HERSCHEL / PLANCK

Planck PLM RF Performance Analysis

Product Code : 22000

Rédigé par/*Written by*	**Responsabilité-Service-Société** ***Responsibility-Office -Company***	**Date**	**Signature**
D. Dubruel	Planck RF Analysis	09/04/04	
Vérifié par/*Verified by*			
JB Riti	Planck PLM Technical Manager	09.04.2004	
E. Pourrier	Product assurance	9/04/2004	
Approbation/*Approved*			
T. Banos	Planck PLM Manager	9/04/04	
J-J. Juillet	Herschel Planck Project Manager	09/04/04	

Data management : G. SERRA

Entité Emettrice : Alcatel Space - Cannes
(détentrice de l'original) :

HERSCHEL/PLANCK	DISTRIBUTION RECORD		
DOCUMENT NUMBER : H-P-3-ASPI-AN-323		Issue 02/ Rev. : 0 Date: 09/04/04	
EXTERNAL DISTRIBUTION		**INTERNAL DISTRIBUTION**	
ESA	**X**	**HP team**	**X**
		Clt Documentation	**Orig.**

ENREGISTREMENT DES EVOLUTIONS / *CHANGE RECORDS*

ISSUE	DATE	§ : DESCRIPTION DES EVOLUTIONS *§ : CHANGE RECORD*	REDACTEUR *AUTHOR*
1		Initial release	D. Dubruel
2	09-04-2004	Document update with CDR data configuration	D. Dubruel

TABLE OF CONTENTS

1. INTRODUCTION 10

1.1 PURPOSE OF THIS NOTE 10
1.2 APPLICABLE DOCUMENTS. 10
1.3 REFERENCE DOCUMENTS 10

2. SELF SPACECRAFT EMISSION ANALYSIS. 11

2.1 SCOPE 11
2.2 SELF SPACECRAFT EMISSION REQUIREMENT 12
2.3 CONVERSION OF THE TEMPERATURE FLUCTUATION LAW INTO POWER FLUCTUATION LAW. 20
2.4 SENSITIVITY ANALYSIS METHOD OF THE TEMPERATURE FLUCTUATION. 25
2.4.1 first phase : method to compute the maximum theoretical fluctuation temperature for each surface element. 25
2.4.2 second phase : method to weight the maximum theoretical fluctuation temperature for each surface element. 26
2.5 RF COUPLING FACTOR EVALUATION 27
2.5.1 Overall amount of relative power evaluation. 27
2.5.2 Relative power evaluation passing through the MLI. 29
2.6 SENSITIVITY ANALYSIS OF THE MAXIMUM ALLOWED TEMPERATURE FLUCTUATION FOR EACH STUCTURAL ELEMENT. 30
2.6.1 primary reflector 31
2.6.2 secondary reflector 34
2.6.3 Top of the SVM 35
2.6.4 Third groove 36
2.6.5 SVM walls 37
2.6.6 solar array (toward the PLM). 39
2.6.7 optical cavity (inside of the baffle) 40
2.6.8 part of the telescope hexagonal frame inside the optical cavity. 41
2.6.9 Sensitivity analysis results. 42
2.7 SELF SPACECRAFT EMISSION EVALUATION 43
2.7.1 Methodology to check the compliance with the specifications. 43
2.7.2 Self spacecraft emission for Planck 44

3. SELF SPACECRAFT EMISSION LEVEL CONCLUSIONS. 47

4. ANALYSIS OF THE RESULTS OF THE 4 PI COMPUTATIONS WITHOUT THE BAFFLE EXTENSION-FIRST RF EXPERTISE 48

4.1 30 GHZ PATTERN ANALYSIS 49
4.2 100 GHZ PATTERN ANALYSIS 51
4.3 353 GHZ PATTERN ANALYSIS 53
4.4 857 GHZ PATTERN ANALYSIS 54
4.5 FAR OUT SIDE LOBE PERFORMANCE SYNTHESIS 55

5. ANALYSIS OF THE RESULTS OF THE 4 PI COMPUTATIONS WITH THE BAFFLE EXTENSION USING GAUSSIAN FEED (4PI-EXT BAF-GAUSS FEED) 57

5.1 30 GHZ PATTERN ANALYSIS (4PI-EXT BAF-GAUSS FEED) 58
5.2 100 GHZ PATTERN ANALYSIS (4PI-EXT BAF-GAUSS FEED) 61
5.3 353 GHZ PATTERN ANALYSIS (4PI-EXT BAF-GAUSS FEED) 64
5.4 857 GHZ PATTERN ANALYSIS (4PI-EXT BAF-GAUSS FEED) 67
5.5 FAR OUT SIDE LOBE PERFORMANCE SYNTHESIS (4PI-EXT BAF-GAUSS FEED) 70

6. ANALYSIS OF THE RESULTS OF THE 4 PI COMPUTATIONS WITH THE BAFFLE EXTENSION USING INSTRUMENT FEED MODEL (4PI-EXT BAF-INST FEED) 72

6.1 30 GHz PATTERN ANALYSIS(4PI-EXT BAF-INST FEED) 73
6.2 100 GHz PATTERN ANALYSIS(4PI-EXT BAF-INST FEED) 1ST DETECTOR POLARISATION ORIENTATION 75
6.3 100 GHz PATTERN ANALYSIS(4PI-EXT BAF-INST FEED) 2ND DETECTOR POLARISATION ORIENTATION 79
6.4 100 GHz PATTERN PRELIMINARY COMPARISON 83
6.5 353 GHz PATTERN ANALYSIS(4PI-EXT BAF-INST FEED) 89
6.6 FAR OUT SIDE LOBE PERFORMANCE SYNTHESIS (4PI-EXT BAF-INST FEED) 91

7. FAR OUT SIDE LOBE PERFORMANCE SYNTHESIS. 92

7.1 PERFORMANCE TOWARD EARTH SUN AND MOON OF THE PLANCK SPACECRAFT WITH PERFECT REFLECTOR SURFACES 92
7.2 QUILTING OR GRATING LOBE IMPACT ON THE FAR OUT SIDE LOBE LEVEL. 93
7.3 IMPACT OF DUST CONTAMINATION ON THE FAR OUT SIDE LOBE LEVEL 95
7.4 IMPACT OF DIFFUSION BY PRIMARY REFLECTOR ON THE FAR OUT SIDE LOBE LEVELS. 97
7.5 FINAL PERFORMANCE REJECTION TOWARD EARTH SUN AND MOON. 99

8. MAIN LOBE PERFORMANCE ANALYSIS 100

8.1 INTRODUCTION 100
8.2 HYPOTHESES AND DATA USED FOR RF BUDGET 101
8.2.1 Planck telescope geometry 101
8.2.2 Horns definition 103
8.2.3 Horns position in the ORDP plane 104
8.3 MAIN LOBES COMPUTATION 108
8.3.1 introduction 108
8.3.2 Requirements 108
8.3.3 Assessment in terms of directivity degradation 109
8.3.4 Simulation Tool 109
8.3.5 LFI radiation pattern 113
8.3.6 HFI radiation pattern 114
8.4 CONTRIBUTORS ANALYSIS 115
8.4.1 Contributors identification 115
8.4.2 Deterministic contributor 116
8.4.3 Statistic contributors 132
8.4.4 Complete Budget 147
8.4.5 Ellipticity deviation 148
8.5 CONCLUSION 148

9. CONCLUSION 149

LIST OF FIGURES

FIGURE 2.2-1 : ALL 5 CURVES FROM TOP : LFI 30,HFI 100,HFI 857 (MERGED), HFI 100 THEN HFI 353 14
FIGURE 2.2-2 : 30 GHZ REQUIREMENT CURVE. 15
FIGURE 2.2-3 :100 GHZ LFI REQUIREMENT CURVE. 16
FIGURE 2.2-4 : 100 GHZ HFI REQUIREMENT CURVE. 17
FIGURE 2.2-5 : 353 GHZ HFI REQUIREMENT CURVE. 18
FIGURE 2.2-6 : 857 GHZ HFI REQUIREMENT CURVE. 19
FIGURE 2.3-1 : NUMERICAL INTEGRATION RESULTS. 22
FIGURE 2.3-2 : PLANCK'S LAW OVER A WIDE FREQUENCY DOMAIN. 22
FIGURE 2.3-3 : PLANCK'S LAW OVER THE 30 –1000 GHZ DOMAIN FOR 100, 200 AND 300 K. 23
FIGURE 2.3-4 : PLANCK'S LAW OVER THE 30 –1000 GHZ DOMAIN FOR 50, 80 AND 150 K. 23
FIGURE 2.3-5 : PLANCK'S LAW DERIVATIVE OVER THE 30 –1000 GHZ DOMAIN FOR 50, 80 AND 150 K 24
FIGURE 2.6-2.6-1 : PRIMARY REFLECTOR ELEMENTS 31
FIGURE 5.1-1 : 4PI DIAGRAM , PHI : -180°, 180°/ THETA : 0,+180° / LEVELS IN DIRECTIVITY DISPLAYED FROM -100 DBI TO 0 DBI 58
FIGURE 5.1-2 : MOON AREA PHI : -180°, 180° / THETA : +148°,+180° / LEVELS IN DIRECTIVITY DISPLAYED FROM -100 DBI TO 0DBI 58
FIGURE 5.1-3 : EARTH AREA PHI : -180°, 180° / THETA : +165°,+180° / LEVELS IN DIRECTIVITY DISPLAYED FROM -150 DBI TO -50DBI 59
FIGURE 5.1-4 : ENLARGED EARTH AREA PHI : -180°, 180° / THETA : +165°,+180° / LEVELS IN DIRECTIVITY DISPLAYED FROM -150 DBI TO -50DBI 59
FIGURE 5.1-5 : SUN AREA PHI : -180°, 180° / THETA : +170°,+180° / LEVELS IN DIRECTIVITY DISPLAYED FROM -150 DBI TO -50DBI 59
FIGURE 5.1-6 : ENLARGED SUN AREA PHI : -180°, 180° / THETA : +170°,+180° / LEVELS IN DIRECTIVITY DISPLAYED FROM -150 DBI TO -40DBI 59
FIGURE 5.1-7 : AREA WHERE THE -65 DB REJECTION IS NOT MET 60
FIGURE 5.2-1 : 4PI DIAGRAM , PHI : -180°, 180° / THETA : 0,+180° / LEVELS IN DIRECTIVITY DISPLAYED FROM -100 DBI TO +0 DBI 61
FIGURE 5.2-2 : MOON AREA PHI : -180°, 180° / THETA : +148°,+180° / LEVELS IN DIRECTIVITY DISPLAYED FROM -150 DBI TO -50 DBI 61
FIGURE 5.2-3 : ENLARGED MOON AREA PHI : -180°, 180° / THETA : +148°,+180° / LEVELS IN DIRECTIVITY DISPLAYED FROM -150 DBI TO -50 DBI. 62
FIGURE 5.2-4 : EARTH AREA PHI : -180°, 180° / THETA : +165°,+180° / LEVELS IN DIRECTIVITY DISPLAYED FROM -150 DBI TO -50DBI. 62
FIGURE 5.2-5 : ENALRGED EARTH AREA PHI : -180°, 180° / THETA : +165°,+180° / LEVELS IN DIRECTIVITY DISPLAYED FROM -150 DBI TO -40DBI 62
FIGURE 5.2-6 : SUN AREA PHI : -180°, 180° / THETA : +170°,+180° / LEVELS IN DIRECTIVITY DISPLAYED FROM -160DBI TO -120 DBI 63
FIGURE 5.2-7 : ENLARGED SUN AREA PHI : -180°, 180° / THETA : +170°,+180° / LEVELS IN DIRECTIVITY DISPLAYED FROM -150 DBI TO -40DBI 63
FIGURE 5.2-8 : AREA WHERE THE -65 DB REJECTION IS NOT MET (DIRECTIVITY LEVEL DISPLAYED FROM 61.6-65=-3.4 DBI TO MAX=61.6 DBI). 63
FIGURE 5.3-1 : 4PI DIAGRAM , PHI : -180°, 180° / THETA : 0,+180° / LEVELS IN DIRECTIVITY DISPLAYED FROM -100 DBI TO +0 DBI 64
FIGURE 5.3-2 : MOON AREA PHI : -180°, 180° / THETA : +148°,+180° / LEVELS IN DIRECTIVITY DISPLAYED FROM -150 DBI TO -50 DBI 64
FIGURE 5.3-3 : ENLARGED MOON AREA PHI : -180°, 180° / THETA : +148°,+180° / LEVELS IN DIRECTIVITY DISPLAYED FROM -150 DBI TO -50 DBI. 65
FIGURE 5.3-4 : EARTH AREA PHI : -180°, 180° / THETA : +165°,+180° / LEVELS IN DIRECTIVITY DISPLAYED FROM -200 DBI TO -100DBI. 65
FIGURE 5.3-5 : ENLARGED EARTH AREA PHI : -180°, 180° / THETA : +165°,+180° / LEVELS IN DIRECTIVITY DISPLAYED FROM -200 DBI TO -100 DBI 65

FIGURE 5.3-6 : SUN AREA PHI : -180°, +180° / THETA : +170°,+180° / LEVELS IN DIRECTIVITY DISPLAYED FROM -200DBI TO -100 DBI 65
FIGURE 5.3-7 : ENLARGED SUN AREA PHI : -180°, 180° / THETA : +170°,+180° / LEVELS IN DIRECTIVITY DISPLAYED FROM -200DBI TO -100 DBI 66
FIGURE 5.3-8 : AREA WHERE THE -65 DB REJECTION IS NOT MET (DIRECTIVITY LEVEL DISPLAYED FROM 69.2-65=4.2 DBI TO MAX=69.2 DBI). 66
FIGURE 5.4-1 : 4PI DIAGRAM , PHI : -180°, 180°/THETA : 0,+180°/LEVELS IN DIRECTIVITY DISPLAYED FROM -100 DBI TO +0 DBI 67
FIGURE 5.4-2 : MOON AREA PHI : -180°, 180° / THETA : +148°,+180° / LEVELS IN DIRECTIVITY DISPLAYED FROM -195 DBI TO -95 DBI 67
FIGURE 5.4-3 : ENLARGED MOON AREA PHI : -180°, 180° / THETA : +148°,+180° / LEVELS IN DIRECTIVITY DISPLAYED FROM -195 DBI TO -95 DBI..... 68
FIGURE 5.4-4 : EARTH AREA PHI : -180°, 180° / THETA : +165°,+180° / LEVELS IN DIRECTIVITY DISPLAYED FROM -195 DBI TO -95DBI 68
FIGURE 5.4-5 : ENLARGED EARTH AREA PHI : -180°, 180° / THETA : +165°,+180° / LEVELS IN DIRECTIVITY DISPLAYED FROM -195 DBI TO -95DBI 68
FIGURE 5.4-6 : SUN AREA PHI : -180°, 180° / THETA : +170°,+180° / LEVELS IN DIRECTIVITY DISPLAYED FROM -235 DBI TO -185 DBI. 69
FIGURE 5.4-7 : SUN AREA PHI : -180°, 180° / THETA : +170°,+180° / LEVELS IN DIRECTIVITY DISPLAYED FROM -235 DBI TO -185 DBI. 69
FIGURE 6.1-1 : 4PI DIAGRAM , PHI : -180°, 180° / THETA : 0,+180° / LEVELS IN DIRECTIVITY DISPLAYED FROM -100 DBI TO +0 DBI (FIRST COMPONENT, XPOL)..... 73
FIGURE 6.1-2 : 4PI DIAGRAM , PHI : -180°, 180° / THETA : 0,+180° / LEVELS IN DIRECTIVITY DISPLAYED FROM -100 DBI TO +0 DBI (SECOND COMPONENT, CO-POL)..... 74
FIGURE 6.1-3 : 4PI DIAGRAM , PHI : -180°, 180° / THETA : 0,+180° / LEVELS IN DIRECTIVITY DISPLAYED FROM -100 DBI TO +0 DBI (LOCAL MAJOR/MINOR COMPONENT)..... 74
FIGURE 6.2-1 : 4PI DIAGRAM , PHI : -180°, 180° / THETA : 0,+180° / LEVELS IN DIRECTIVITY DISPLAYED FROM -100 DBI TO +0 DBI (FIRST COMPONENT, XPOL)..... 75
FIGURE 6.2-2 : 4PI DIAGRAM , PHI : -180°, 180° / THETA : 0,+180° / LEVELS IN DIRECTIVITY DISPLAYED FROM -100 DBI TO +0 DBI (SECOND COMPONENT, CO-POL)..... 76
FIGURE 6.2-3 : 4PI DIAGRAM , PHI : -180°, 180° / THETA : 0,+180° / LEVELS IN DIRECTIVITY DISPLAYED FROM -100 DBI TO +0 DBI (LOCAL MAJOR/MINOR COMPONENT)..... 76
FIGURE 6.2-4 : MOON AREA PHI : -180°, 180° / THETA : +148°,+180° / LEVELS IN DIRECTIVITY DISPLAYED FROM -150 DBI TO -50 DBI 77
FIGURE 6.2-5 : ENLARGED MOON AREA PHI : -180°, 180° / THETA : +148°,+180° / LEVELS IN DIRECTIVITY DISPLAYED FROM -150 DBI TO -50 DBI (LOCAL MAJOR/MINOR COMPONENT)..... 77
FIGURE 6.2-6 : EARTH AREA PHI : -180°, 180° / THETA : +165°,+180° / LEVELS IN DIRECTIVITY DISPLAYED FROM -150 DBI TO -50DBI (LOCAL MAJOR/MINOR COMPONENT)..... 77
FIGURE 6.2-7 : ENLARGED EARTH AREA PHI : -180°, 180° / THETA : +165°,+180° / LEVELS IN DIRECTIVITY DISPLAYED FROM -150 DBI TO -50DBI (LOCAL MAJOR/MINOR COMPONENT)..... 78
FIGURE 6.2-8 : SUN AREA PHI : -180°, 180° / THETA : +170°,+180° / LEVELS IN DIRECTIVITY DISPLAYED FROM -1600 DBI TO -120DBI (LOCAL MAJOR/MINOR COMPONENT 78
FIGURE 6.2-9 : SUN AREA PHI : -180°, 180° / THETA : +170°,+180° / LEVELS IN DIRECTIVITY DISPLAYED FROM -160 DBI TO -120DBI (LOCAL MAJOR/MINOR COMPONENT 78
FIGURE 6.3-1 : 4PI DIAGRAM , PHI : -180°, 180° / THETA : 0,+180° / LEVELS IN DIRECTIVITY DISPLAYED FROM -100 DBI TO +0 DBI (FIRST COMPONENT, XPOL)..... 79
FIGURE 6.3-2 : 4PI DIAGRAM , PHI : -180°, 180° / THETA : 0,+180° / LEVELS IN DIRECTIVITY DISPLAYED FROM -100 DBI TO +0 DBI (SECOND COMPONENT, CO-POL)..... 80
FIGURE 6.3-3 : 4PI DIAGRAM , PHI : -180°, 180° / THETA : 0,+180° / LEVELS IN DIRECTIVITY DISPLAYED FROM -100 DBI TO +0 DBI (LOCAL MAJOR/MINOR COMPONENT)..... 80
FIGURE 6.3-4 : MOON AREA PHI : -180°, 180° / THETA : +148°,+180° / LEVELS IN DIRECTIVITY DISPLAYED FROM -150 DBI TO -50 DBI 81
FIGURE 6.3-5 : ENLARGED MOON AREA PHI : -180°, 180° / THETA : +148°,+180° / LEVELS IN DIRECTIVITY DISPLAYED FROM -100 DBI TO 0 DBI (LOCAL MAJOR/MINOR COMPONENT) 81
FIGURE 6.3-6 : EARTH AREA PHI : -180°, 180° / THETA : +165°,+180° / LEVELS IN DIRECTIVITY DISPLAYED FROM -150 DBI TO -50DBI (LOCAL MAJOR/MINOR COMPONENT)..... 81

FIGURE 6.3-7 : SUN AREA PHI : -180°, 180° / THETA : +170°,+180° / LEVELS IN DIRECTIVITY DISPLAYED FROM -150 DBI TO -50DBI (LOCAL MAJOR/MINOR COMPONENT 82
FIGURE 6.4-1 : LOCAL AREA MODIFIED BY MORE THAN 30 DB (RED PIXELS TO BE DISGARDED) 84
FIGURE 6.4-2 :LOCAL AREA MODIFIED BY MORE THAN 20 DB (RED PIXELS TO BE DISGARDED). 85
FIGURE 6.4-3 : LOCAL AREA MODIFIED BY MORE THAN 10 DB .....AND NO MORE THAN 20 DB (RED PIXELS TO BE DISGARDED) 86
FIGURE 6.4-4 LOCAL AREA MODIFIED BY MORE THAN 10 DB (RED PIXELS TO BE DISGARDED). 87
FIGURE 6.4-5 :LOCAL AREA MODIFIED BY NO MORE THAN 10 DB (RED PIXELS TO BE DISGARDED). 88
FIGURE 6.5-1 : 4PI DIAGRAM , PHI : -180°, 180° / THETA : 0,+180° / LEVELS IN DIRECTIVITY DISPLAYED FROM -100 DBI TO +0 DBI (LOCAL MAJOR/MINOR COMPONENT) 89
FIGURE 6.5-2 : MOON AREA PHI : -180°, 180° / THETA : +148°,+180° / LEVELS IN DIRECTIVITY DISPLAYED FROM -100 DBI TO -0 DBI 89
FIGURE 6.5-3 : EARTH AREA PHI : -180°, 180° / THETA : +165°,+180° / LEVELS IN DIRECTIVITY DISPLAYED FROM -150 DBI TO -50DBI (LOCAL MAJOR/MINOR COMPONENT) 89
FIGURE 6.5-4 : SUN AREA PHI : -180°, 180° / THETA : +170°,+180° / LEVELS IN DIRECTIVITY DISPLAYED FROM -150 DBI TO -50DBI (LOCAL MAJOR/MINOR COMPONENT 90
FIGURE 7.4-1 :PLANCK REFLECTOR ILLUMINATED AREA 97
FIGURE 8.2-8.2-1: PLANCK TELESCOPE COORDINATE SYSTEMS 102
FIGURE 8.2-2 : LFI HORNS IN THE ORDP PLANE 105
FIGURE 8.2-3: HFI HORNS IN THE ORDP PLANE 107
FIGURE 8.2-4 DETECTORS VIEW IN THE FOCAL PLANE 107
FIGURE 8.3-1 TELESCOPE SPECIFICATIONS: GAIN DEGRADATION 108
FIGURE 8.3-2: RADIATION PATTERN OF THE TELESCOPE FOR LFI HORNS 113
FIGURE 8.3-3. RADIATION PATTERN OF THE TELESCOPE FOR HFI HORNS 114
FIGURE 8.4-1 CONTRIBUTORS IDENTIFICATION 115
FIGURE 8.4-2 DETERMINISTIC CASE 116
FIGURE 8.4-3 RESIDUAL DEFORMATIONS ON THE MAIN REFLECTOR (UNITY IN FIGURE :MM) (RMS≈ 10 µM) 118
FIGURE 8.4-4 RESIDUAL DEFORMATIONS ON THE SUB REFLECTOR (UNITY IN FIGURE :M) (RMS ≈ 20 µM) 118
FIGURE 8.4-5 GAIN DEGRADATION DUE TO DETERMINISTIC LOAD CASE 119
FIGURE 8.4-6 CELL DECOMPOSITION 121
FIGURE 8.4-7 QUILTING IMPACT ON REFLECTOR 122
FIGURE 8.4-8 CELL DECOMPOSITION OF THE REFLECTOR (MAGNIFIED) 122
FIGURE 8.4-9 QUILTING IMPACT ON THE REFLECTOR (CELL MAGNIFIED) 123
FIGURE 8.4-10 : GAIN DEGRADATION DUE TO QUILTING EFFECTS 124
FIGURE 8.4-11 DETERMINIST: BUDGET 131
FIGURE 8.4-12 : RANDOM CASES 1 TO 70 (2σ) 145
FIGURE 8.4-13 TOTAL RF BUDGET OF PLANCK TELESCOPE (2σ) 148

LIST OF TABLES

TABLE 2.2-1 : MINIMUM AND MAXIMUM AMPLITUDE DEVIATIONS OF THE ASD. 13
TABLE 2-2.5-1 : OUTPUT OF THE TICRA RF EXPERTISE. 28
TABLE 2-2.7-1 : SPACECRAFT TEMPERATURE RESULTS FROM THERMAL ANALYSIS (SEE RD1 AND RD2) 44
TABLE 2.7-2 : 30 GHZ CHANNEL ASD PERFORMANCE DISPLAY (WORST CASE COMPONENT AT 1/60 HZ). 45
TABLE 2.7-3 : 100 GHZ HFI CHANNEL ASD PERFORMANCE DISPLAY (WORST CASE COMPONENT AT 1/60 HZ). 46
TABLE 2.7-4 : 353 GHZ CHANNEL ASD PERFORMANCE DISPLAY (WORST CASE COMPONENT AT 1/60 HZ). 46
TABLE 4.5-1 :PERFORMANCE SYNTHESIS. 56
TABLE 5.5-1 : PERFORMANCE SYNTHESIS. 71
TABLE 7.1-1 : REJECTION PERFORMANCE SYNTHESIS. 92
TABLE 7.2-1 : GRATING LOBES LEVEL 94
TABLE 7.2-2 : ANGULAR POSITION OF THE GRATING LOBE INDUCED BY THE SECONDARY REFLECTOR QUILTING 94
TABLE 7.2-3 : ANGULAR POSITION OF THE GRATING LOBE INDUCED BY THE PRIMARY REFLECTOR QUILTING 94
TABLE 7.3-1 :REJECTION LEVEL @857 GHZ INDUCED BY REFLECTOR CONTAMINATION. 95

TABLE 7.3-2 : MARGIN @857 GHZ WRT THE REQUIREMENTS AND THE GOALS. 95
TABLE 7.3-3 : REJECTION LEVEL @353 GHZ INDUCED BY REFLECTOR CONTAMINATION. 96
TABLE 7.3-4 : MARGIN @353 GHZ WRT THE REQUIREMENTS AND THE GOALS. 96
TABLE 7.3-5 REJECTION LEVEL @100 GHZ INDUCED BY REFLECTOR CONTAMINATION. 96
TABLE 7.3-6 : MARGIN @100 GHZ WRT THE REQUIREMENTS AND THE GOALS. 96
TABLE 7.4-1 : SUMMARY OF EFFECTIVE ANTENNA TEMPERATURE. 97
TABLE 7.5-1 : FINAL PERFORMANCE REJECTION COMPARISON WRT TO THE REQUIREMENTS AND THE GOALS. 99
TABLE 8.2-1 TAPER OF HORNS 103
TABLE 8.2-2 : LFI HORNS POSITIONS AND ORIENTATIONS 104
TABLE 8.2-3 POSITIONS OF HFI HORNS 106
TABLE 8.3-1 : SURFACE ERROR (μM RMS) AND GAIN DEGRADATION BY RUZE 110
TABLE 8.3-2 CONVERGENCE BETWEEN PO-PO AND MGTD (REFLECTION)-PO 112
TABLE 8.4-1 DETERMINISTIC LOAD CASE : BFE AND DEFOCUS 117
TABLE 8.4-2 : GAIN DEGRADATION DUE TO THE DETERMINISTIC LOAD CASE 120
TABLE 8.4-3 GAIN DEGRADATION DUE TO OHMIC LOSSES 126
TABLE 8.4-4 GAIN DEGRADATION DUE TO ROUGHNESS 127
TABLE 8.4-5 GAIN DEGRADATION DUE TO CONTAMINATION (NS :NOT SIGNIFICANT) 129
TABLE 8.4-6 DETERMINIST : BUDGET (NS : NOT SIGNIFICANT) 130
TABLE 8.4-7 WFE PER HORN 133
TABLE 8.4-8 INPUT PARAMETERS FOR THE SENSITIVITY ANALYSIS. RANDOM CASE 135
TABLE 8.4-9 INPUT PARAMETERS FOR SENSITIVITY ANALYSIS : RANDOM CASE 136
TABLE 8.4-10 DESCRIPTIONS OF THE COLUMNS 137
TABLE 8.4-11 RANDOM CASE (1 TO 10) (2σ) 138
TABLE 8.4-12 RANDOM CASE (11 TO 20) (2σ) 139
TABLE 8.4-13 RANDOM CASE (21 TO 30) (2σ) 140
TABLE 8.4-14 RANDOM CASE (31 TO 40) (2σ) 141
TABLE 8.4-15 RANDOM CASE (41 TO 50) (2σ) 142
TABLE 8.4-16 RANDOM CASE (51 TO 60) (2σ) 143
TABLE 8.4-17 RANDOM CASE (61 TO 70) (2σ) 144
TABLE 8.4-18 TOTAL RANDOM CASE (2σ) 146
TABLE 8.4-19 COMPLETE BUDGET (2σ) 147

1. INTRODUCTION

1.1 Purpose of this note

This note updates the PDR analysis.

1.2 Applicable documents.

[AD 1] System requirements specification – SCI – PR-RS-05991- issue 2/ 0- 13 july 2001

[AD 2] H-P-3-ASPI-SP-0274 -issue 1 - rev 0 -Planck Telescope optical and RF system specification.

1.3 Reference documents

[RD 1] Planck RF expertise Phase B - WP4 - RF calculation report : Incident RF power exchange between detector and structural elements - October, 2002 - S-1117-07

[RD 2] SVM thermal analysis report - H-P-TN-AI-0005 - issue 2 - 14/06/2002.

[RD 3] Planck PLM thermal analysis - H-P-3-ASPI-AN-330 - issue 1 - 01/07/2002.

[RD 4] Planck RF expertise model verification & computations WP 2 & WP3 - November , 2003 -TICRA - s-1188-03

[RD 5] Update of the inputs for the RF numerical model - H-P-3-ASP-TN-0564 - issue 1 - rev 0 - 16/09/2003

[RD 6] H-P-3-ASPI-TN-0517 -issue 1 - rev 0 - Planck LFI detector data processing.

[RD 7] H-P-3-ASPI-TN-0559 -issue 1 - rev 2 - HFI detector data processing.

[RD 8] Planck RF expertise - Manual for computations of far out side lobe patterns - November, 2003 - s1188-04

[RD 9] Planck PLM RF Performance Analysis, PDR Analysis, H-P-3-ASPI-AN-0323, july 2002.

[RD 10] NIL

[RD 11] NIL.

[RD 12] Planck Optical Analysis, Inputs for WFE and Gain Budgets, H-P-3-ASPI-TN-0742- , Apr. 2004.

[RD 13] Planck Payload Optical Performance Analysis, H-P-3-ASPI-TN-0331, Apr. 2004.

[RD 14] Analysis of the diffusion by primary reflector using the MAP method - H-P-3-ASP-TN-0528 - issue 1 - rev 0 - 11/06/2003.

[RD 15] Dust contamination analysis - H-P-3-TN-0468 - issue 1 - rev 0 - 27 /05 /2003

2. SELF SPACECRAFT EMISSION ANALYSIS.

2.1 Scope

This section presents the analysis of the self spacecraft emission level.

The analysis starts with the understanding of the requirement. Then the sensitivity analysis method is explained and applied. This sensitivity analysis allows to identify the most critical surface element wrt to the performance.

The last phase is the performance budget based upon the results of the thermal analysis.

The main update wrt the PDR analysis are the following :

-analysis of the Fourier processing of the temporal thermal law performed by Alenia.
-Fourier transform of the updated temporal thermal law provided by Alenia.
-use of the coupling factor computed by TICRA in the frame of the RF expertise.

From that point the PDR fourier analysis of Alenia has been kept (worst case value).

2.2 Self spacecraft emission requirement

The self spacecraft emission requirement is defined in the System Requirement Specification (requirement ref SPER 065 P).

****

The ASD (in Watts / √Hz) of each frequency component between 0.01 Hz and 100 Hz shall be such that :

Frequency [GHz]	**ASD** [Watt / √Hz]
30	< 3.4 E-18 X
100 (LFI)	< 1.1 E-17 X
100 (HFI)	< 2.1 E-18 X
353	< 1.8 E-18 X
857	< 2.2 E-17 X

Note :
X is equal to one for any frequency component fo of the fluctuation source synchronous with the Planck S/C spinning rate (i.e. multiple of f.spin = 1 / 60 Hz).

Otherwise , X = (B * t.obs * Delta.f) , where Delta.f = fo – k * f.spin and k is chosen to minimise Delta.f .
t.obs = 3600 * FWHM / 2.5 arcmin , and FWHM is the angular resolution of the antenna radiation pattern in arc minutes .

****

The above requirement is derived in order to obtain for any component f_o of the fluctuating source, the maximum allowed level of ASD.

Delta_f is the difference between the fluctuating component f_o and the nearest multiple of the spin frequency. Then $(Delta\_f)_{max}$ is equal to f_spin/2.

If f_o = k*f_spin then X=1.
If f_o different from f_spin X is a linear function varying with f_o. X is a periodic function. The period is f_spin.

For f_o varying from k*f_spin to k*(f_spin+f_spin/2), X is linearly increasing from 1 up to PI*t_obs*f_spin/2.

For f_o varying from k*(f_spin+f_spin/2) to (k+1)*f_spin, X is linearly decreasing from PI*t_obs*f_spin/2 down to 1.

The following table details for each frequency the ASD allowed deviation. The Second column is obtained from the computation of the telescope main lobe. The fourth column is the requirement to be multiplied by X function of f_o.

In this table (Table 2.2-1) the most stringent requirement is only applicable to spin-synchronous fluctuating sources. The most relaxed requirement is applicable to sources fluctuating at f=k*3/2*f_spin.

Central frequency (GHz)	FWHM (arcmin)	PI*t_obs(s)	Qantity (to multiplied by X)	X_max	ASD_min (W/Hz^-05) = ASD * 1	ASD_min (dBW/Hz^-0.5)	ASD_max (W/Hz^-0.5	ASD_max (dBW/Hz^-0.5)
30	33	149288.48	3.40E-18	1244.07	3.40E-18	-174.69	4.23E-15	-143.74
100 (LFI)	10	45238.93	1.10E-17	376.99	1.10E-17	-169.59	4.15E-15	-143.82
100 (HFI)	10	45238.93	2.10E-18	376.99	2.10E-18	-176.78	7.92E-16	-151.01
353	5.0	22619.47	1.80E-18	188.50	1.80E-18	-177.45	3.39E-16	-154.69
857	5.0	22619.47	2.20E-17	188.50	2.20E-17	-166.58	4.15E-15	-143.82

Table 2.2-1 : Minimum and Maximum amplitude deviations of the ASD.

The Figure 2.2-1 presents all the five curves on the same plot. The maxima of the LFI 30 LFI 100 and HFI 857 are almost the same. The three corresponding curves appear merged. The most stringent requirement is the one for the HFI 353 GHz channel.

The Figure 2.2-2 and Figure 2.2-6 present the requirements curves one by one for each specified frequency.

The curves are plotted for the first few multiples of the spin frequency. Due to the wide dynamic variation, the ordinate is plotted as 10*log10(ASD). Hence the linear behaviour of the requirement is plotted as a logarithmic curve instead of a linear curve.

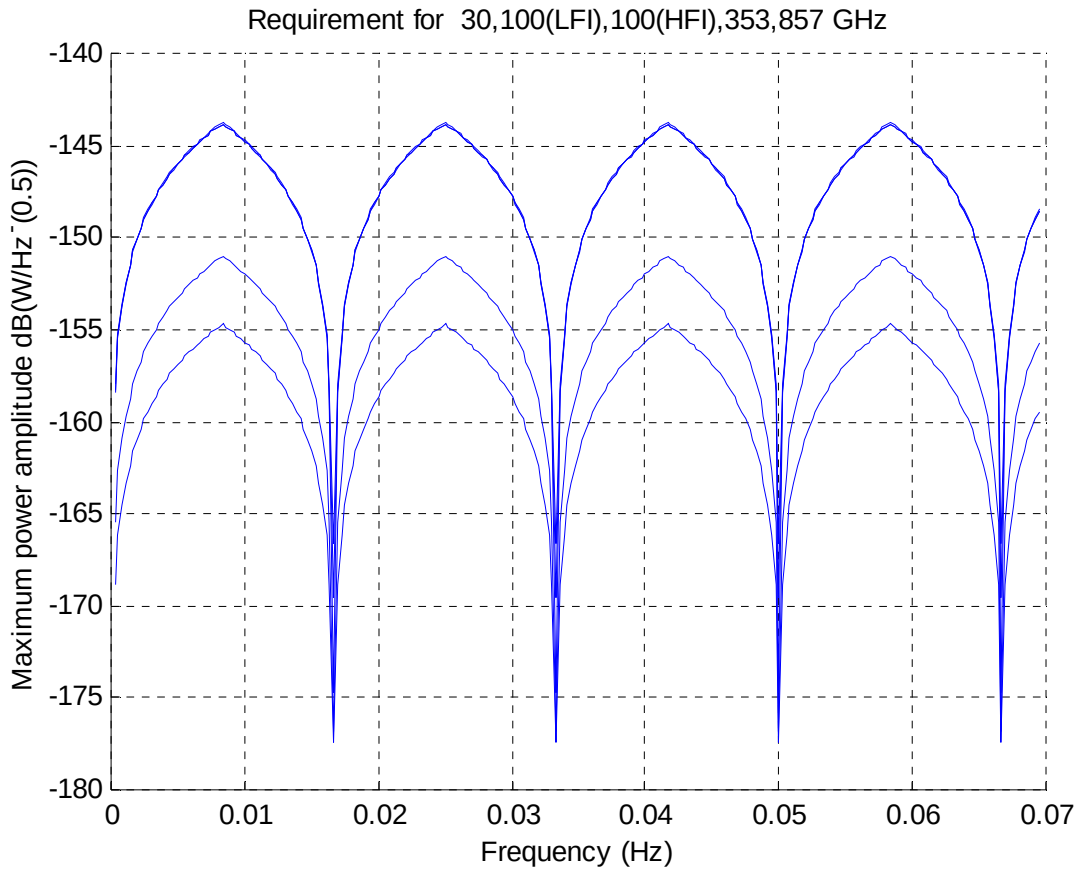

Figure 2.2-1 : All 5 curves from top : LFI 30,HFI 100,HFI 857 (merged), HFI 100 then HFI 353

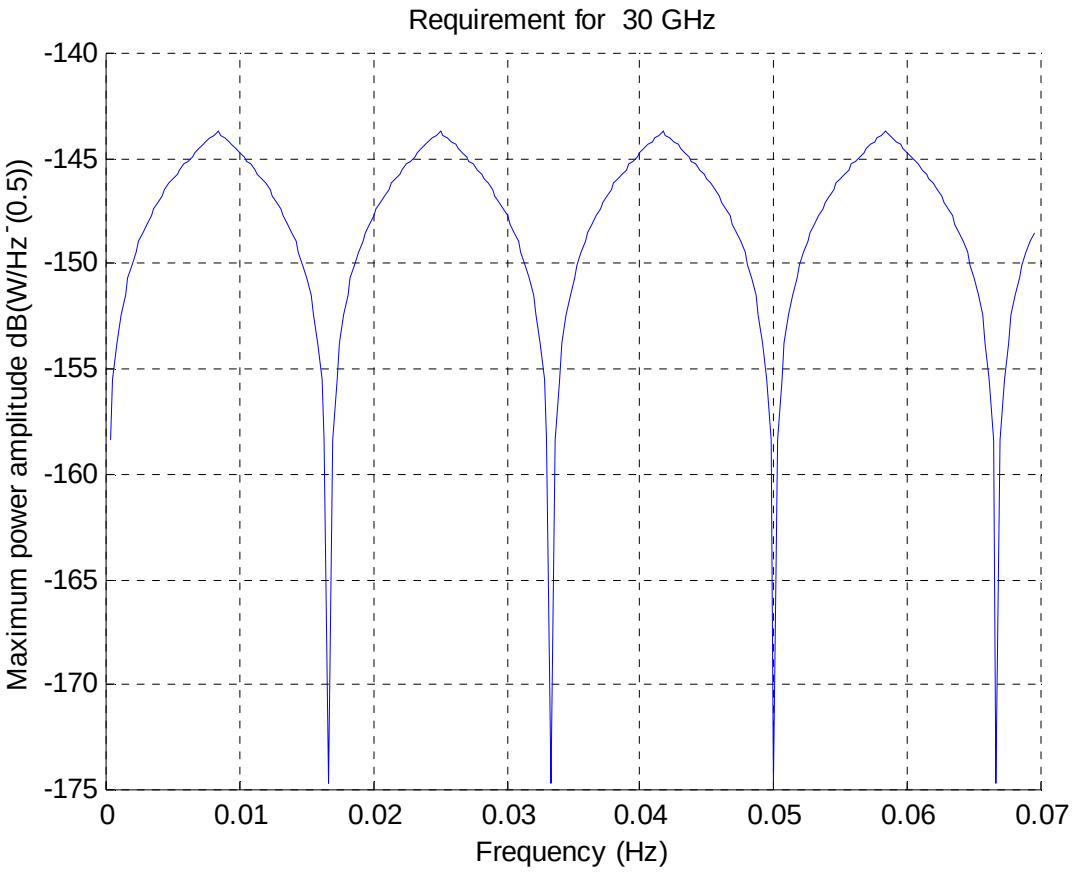

Figure 2.2-2 : 30 GHz requirement curve.

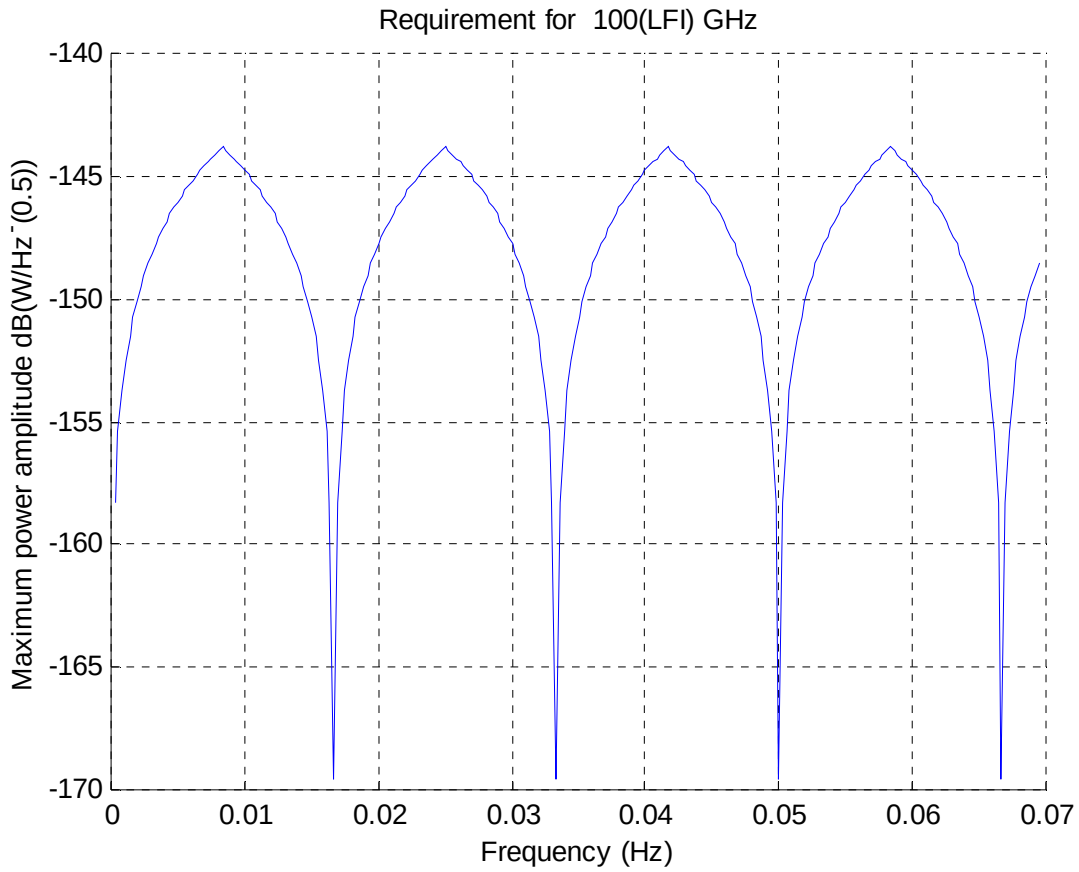

Figure 2.2-3 :100 GHz LFI requirement curve.

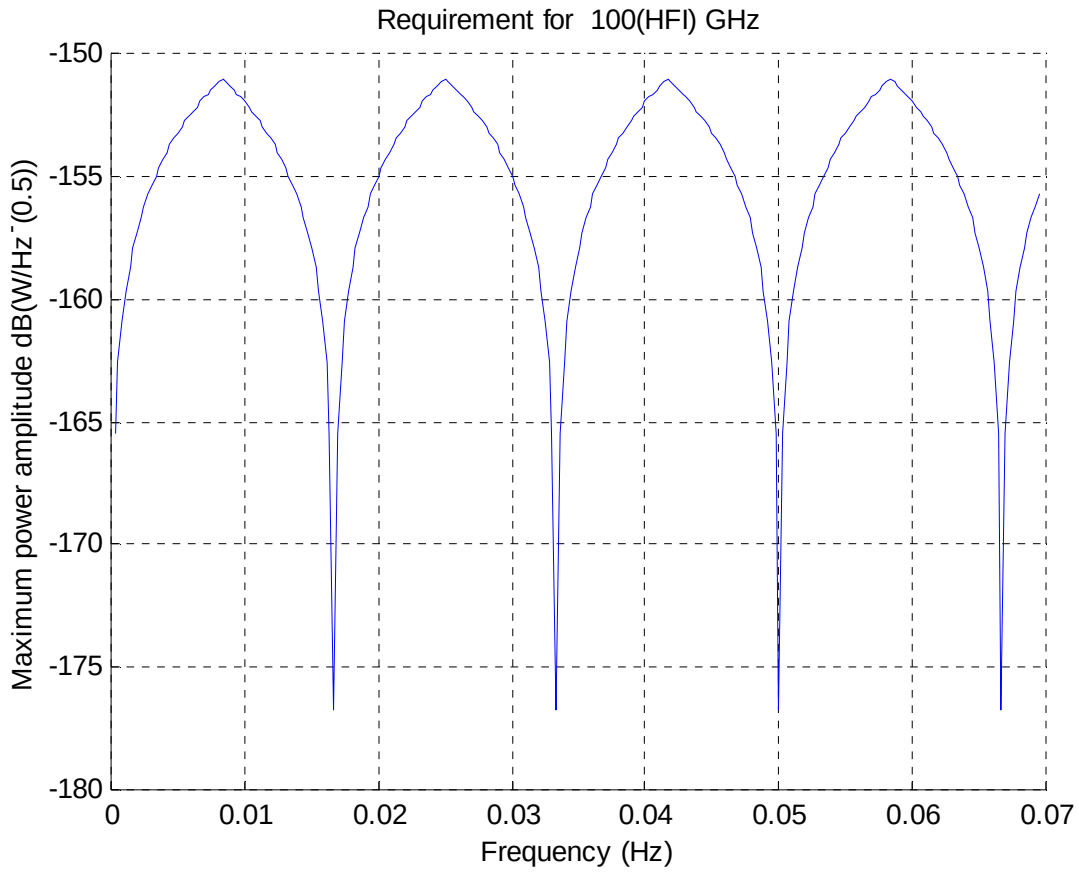

Figure 2.2-4 : 100 GHz HFI requirement curve.

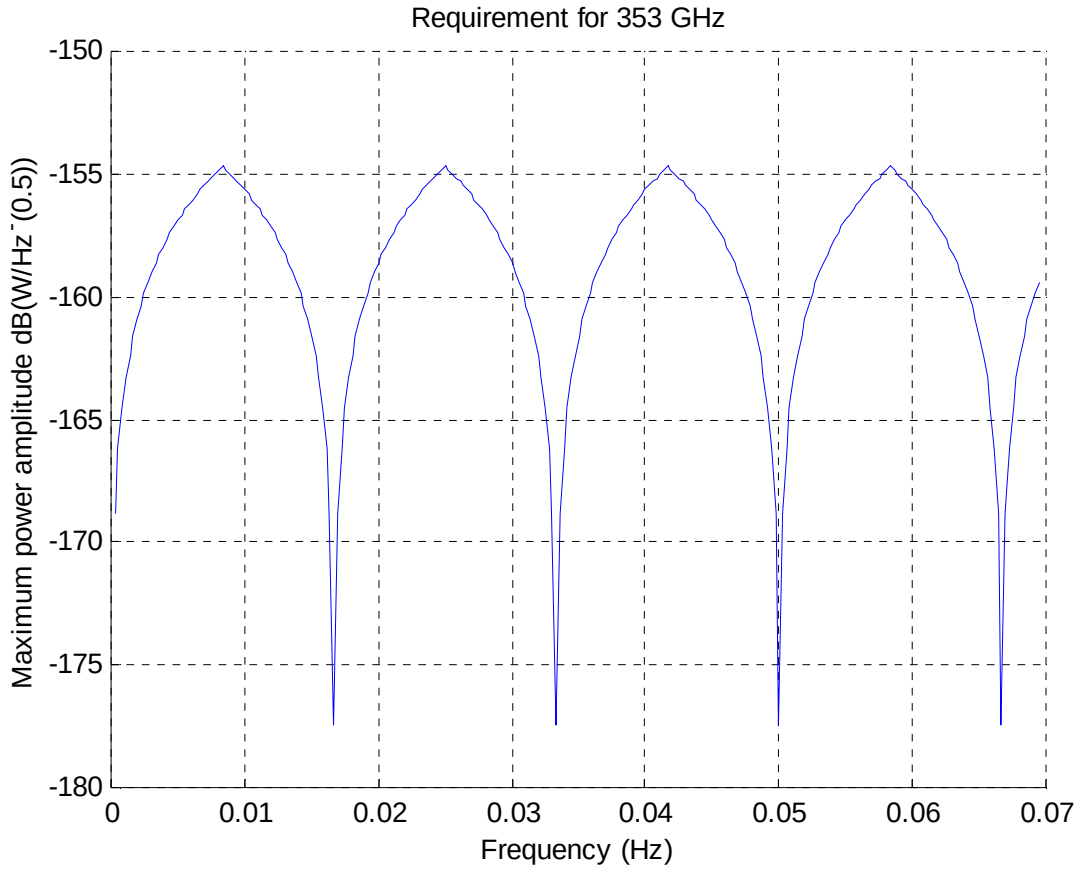

Figure 2.2-5 : 353 GHz HFI requirement curve.

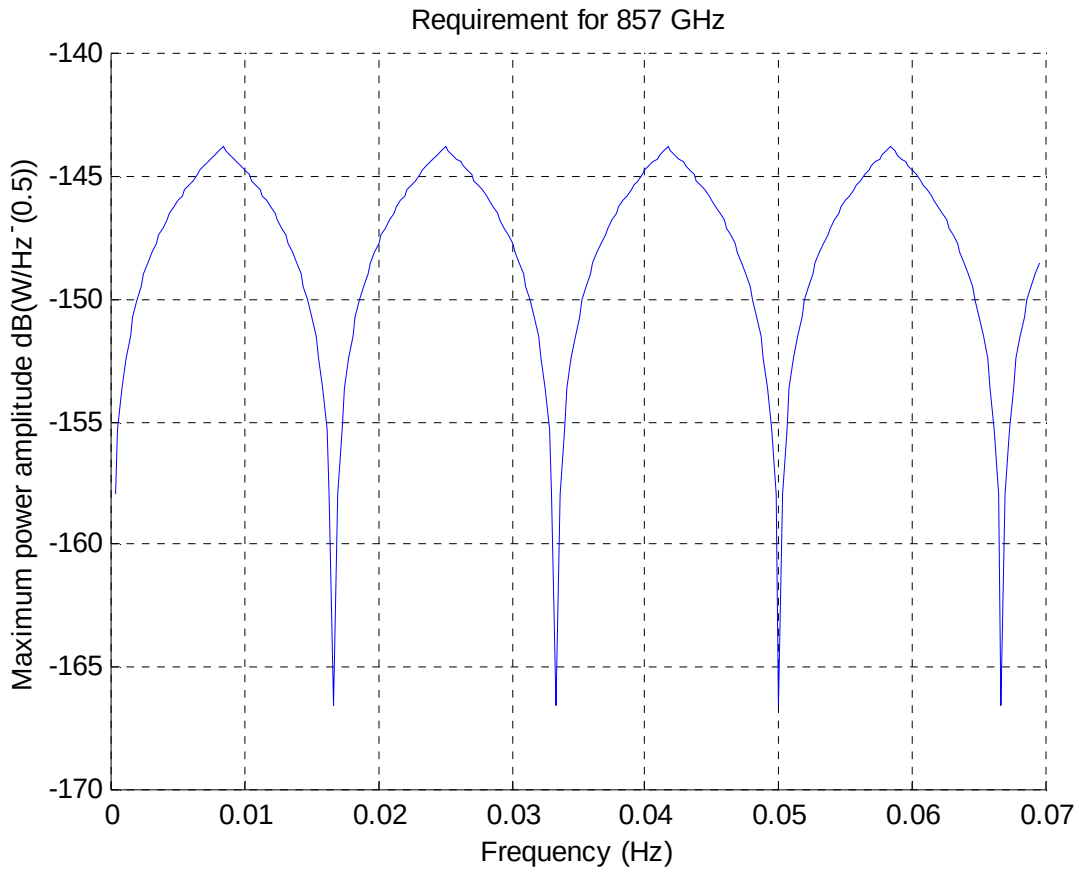

Figure 2.2-6 : 857 GHz HFI requirement curve.

2.3 Conversion of the temperature fluctuation law into power fluctuation law.

The SPER 065 P requirement is expressed in terms of power fluctuation. The input for the analysis is provided as temperature deviation. Hence it is necessary to convert the temperature fluctuation law into a power fluctuation law. The conversion is detailed here below.

The received power by a detector is :

$$P = \frac{A_r}{2} \int_{f1}^{f2} \iint_{4\pi} B(\theta,\varphi, f, T)\, f_n(\theta,\varphi) d\Omega df \quad [1]$$

$$B(\theta,\varphi, f, T) = \frac{(\frac{2.h}{c^2}).f^3}{\exp(\frac{h.f}{k.T}) - 1}$$ [2] is the spectral brightness of a black body (Planck's law)

T : black body temperature
f_n : normalised power radiation pattern of the detector
f_1,f_2 : bandwidth limit
A_r : effective area of horn

The power fluctuations are :

$$\Delta P = \frac{\partial P}{\partial T} * \Delta T \quad [3]$$

then

$$\frac{\partial P}{\partial T} = \frac{A_r}{2} \int_{f1}^{f2} \iint_{4\pi} f_n(\theta,\varphi) \frac{\partial B(\theta,\varphi, f, T)}{\partial T} d\Omega df \quad [4]$$

$$\frac{\partial}{\partial T}(B(\theta,\varphi, f, T)) = (\frac{2.h^2.f^4}{k.c^2.T^2}).\frac{\exp(\frac{h.f}{k.T})}{\left(\exp(\frac{h.f}{k.T}) - 1\right)^2} \quad [5]$$

$$\Delta P = \frac{A_r}{2} \Delta T \iint_{4\pi} f_n(\theta,\varphi) (\int_{f_1}^{f_2} \frac{\partial B(\theta,\varphi, f, T)}{\partial T} df).d\Omega \quad [6]$$

Let consider :

$$I(T(\theta,\varphi)) = \int_{f_1}^{f_2} \frac{\partial B(\theta,\varphi, f, T)}{\partial T} df \quad [7]$$

The fluctuating surface considered as a black body is seen by the horn inside a solid angle Ω_S , then $I(\theta,\varphi) = 0$ outside Ω_S :

$$\Delta P = \Delta T.\frac{A_r}{2}\iint_{4\pi} f_n(\theta,\varphi).I(T(\theta,\varphi)).d\Omega = \Delta T.\frac{A_r}{2}.I.\iint_{\Omega_S} f_n(\theta,\varphi).d\Omega \qquad [8]$$

The effective area is defined by :

$$A_r = \frac{\lambda^2}{\iint_{4\pi} f_n(\theta,\varphi).d\Omega} \qquad [9]$$

Then

$$\Delta P = \frac{\Delta T}{2}.\lambda^2.I.\frac{\iint_{\Omega_S} f_n(\theta,\varphi).d\Omega}{\iint_{4\pi} f_n(\theta,\varphi).d\Omega} \qquad [10]$$

The following IP quantity is the incident power computed with grasp8.

$$IP = \frac{\iint_{\Omega_S} f_n(\theta,\varphi).d\Omega}{\iint_{4\pi} f_n(\theta,\varphi).d\Omega} \qquad [11]$$

On final the power fluctuation is expressed as

$$\Delta P = \frac{\Delta T}{2} * \lambda^2 * I * IP \qquad [12]$$

The detector efficiency and the surface emissivity have to be taken into account ($\eta = 1$ for the LFI and $\eta = 0.3$ for the HFI)

$$\Delta P = \frac{\Delta T}{2} * \lambda^2 * I * IP * \eta * \varepsilon \qquad [13]$$

The integral I is numerically computed as follow :

$$I = \int_{f_1}^{f_2} \frac{\partial B(\theta,\varphi,f,T)}{\partial T} df = \sum_{i=1}^{N} \frac{\partial}{\partial T}(B(\theta,\varphi,f,T)).\Delta f \qquad [14] \text{ with } \begin{cases} \Delta f = \dfrac{f_2 - f_1}{N} \\ f_i = f_1 + i.\Delta f \end{cases}$$

Numerical computation of I.

$$I = \sum_{i=1}^{N} \frac{\partial}{\partial T}(B(\theta, \varphi, f, T)).\Delta f \qquad [15]$$

The former quantity is computed for all frequencies and for different average surface temperatures (fig 3-1).

Central frequency (GHz)	Lowest frequency (GHz)	Highest frequency (GHz)	Temperature (K)	I (ISU)
30	27	30	50	1.6646E-09
30	27	30	80	1.6647E-09
30	27	30	150	1.6647E-09
100	90	110	50	6.1608E-08
100	90	110	80	6.1638E-08
100	90	110	150	6.1652E-08
353	317.7	388.3	50	2.6857E-06
353	317.7	388.3	80	2.7016E-06
353	317.7	388.3	150	2.7090E-06
857	771.3	942.7	50	3.6656E-05
857	771.3	942.7	80	3.7948E-05
857	771.3	942.7	150	3.8559E-05

Figure 2.3-1 : Numerical integration results.

The numerical result is varying with the frequency but not with the average temperature. This is explained by looking at the Planck's law behavior and at its associated derivative. The derivative curves are quasi identical over the Planck average temperature range. (see fig 3-2 to 3-5)

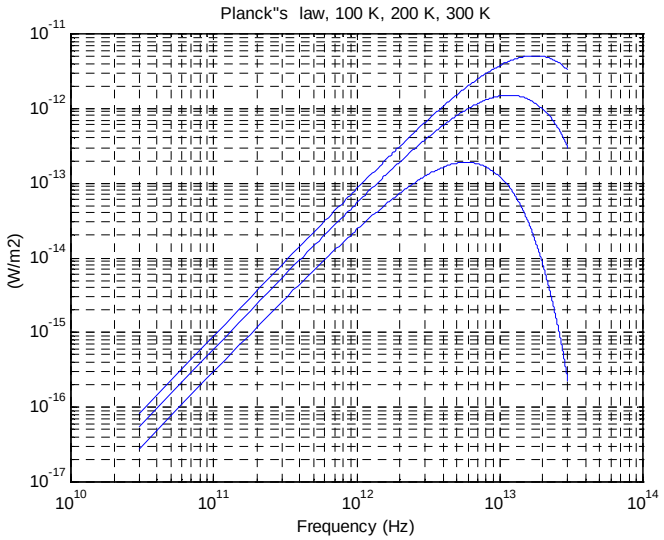

Figure 2.3-2 : Planck's law over a wide frequency domain.

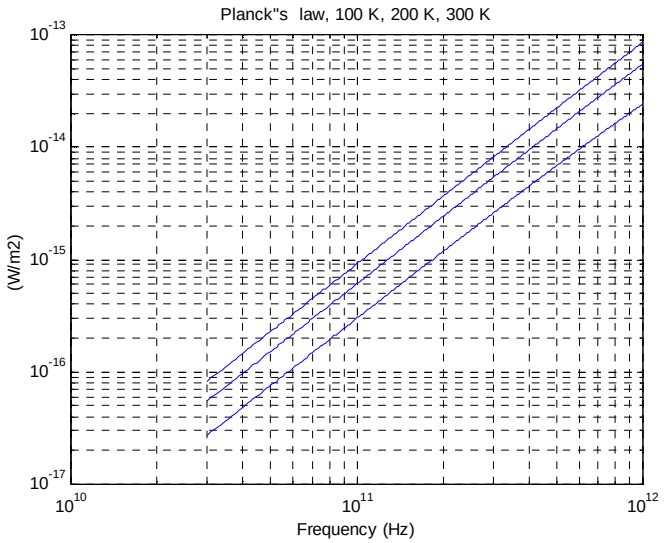

Figure 2.3-3 : Planck's law over the 30 –1000 GHz domain for 100, 200 and 300 K.

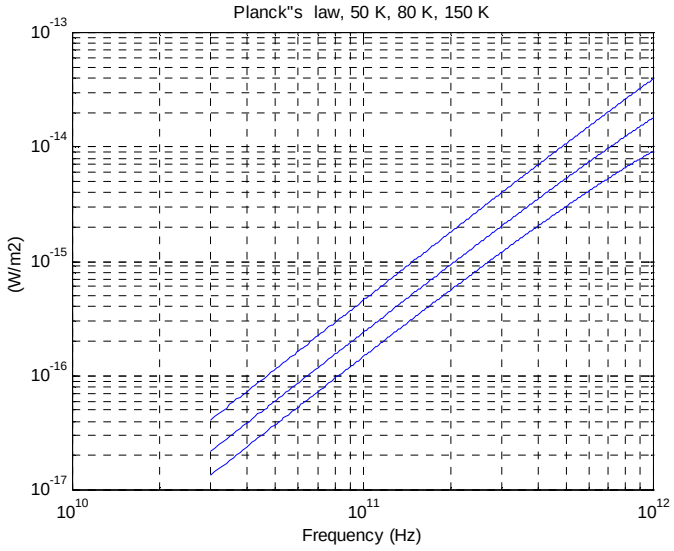

Figure 2.3-4 : Planck's law over the 30 –1000 GHz domain for 50, 80 and 150 K.

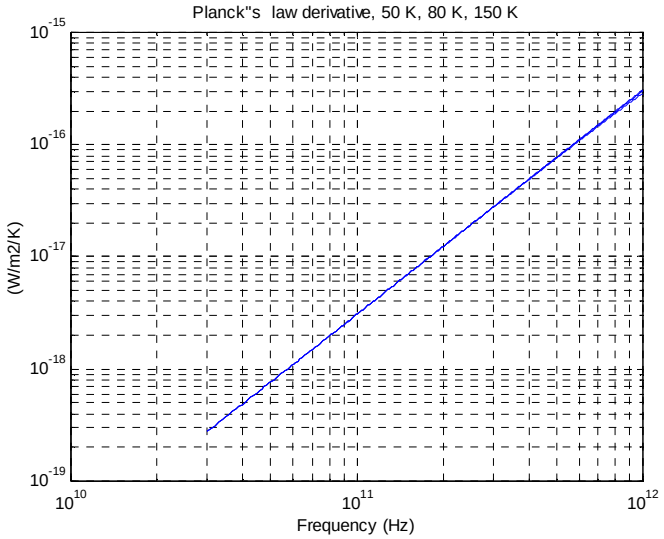

Figure 2.3-5 : Planck's law derivative over the 30 –1000 GHz domain for 50, 80 and 150 K

As a conclusion the power reaching a detector is expressed as :

$$\Delta P = \frac{\Delta T}{2} * \lambda^2 * I * IP * \eta * \varepsilon$$

where η is the detector efficiency ($\eta = 1$ for the LFI and $\eta = 0.3$ for the HFI)

IP is the incident power of RF coupling factor from the thermal source to the detector.

ε is the surface emissivity of the thermal source

λ is the wavelength of the observation channel

ΔT is the physical thermal deviation of the thermal source.

I is the Numerical integration over the channel bandwidth of the thermal derivative of the Planck's law.

Central frequency (GHz)	I (ISU)
30	1.6646E-09
100	6.1652E-08
353	2.7090E-06
857	3.8559E-05

2.4 Sensitivity analysis method of the temperature fluctuation.

The former section has shown how to convert a temperature fluctuation into power fluctuation. Now it is necessary to perform the conversion for each surface of the spacecraft and to sum up all contribution.

The sensitivity analysis is performed so as to determine what are the most critical surface element wrt the performance. The first phase is then to compute the maximum theoretical fluctuation allowed for each surface considered alone.

The second phase is to weight all the obtain temperature so as to obtain a total power performance equal to the requirement

2.4.1 first phase : method to compute the maximum theoretical fluctuation temperature for each surface element.

The total power reaching a detector is the linear sum of all the elementary power of each surface of the spacecraft.

$$\Delta P_{total} = \sum_{i=1}^{n\_surface} \Delta P_{surface(i)} \quad [1]$$

$$\Delta P_{total} = \sum_{i=1}^{n\_surface} \frac{\Delta T_{surface(i)}}{2} * \lambda^2 * I * IP_{surface(i)} * \eta * \varepsilon_{surface(i)} \quad [2]$$

n_surface : number of fluctuating surfaces considered on the spacecraft.

Under this assumption the power allocation for each surface is the following :

$$\Delta P_{surface(i)} = \alpha_i * \Delta P_{total} \quad [3]$$

$$\text{with} \quad \sum_{i=1}^{n\_surface} \alpha_i = 1$$

The temperature allocation consists in computing the temperature of each considered surface alone. This means that the considered surface will induce a power at detector level equal to the requirement.
The procedure is then :

$$\Delta P_{total} = \frac{ASD_{requirement}}{\sqrt{t_{obs}}} \quad [4] \qquad \text{with} \qquad t_{obs} = 3600 \cdot \frac{FWHM[arc\,\min]}{2.5\,arc\,\min} \quad [5]$$

Then

$$\Delta T_{surface\_alone} = 2 * \Delta P_{total} / (\lambda^2 * I * IP_{surface} * \eta * \varepsilon_{surface}) \quad [6]$$

Then in order to take into account the other surfaces, this temperature has to be weighted.

2.4.2 second phase : method to weight the maximum theoretical fluctuation temperature for each surface element.

The sum of each individual surface contribution has to generate an amount of power at detector level lower than the requirement. Hence the weighted temperature fluctuation of each surface is

$$\Delta T_{surface} = \alpha_i * \Delta T_{surface\_alone} \quad [7]$$

$$\text{with} \quad \sum_{i=1}^{n\_surface} \alpha_i = 1$$

Rem the weighting coefficient are the same as the one used in former section:

2.5 RF coupling factor evaluation

2.5.1 Overall amount of relative power evaluation.

The TICRA RF expertise study (reference document [RD 1]) is producing the incident power or RF coupling factor from the structural element to the detector. The computed values are detailed in table 2-1. Those RF coupling factor have not been recomputed for the new baffle configuration as far as the values are already very low and provide significant margin. Anyhow those value are an update wrt the PDR configuration.

The values presented in these tables correspond to the relative incident power exchanged between the detector and the corresponding element. The computation have been performed at 30 and 100 GHz only. At 857 GHz there's numerically no RF power exchanged between the detector and any of the spacecraft elements. This is due to the location in the center of the Focal plane unit of the 857 GHz and to its gaussian radiation pattern. Hence there's no self spacecraft emission at 857 GHz.

As a worst case the 353 GHz incident power numerical value are considered to be the ones at 100 GHz.

The following table shows a significant difference between the relative power exchanged with a structural element inside or outside the baffle cavity.

Structural element	Method used in analysis	Total relative power. Field from the 30 GHz LFI27 feed.	Total relative power. Field from the HFI_100_1 feed at 100 GHz
Baffle A	1	0.000168	0.000457
Baffle B	1	0.000310	0.000536
Baffle C	1	0.000249	0.000220
Baffle D	1	0.000081	0.000111
Baffle E	1	0.000183	0.000164
Baffle F	1	0.000674	0.000404
Baffle G	1	0.000417	0.000304
Baffle H	1	0.000085	0.000178
FPU	1	0.000047	0.000124
Hexagon side 2	1	0.000002	7.4E-7
Groove 3	1 and 2	1.09E-7 (Method 1)	1.95E-8 (Method 1)
Solar array	2	5.5E-13	1.1E-14
SVM shield	2	4E-13	3.5E-15
Side A of the SVM box	2	8.6E-15	2.4E-18

table 2-2.5-1 : output of the TICRA RF expertise.

2.5.2 Relative power evaluation passing through the MLI.

The SVM is covered by a MLI for thermal purposes. This MLI is composed of 15 layers made of Aluminium with a thickness of 800 angströms (0.08^{e}-6 m). From the RF point of view these successive layers of thin metallic sheet have a frequency dependent behavior wrt the frequency range. The MLI has a transmission coefficient decreasing with the frequency.

This sub section introduces the detailed computation of the relative power passing through the MLI and going to the structural top of the SVM. In that case the emissivity of the structural element is 0.95.

The fist step consists in computing the equivalent number of skin depth (thickness) at each frequency.

Frequency (GHz)	30	100	353	857
skin depth (m)	4.770E-07	2.610E-07	1.390E-07	8.900E-08
MLI thickness	8.00E-08	8.00E-08	8.00E-08	8.00E-08
Number of layer	15	15	15	15
total thickness (m)	1.20E-06	1.20E-06	1.20E-06	1.20E-06
Equivalent number of thickness	2.52	4.60	8.63	13.48

The second step consists in computing the RF power attenuation knowing that for 1 skin depth the attenuation is 10*log(e) =10 / ln(10) =4.3 dB.

Power attenuation for 1 skin depth (dB)	4.3	4.3	4.3	4.3
Total power attenuation (dB)	10.82	19.77	37.12	57.98

On final each relative power is computed through the MLI.
Rem : The relative power at 353 GHz is assumed to be the same as the one at 100 GHz (conservative approach).

	30 GHz	100 GHz	353 GHz
Solar Array			
Solar array top of MLI	5.50E-13	1.10E-14	1.10E-14
Solar array structural face (below the MLI)	4.56E-14	1.16E-16	2.13E-18
SVM shield			
SVM shield top of MLI	4.00E-13	3.50E-15	3.50E-15
SVM shield structural face (below the MLI)	3.31E-14	3.69E-17	6.79E-19
SVM walls			
Side A of SVM box top of MLI	8.60E-15	2.40E-18	2.40E-18
Side A of SVM structural face (below the MLI)	7.12E-16	2.53E-20	4.66E-22

2.6 sensitivity analysis of the maximum allowed temperature fluctuation for each stuctural element.

This section presents for each surface element of the spacecraft the numerical result for the temperature allocation.
This correspond to the numerical implementation of :

$$\Delta T_{surface\_alone} = 2 * \Delta P_{total} / (\lambda^2 * I * IP_{surface} * \eta * \varepsilon_{surface}) \quad [1]$$

$$\Delta P_{total} = \frac{ASD_{requirement}}{\sqrt{t_{obs}}} \quad [2]$$

For each surface the relative power or incident power ($IP_{surface}$) is used.

The relative power computation is available at 30 GHz and 100 GHz. For the higher frequencies (353 and 857 GHz) the same value as the one available at 100 GHz is used. This choice corresponds to a worst case for the following reasons.

1) The high frequency (353 GHz) detectors are closer to the focal point hence providing a greater apodization at the edge of the secondary reflector.
2) For the structural element outside the baffle cavity the edge of the baffle has a diffraction behaviour providing a better rejection.

The emissivity parameter for each surface is also used (0.02 for reflector, 0.05 for MLI, 0.95 for carbon structure etc …)
The computation is performed for each channel (5 wavelengths).

As a summary the temperature allocation is performed in two phases :

-the first phase consists in computing the maximum allowed temperature fluctuation for each indidual surface element inducing a self spacecraft emission level equal to the requirement. This first phase is a sensitivity analysis allowing to see the contribution of each element.

-the second phase consists in taking into account all the surface element contribution. A weighting is performed so as to obtain a summation of all power contibution from each surface equal to the requirement. The corresponding power is computed for each surface element and linearly summed up.

2.6.1 primary reflector

The primary reflector is split in different sub-parts.

The computation is performed using the grasp8 numerical model. The aim is to find the incident power exchanged with the detector and the different reflector parts. In figure 2.6-1 (left view) a hole has been numerically performed so as to keep only the rays going to the outer part of the primary reflector. In figure 2.6-1 (left view), a dummy squared reflector is used so as to block the rays and to keep only the rays going to the upper part of the baffle.

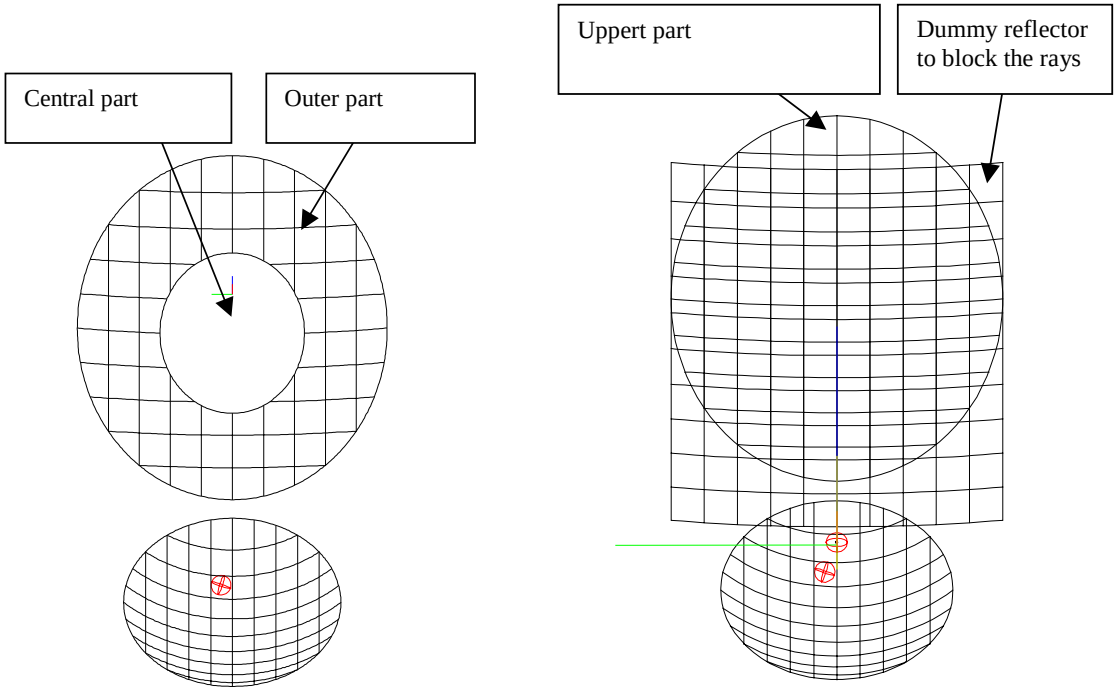

Figure 2.6-2.6-1 : primary reflector elements.

2.6.1.1 primary reflector upper part

The following table presents the numerical application of the relation [1] (sect 2.6). The numerical result is contained in the last column (delta_T). This computation corresponds to the most stringent requirement at the spin frequency (1/60 Hz).

PR Upper part

	ASD Spec (W/Hz^0.5)	ASD / t_obs^0.5 (W)	I (SI)	Lambda (m)	I*lambda^2/2 (W/Hz)	Incident power	Eta	Epsilon	delta_T (K)
30	3.40E-18	1.64E-20	1.66E-09	0.01000	8.32E-14	0.000614	1	0.02	1.60E-02
100 (LFI)	1.10E-17	9.17E-20	6.16E-08	0.00300	2.77E-13	0.000614	1	0.02	2.70E-02
100 (HFI)	2.10E-18	1.75E-20	6.16E-08	0.00300	2.77E-13	0.000614	0.3	0.02	1.71E-02
353	1.80E-18	2.12E-20	2.70E-06	0.00085	9.76E-13	0.000614	0.3	0.02	5.90E-03
857	2.20E-17	2.59E-19	3.79E-05	0.00035	2.33E-12	0.000614	0.3	0.02	3.03E-02

Worst Case
5.90E-03

Assumptions : Primary reflector emmissivity 0.02.
Incident power constant for all frequencies, computed at 30 GHz only. The incident power at higher frequency is assumed to be lower due to a better location of the detector in the focal plane. Hence the relative power value computed at 30 GHz is the highest one and leads to a conservative temperature. For instance the actual relative power at 353 GHz is smaller than the one used (here 0.000614) which is the value computed at 30 GHz.

The temperature allocation (right column) on this part is driven by the requirement of the HFI channel at 353 GHz.

Results wil be discussed in section 2.6.9.

2.6.1.2 primary reflector circular central part

The following table presents the numerical application of the relation [1]. The numerical result is contained in the last column (delta_T). This computation corresponds to the most stringent requirement at the spin frequency (1/60 Hz).

PR circular central part

	ASD Spec (W/Hz^0.5)	ASD / t_obs^0.5 (W)	I (SI)	Lambda (m)	I*lambda^2/2 (W/Hz)	Incident power	Eta	Epsilon	delta_T (K)
30	3.40E-18	1.64E-20	1.66E-09	0.01000	8.32E-14	0.7362	1	0.02	1.33E-05
100 (LFI)	1.10E-17	9.17E-20	6.16E-08	0.00300	2.77E-13	0.7362	1	0.02	2.25E-05
100 (HFI)	2.10E-18	1.75E-20	6.16E-08	0.00300	2.77E-13	0.7362	0.3	0.02	1.43E-05
353	1.80E-18	2.12E-20	2.70E-06	0.00085	9.76E-13	0.7362	0.3	0.02	4.92E-06
857	2.20E-17	2.59E-19	3.79E-05	0.00035	2.33E-12	0.7362	0.3	0.02	2.52E-05

Worst Case
4.92E-06

Assumptions : Primary reflector emmissivity 0.02.
Incident power constant for all frequencies, computed at 30 GHz only. The incident power at higher frequency is assumed to be lower due to a better location of the detector in the focal plane.

Hence the relative power value computed at 30 GHz is the highest one and leads to a conservative temperature for all the other channels.

The temperature allocation on this part is driven by the requirement of the HFI channel at 353 GHz.

Results wil be discussed in section 2.6.9.

2.6.1.3 primary reflector outer part.

The following table presents the numerical application of the relation [1]. The numerical result is contained in the last column (delta_T). This computation corresponds to the most stringent requirement at the spin frequency (1/60 Hz).

PR Circular outer part

	ASD Spec (W/Hz^0.5)	ASD / t_obs^0.5 (W)	I (SI)	Lambda (m)	I*lambda^2/2 (W/Hz)	Incident power	Eta	Epsilon	delta_T (K)
30	3.40E-18	1.64E-20	1.66E-09	0.01000	8.32E-14	0.258400	1	0.02	3.80E-05
100 (LFI)	1.10E-17	9.17E-20	6.16E-08	0.00300	2.77E-13	0.258400	1	0.02	6.41E-05
100 (HFI)	2.10E-18	1.75E-20	6.16E-08	0.00300	2.77E-13	0.258400	0.3	0.02	4.07E-05
353	1.80E-18	2.12E-20	2.70E-06	0.00085	9.76E-13	0.258400	0.3	0.02	1.40E-05
857	2.20E-17	2.59E-19	3.79E-05	0.00035	2.33E-12	0.258400	0.3	0.02	7.19E-05
								Worst Case	
								1.40E-05	

Assumptions : Primary reflector emmissivity 0.02.
Incident power constant for all frequencies, computed at 30 GHz only. The incident power at higher frequency is assumed to be lower due to a better location of the detector in the focal plane. Hence the relative power value computed at 30 GHz is the highest one and leads to a conservative temperature for all the other channels.

The temperature allocation on this part is driven by the requirement of the HFI channel at 353 GHz.

Results wil be discussed in section 2.6.9.

2.6.2 secondary reflector

The following table presents the numerical application of the relation [1]. The numerical result is contained in the last column (delta_T). This computation corresponds to the most stringent requirement at the spin frequency (1/60 Hz).

SR

	ASD Spec (W/Hz^0.5)	ASD / t_obs^0.5 (W)	I (SI)	Lambda (m)	I*lambda^2/2 (W/Hz)	Incident power	Eta	Epsilon	delta_T (K)
30	3.40E-18	1.64E-20	1.66E-09	0.01000	8.32E-14	1	1	0.02	9.83E-06
100 (LFI)	1.10E-17	9.17E-20	6.16E-08	0.00300	2.77E-13	1	1	0.02	1.66E-05
100 (HFI)	2.10E-18	1.75E-20	6.16E-08	0.00300	2.77E-13	1	0.3	0.02	1.05E-05
353	1.80E-18	2.12E-20	2.70E-06	0.00085	9.76E-13	1	0.3	0.02	3.62E-06
857	2.20E-17	2.59E-19	3.79E-05	0.00035	2.33E-12	1	0.3	0.02	1.86E-05
									Worst Case
									3.62E-06

Assumptions : Secondary reflector emissivity 0.02.
Incident power rounded to 1 for all frequencies (instead of 0.997 at 30 GHz for instance).

The temperature allocation on this part is driven by the requirement of the HFI channel at 353 GHz.

Results wil be discussed in section 2.6.9.

2.6.3 Top of the SVM

The following table presents the numerical application of the relation [1]. The numerical result is contained in the last column (delta_T). This computation corresponds to the most stringent requirement at the spin frequency (1/60 Hz).

MLI OF THE SVM UPPER PANEL (+X face)

	ASD Spec (W/Hz^0.5)	ASD / t_obs^0.5 (W)	I (SI)	Lambda (m)	I*lambda^2/2 (W/Hz)	Incident power	Eta	Epsilon	delta_T (K)
30	3.40E-18	1.64E-20	1.66E-09	0.01000	8.32E-14	4.00E-13	1	0.05	9.83E+06
100 (LFI)	1.10E-17	9.17E-20	6.16E-08	0.00300	2.77E-13	3.50E-15	1	0.05	1.89E+09
100 (HFI)	2.10E-18	1.75E-20	6.16E-08	0.00300	2.77E-13	3.50E-15	0.3	0.05	1.20E+09
353	1.80E-18	2.12E-20	2.70E-06	0.00085	9.76E-13	3.50E-15	0.3	0.05	4.14E+08
857	2.20E-17	2.59E-19	3.79E-05	0.00035	2.33E-12	3.50E-15	0.3	0.05	2.12E+09
									Worst Case
									9.83E+06

The RF power is passing through the MLI and reaches the structural face (emmissivity of 0.95). Results are presented in the following table. The computation of the attenuated relative power is presented in section 2.5.2.

SVM UPPER PANEL (below the MLI)

	ASD Spec (W/Hz^0.5)	ASD / t_obs^0.5 (W)	I (SI)	Lambda (m)	I*lambda^2/2 (W/Hz)	Incident power past the MLI	Eta	Epsilon	delta_T (K)
30	3.40E-18	1.64E-20	1.66E-09	0.01000	8.32E-14	3.31E-14	1	0.95	6.24E+06
100 (LFI)	1.10E-17	9.17E-20	6.16E-08	0.00300	2.77E-13	3.69E-17	1	0.95	9.45E+09
100 (HFI)	2.10E-18	1.75E-20	6.16E-08	0.00300	2.77E-13	3.69E-17	0.3	0.95	6.00E+09
353	1.80E-18	2.12E-20	2.70E-06	0.00085	9.76E-13	6.79E-19	0.3	0.95	1.12E+11
857	2.20E-17	2.59E-19	3.79E-05	0.00035	2.33E-12	6.79E-19	0.3	0.95	5.76E+11
									Worst Case
									6.24E+06

Results wil be discussed in section 2.6.9.

2.6.4 Third groove

The following table presents the numerical application of the relation [1]. The numerical result is contained in the last column (delta_T). This computation corresponds to the most stringent requirement at the spin frequency (1/60 Hz).

Groove 3 (outside the optical cavity)

	ASD Spec (W/Hz^0.5)	ASD / t_obs^0.5 (W)	I (SI)	Lambda (m)	I*lambda^2/2 (W/Hz)	Incident power	Eta	Epsilon	delta_T (K)
30	3.40E-18	1.64E-20	1.66E-09	0.01000	8.32E-14	1.09E-07	1	0.9	2.00E+00
100 (LFI)	1.10E-17	9.17E-20	6.16E-08	0.00300	2.77E-13	1.95E-08	1	0.9	1.89E+01
100 (HFI)	2.10E-18	1.75E-20	6.16E-08	0.00300	2.77E-13	1.95E-08	0.3	0.9	1.20E+01
353	1.80E-18	2.12E-20	2.70E-06	0.00085	9.76E-13	1.95E-08	0.3	0.9	4.13E+00
857	2.20E-17	2.59E-19	3.79E-05	0.00035	2.33E-12	1.95E-08	0.3	0.9	2.12E+01
									Worst Case
									2.00E+00

Assumptions : third groove emmissivity 0.9 (open honeycomb)

Results wil be discussed in section 2.6.9.

2.6.5 SVM walls

The SVM walls are either covered of MLI or black painted. For the walls covered by the MLI the RF power goes to the external face of the MLI (emissivity of 0.05) and some of this energy is passing through the MLI and goes to the structural panel (emissivity of 0.95). For the black painted walls, the emmissivity is of 0.78.

2.6.5.1 SVM walls covered by the MLI

The following table presents the numerical application of the relation [1]. The numerical result is contained in the last column (delta_T). This computation corresponds to the most stringent requirement at the spin frequency (1/60 Hz).

MLI of the SVM lateral panel (side of SVM box)

	ASD Spec (W/Hz^0.5)	ASD / t_obs^0.5 (W)	I (SI)	Lambda (m)	I*lambda^2/2 (W/Hz)	Incident power	Eta	Epsilon	delta_T (K)
30	3.40E-18	1.64E-20	1.66E-09	0.01000	8.32E-14	8.60E-15	1	0.05	4.57E+08
100 (LFI)	1.10E-17	9.17E-20	6.16E-08	0.00300	2.77E-13	2.40E-18	1	0.05	2.76E+12
100 (HFI)	2.10E-18	1.75E-20	6.16E-08	0.00300	2.77E-13	2.40E-18	0.3	0.05	1.75E+12
353	1.80E-18	2.12E-20	2.70E-06	0.00085	9.76E-13	2.40E-18	0.3	0.05	6.04E+11
857	2.20E-17	2.59E-19	3.79E-05	0.00035	2.33E-12	2.40E-18	0.3	0.05	3.10E+12
									Worst Case
									4.57E+08

The RF power is passing through the MLI and reaches the structural face (emmissivity of 0.95), results are presented in the following table.

SVM lateral panel (below the MLI)

	ASD Spec (W/Hz^0.5)	ASD / t_obs^0.5 (W)	I (SI)	Lambda (m)	I*lambda^2/2 (W/Hz)	Incident power	Eta	Epsilon	delta_T (K)
30	3.40E-18	1.64E-20	1.66E-09	0.01000	8.32E-14	7.12E-16	1	0.95	2.90E+08
100 (LFI)	1.10E-17	9.17E-20	6.16E-08	0.00300	2.77E-13	2.53E-20	1	0.95	1.38E+13
100 (HFI)	2.10E-18	1.75E-20	6.16E-08	0.00300	2.77E-13	2.53E-20	0.3	0.95	8.75E+12
353	1.80E-18	2.12E-20	2.70E-06	0.00085	9.76E-13	4.66E-22	0.3	0.95	1.64E+14
857	2.20E-17	2.59E-19	3.79E-05	0.00035	2.33E-12	4.66E-22	0.3	0.95	8.40E+14
									Worst Case
									2.90E+08

Results wil be discussed in section 2.6.9.

2.6.5.2 black painted SVM walls

The following table presents the numerical application of the relation [1]. The numerical result is contained in the last column (delta_T). This computation corresponds to the most stringent requirement at the spin frequency (1/60 Hz).

SVM lateral black painted panel

	ASD Spec (W/Hz^0.5)	ASD / t_obs^0.5 (W)	l (SI)	Lambda (m)	l*lambda^2/2 (W/Hz)	Incident power	Eta	Epsilon	delta_T (K)
30	3.40E-18	1.64E-20	1.66E-09	0.01000	8.32E-14	8.60E-15	1	0.78	2.93E+07
100 (LFI)	1.10E-17	9.17E-20	6.16E-08	0.00300	2.77E-13	2.40E-18	1	0.78	1.77E+11
100 (HFI)	2.10E-18	1.75E-20	6.16E-08	0.00300	2.77E-13	2.40E-18	0.3	0.78	1.12E+11
353	1.80E-18	2.12E-20	2.70E-06	0.00085	9.76E-13	2.40E-18	0.3	0.78	3.87E+10
857	2.20E-17	2.59E-19	3.79E-05	0.00035	2.33E-12	2.40E-18	0.3	0.78	1.99E+11
									Worst Case
									2.93E+07

Results wil be discussed in section 2.6.9.

2.6.6 solar array (toward the PLM).

The following table presents the numerical application of the relation [1]. The numerical result is contained in the last column (delta_T). This computation corresponds to the most stringent requirement at the spin frequency (1/60 Hz).

Solar array +X face of the MLI

	ASD Spec (W/Hz^0.5)	ASD / t_obs^0.5 (W)	I (SI)	Lambda (m)	I*lambda^2/2 (W/Hz)	Incident power	Eta	Epsilon	delta_T (K)
30	3.40E-18	1.64E-20	1.66E-09	0.01000	8.32E-14	5.50E-13	1	0.05	7.15E+06
100 (LFI)	1.10E-17	9.17E-20	6.16E-08	0.00300	2.77E-13	1.10E-14	1	0.05	6.02E+08
100 (HFI)	2.10E-18	1.75E-20	6.16E-08	0.00300	2.77E-13	1.10E-14	0.3	0.05	3.83E+08
353	1.80E-18	2.12E-20	2.70E-06	0.00085	9.76E-13	1.10E-14	0.3	0.05	1.32E+08
857	2.20E-17	2.59E-19	3.79E-05	0.00035	2.33E-12	1.10E-14	0.3	0.05	6.76E+08
									Worst Case
									7.15E+06

The RF power is passing through the MLI and reaches the structural face (emmissivity of 0.95). Results are presented in the following table.

Solar array +X face (below the MLI)

	ASD Spec (W/Hz^0.5)	ASD / t_obs^0.5 (W)	I (SI)	Lambda (m)	I*lambda^2/2 (W/Hz)	Incident power	Eta	Epsilon	delta_T (K)
30	3.40E-18	1.64E-20	1.66E-09	0.01000	8.32E-14	4.56E-14	1	0.95	4.54E+06
100 (LFI)	1.10E-17	9.17E-20	6.16E-08	0.00300	2.77E-13	1.16E-16	1	0.95	3.01E+09
100 (HFI)	2.10E-18	1.75E-20	6.16E-08	0.00300	2.77E-13	1.16E-16	0.3	0.95	1.91E+09
353	1.80E-18	2.12E-20	2.70E-06	0.00085	9.76E-13	2.13E-18	0.3	0.95	3.58E+10
857	2.20E-17	2.59E-19	3.79E-05	0.00035	2.33E-12	2.13E-18	0.3	0.95	1.83E+11
									Worst Case
									4.54E+06

Results wil be discussed in section 2.6.9.

2.6.7 optical cavity (inside of the baffle)

The optical cavity is composed of the baffle and the baffle floor. The baffle floor is the groove 3 part inside the baffle.

2.6.7.1 Baffle

The following table presents the numerical application of the relation [1]. The numerical result is contained in the last column (delta_T). This computation corresponds to the most stringent requirement at the spin frequency (1/60 Hz).

Baffle

	ASD Spec (W/Hz^0.5)	ASD / t_obs^0.5 (W)	I (SI)	Lambda (m)	I*lambda^2/2 (W/Hz)	Incident power	Eta	Epsilon	delta_T (K)
30	3.40E-18	1.64E-20	1.66E-09	0.01000	8.32E-14	0.002167	1	0.05	1.81E-03
100 (LFI)	1.10E-17	9.17E-20	6.16E-08	0.00300	2.77E-13	0.002374	1	0.05	2.79E-03
100 (HFI)	2.10E-18	1.75E-20	6.16E-08	0.00300	2.77E-13	0.002374	0.3	0.05	1.77E-03
353	1.80E-18	2.12E-20	2.70E-06	0.00085	9.76E-13	0.002374	0.3	0.05	6.11E-04
857	2.20E-17	2.59E-19	3.79E-05	0.00035	2.33E-12	0.002374	0.3	0.05	3.13E-03
									Worst Case
									6.11E-04

Results wil be discussed in section 2.6.9.

2.6.7.2 baffle floor or groove 3 part inside the baffle.

The following table presents the numerical application of the relation [1]. The numerical result is contained in the last column (delta_T). This computation corresponds to the most stringent requirement at the spin frequency (1/60 Hz).

Groove 3 (baffle floor inside the optical cavity)

	ASD Spec (W/Hz^0.5)	ASD / t_obs^0.5 (W)	I (SI)	Lambda (m)	I*lambda^2/2 (W/Hz)	Incident power	Eta	Epsilon	delta_T (K)
30	3.40E-18	1.64E-20	1.66E-09	0.01000	8.32E-14	1.35E-04	0.05	0.9	3.24E-02
100 (LFI)	1.10E-17	9.17E-20	6.16E-08	0.00300	2.77E-13	2.28E-04	0.05	0.9	3.23E-02
100 (HFI)	2.10E-18	1.75E-20	6.16E-08	0.00300	2.77E-13	2.28E-04	0.05	0.9	6.15E-03
353	1.80E-18	2.12E-20	2.70E-06	0.00085	9.76E-13	2.28E-04	0.05	0.9	2.12E-03
857	2.20E-17	2.59E-19	3.79E-05	0.00035	2.33E-12	2.28E-04	0.05	0.9	1.09E-02
									Worst Case
									2.12E-03

Results wil be discussed in section 2.6.9.

2.6.8 part of the telescope hexagonal frame inside the optical cavity.

Hexagon side 2

	ASD Spec (W/Hz^0.5)	ASD / t_obs^0.5 (W)	I (SI)	Lambda (m)	I*lambda^2/2 (W/Hz)	Incident power	Eta	Epsilon	delta_T (K)
30	3.40E-18	1.64E-20	1.66E-09	0.01000	8.32E-14	0.000002	1	0.1	9.83E-01
100 (LFI)	1.10E-17	9.17E-20	6.16E-08	0.00300	2.77E-13	7.40E-07	1	0.1	4.48E+00
100 (HFI)	2.10E-18	1.75E-20	6.16E-08	0.00300	2.77E-13	7.40E-07	0.3	0.1	2.84E+00
353	1.80E-18	2.12E-20	2.70E-06	0.00085	9.76E-13	7.40E-07	0.3	0.1	9.79E-01
857	2.20E-17	2.59E-19	3.79E-05	0.00035	2.33E-12	7.40E-07	0.3	0.1	5.02E+00
									Worst Case
									9.79E-01

Results wil be discussed in section 2.6.9.

2.6.9 Sensitivity analysis results.

Each worst case performance obtained in the section 2.6.1 to 2.6.8 are synthesized in the following table.

The synthesis is displayed in two sets of data. The performance data for the structural element inside the baffle or optical cavity and the performance data for the structural element outside the optical cavity.

This sensistivity analysis allows to check the relative impact on the performance from each structural element. The results synthesized in the following table does not represent a physical thermal law but the maximum thermal performance theoritically allowed for each surface considered alone. This value corresponds to an upper fluctuation limit. If the limit is reached then the power reaching the detector would be equal to the requirement.

The sensitivity analysis shows that the structural elements outside the optical cavity have a neglegible impact compared to the structural element inside the optical cavity. This is due to the very low level of relative power reaching the element outside the optical cavity.

	delta_T (K)
PR circular central part	4.92^{E}-06
PR Upper part	5.90^{E}-03
PR Circular outer part	1.40^{E}-05
SR	3.62^{E}-06
Baffle	6.11^{E}-04
Hexagon side 2	9.79^{E}-01
Groove 3 (baffle floor inside the optical cavity)	2.12^{E}-03

Table 2.6-1 : performance synthesis for the element inside the optical cavity

	delta_T (K)
Groove 3 (outside the optical cavity)	2.00E+00
Solar array +X face of the MLI	7.15E+06
Solar array +X face (below the MLI)	4.54E+06
MLI OF THE SVM UPPER PANEL (+X face)	9.83E+06
SVM UPPER PANEL (below the MLI)	6.24E+06
MLI of the SVM lateral panel (side of SVM box)	4.57E+08
SVM lateral panel (below the MLI)	2.90E+08
SVM lateral black painted panel	2.93E+07

Table 2.6-2 : performance synthesis for the element outside the optical cavity

2.7 Self spacecraft emission evaluation

2.7.1 Methodology to check the compliance with the specifications.

To check compliance with the specifications, which are given in terms of ASD [W/Hz$^{1/2}$], the following must be compared:

$$\Delta P_{\det ector} < \frac{ASD}{\sqrt{t_{obs}}} \qquad \Delta P = \frac{\Delta T}{2} * \lambda^2 * I * IP * \eta * \varepsilon$$

where:

$$t_{obs} = 3600 \cdot \frac{FWHM[arc\min]}{2.5 arc\min}$$

ΔT is obtained by computing the ASD of the temporal thermal law over 7200 s.

Then $\Delta T = \frac{ASD(T(t))}{\sqrt{t_{obs}}}$

Hence the following value has to be compared to the requirements.

$$ASD(Power) = \frac{1}{2} * \lambda^2 * I * IP * \eta * \varepsilon * ASD(T(t))$$

2.7.2 Self spacecraft emission for Planck .

For each structural element of the SVM a time domain thermal law has been computed and Fourier transformed for the PDR. The reference documents RD1 and RD2 contain the PDR analysis. Since this analysis, new temporal thermal laws (issued from SVM thermal control system CDR) have been fourier transformed and compared to the PDR fourier analysis. The PDR value have been kept as worst case.

For the PLM elements, the direct component at 1/60 Hz has been used.

The following table displays the comparison of the computed thermal deviation obtained at 1/60 Hz. The ASD thermal performance expressed in K/Hz ^ 1/2 is divided by the observation defined for each channel. Then the corresponding ΔT at 1/60Hz is displayed for each channel.

	ASD requirement at 1/60 Hz (K/Hz^1/2)	ASD performance at 1/60 Hz (K/Hz^1/2)	DT at 1/60 Hz 30 GHz (µK)	DT at 1/60 Hz 100 GHz (µK)	DT at 1/60 Hz 100 GHz HFI (µK)	DT at 1/60 Hz 353 GHz (µK)	DT at 1/60 Hz 857 GHz (µK)
PR circular central part			0.2	0.2	0.2	0.2	0.2
PR Upper part			1.3	1.3	1.3	1.3	1.3
PR Circular outer part			1.1	1.1	1.1	1.1	1.1
SR		6.00E-07	2.89E-03	5.00E-03	5.00E-03	7.07E-03	7.07E-03
Baffle			30	30	30	30	30
Groove 3 (baffle floor inside the optical cavity)			30	30	30	30	30
MLI OF THE SVM UPPER PANEL (+X face)	0.01	3.68E-04	1.77E+00	3.07E+00	3.07E+00	4.34E+00	4.34E+00
SVM UPPER PANEL (below the MLI)	0.01	3.68E-04	1.77E+00	3.07E+00	3.07E+00	4.34E+00	4.34E+00
Groove 3 (outside the optical cavity)		1.10E-04	5.29E-01	9.17E-01	9.17E-01	1.30E+00	1.30E+00
SVM lateral black painted panel	0.01	1.28E-01	6.16E+02	1.07E+03	1.07E+03	1.51E+03	1.51E+03
MLI of the SVM lateral panel (side of SVM box)	0.01	4.62E-06	2.22E-02	3.85E-02	3.85E-02	5.44E-02	5.44E-02
Solar array +X face of the MLI	0.01	7.97E-06	3.83E-02	6.64E-02	6.64E-02	9.39E-02	9.39E-02
Solar array +X face (below the MLI)	0.01	7.97E-06	3.83E-02	6.64E-02	6.64E-02	9.39E-02	9.39E-02

Table 2-2.7-1 : spacecraft temperature results from thermal analysis (see RD1 and RD2)

The following tables display the ASD computed using the data coming from the thermal analysis. Only the surface element inside the optical cavity are taken into account. This choice is justified because the impact of the element oustide the optical cavity is many order of magnitude lower than the one inside the optical cavity.

A system contingency is defined as 20% of the requirement This system contingency is then summed up in order to obtain the total performance.

Performance at 30 GHz

F (GHz)	λ (mm)	Eta	I (SI)	T obs (s)
30	1.00E+01	1	1.66E-09	43200

		ΔT performance at 1/60 Hz (K.Hz^-0.5)	Emissivity of the surface	IP	ASD Performance (W/Hz^0.5)
PR circular central part		2.00E-01	0.02	2.58E-01	1.79E-20
PR Upper part		1.30E+00	0.02	6.14E-04	2.76E-22
PR Circular outer part		1.10E+00	0.02	2.58E-01	9.83E-20
SR		2.89E-03	0.02	1.00E+00	9.99E-22
Baffle		3.00E+01	0.05	2.17E-03	5.62E-20
Groove 3 (baffle floor inside the optical cavity)		3.00E+01	0.05	2.00E-06	5.19E-23
System contingency					6.80E-19
Total ASD (W/Hz^0.5)					8.54E-19
ASD Spec (W/Hz^0.5)					3.40E-18

table 2.7-2 : 30 GHz channel ASD performance display (worst case component at 1/60 Hz).

Performance at 100 GHz (HFI)	F (GHz)	λ (mm)	Eta	I (SI)	T obs (s)
	100	3.00E+00	0.3	6.16E-08	14400

		ΔT performance at 1/60 Hz (μK)	Emissivity of the surface	IP	ASD Performance (W/Hz^0.5)
PR circular central part		2.00E-01	0.02	0.2584	1.03E-20
PR Upper part		1.30E+00	0.02	0.000614	1.59E-22
PR Circular outer part		1.10E+00	0.02	0.2584	5.67E-20
SR		5.00E-03	0.02	1	9.98E-22
Baffle		3.00E+01	0.05	0.002374	3.55E-20
Groove 3 (baffle floor inside the optical cavity)		3.00E+01	0.05	0.00000074	1.11E-23
System contingency					4.20E-19
Total ASD (W/Hz^0.5)					4.20E-19
ASD Spec (W/Hz^0.5)					2.10E-18

table 2.7-3 : 100 GHz HFI channel ASD performance display (worst case component at 1/60 Hz).

Performance at 353 GHz (HFI)	F (GHz)	λ (mm)	Eta	I (SI)	T obs (s)
	353	8.50E-01	0.3	2.70E-06	7200

		ΔT performance at 1/60 Hz (μK)	Emissivity of the surface	IP	ASD Performance (W/Hz^0.5)
PR circular central part		2.00E-01	0.02	0.2584	2.57E-20
PR Upper part		1.30E+00	0.02	0.000614	3.96E-22
PR Circular outer part		1.10E+00	0.02	0.2584	1.41E-19
SR		7.07E-03	0.02	1	3.51E-21
Baffle		3.00E+01	0.05	0.002374	8.84E-20
Groove 3 (baffle floor inside the optical cavity)		3.00E+01	0.05	0.00000074	2.76E-23
System contingency					3.60E-19
Total ASD (W/Hz^0.5)					4.48E-19
ASD Spec (W/Hz^0.5)					1.80E-18

table 2.7-4 : 353 GHz channel ASD performance display (worst case component at 1/60 Hz).

As far as there's no RF power exchanged between the detector and the spacecraft surfaces there's no self spacecraft emission level at 857 GHz from a numerical point of view.

As a conclusion the self spacecraft emission level is well below the requirements.

3. SELF SPACECRAFT EMISSION LEVEL CONCLUSIONS.

The section 2.7.2 shows two main results. The first one is that the self spacecraft emission level is driven by the PLM elements contained inside the baffle cavity. The second result is that compared to initial issue of this document (PDR data package in June 2002) the relative power going to the baffle has been re-evaluated thanks to refined computation by TICRA.

4. ANALYSIS OF THE RESULTS OF THE 4 PI COMPUTATIONS WITHOUT THE BAFFLE EXTENSION-FIRST RF EXPERTISE.

This section reviews the 4 PI computation results obtained by TICRA in the frame of the first RF expertise (kicked off in november 2001). These results have been obtained for the baffle without extension, they are not part of the CDR current budget. These results are mentionned for information so as to see the impact of the baffle extension by comparing the results with the CDR ones provided in section 5.

For each frequency, the 4PI diagram is displayed in the same graphical representation, as the ones in the TICRA reports.

Then the sub area where the Moon is located (half cone angle of 32° along the spacecraft spin axis) is extracted. The maximum directivity within this area is labelled the Edge of Cone (EOC) directivity. This directivity is then compared to the maximum on axis gain in order to obtain the achieved rejection. The objectives are to compare these rejections to the required rejections (req SPER 060).

The same process is applied for the cone containing the Earth and Sun.

In addition the pattern area where a -65 dB rejection is not achieved is displayed in order to check the status wrt the Milky way nota.

The modeling have been performed using the following detector model definition.:

- 30 GHz LFI horn radiation pattern.
- 100 GHz horn radiation pattern coming from the PPLM A study.
- 353 GHz gaussian feed (-30 dB at 19.4°).
- 857 GHz gaussian feed (-30 dB at 19.4°).

On final a table summarizes the performances for the rejection toward Earth Sun and Moon.

4.1 30 GHz Pattern analysis

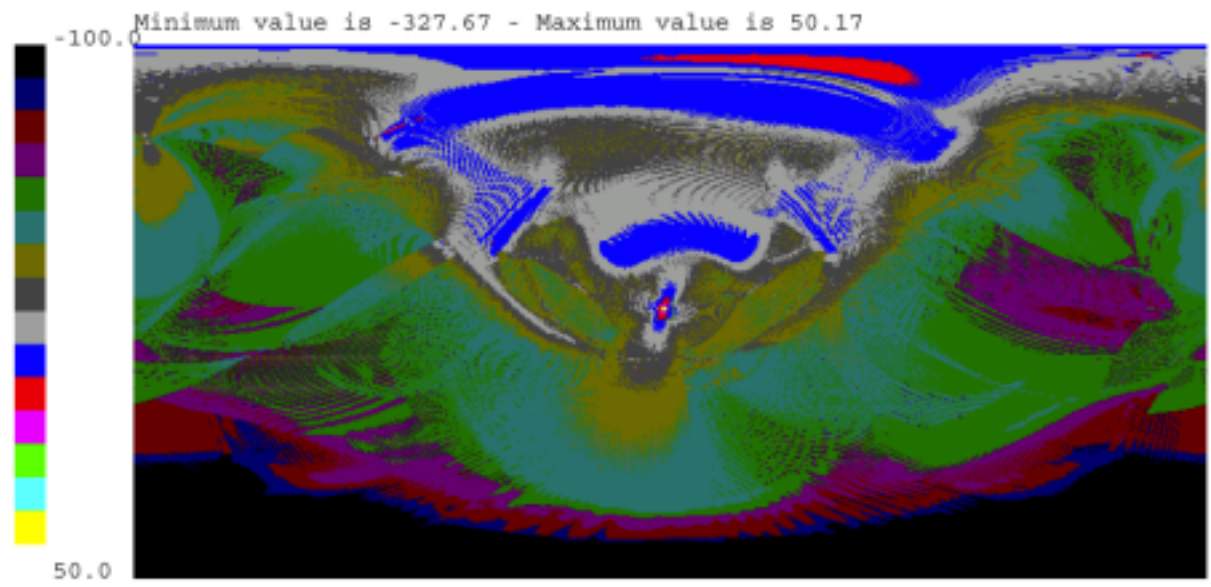

4PI diagram , phi : -180°, 180° / theta : 0,+180° / levels in directivity displayed from -100 dBi to +50 dBi

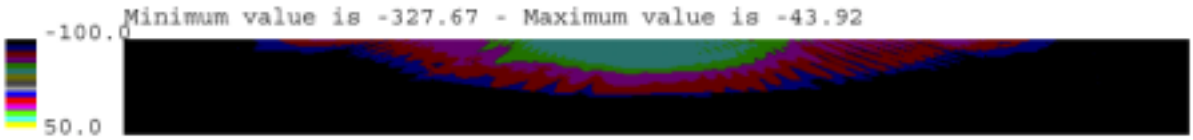

Moon area phi : -180°, 180° / theta : +148°,+180° / levels in directivity displayed from -100 dBi to +50 dBi

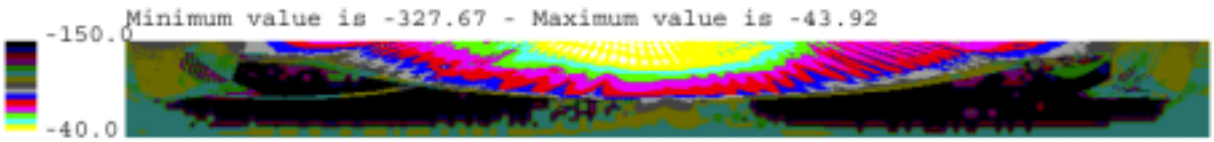

Moon area phi : -180°, 180° / theta : +148°,+180° / levels in directivity displayed from -150 dBi to -40dBi

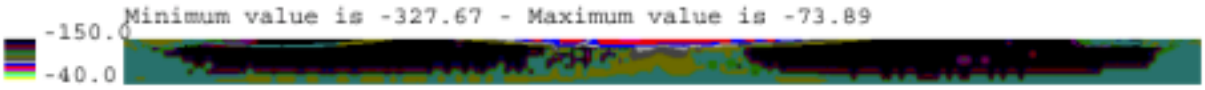

Earth area phi : -180°, 180° / theta : +165°,+180° / levels in directivity displayed from -150 dBi to -40dBi

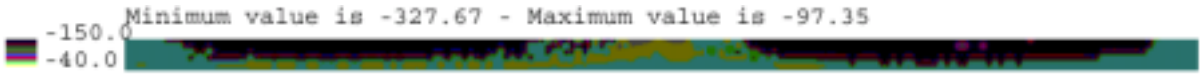

Sun area phi : -180°, 180° / theta : +170°,+180° / levels in directivity displayed from -150 dBi to -40dBi

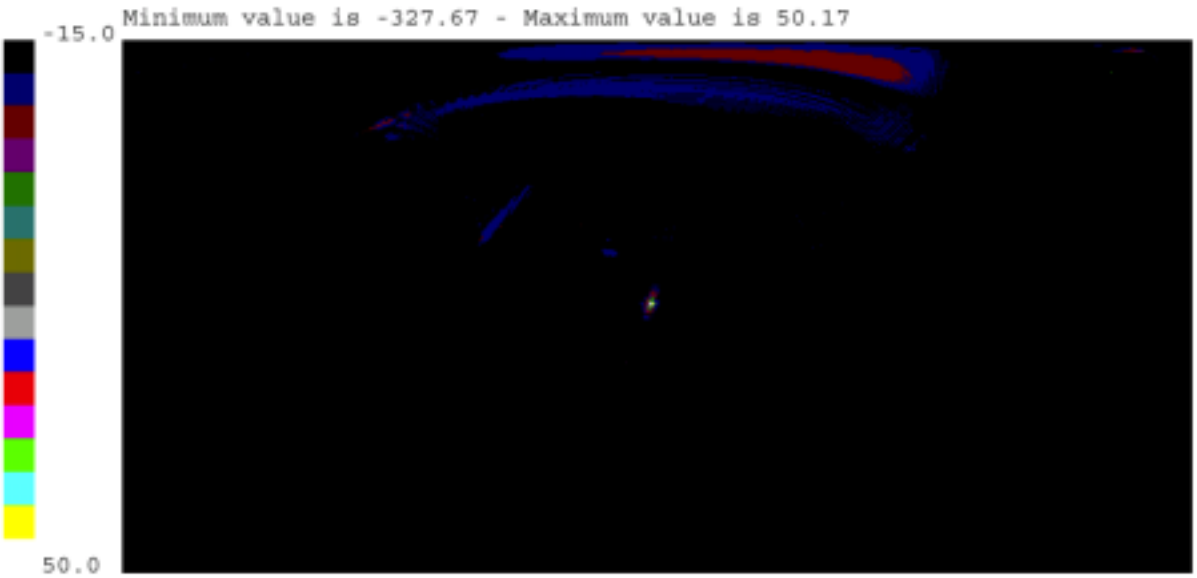

Area where the -65 dB rejection is not met (directivity level from 50-65=-15 dBi to max=50 dBi. This area corresponds to the angular direction where the spill over lobe past the primary is located and the area of the main lobe as well.

4.2 100 GHz Pattern analysis

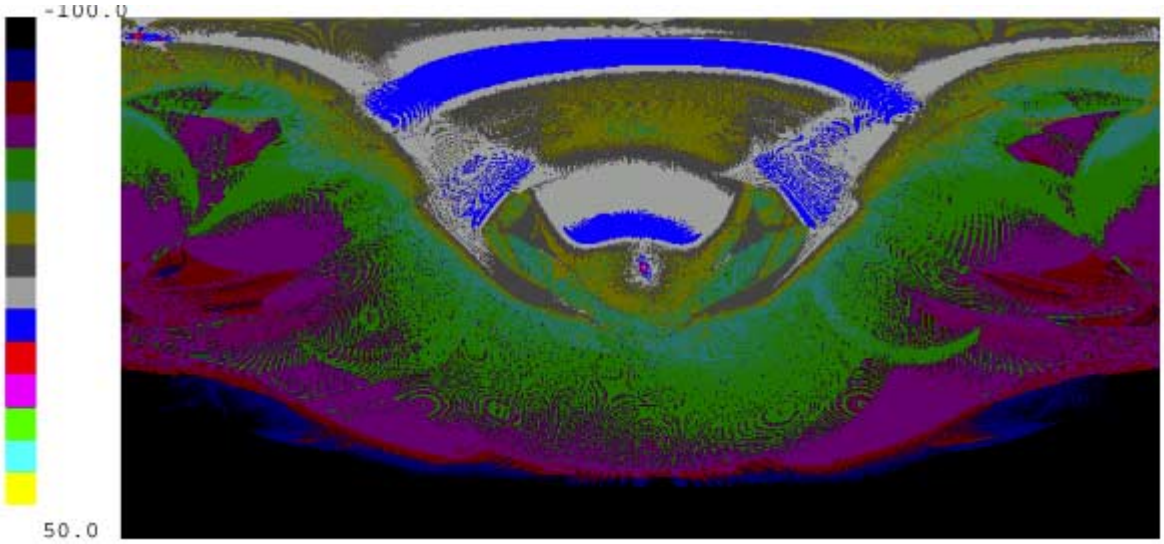

4PI diagram , phi : -180°, 180° / theta : 0,+180° / levels in directivity displayed from -100 dBi to +50 dBi

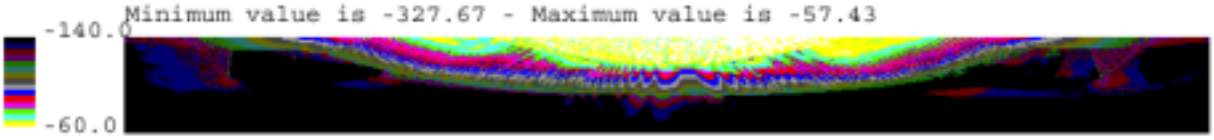

Moon area phi : -180°, 180° / theta : +148°,+180° / levels in directivity displayed from -140 dBi to -60 dBi

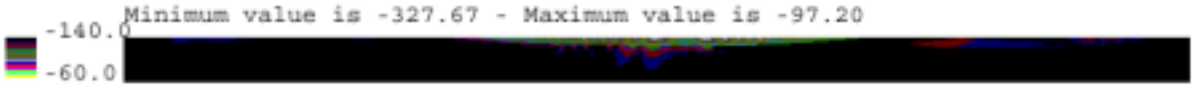

Earth area phi : -180°, 180° / theta : +165°,+180° / levels in directivity displayed from -150 dBi to -40dBi

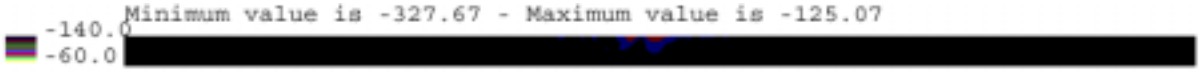

Sun area phi : -180°, 180° / theta : +170°,+180° / levels in directivity displayed from -150 dBi to -40dBi

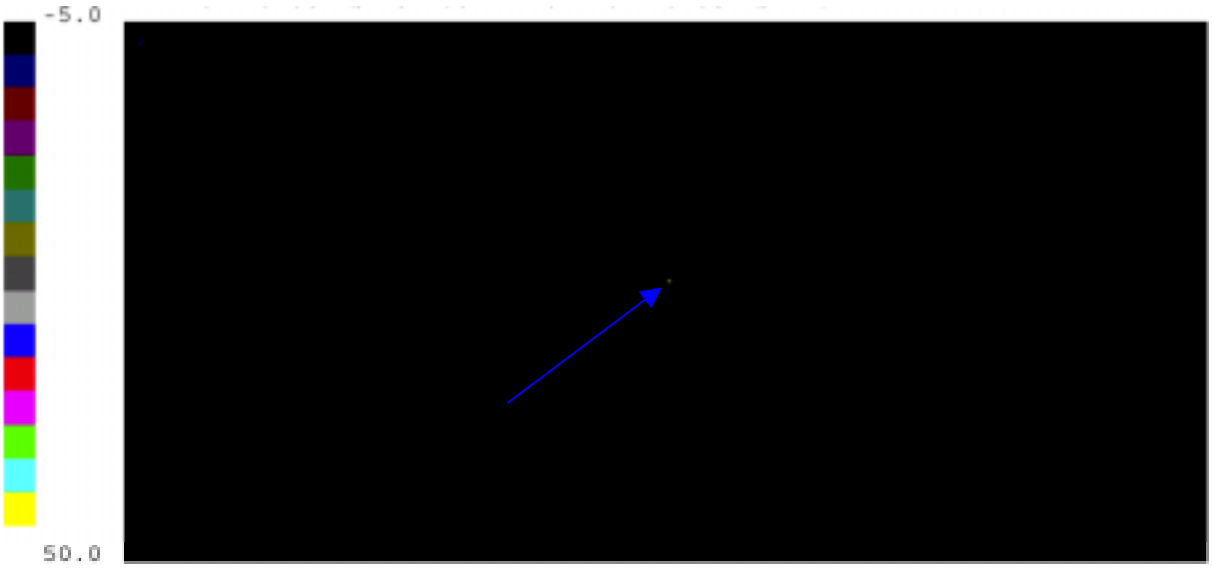

Area where the -65 dB rejection is not met (directivity level displayed from 60-65=-5 dBi to max=60 dBi).

Only the main lobe area is over the -65 dB rejection. The corresponding pixel is pointed out by the blue arrow.

4.3 353 GHz Pattern analysis

The pattern is only computed in 8 characteristic half_cut. The directivity at 148° is -90 dBi worst case. As far as the on-axis gain is of 69.2 dBi the rejection is then -159 dB in a worst case.

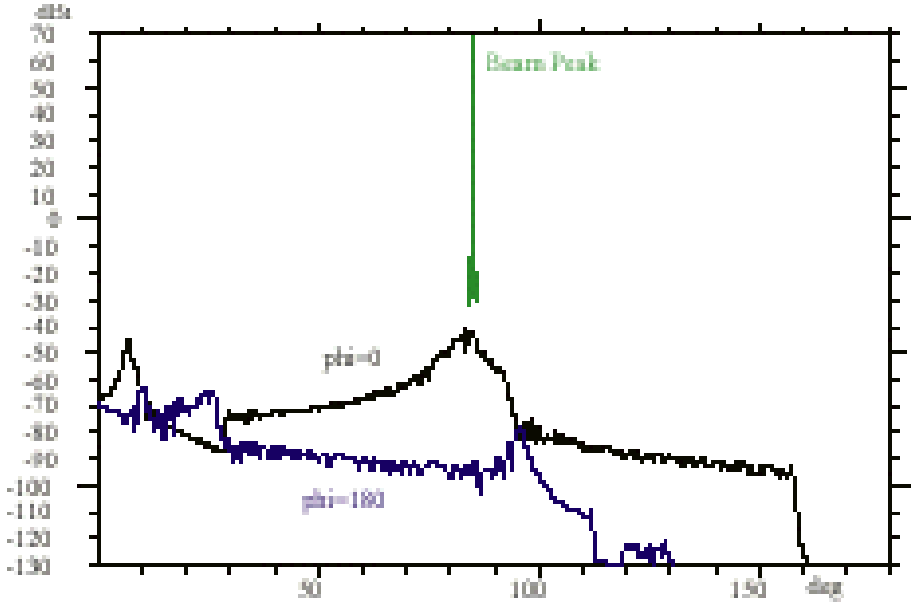

Figure 11-4 Total field for ϕ = 0.°, HFI_353_1.

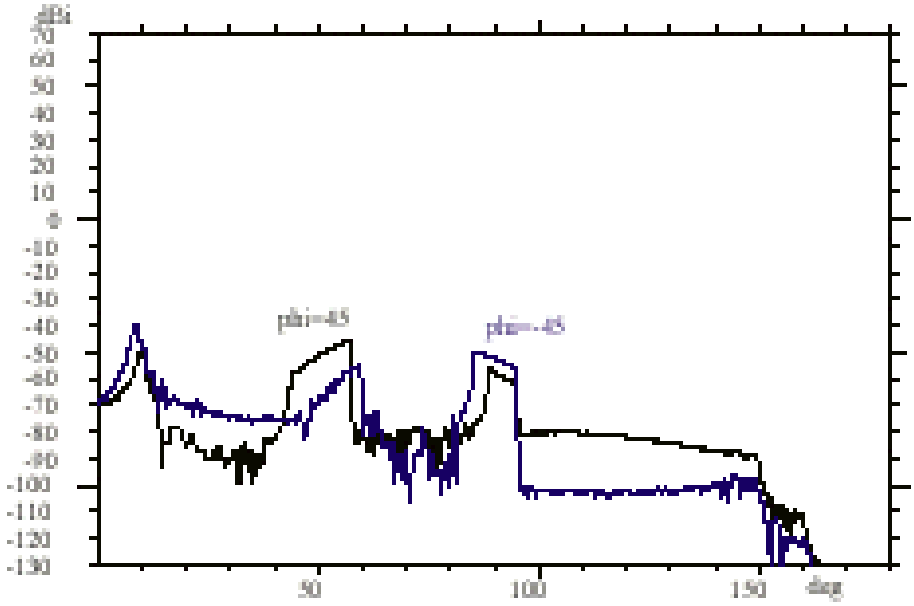

Figure 11-5 Total field for ϕ = ±45°, HFI_353_1.

4.4 857 GHz Pattern analysis

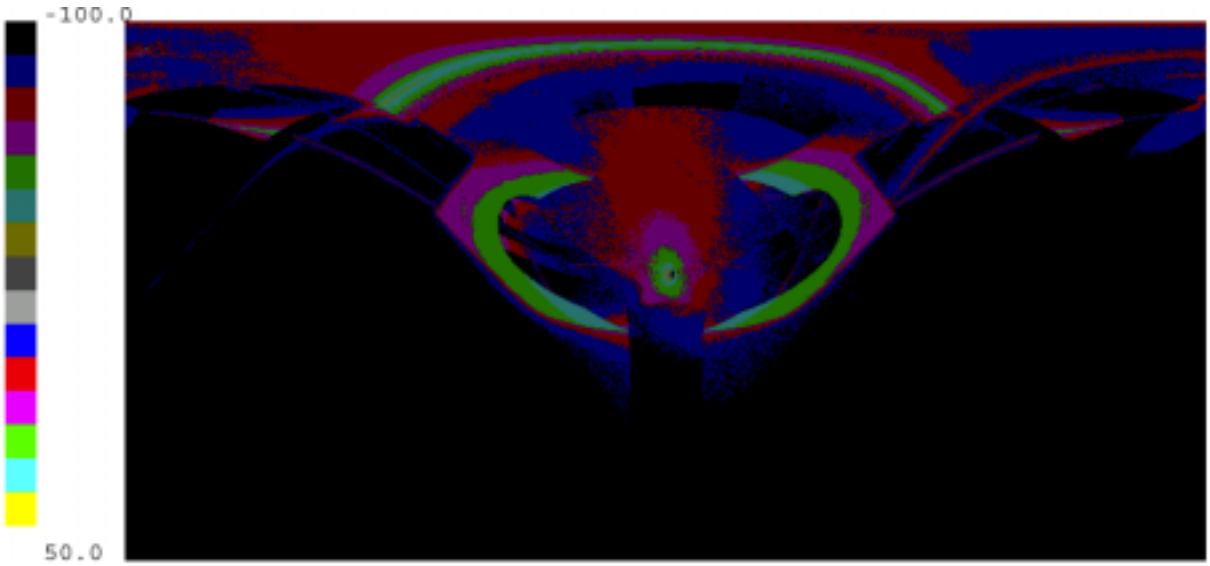

4PI diagram , phi : -180°, 180° / theta : 0,+180° / levels in directivity displayed from -100 dBi to +50 dBi

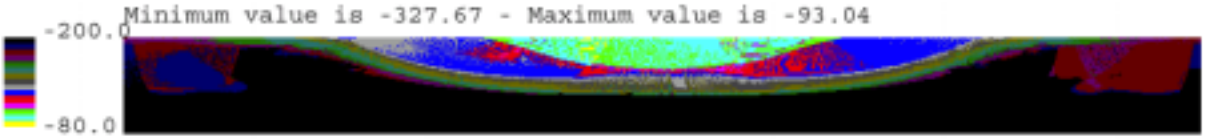

Moon area phi : -180°, 180° / theta : +148°,+180° / levels in directivity displayed from -140 dBi to -60 dBi

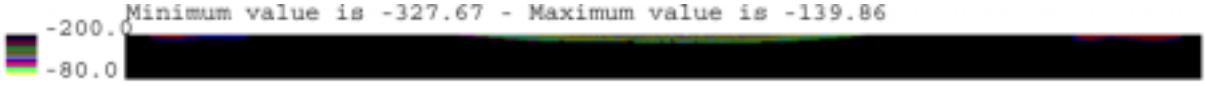

Earth area phi : -180°, 180° / theta : +165°,+180° / levels in directivity displayed from -200 dBi to -80dBi

Sun area phi : -180°, 180° / theta : +170°,+180° / levels in directivity displayed from -300 dBi -150dBi.

There's no angular direction with rejection greater than -65 dB. Except for the main lobe.

4.5 FAR OUT SIDE LOBE Performance synthesis

The requirements are defined as follows in [AD 1].

SPER-060 P	*The system rejection at the detectors for Sun, Earth, Moon at worst case locations shall be , at least :*
	30 GHz : *-91 dB , -78 dB and -71 dB respectively.*
	100 GHz (HFI) : *-91.5 dB (-99 dB), -78.5 dB (-86 dB) and -71.5 dB (-73 db) respectively*
	353 GHz : *-92 dB (-108 dB), -79 dB (-95 dB) and -72 dB (-81 dB) respectively.*
	857 GHz : *-98 dB (-122 dB), -85 dB (-109 dB) and -78 dB (-95 dB) respectively.*
Notes	1) The requirement for the Milky Way is of order –65 dB from peak but is driven by the telescope in free-standing configuration.
	2) The values between brackets shall be taken as goals .

The performance analysis is performed by using the worst case result in terms of directivity toward the Moon, the Earth and the Sun. This worst case directivity is the maximum directivity inside the angular area.

This directivity is compared to the maximum on axis directivity and the rejection is computed as :

Rejection (dB) = EOC_directivity (dBi) - On_axis_gain (dBi).

The margin wrt the requirements is defined as :

Margin (dB) = requirement (dB) - achieved_rejection (dB)

Rem : A positive margin value means of course that the requirement is achieved.

The following table displays the worst case performance synthesis. The results are output directly from the numerical model. Some value can be considered as not physical such as value greater than 200 dB. Anyway the raw data allow to see the nice behaviour of the numerical model. As expected, the highest the frequency is the lower the rejection is.

Conclusion : The result of the computation performed in the frame of the RF expertise (ideal reflector surfaces, no dust, sharp edges) show a significant margin towards the Earth Sun and Moon rejection. Both requirements and goals are achieved.

30 GHz

	Aspect angle (°)	Theta value (°)	EOC directivity (dBi)	On axis max gain (dBi)	Rejection (dB)	Rejection requirement (dB)	Rejection goal (dB)	Margin (dB)
Moon	32	148	-43	50	-93	-71	NA	**22**
Earth	15	165	-73	50	-123	-78	NA	**45**
Sun	10	170	-97	50	-147	-91	NA	**56**

100 GHz

	Aspect angle (°)	Theta value (°)	EOC directivity (dBi)	On axis max gain (dBi)	Rejection (dB)	Rejection requirement (dB)	Rejection goal (dB)	Margin (dB)
Moon	32	148	-57	61	-118	-71.5	-73	**46.5**
Earth	15	165	-97	61	-158	-78.5	-86	**79.5**
Sun	10	170	-125	61	-186	-91.5	-99	**94.5**

353 GHz

	Aspect angle (°)	Theta value (°)	EOC directivity (dBi)	On axis max gain (dBi)	Rejection (dB)	Rejection requirement (dB)	Rejection goal (dB)	Margin (dB)
Moon	32	148	-90 (WC)	69	-159	-72	-81	**87**
Earth	15	165	-90 (WC)	69	-159	-79	-95	**80**
Sun	10	170	-90 (WC)	69	-159	-92	-108	**67**

857 GHz

	Aspect angle (°)	Theta value (°)	EOC directivity (dBi)	On axis max gain (dBi)	Rejection (dB)	Rejection requirement (dB)	Rejection goal (dB)	Margin (dB)
Moon	32	148	-93	76	-169	-78	-95	**91**
Earth	15	165	-139	76	-215	-85	-109	**130**
Sun	10	170	-202	76	-278	-98	-122	**180**

Table 4.5-1 :performance synthesis.

5. ANALYSIS OF THE RESULTS OF THE 4 PI COMPUTATIONS WITH THE BAFFLE EXTENSION USING GAUSSIAN FEED (4PI-EXT BAF-GAUSS FEED)

This section introduces the update analysis of the TICRA results (released in november 2003). All TICRA computation results and analysis are provided in [RD 4]. Those results are the ones used for the CDR budget.

Then the sub area where the Moon is located (half cone angle of 32° along the spacecraft spin axis) is extracted. The maximum directivity within this area is labelled the Edge of Cone (EOC) directivity. This directivity is then compared to the maximum on axis gain in order to obtain the achieved rejection.

The same process is applied for the angular cone containing the Earth and Sun.

In addition the pattern area where a -65 dB rejection is not achived is displayed in order to check the status wrt the Milky way nota.

The RF numerical model (extended baffle etc etc …) is fully defined in the document " Update of the inputs for the RF numerical model" (RD 5).
The feed model are recalled hereafter (see RD 5) :

- 30 GHz gaussian feed model with 30 dB taper at 23.6° off axis.

100 GHz gaussian feed model with 30 dB taper at 26.8° off axis.
353 GHz gaussian feed model with 30 dB taper at 19.4°.
857 GHz gaussian feed model with 30 dB taper at 19.4°.

On final a table summarizes the performances for the rejection toward Earth Sun and Moon.

5.1 30 GHz Pattern analysis (4pi-ext baf-gauss feed)

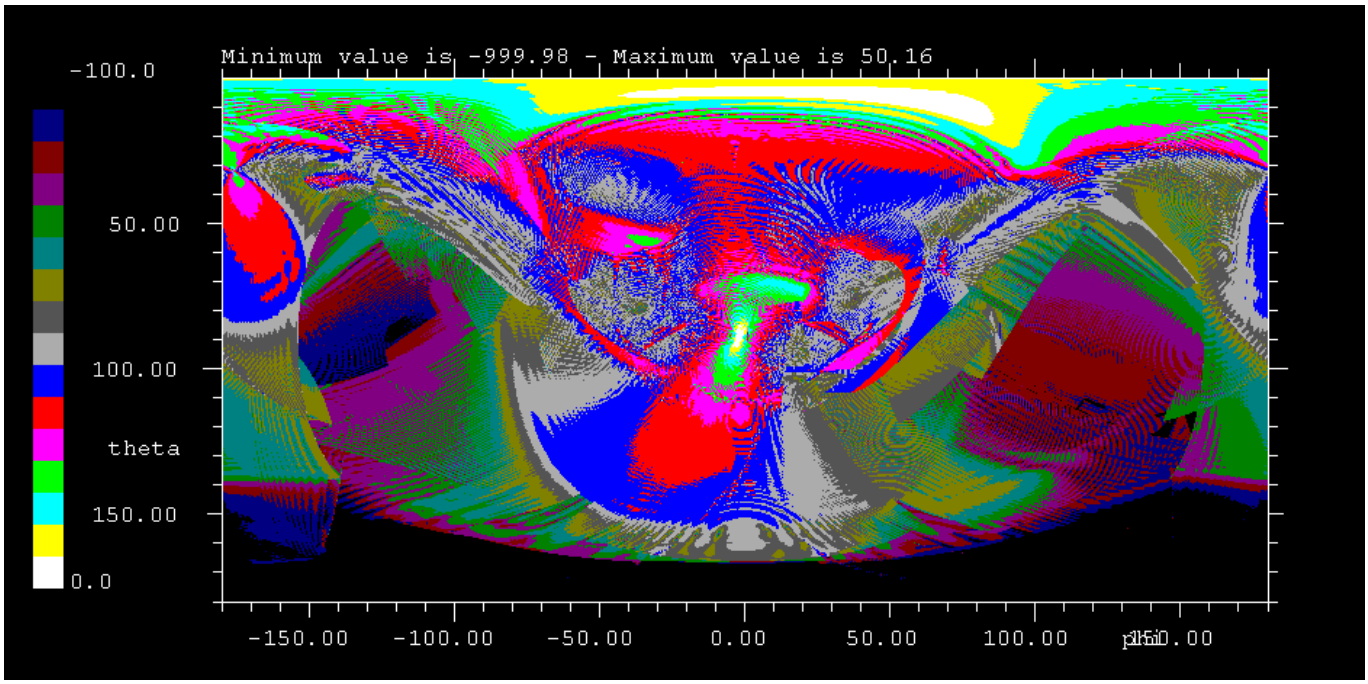

Figure 5.1-1 : 4PI diagram , phi : -180°, 180° / theta : 0,+180° / levels in directivity displayed from -100 dBi to 0 dBi

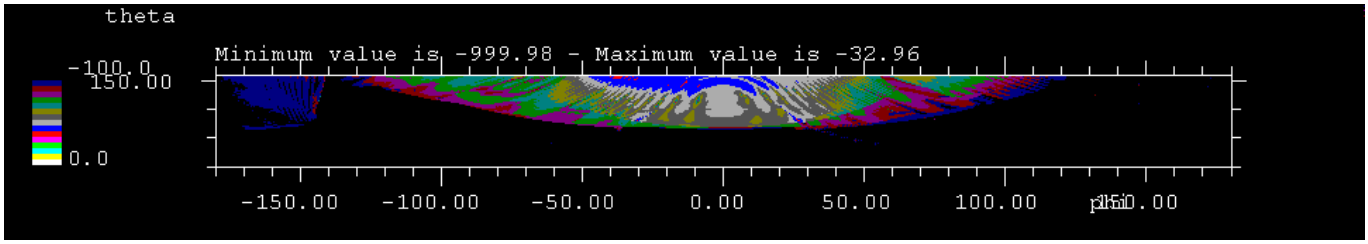

Figure 5.1-2 : Moon area phi : -180°, 180° / theta : +148°,+180° / levels in directivity displayed from -100 dBi to 0dBi

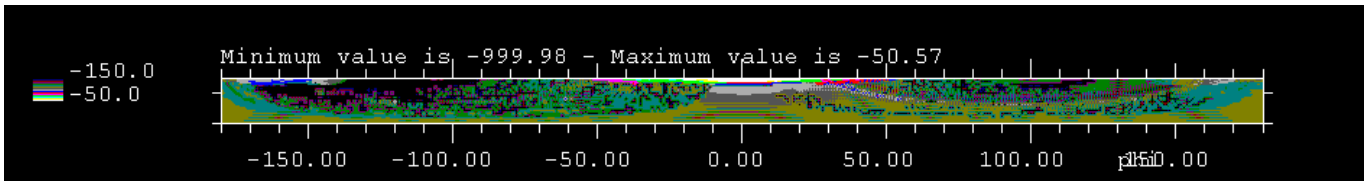

Figure 5.1-3 : Earth area phi : -180°, 180° / theta : +165°,+180° / levels in directivity displayed from -150 dBi to -50dBi

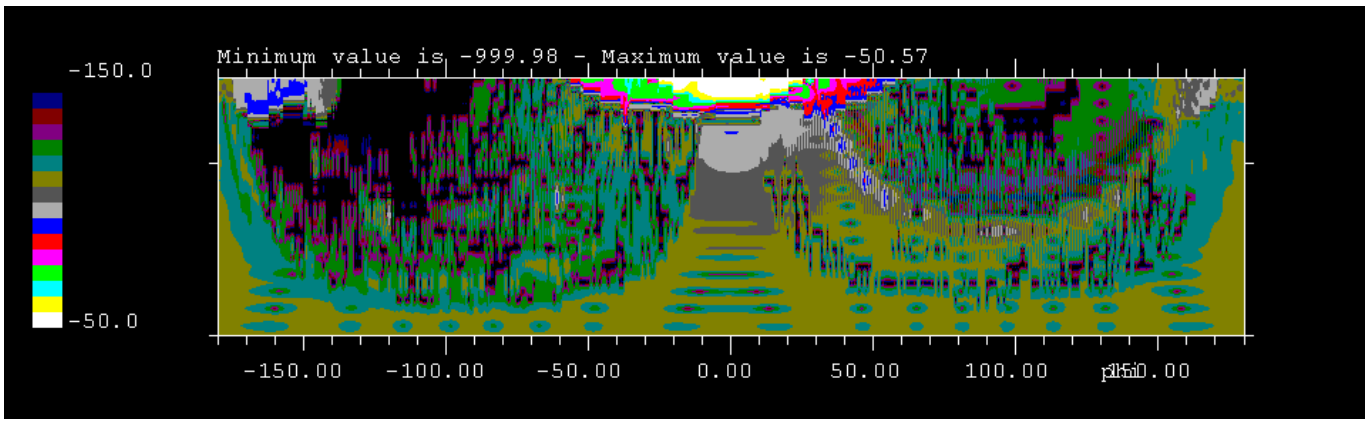

Figure 5.1-4 : Enlarged Earth area phi : -180°, 180° / theta : +165°,+180° / levels in directivity displayed from -150 dBi to -50dBi

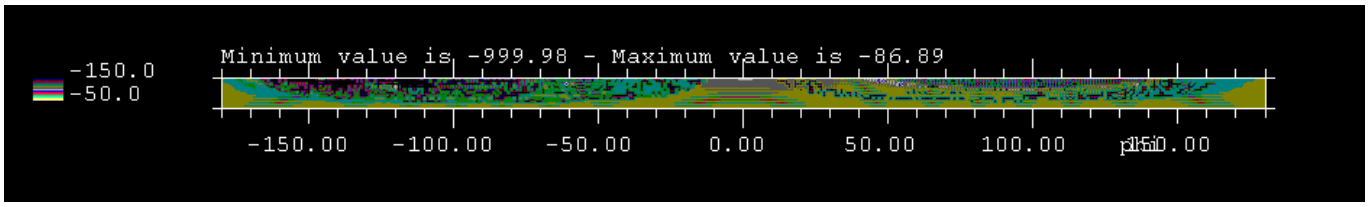

Figure 5.1-5 : Sun area phi : -180°, 180° / theta : +170°,+180° / levels in directivity displayed from -150 dBi to -50dBi

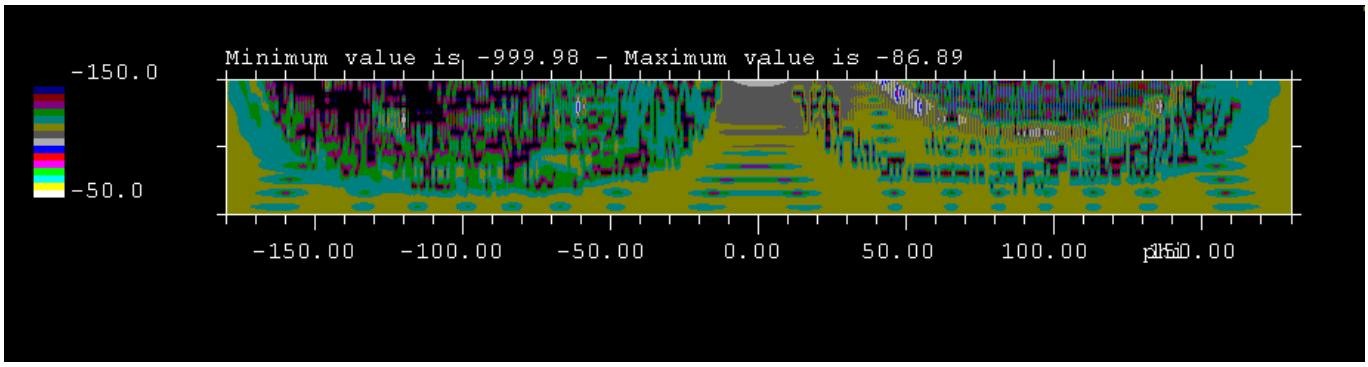

Figure 5.1-6 : Enlarged sun area phi : -180°, 180° / theta : +170°,+180° / levels in directivity displayed from -150 dBi to -40dBi

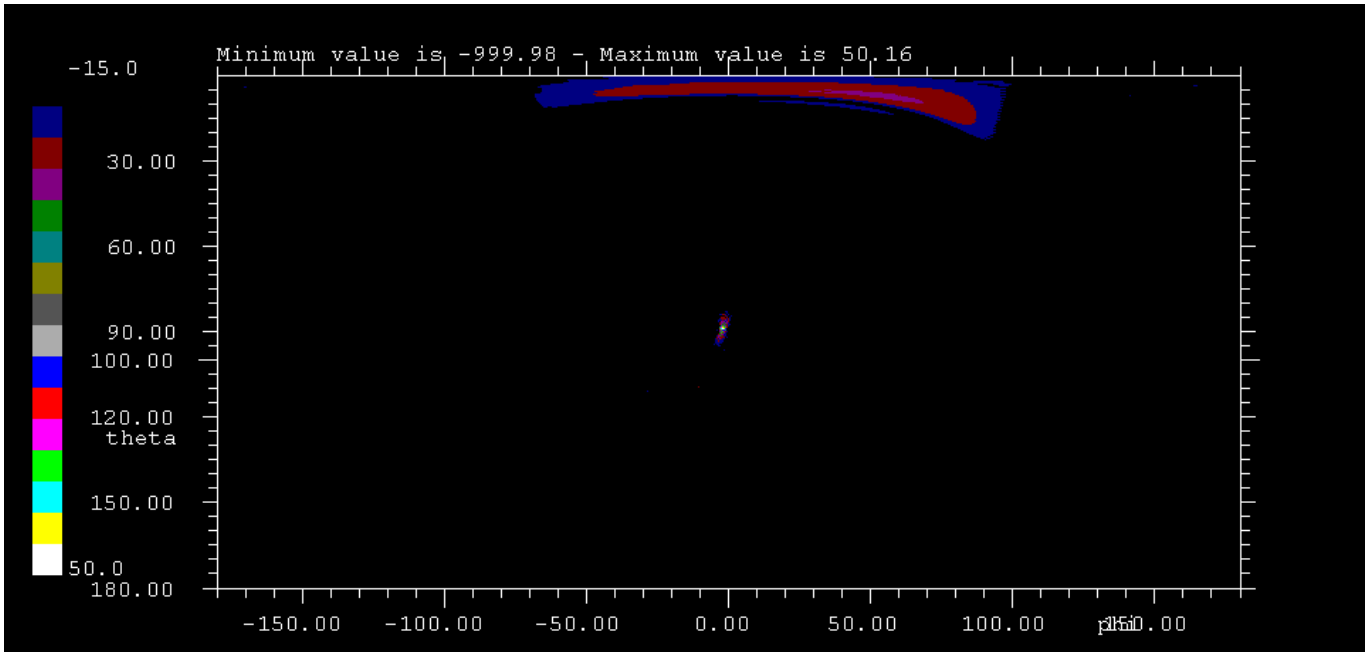

Figure 5.1-7 : Area where the -65 dB rejection is not met

Area where the -65 dB rejection is not met (directivity level from 50-65=-15 dBi to max=50 dBi. This area corresponds to the angular direction where the spill over lobe past the primary is located and the area of the main lobe as well.

5.2 100 GHz Pattern analysis (4pi-ext baf-gauss feed)

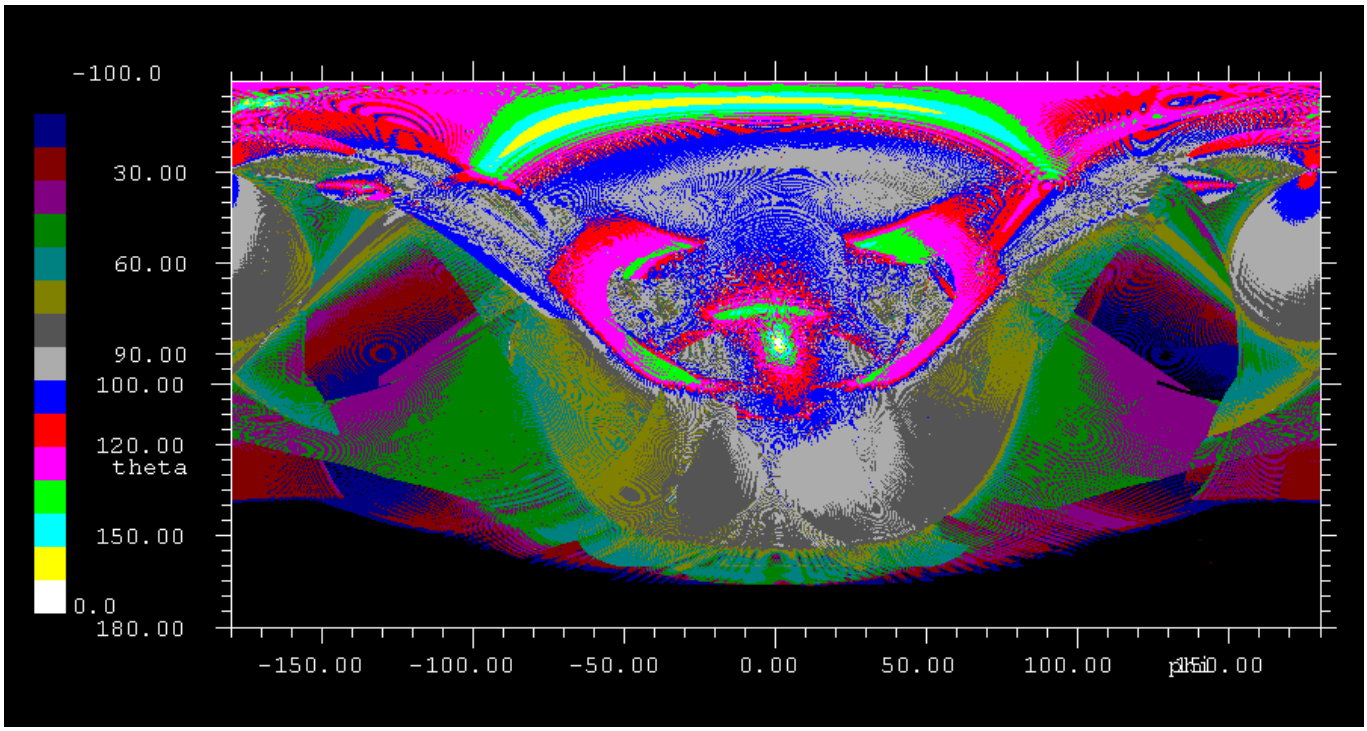

Figure 5.2-1 : 4PI diagram , phi : -180°, 180° / theta : 0,+180° / levels in directivity displayed from -100 dBi to +0 dBi

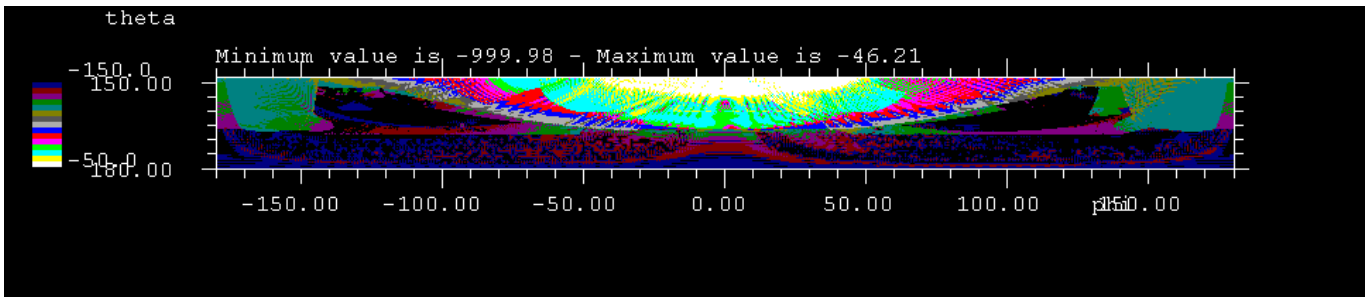

Figure 5.2-2 : Moon area phi : -180°, 180° / theta : +148°,+180° / levels in directivity displayed from -150 dBi to -50 dBi

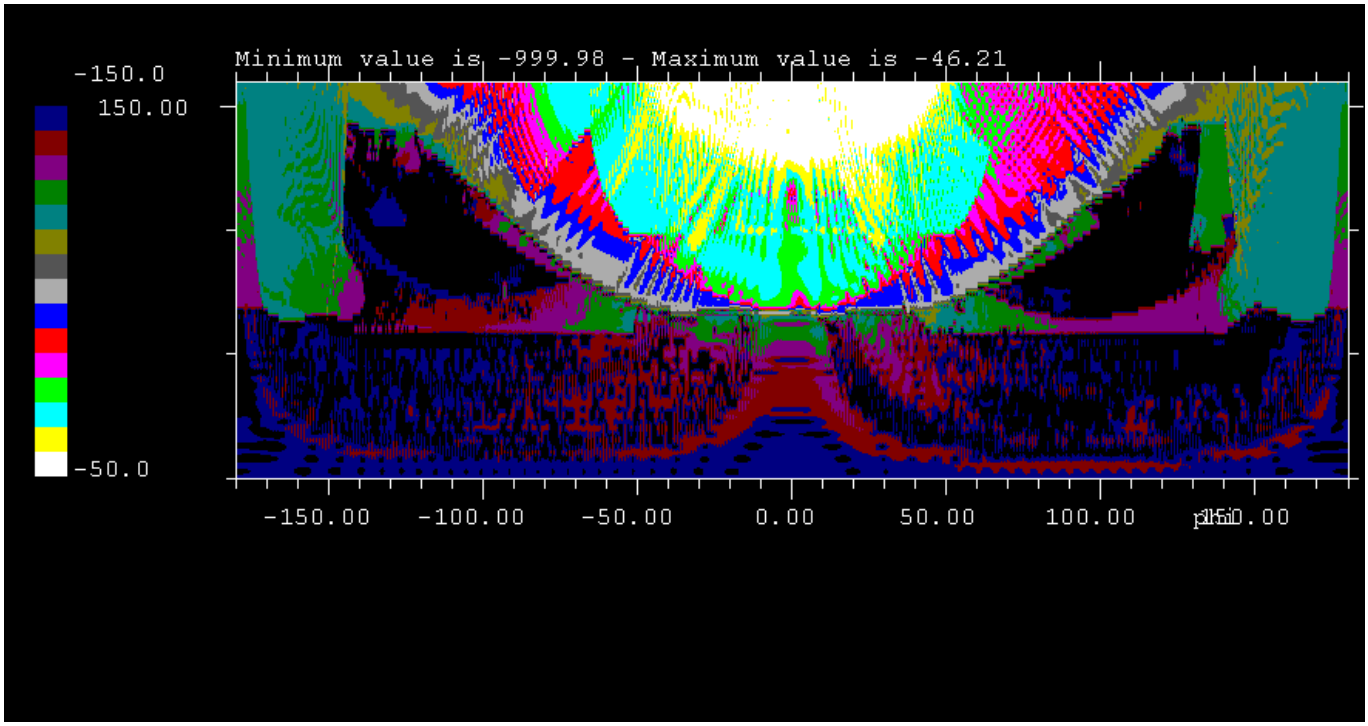

Figure 5.2-3 : Enlarged Moon area phi : -180°, 180° / theta : +148°,+180° / levels in directivity displayed from -150 dBi to -50 dBi

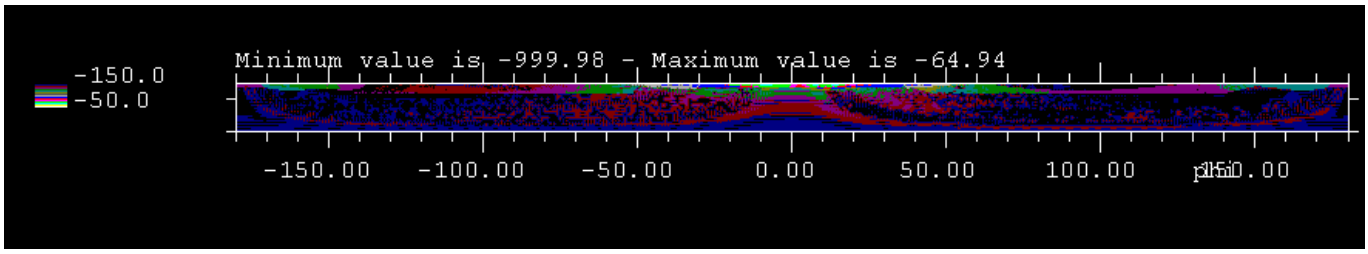

Figure 5.2-4 : Earth area phi : -180°, 180° / theta : +165°,+180° / levels in directivity displayed from -150 dBi to -50dBi.

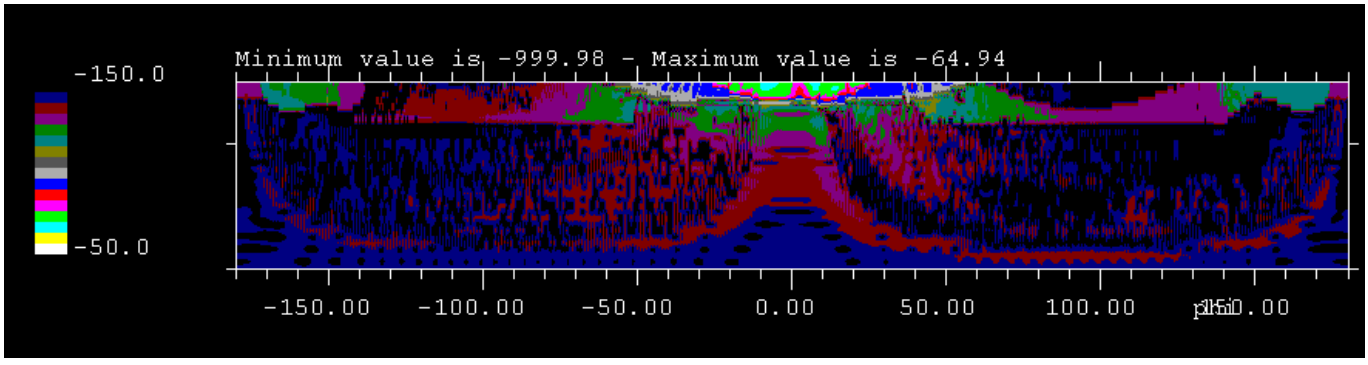

Figure 5.2-5 : Enalrged Earth area phi : -180°, 180° / theta : +165°,+180° / levels in directivity displayed from -150 dBi to -40dBi

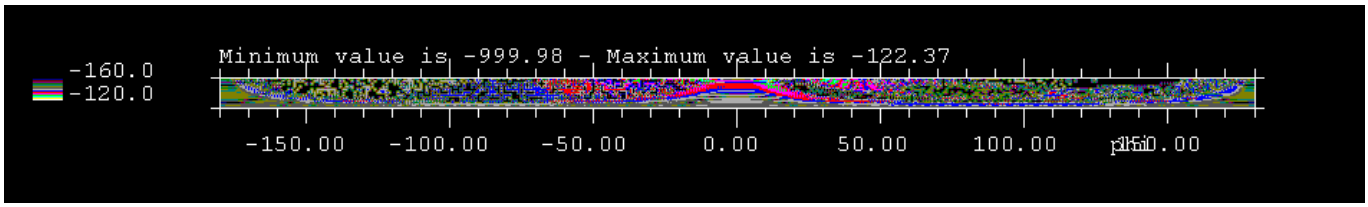

Figure 5.2-6 : Sun area phi : -180°, 180° / theta : +170°,+180° / levels in directivity displayed from -160dBi to -120 dBi

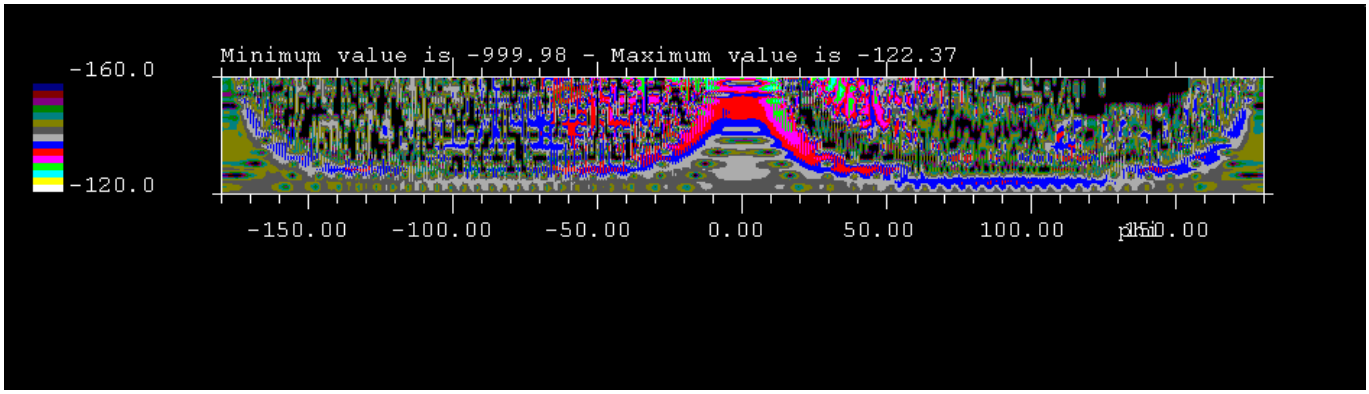

Figure 5.2-7 : Enlarged Sun area phi : -180°, 180° / theta : +170°,+180° / levels in directivity displayed from -150 dBi to -40dBi

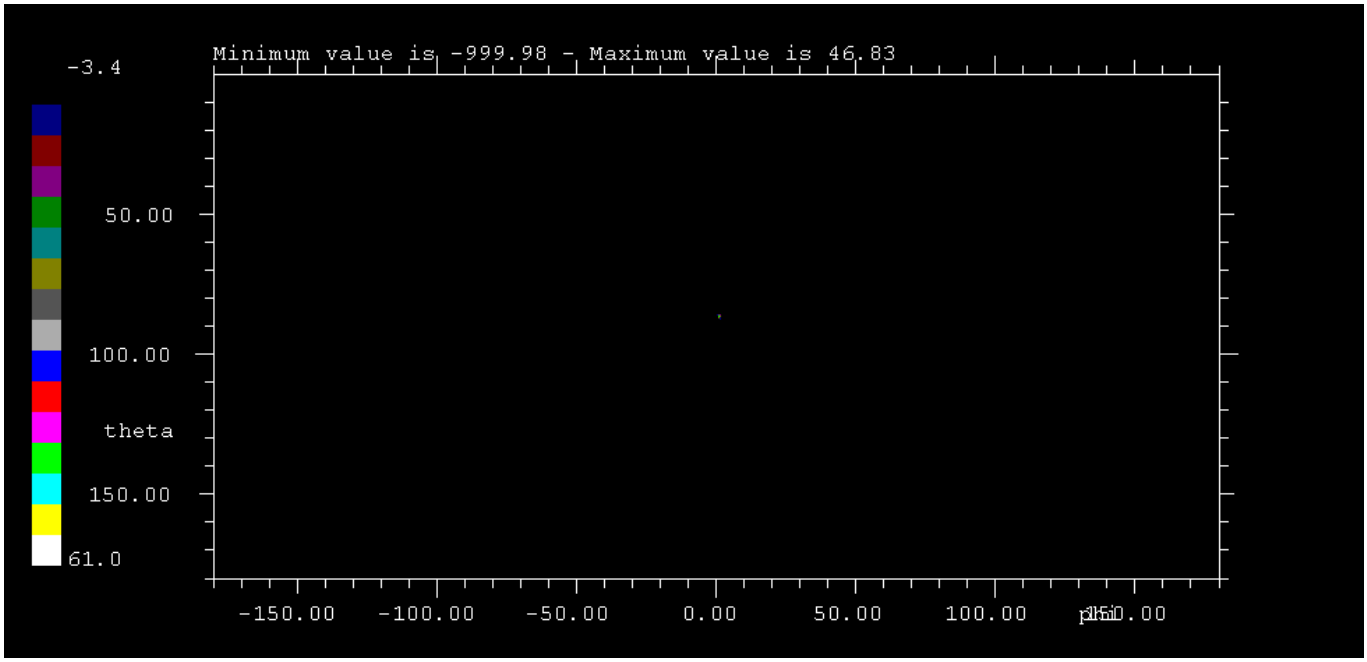

Figure 5.2-8 : Area where the -65 dB rejection is not met (directivity level displayed from 61.6-65=-3.4 dBi to max=61.6 dBi).

Only the main lobe area is over the -65 dB rejection.

5.3 353 GHz Pattern analysis (4pi-ext baf-gauss feed)

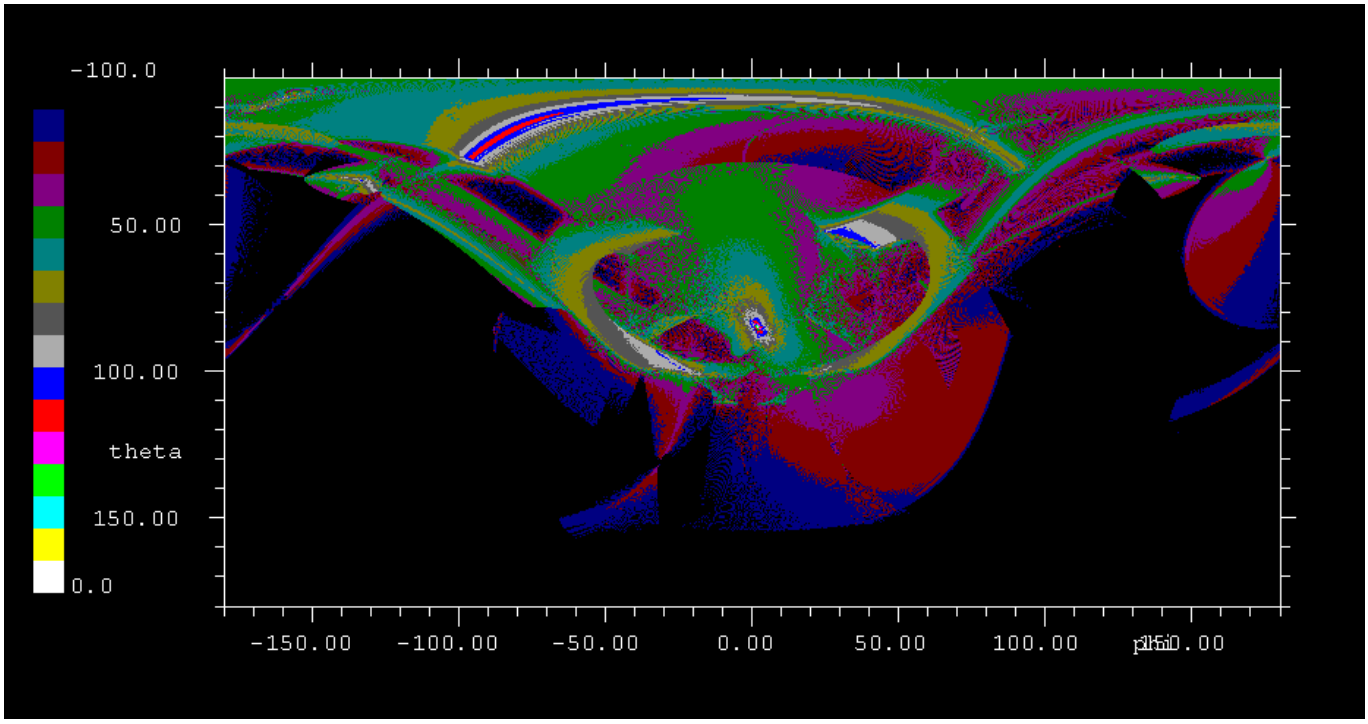

Figure 5.3-1 : 4PI diagram , phi : -180°, 180° / theta : 0,+180° / levels in directivity displayed from -100 dBi to +0 dBi

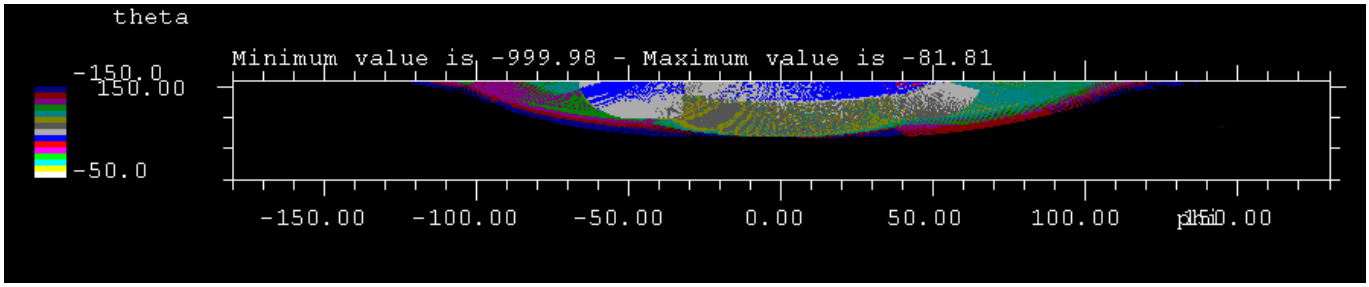

Figure 5.3-2 : Moon area phi : -180°, 180° / theta : +148°,+180° / levels in directivity displayed from -150 dBi to -50 dBi

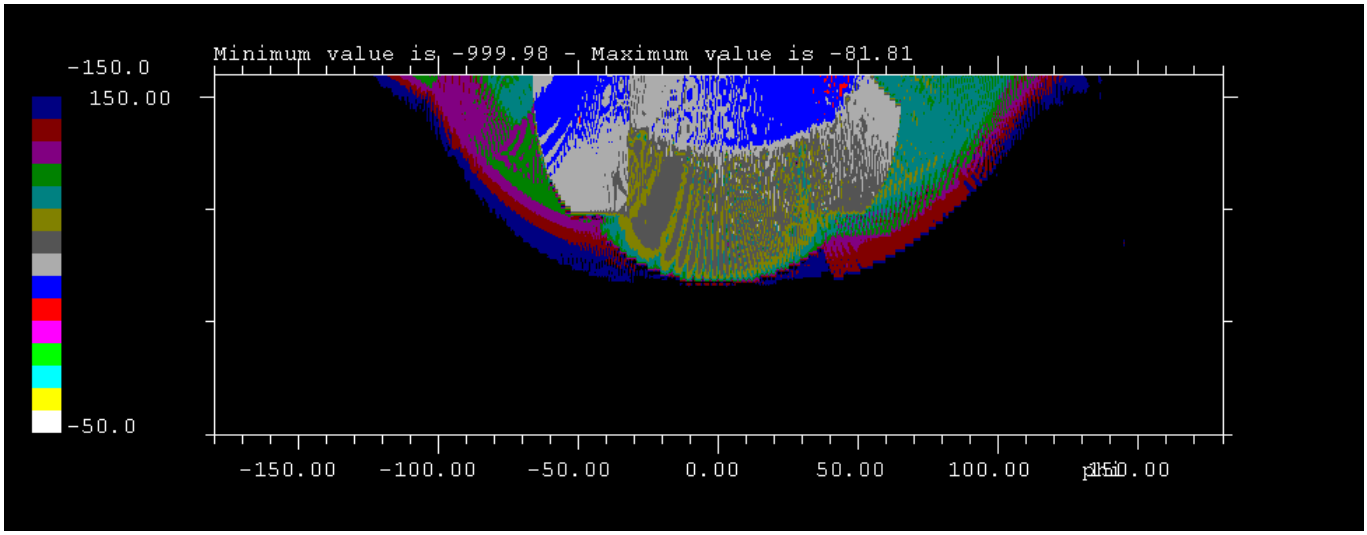

Figure 5.3-3 : Enlarged Moon area phi : -180°, 180° / theta : +148°,+180° / levels in directivity displayed from -150 dBi to -50 dBi

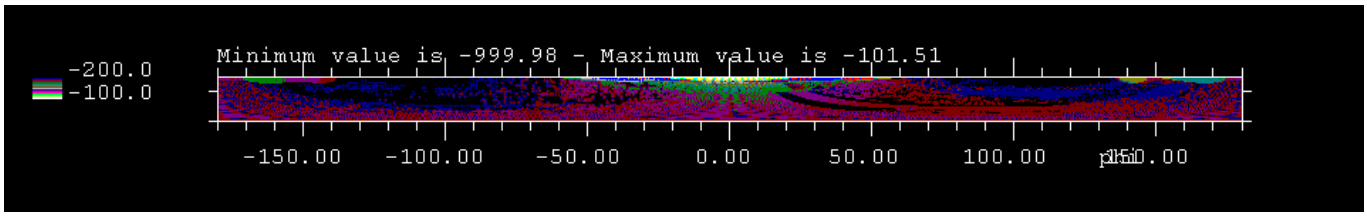

Figure 5.3-4 : Earth area phi : -180°, 180° / theta : +165°,+180° / levels in directivity displayed from -200 dBi to -100dBi.

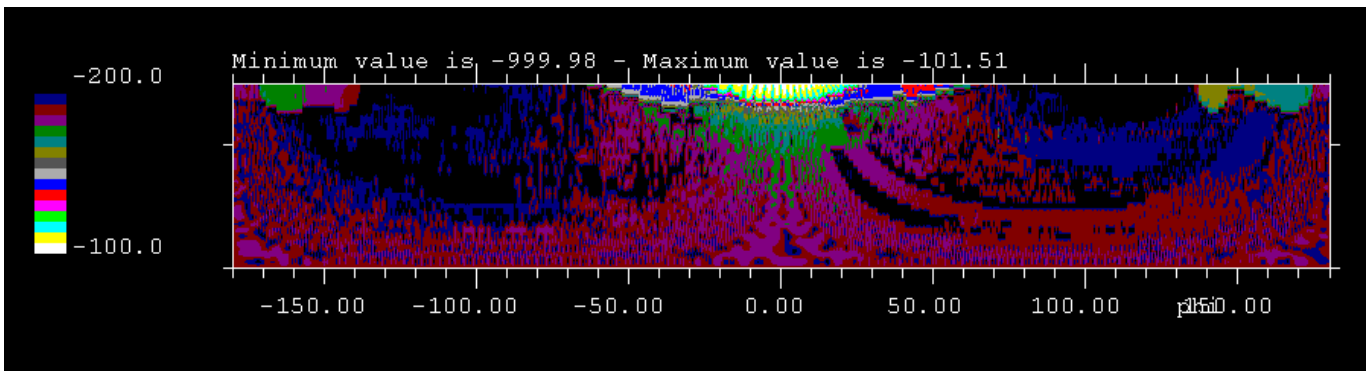

Figure 5.3-5 : Enlarged Earth area phi : -180°, 180° / theta : +165°,+180° / levels in directivity displayed from -200 dBi to -100 dBi

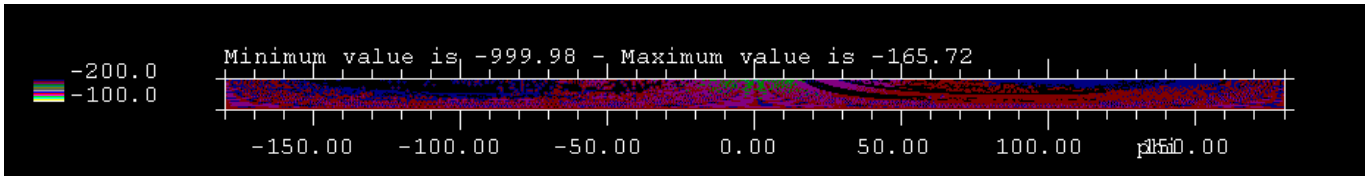

Figure 5.3-6 : Sun area phi : -180°, +180° / theta : +170°,+180° / levels in directivity displayed from -200dBi to -100 dBi

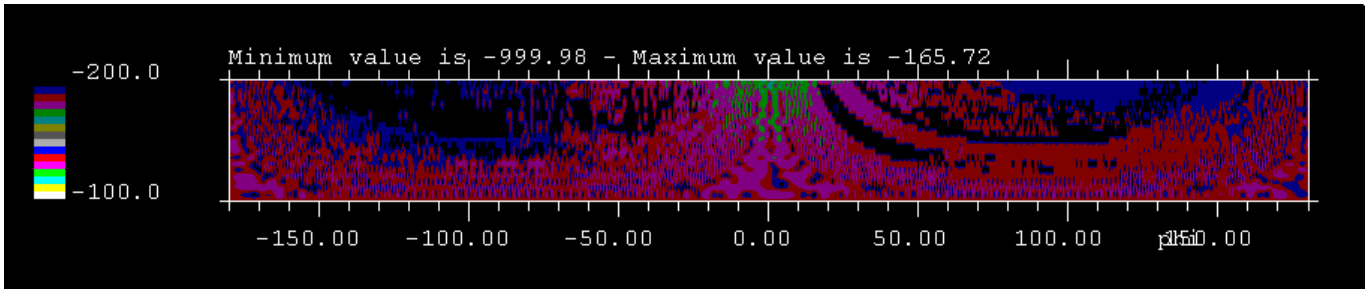

Figure 5.3-7 : Enlarged Sun area phi : -180°, 180° / theta : +170°,+180° / levels in directivity displayed from -200dBi to -100 dBi

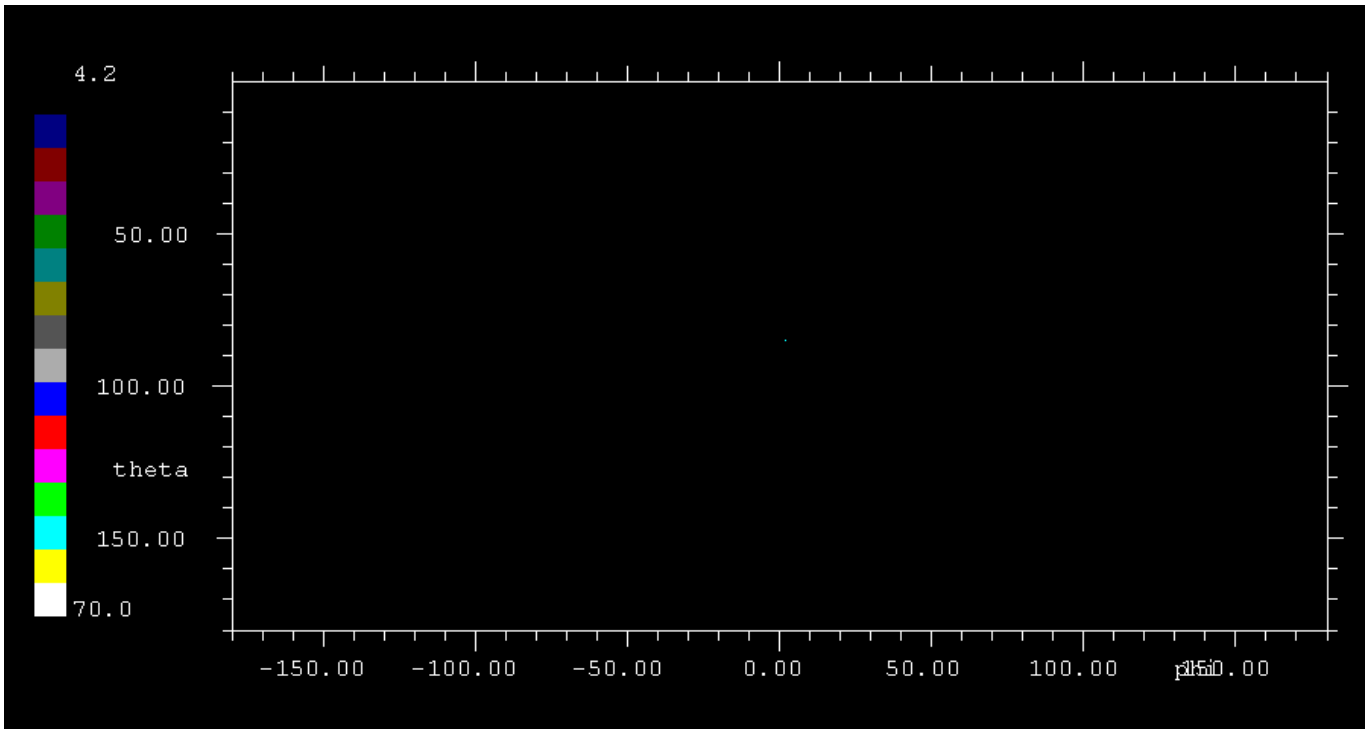

Figure 5.3-8 : Area where the -65 dB rejection is not met (directivity level displayed from 69.2-65=4.2 dBi to max=69.2 dBi).

Only the main lobe area is over the -65 dB rejection.

5.4 857 GHz Pattern analysis (4pi-ext baf-gauss feed)

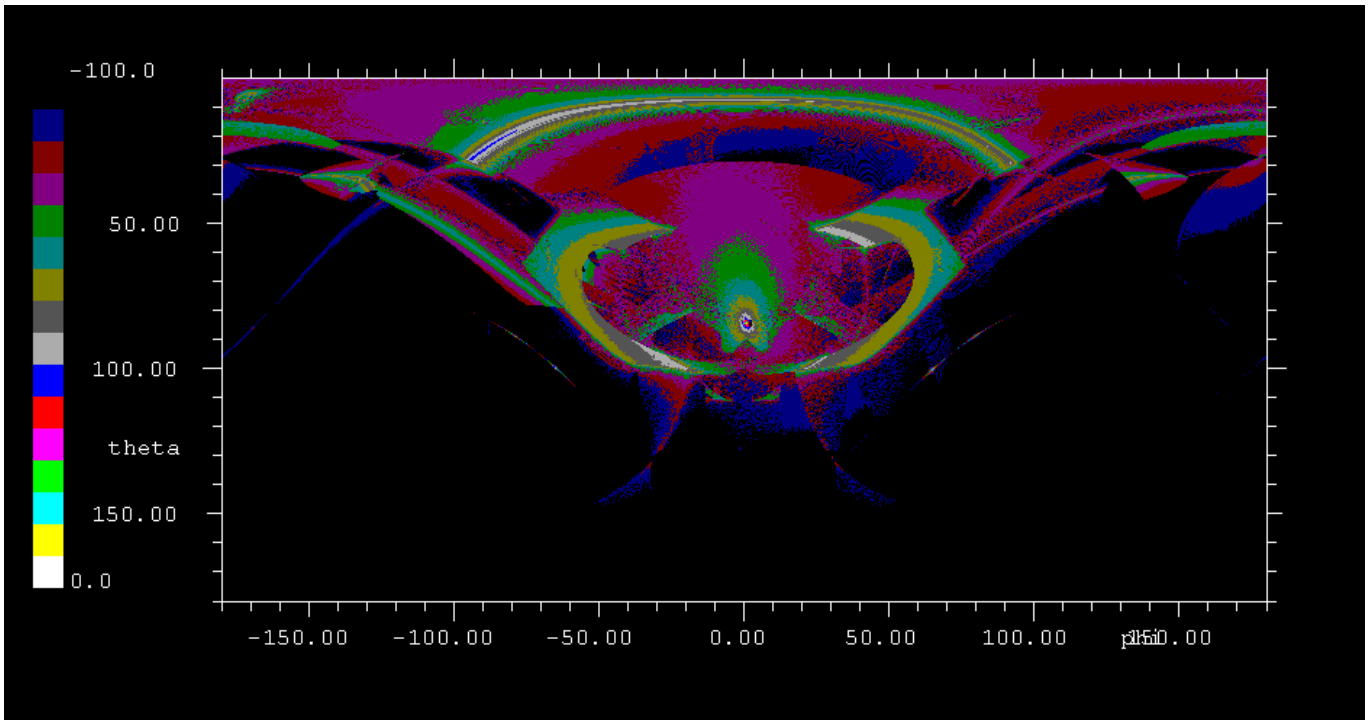

Figure 5.4-1 : 4PI diagram , phi : -180°, 180°/theta : 0,+180°/levels in directivity displayed from -100 dBi to +0 dBi

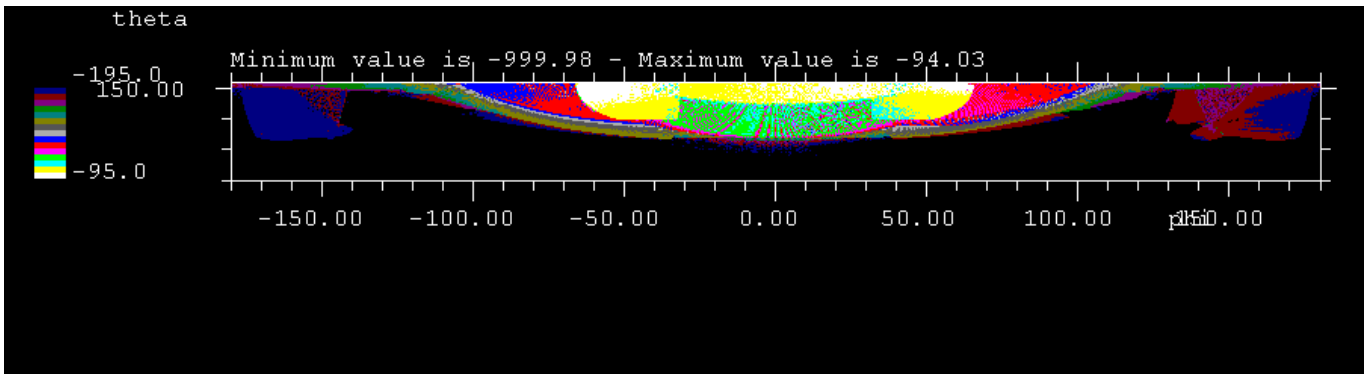

Figure 5.4-2 : Moon area phi : -180°, 180° / theta : +148°,+180° / levels in directivity displayed from -195 dBi to -95 dBi

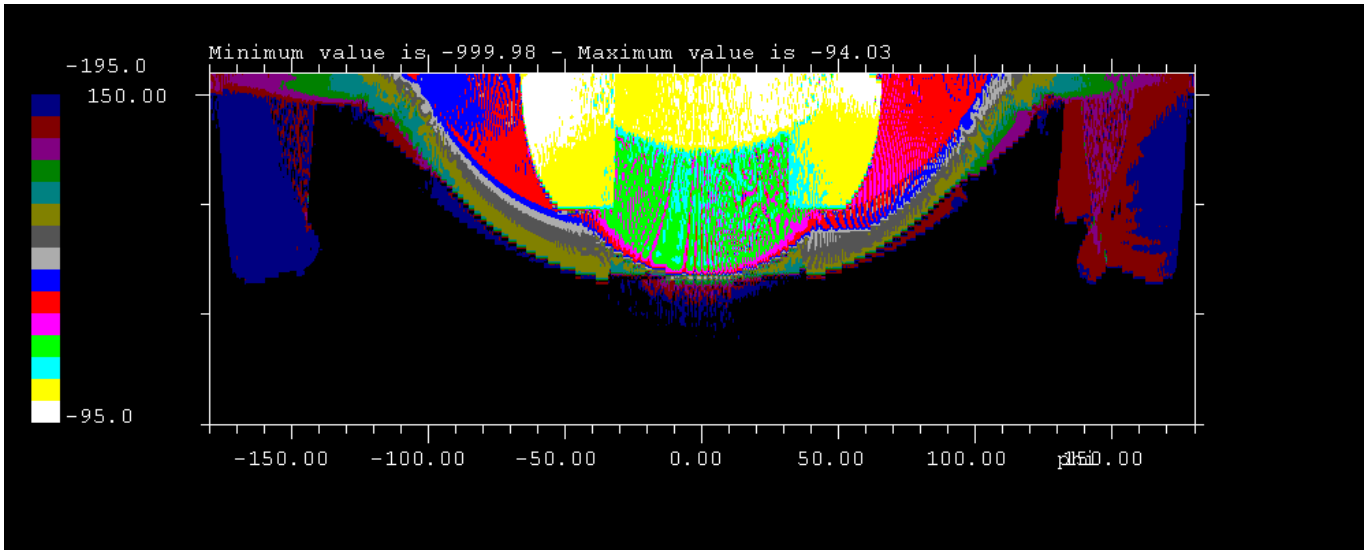

Figure 5.4-3 : Enlarged Moon area phi : -180°, 180° / theta : +148°,+180° / levels in directivity displayed from -195 dBi to -95 dBi

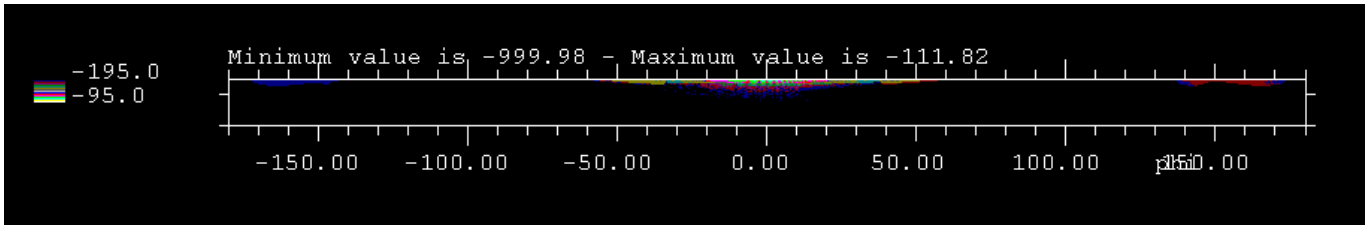

Figure 5.4-4 : Earth area phi : -180°, 180° / theta : +165°,+180° / levels in directivity displayed from -195 dBi to -95dBi

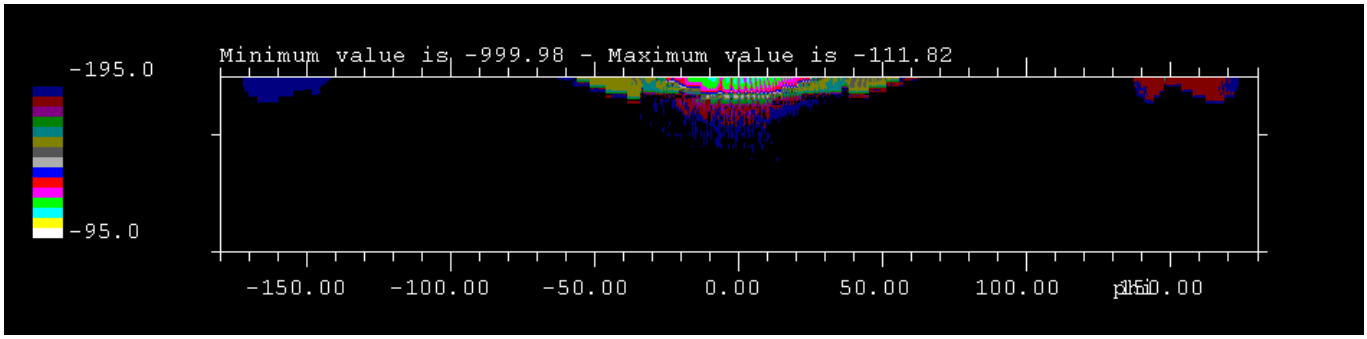

Figure 5.4-5 : Enlarged Earth area phi : -180°, 180° / theta : +165°,+180° / levels in directivity displayed from -195 dBi to -95dBi

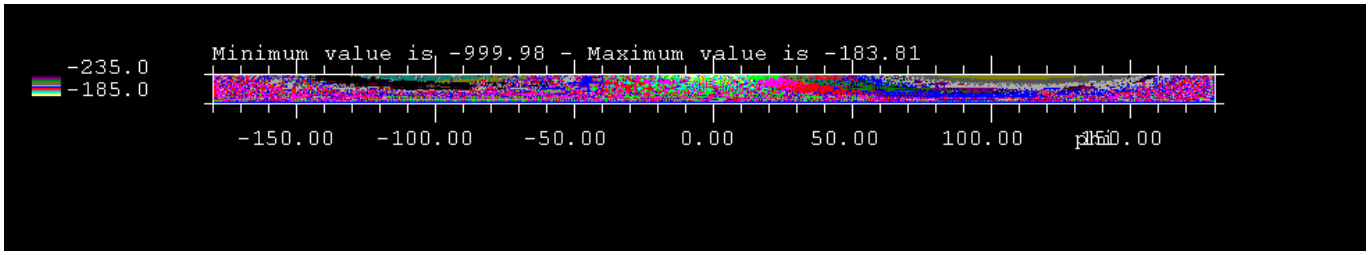

Figure 5.4-6 : Sun area phi : -180°, 180° / theta : +170°,+180° / levels in directivity displayed from -235 dBi to -185 dBi.

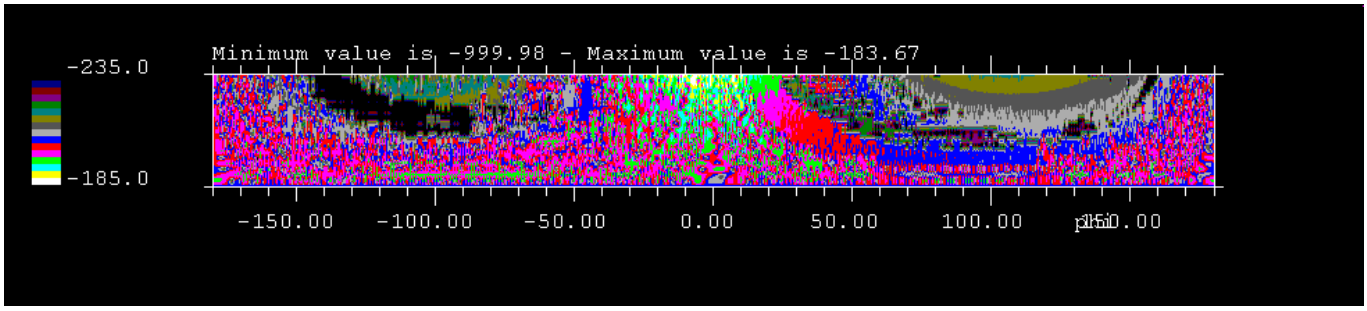

Figure 5.4-7 : Sun area phi : -180°, 180° / theta : +170°,+180° / levels in directivity displayed from -235 dBi to -185 dBi.

There's no angular direction with rejection greater than -65 dB. Except for the main lobe.

5.5 FAR OUT SIDE LOBE Performance synthesis (4pi-ext baf-gauss feed)

The requirements are defined as follows.

SPER-060 P	*The system rejection at the detectors for Sun, Earth, Moon at worst case locations shall be , at least :*
	30 GHz : *-91 dB , -78 dB and -71 dB respectively.*
	100 GHz (HFI) : *-91.5 dB (-99 dB), -78.5 dB (-86 dB) and -71.5 dB (-73 db) respectively*
	353 GHz : *-92 dB (-108 dB), -79 dB (-95 dB) and -72 dB (-81 dB) respectively.*
	857 GHz : *-98 dB (-122 dB), -85 dB (-109 dB) and -78 dB (-95 dB) respectively.*
Notes	1) The requirement for the Milky Way is of order –65 dB from peak but is driven by the telescope in free-standing configuration.
	2) The values between brackets shall be taken as goals .

The performance analysis is performed by using the worst case result in terms of directivity toward the Moon, the Earth and the Sun. This worst case directivity is the maximum directivity inside the angular area.

This directivity is compared to the maximum on axis directivity and the rejection is computed as :

Rejection (dB) = EOC_directivity (dBi) - On_axis_gain (dBi).

The margin wrt the requirements is defined as :

Margin (dB) = requirement (dB) - achieved_rejection (dB)

Rem : A positive margin value means of course that the requirement is achieved.

The following table (5.5-1) displays the worst case performance synthesis. The results are output directly from the numerical model. Some value can be considered as not physical such as value greater than 200 dB. Anyway the raw data allow to see the nice behaviour of the numerical model. As expected, the highest the frequency is the lower the rejection is.

Conclusion : The result of the computation performed in the frame of the RF expertise (ideal reflector surfaces, no dust, sharp edges) show a significant margin towards the Earth Sun and Moon rejection. Both requirements and goals are achieved.

30 GHz

	Aspect angle (°)	Theta value (°)	EOC directivity (dBi)	On axis max gain (dBi)	Rejection (dB)	Rejection requirement (dB)	Rejection goal (dB)	Margin (dB)
Moon	32	148	-33	50	-83	-71	NA	**12**
Earth	15	165	-50	50	-100	-78	NA	**22**
Sun	10	170	-86	50	-136	-91	NA	**45**

100 GHz

	Aspect angle (°)	Theta value (°)	EOC directivity (dBi)	On axis max gain (dBi)	Rejection (dB)	Rejection requirement (dB)	Rejection goal (dB)	Margin (dB)
Moon	32	148	-46	61	-107	-71.5	-73	**36**
Earth	15	165	-64	61	-125	-78.5	-86	**47**
Sun	10	170	-122	61	-183	-91.5	-99	**92**

353 GHz

	Aspect angle (°)	Theta value (°)	EOC directivity (dBi)	On axis max gain (dBi)	Rejection (dB)	Rejection requirement (dB)	Rejection goal (dB)	Margin (dB)
Moon	32	148	-81	69	-150	-72	-81	**78**
Earth	15	165	-101	69	-170	-79	-95	**91**
Sun	10	170	-165	69	-234	-92	-108	**142**

857 GHz

	Aspect angle (°)	Theta value (°)	EOC directivity (dBi)	On axis max gain (dBi)	Rejection (dB)	Rejection requirement (dB)	Rejection goal (dB)	Margin (dB)
Moon	32	148	-94	76	-170	-78	-95	**92**
Earth	15	165	-111	76	-187	-85	-109	**102**
Sun	10	170	-183	76	-259	-98	-122	**161**

Table 5.5-1 : performance synthesis.

6. ANALYSIS OF THE RESULTS OF THE 4 PI COMPUTATIONS WITH THE BAFFLE EXTENSION USING INSTRUMENT FEED MODEL (4PI-EXT BAF-INST FEED)

One parameter of interest is the detector feed model. For development phase purposes it has not been possible to use for the intiial run the QM or FM flight RF model of the feed. Those feed model are called instrument model or instrument feed (inst-feed). The detailed RF analysis of those detectors is provided in the documents [RD 6] [RD 7].

This section presents the re-run of the TICRA grasp file where the gaussian feed models have been replaced by the computed radiation pattern of the actual feed (QM or FM). No other parameters have been changed. The feeds ared located at the same position with the same polarization orientation at detector level for the polarized detector. In other word all geometrical elements are defined in [RD 5] and the RF feed models are defined in [RD 6] and [RD 7].

In addition for each frequency, two computations have been performed : one for each polarization of the detector in the focal plane in line with the detector orientation provided by the instruments.

Then the sub area where the Moon is located (half cone angle of 32° along the spacecraft spin axis) is extracted. The maximum directivity within this area is labelled the Edge of Cone (EOC) directivity. This directivity is then compared to the maximum on axis gain in order to obtain the achieved rejection.

The same process is applied for the Earth and Sun.

The modeling are performed using the up to date available data (see [RD 6] and [RD 7]). Hence the following data have been used :

- -30 GHz LFI detector radiation pattern (see [RD 6]) , dual orthogonal polarization
- -100 GHz HFI horn pattern (see [RD 7]) , dual orthogonal polarization
- -353 GHz HFI horn pattern (see [RD 7])
- -857 GHz no computation as far as multi moded horn characteristic is not available.

On final a table summarizes the performances for the rejection toward Earth Sun and Moon.

6.1 30 GHz Pattern analysis(4pi-ext baf-inst feed)

The following figure (fig 6.1-1) displays the 4 PI radiation pattern of the LFI 30 GHz radiation pattern inserted in the Planck geometry. The computation is performed as explained in (RD 8]. The numerical computation is performed as different sequence of ray combination or physical optics local computations. Then all elementary pattern are recombined so as to provide the 4 Pi radiation pattern. As visible on the following figure a sub pattern (see square shape) located bewteen phi values of 90° to 105° and theta values of 97.5° to 122.5° is badly located. The error is not located in the computation itself but in the parameters setting of the different pattern window size. Unfortunatelly the investigation are not over for the release of this document.

Anyhow all pattern corresponding to all elementary ray combination are computed and ready to be recombined.

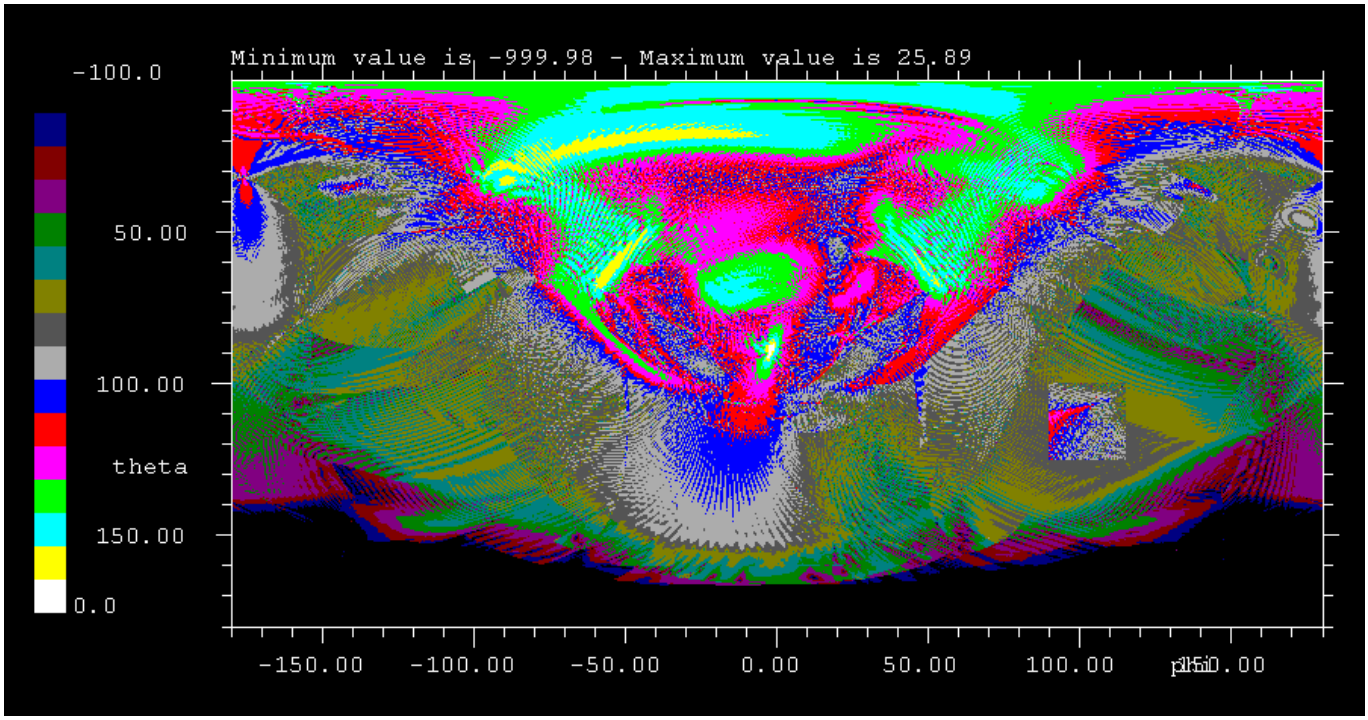

Figure 6.1-1 : 4PI diagram , phi : -180°, 180° / theta : 0,+180° / levels in directivity displayed from -100 dBi to +0 dBi (first component, Xpol)

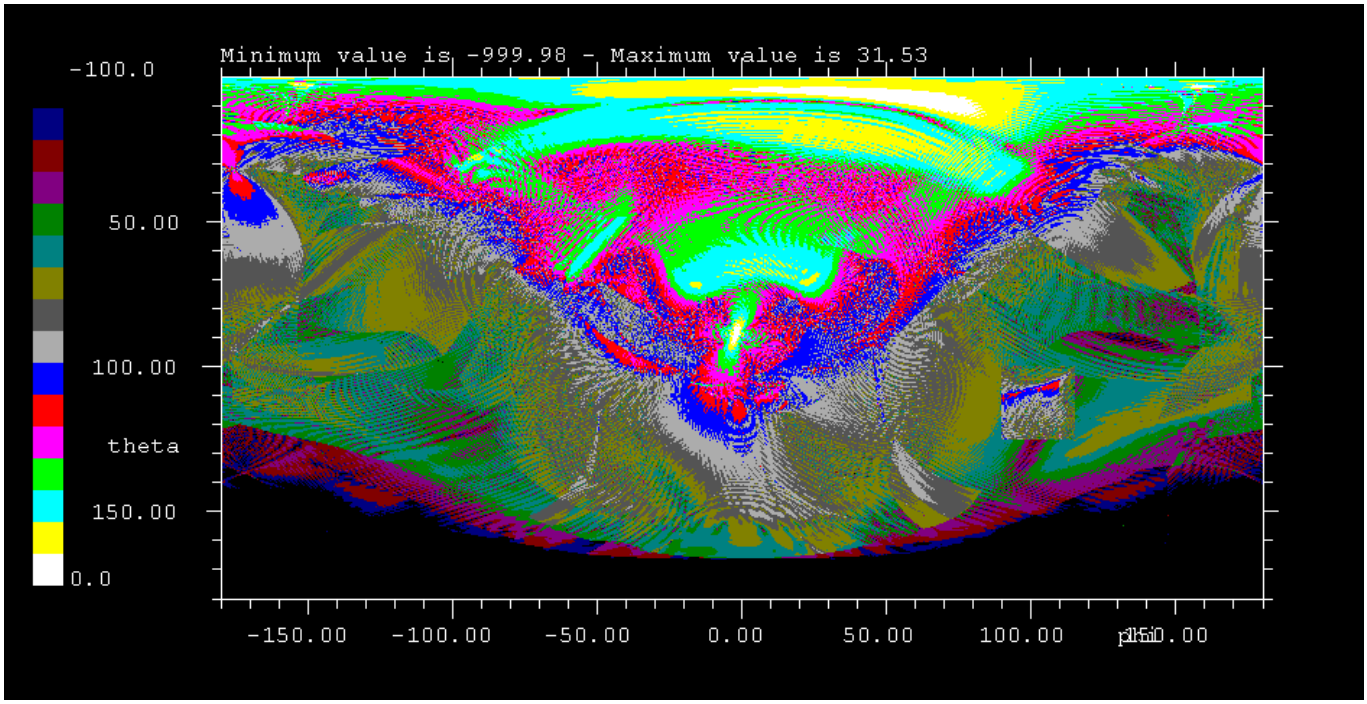

Figure 6.1-2 : 4PI diagram , phi : -180°, 180° / theta : 0,+180° / levels in directivity displayed from -100 dBi to +0 dBi (second component, co-pol)

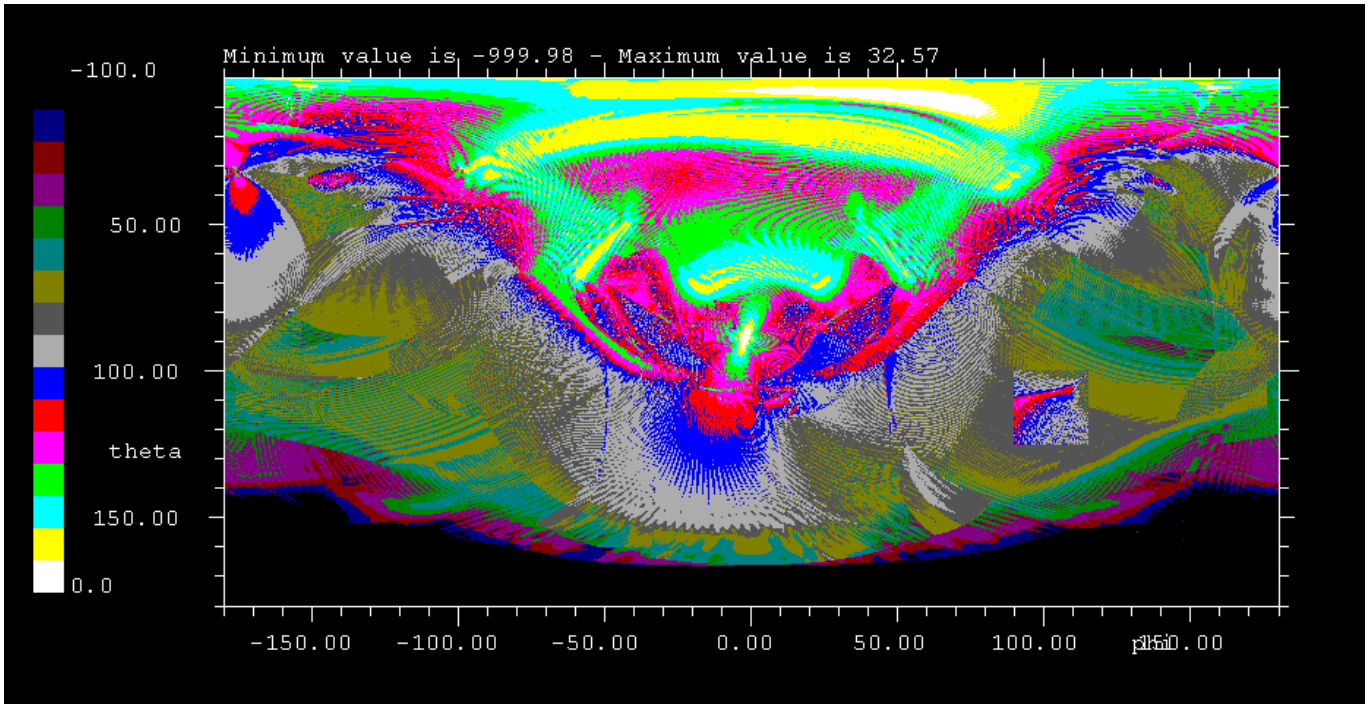

Figure 6.1-3 : 4PI diagram , phi : -180°, 180° / theta : 0,+180° / levels in directivity displayed from -100 dBi to +0 dBi (local major/minor component)

6.2 100 GHz Pattern analysis(4pi-ext baf-inst feed) 1st detector polarisation orientation

The detector phase center is located in the RDP coordinate such that :

x:-47.57 mm, y:-32.966 mm, z: 14.847 mm

The X_axis vector of the detector coordinate system is :
x_axis (x: 0.99540745 , y:-0.00331985, z:-0.09567128)
The Y_axis vector :
y_axis (x:-0.00331985, y: 0.99760016 , z:-0.06915857)
The Z_axis vector :
z_axis : (x :0.09567128 , y: 0.06915857 , z:-0.99300760)

For the 1st detector polarization orientation, the polarization vector of the feed is oriented along the Y axis.

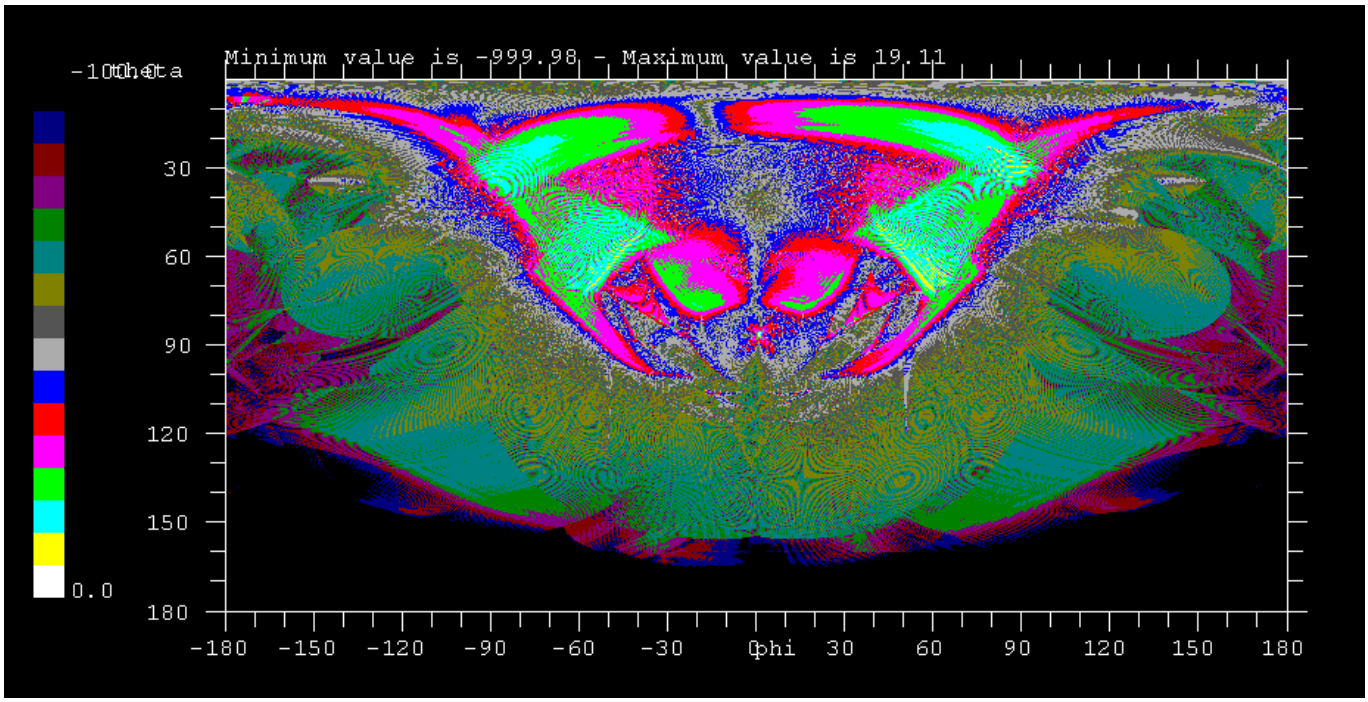

Figure 6.2-1 : 4PI diagram , phi : -180°, 180° / theta : 0,+180° / levels in directivity displayed from -100 dBi to +0 dBi (first component, Xpol)

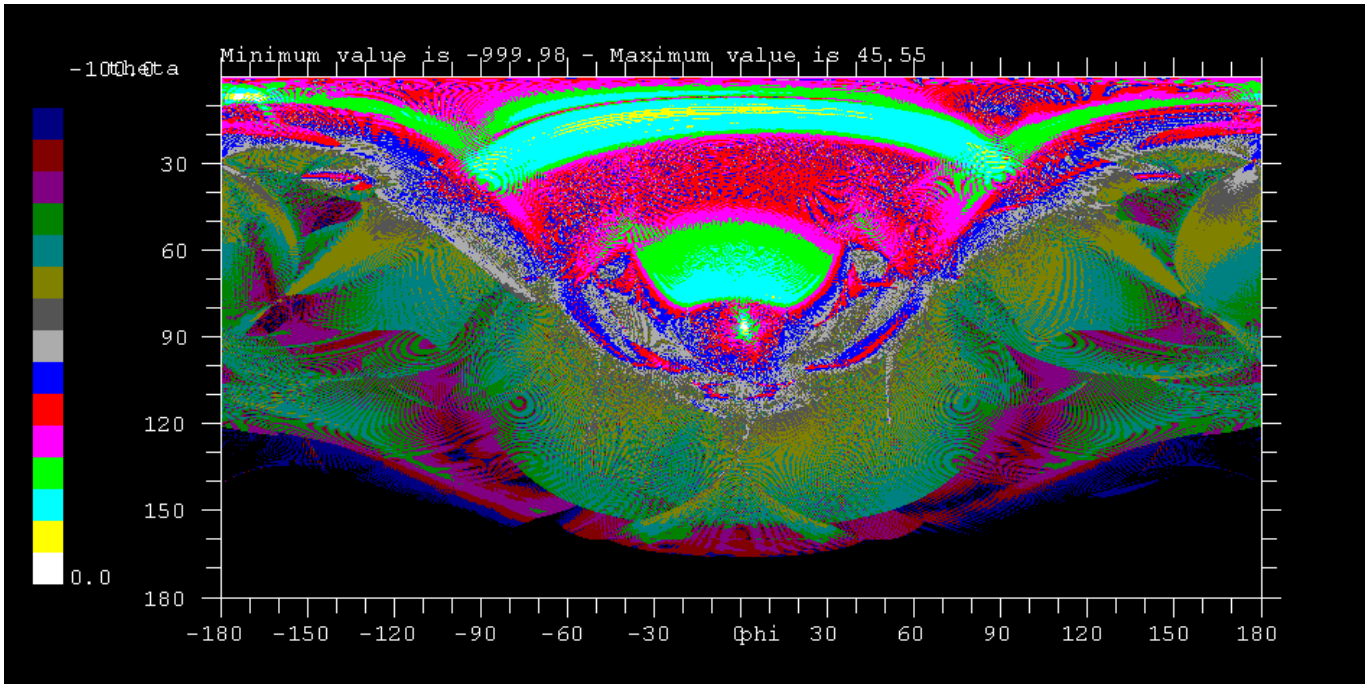

Figure 6.2-2 : 4PI diagram , phi : -180°, 180° / theta : 0,+180° / levels in directivity displayed from -100 dBi to +0 dBi (second component, co-pol)

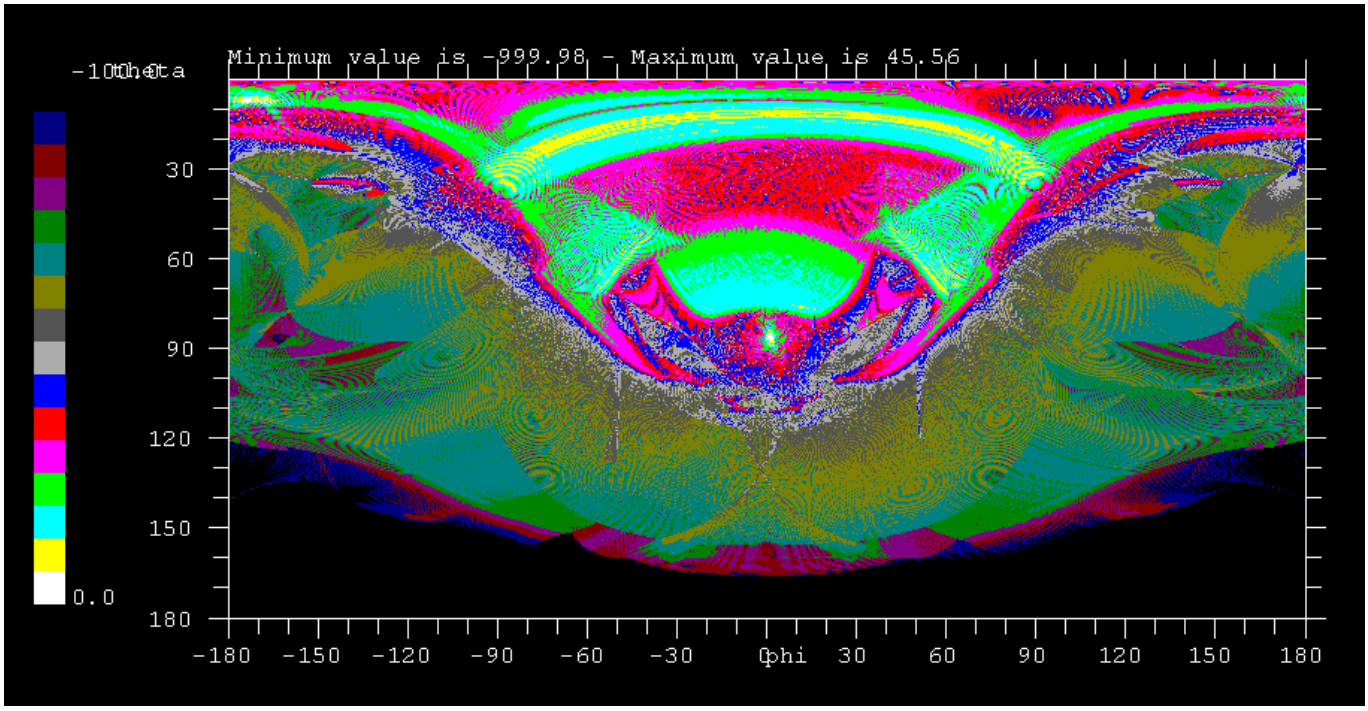

Figure 6.2-3 : 4PI diagram , phi : -180°, 180° / theta : 0,+180° / levels in directivity displayed from -100 dBi to +0 dBi (local major/minor component)

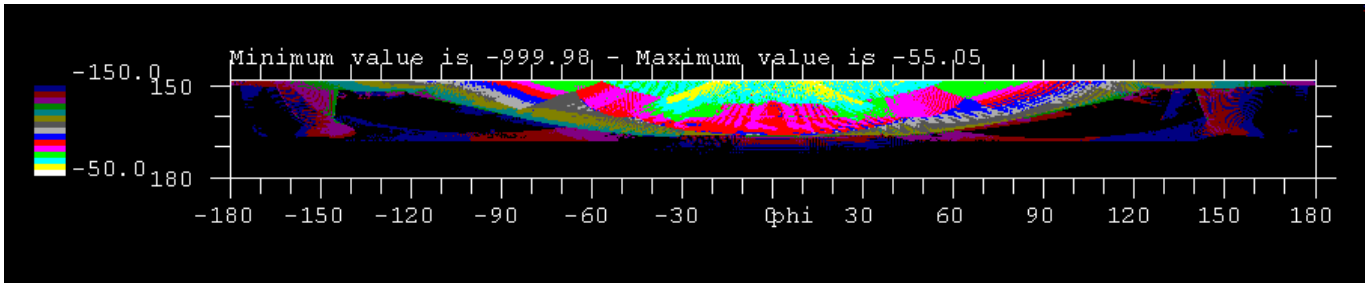

Figure 6.2-4 : Moon area phi : -180°, 180° / theta : +148°,+180° / levels in directivity displayed from -150 dBi to -50 dBi

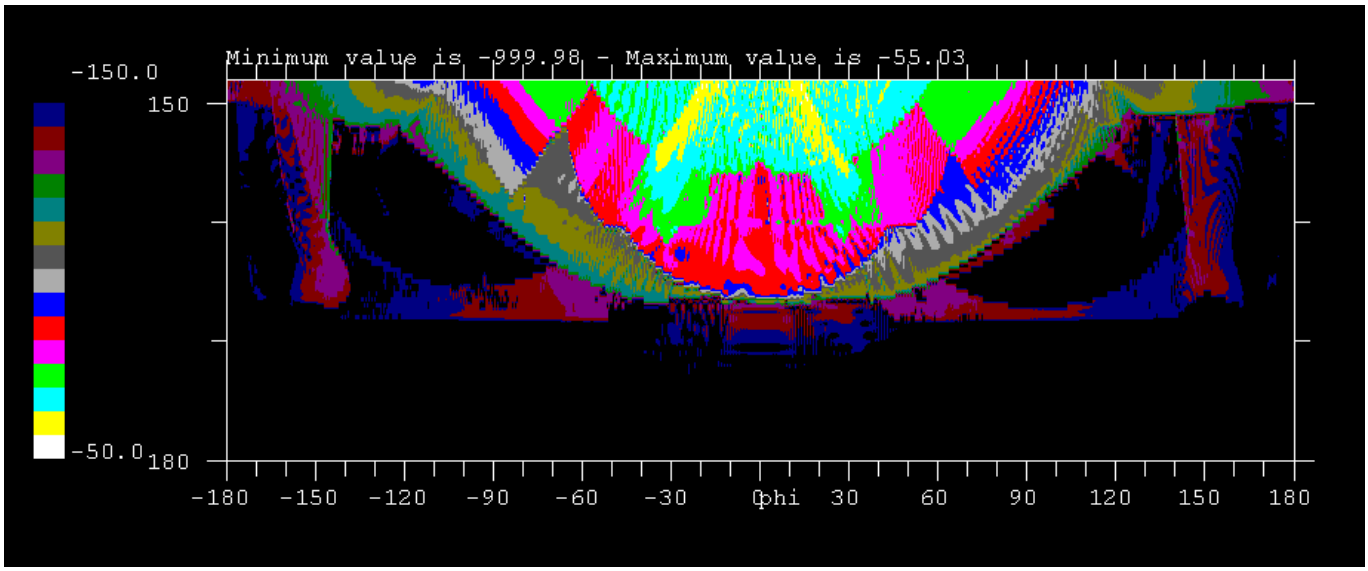

Figure 6.2-5 : enlarged Moon area phi : -180°, 180° / theta : +148°,+180° / levels in directivity displayed from -150 dBi to -50 dBi (local major/minor component)

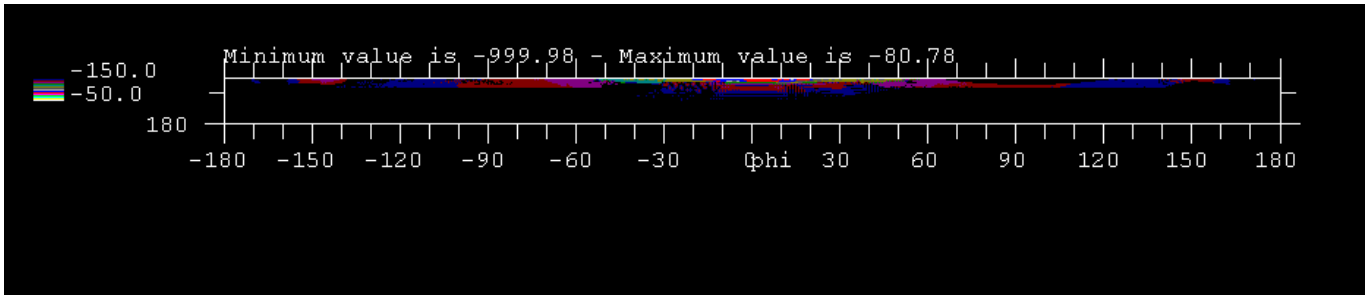

Figure 6.2-6 : Earth area phi : -180°, 180° / theta : +165°,+180° / levels in directivity displayed from -150 dBi to -50dBi (local major/minor component)

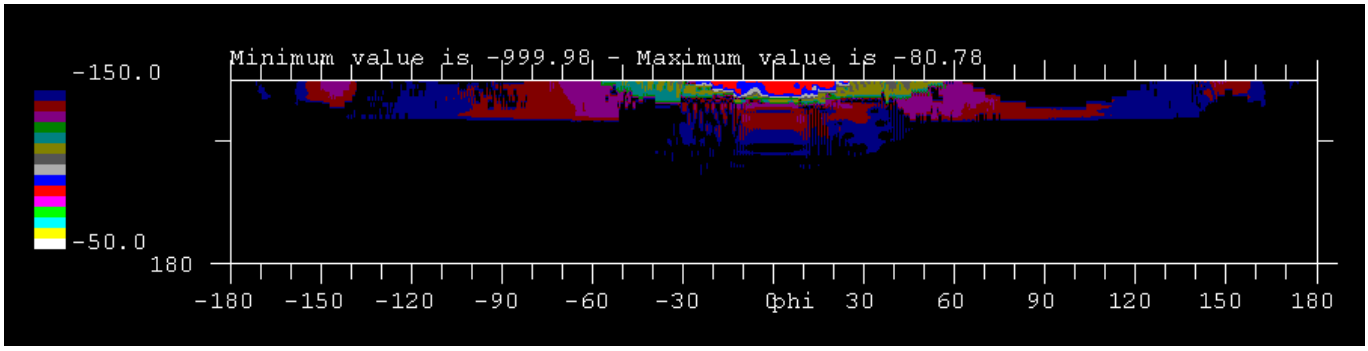

Figure 6.2-7 : Enlarged Earth area phi : -180°, 180° / theta : +165°,+180° / levels in directivity displayed from -150 dBi to -50dBi (local major/minor component)

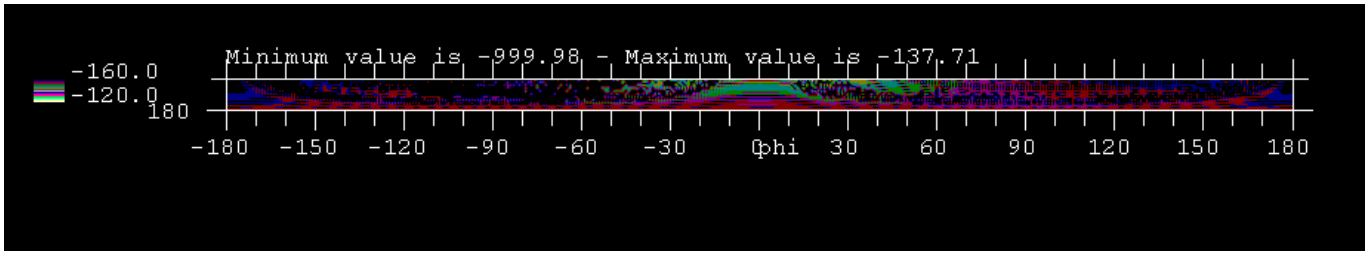

Figure 6.2-8 : Sun area phi : -180°, 180° / theta : +170°,+180° / levels in directivity displayed from -1600 dBi to -120dBi (local major/minor component

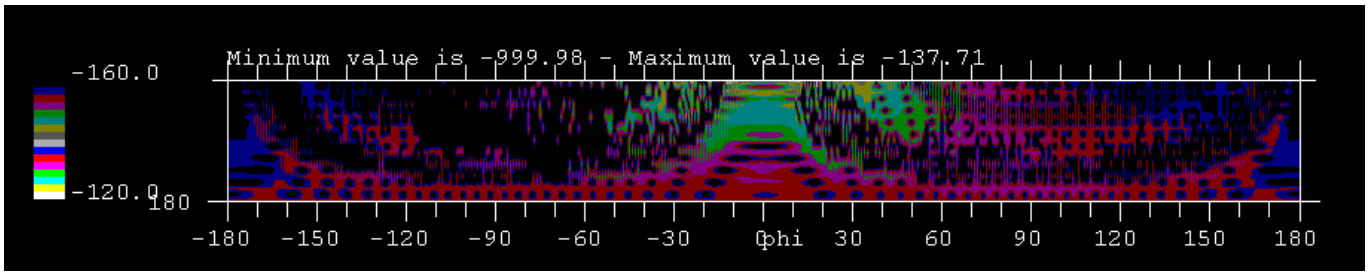

Figure 6.2-9 : Sun area phi : -180°, 180° / theta : +170°,+180° / levels in directivity displayed from -160 dBi to -120dBi (local major/minor component

Only the main lobe area is over the -65 dB rejection.

6.3 100 GHz Pattern analysis(4pi-ext baf-inst feed) 2nd detector polarisation orientation

The detector phase center is located in the RDP coordinate such that :

x:-47.57 mm, y:-32.966 mm, z: 14.847 mm

The X_axis vector of the detector coordinate system is :
x_axis (x: 0.99540745 , y:-0.00331985, z:-0.09567128)
The Y_axis vector :
y_axis (x:-0.00331985, y: 0.99760016 , z:-0.06915857)
The Z_axis vector :
z_axis : (x :0.09567128 , y: 0.06915857 , z:-0.99300760)

For the 2nd detector polarization orientation, the polarization vector of the feed is oriented along the X axis.

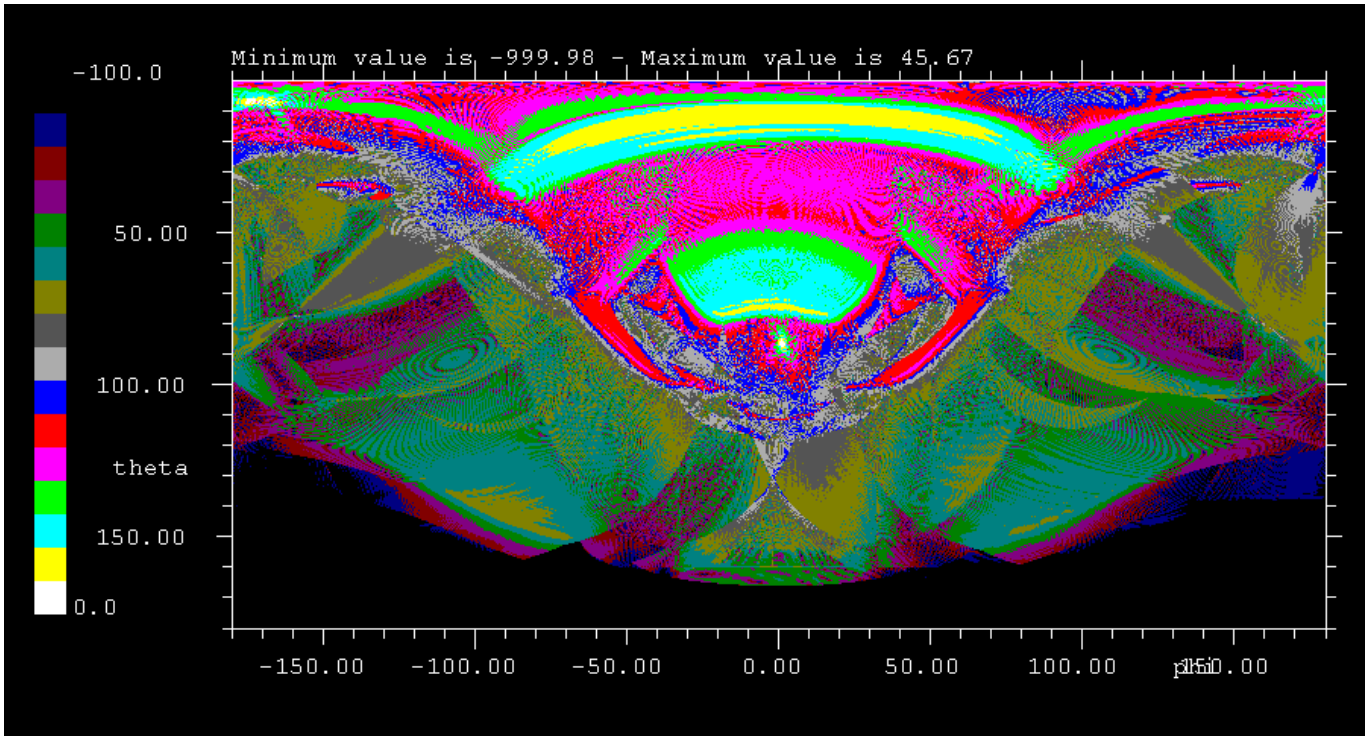

Figure 6.3-1 : 4PI diagram , phi : -180°, 180° / theta : 0,+180° / levels in directivity displayed from -100 dBi to +0 dBi (first component, Xpol)

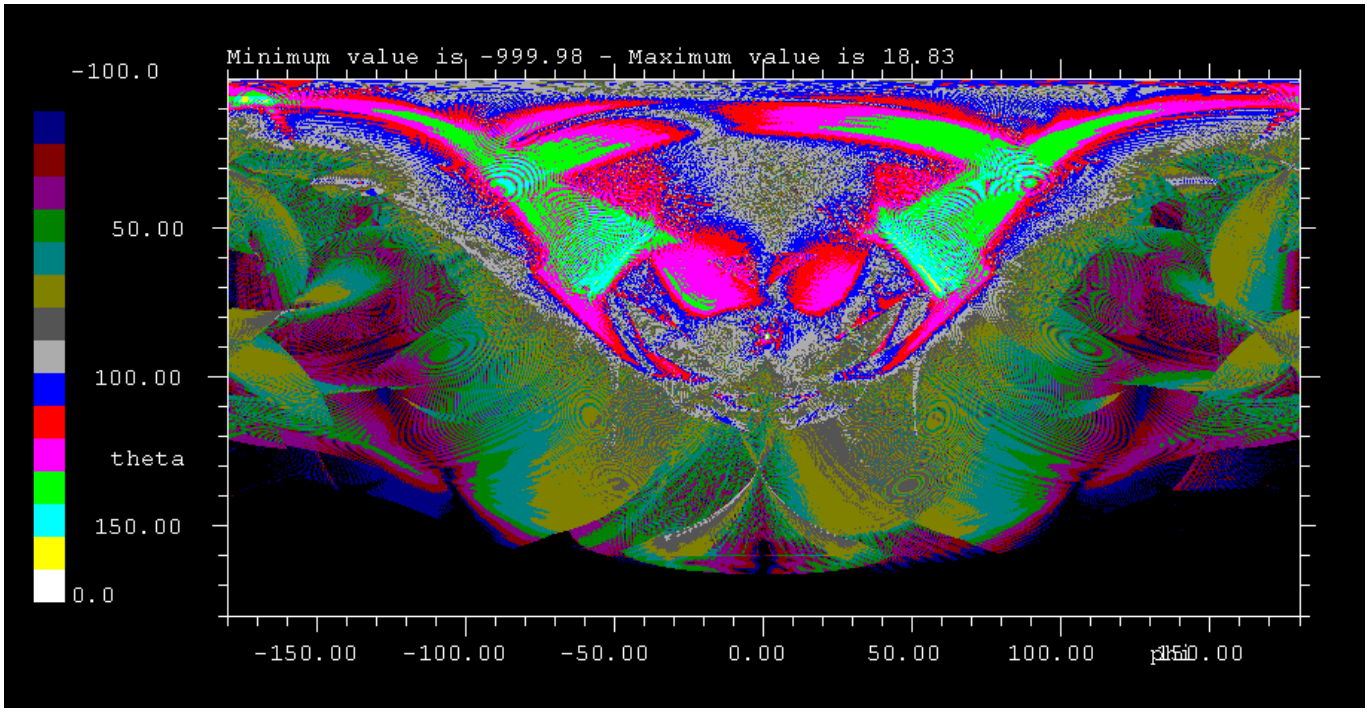

Figure 6.3-2 : 4PI diagram , phi : -180°, 180° / theta : 0,+180° / levels in directivity displayed from -100 dBi to +0 dBi (second component, co-pol)

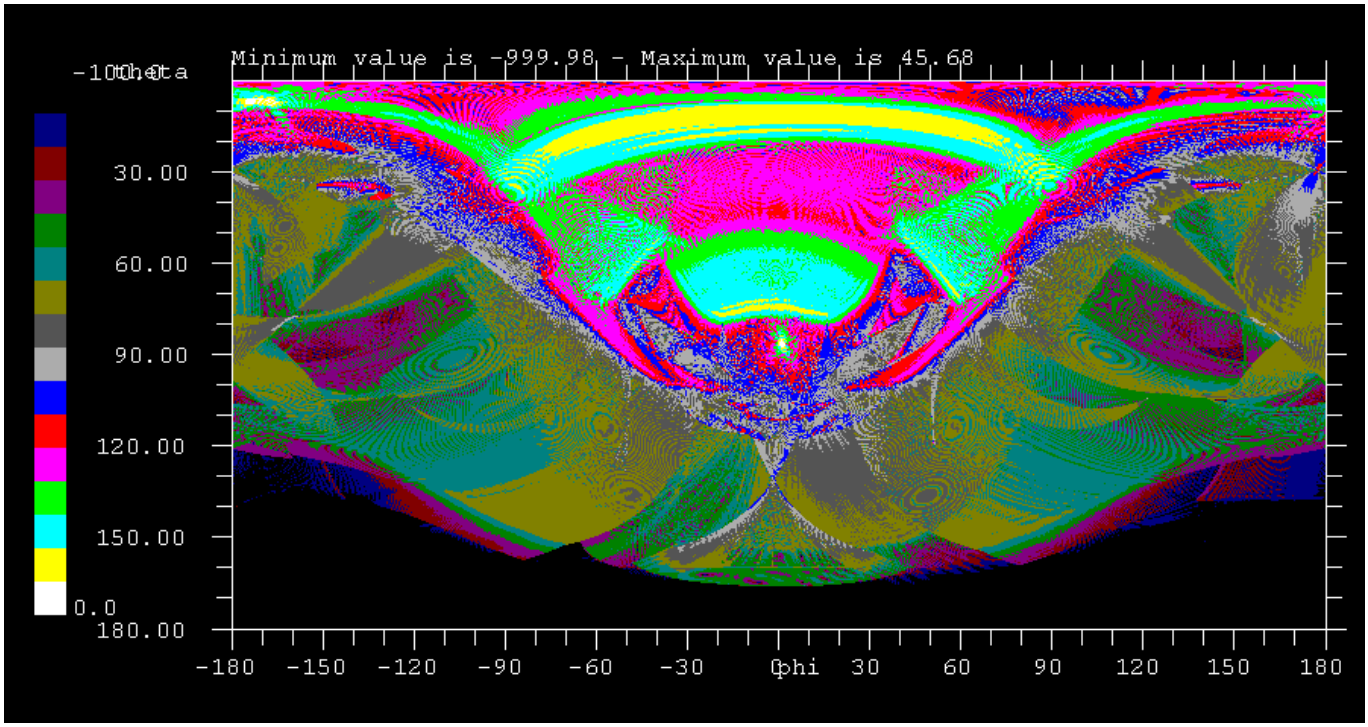

Figure 6.3-3 : 4PI diagram , phi : -180°, 180° / theta : 0,+180° / levels in directivity displayed from -100 dBi to +0 dBi (local major/minor component)

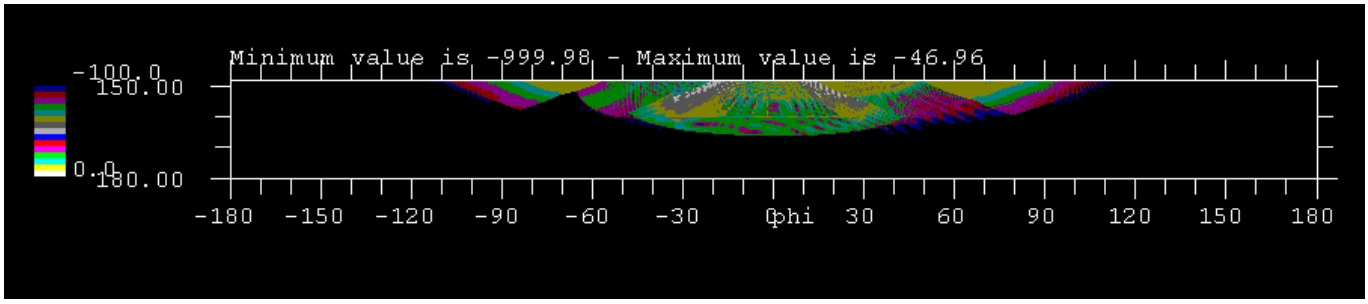

Figure 6.3-4 : Moon area phi : -180°, 180° / theta : +148°,+180° / levels in directivity displayed from -150 dBi to -50 dBi

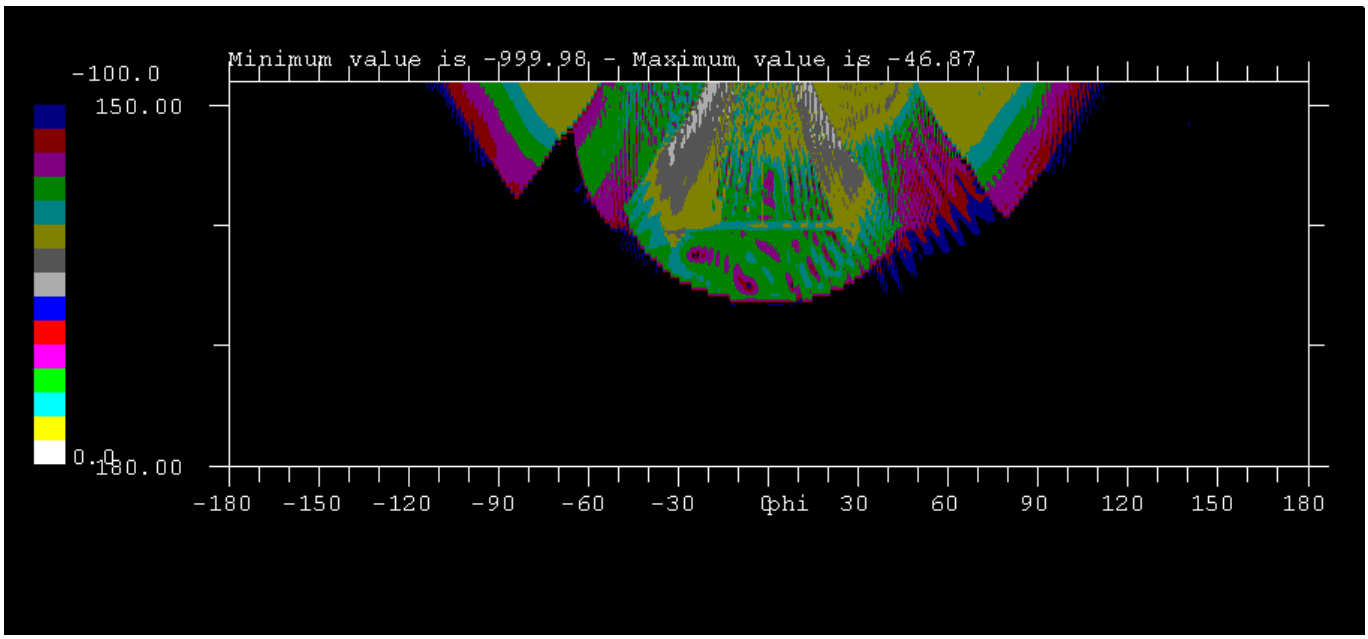

Figure 6.3-5 : enlarged Moon area phi : -180°, 180° / theta : +148°,+180° / levels in directivity displayed from -100 dBi to 0 dBi (local major/minor component)

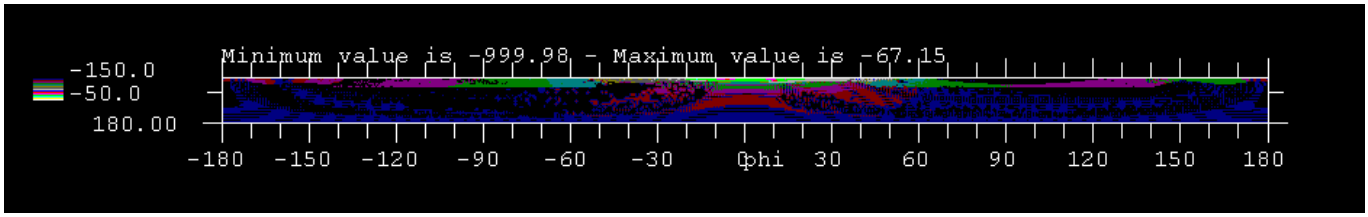

Figure 6.3-6 : Earth area phi : -180°, 180° / theta : +165°,+180° / levels in directivity displayed from -150 dBi to -50dBi (local major/minor component)

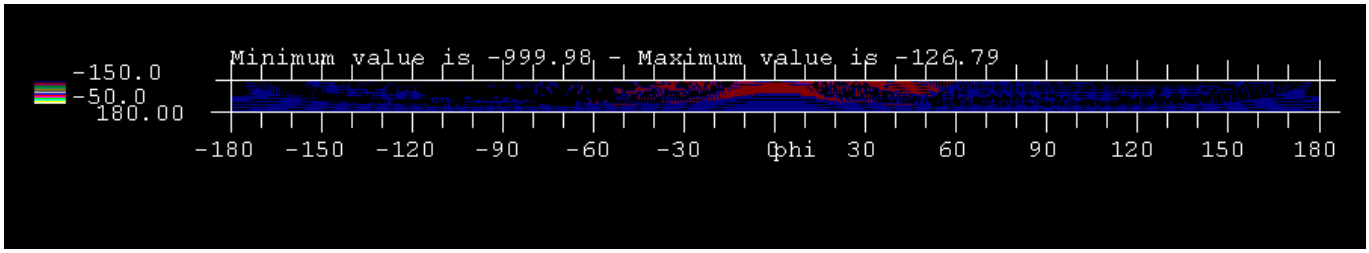

Figure 6.3-7 : Sun area phi : -180°, 180° / theta : +170°,+180° / levels in directivity displayed from -150 dBi to -50dBi (local major/minor component

6.4 100 GHz pattern preliminary comparison

As far as the 100 GHz 4 pi pattern have been computed for two orthogonal polarization orientations at the focal plane level, it is then possible to compare the difference on the overall pattern.

The comparison is performed on the pattern expressed in local major/minor polarisation component. Only the major axis of polarisation ellipse is displayed and compared.

The comparison consists in computing the ratio between the major polarization axis of each pattern. The first pattern is computed as described in section 6.2 for the first polarization orientation of the detector. The second pattern is computed for the orhtogonal polarization orientation (see section 6.3).

The pattern difference is performed by computing the linear ratio for each direction between the first and second pattern. Then the display is performed in dB. For graphical purpose the ratio has been performed twice (fist / second) then (second / first). This is useful to obtain only coloured pixel of interest on the plots. For instance the pattern difference is plotted over a dB range (eg ratio variation from -20 dB to -10 dB and +10 dB to +20 dB). In both cases the values over the upper limit are plotted in black pixels and the values below the lower limit are plotted as red pixels. Then all red pixels have to be disgarded or considered as black for graphical readibility.

The figure 6.4-1 shows that very few pixels are impacted by more than 30 dB gain variation. Such variation can be attributed to the coarse meshing of 0.5° by 0.5°. The highest variation are obtained in the Earth Sun and Moon cone are (theta values varying from 148° to 180°).

The figure 6.4-3 displays some quasi continuous area (not only isolated pixel) where the gain variation is between (+10 dB and +20 dB) and (-20 dB and -10 dB). This area is located between phi=-150° and phi=-100° and theta=70° to theta=90°.

On final the figure 6.4-4 and 6.4-5 show that almost all pattern direction are affected by the polarization detector orientation change by a value of 10 dB.

As a conclusion a raw result is that the detector polarization rotation by 90° generate a pattern global pattern difference of 10 dB on the far out side lobes.

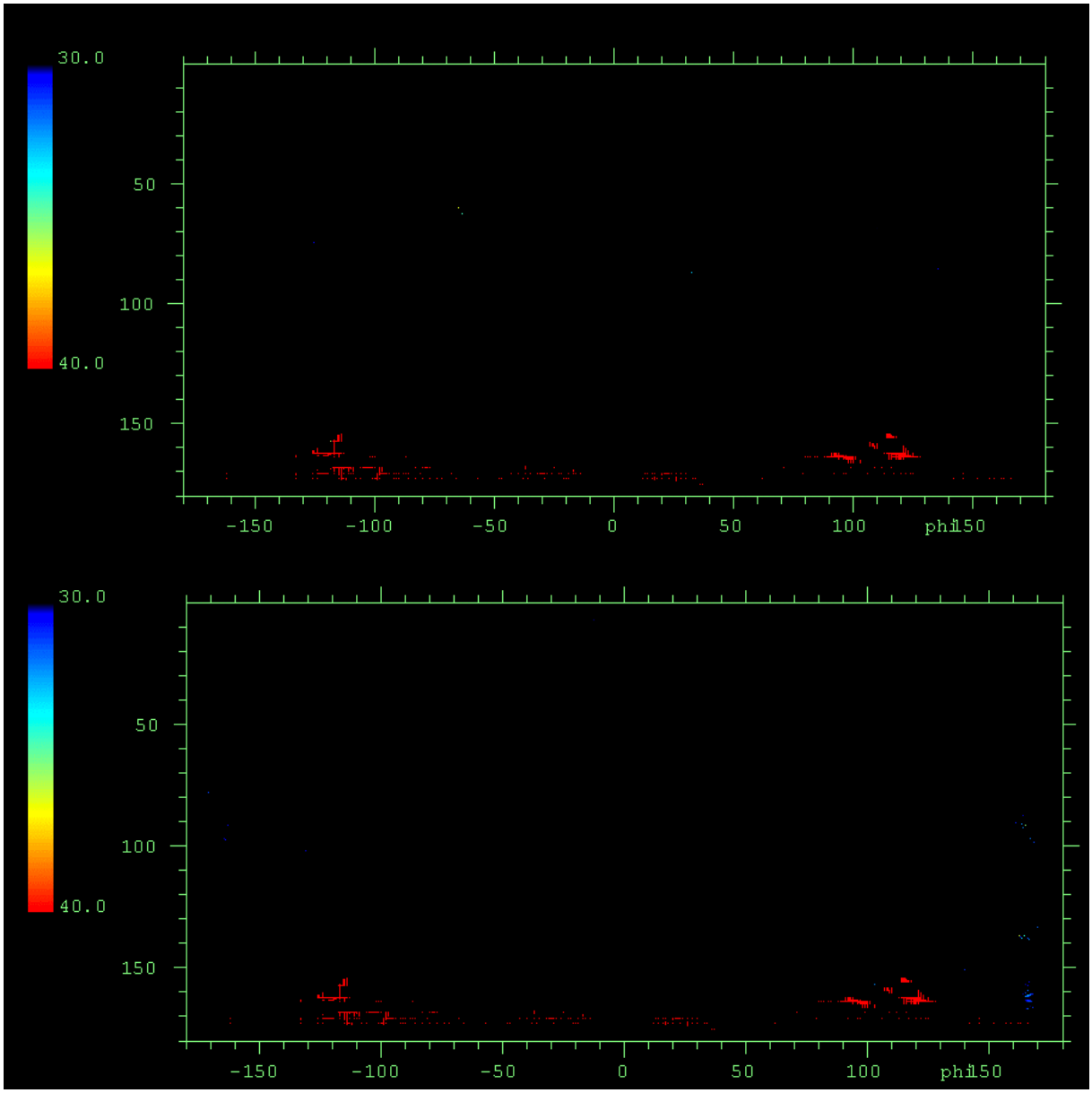

Figure 6.4-1 : local area modified by more than 30 dB (red pixels to be disgarded)

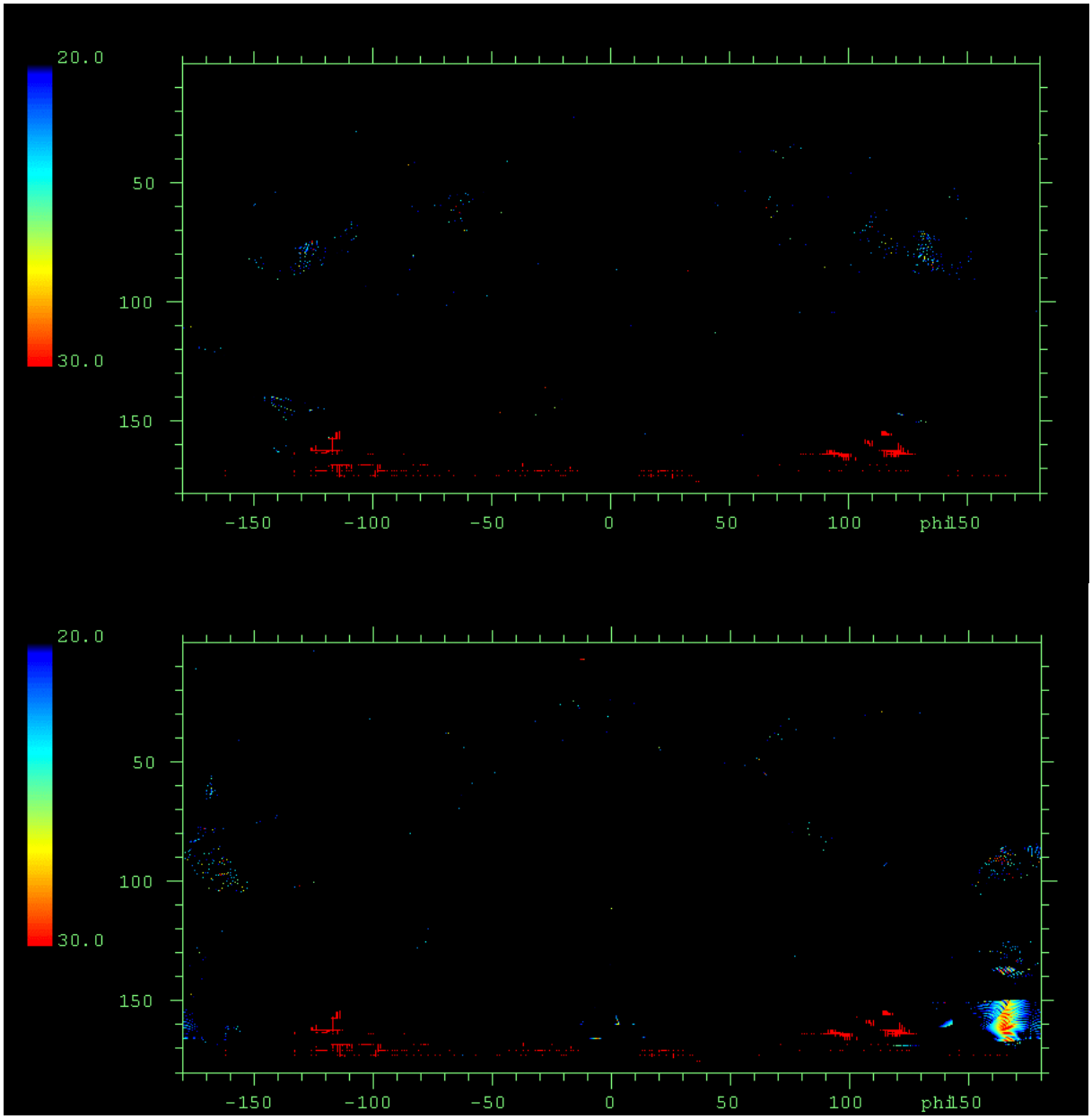

Figure 6.4-2 :local area modified by more than 20 dB (red pixels to be disgarded).

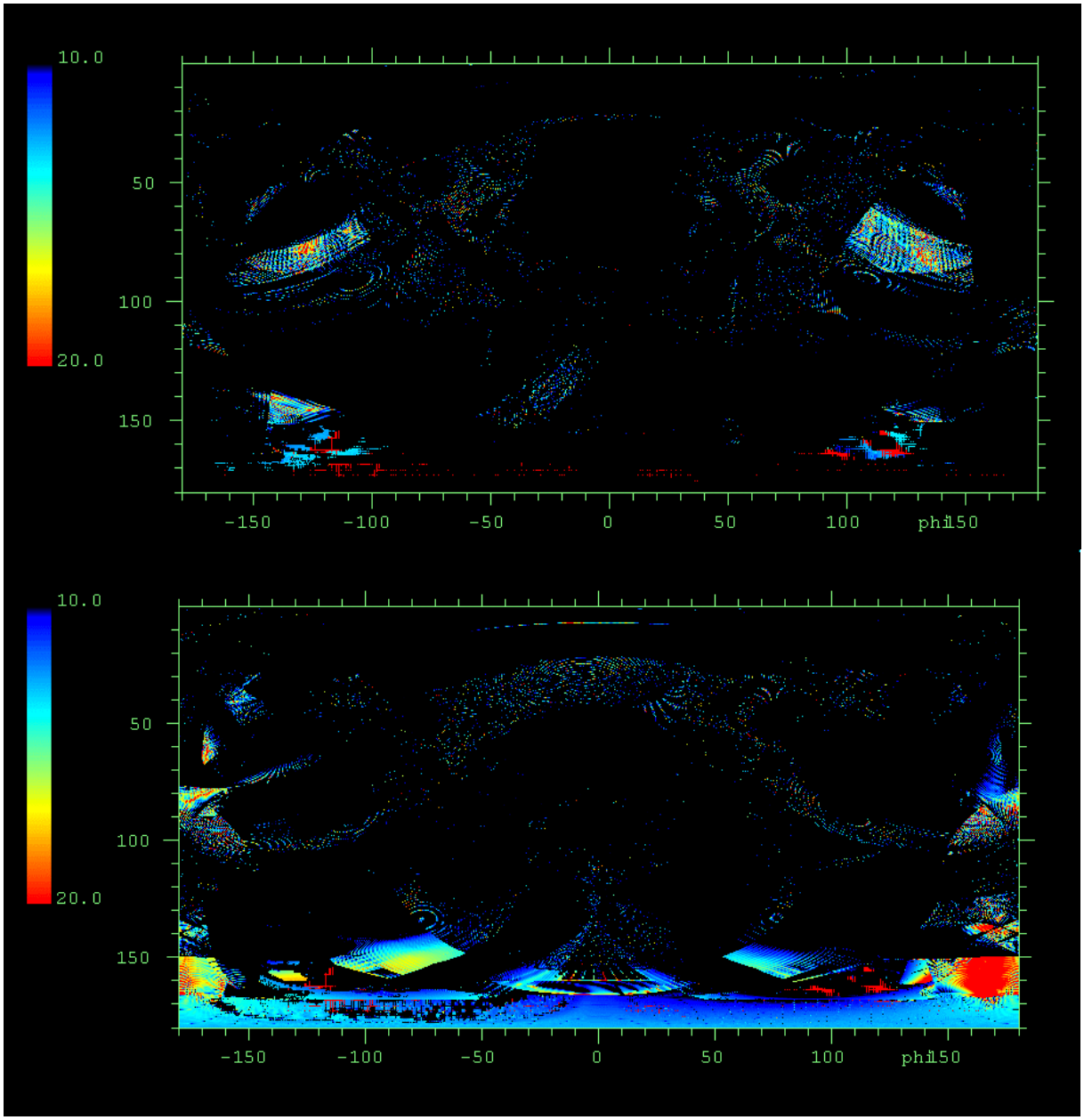

Figure 6.4-3 : local area modified by more than 10 dB and no more than 20 dB (red pixels to be disgarded)

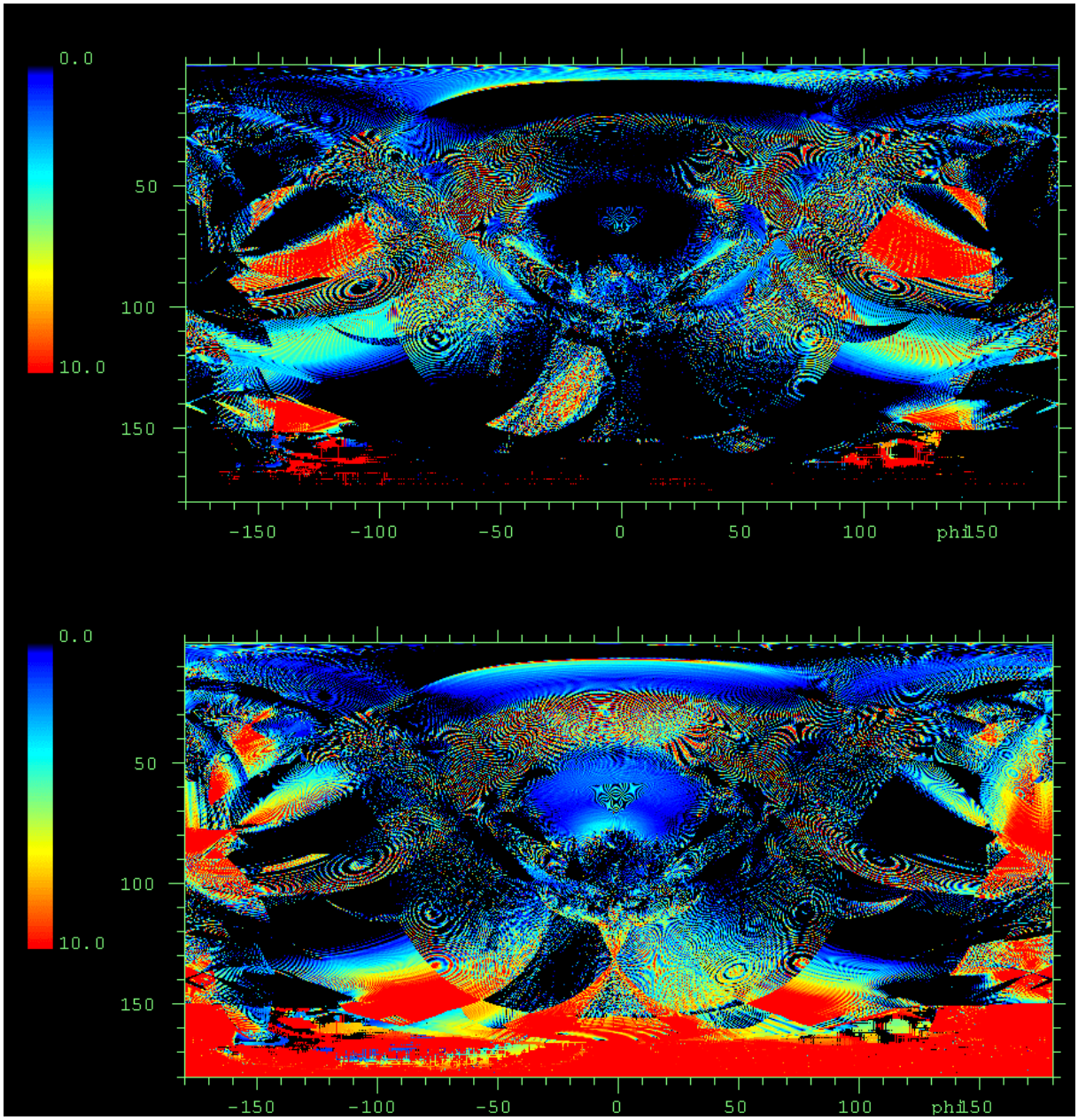

Figure 6.4-4 local area modified by more than 10 dB (red pixels to be disgarded).

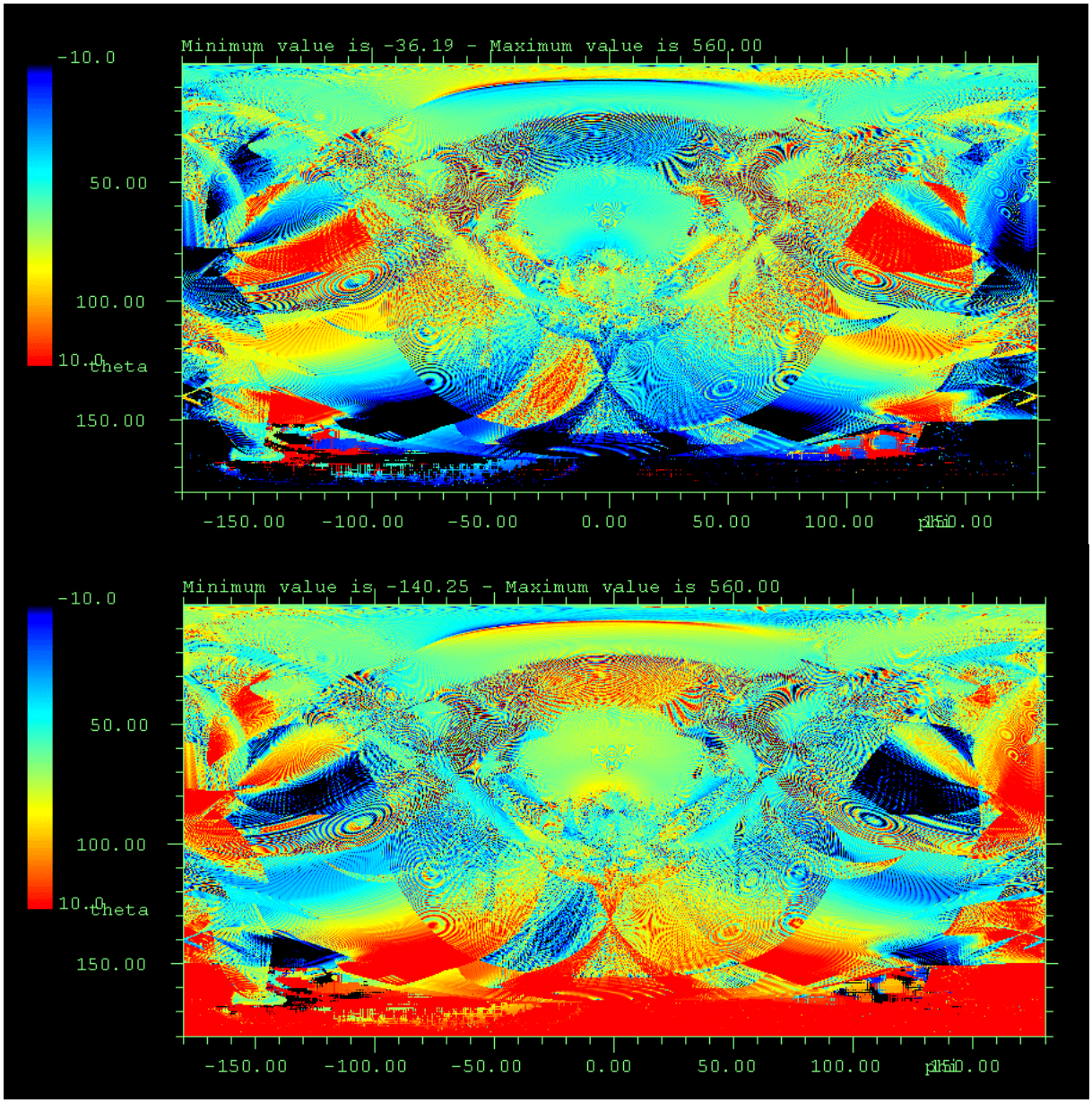

Figure 6.4-5 :local area modified by no more than 10 dB (red pixels to be disgarded).

6.5 353 GHz Pattern analysis(4pi-ext baf-inst feed)

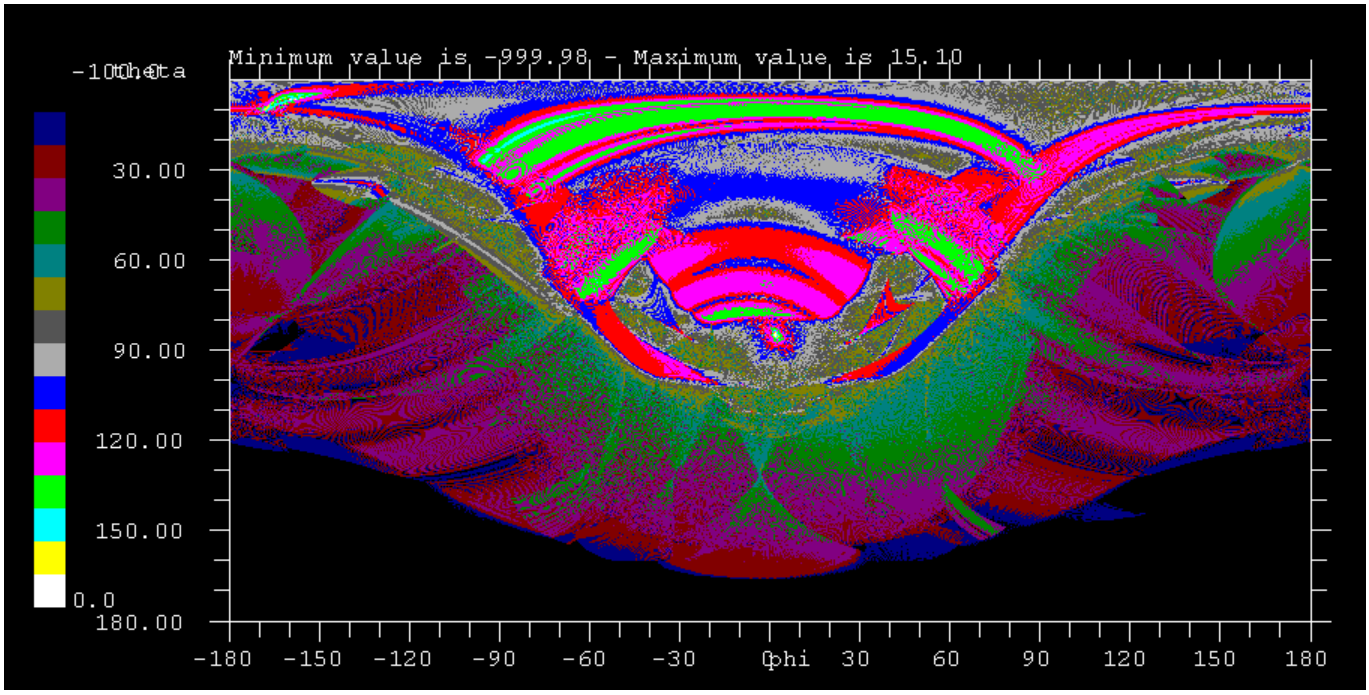

Figure 6.5-1 : 4PI diagram , phi : -180°, 180° / theta : 0,+180° / levels in directivity displayed from -100 dBi to +0 dBi (local major/minor component)

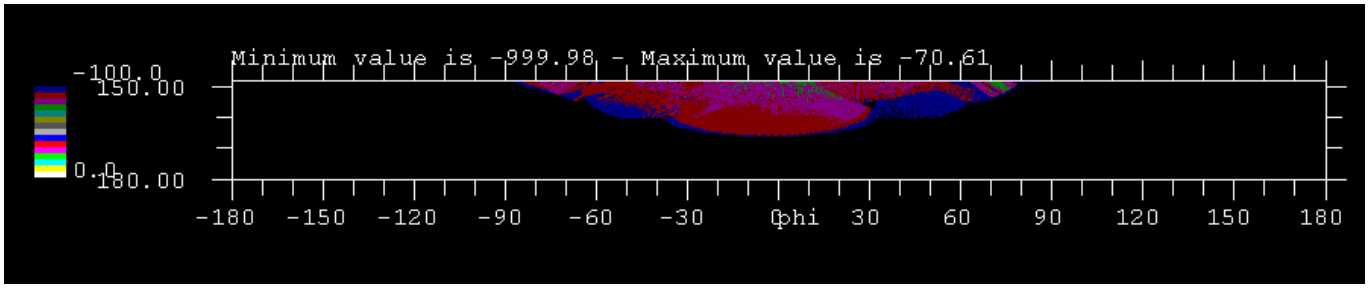

Figure 6.5-2 : Moon area phi : -180°, 180° / theta : +148°,+180° / levels in directivity displayed from -100 dBi to -0 dBi

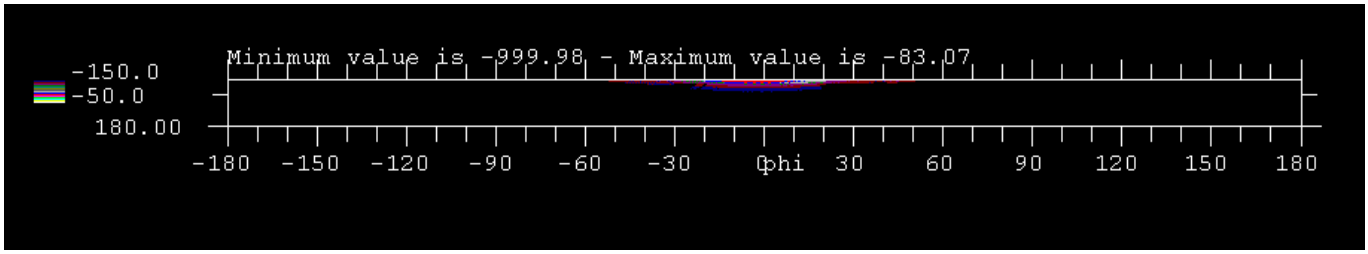

Figure 6.5-3 : Earth area phi : -180°, 180° / theta : +165°,+180° / levels in directivity displayed from -150 dBi to -50dBi (local major/minor component)

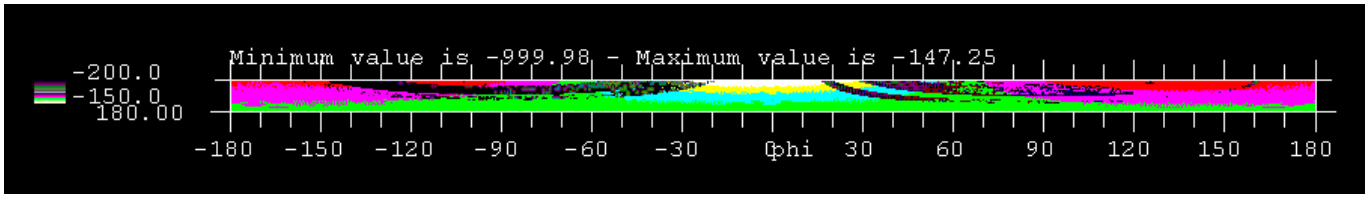

Figure 6.5-4 : Sun area phi : -180°, 180° / theta : +170°,+180° / levels in directivity displayed from -150 dBi to -50dBi (local major/minor component

6.6 FAR OUT SIDE LOBE Performance synthesis (4pi-ext baf-inst feed)

30 GHz					
	Aspect angle (°)	Theta value (°)	EOC directivity (dBi)	On axis max gain (dBi)	Rejection (dB)
Moon	32	148	TBC	50	TBC
Earth	15	165	TBC	50	TBC
Sun	10	170	TBC	50	TBC

100 GHz	feed polarization 1				
	Aspect angle (°)	Theta value (°)	EOC directivity (dBi)	On axis max gain (dBi)	Rejection (dB)
Moon	32	148	-55	61	-116
Earth	15	165	-80	61	-141
Sun	10	170	-137	61	-198

100 GHz	feed polarization 2				
	Aspect angle (°)	Theta value (°)	EOC directivity (dBi)	On axis max gain (dBi)	Rejection (dB)
Moon	32	148	-46	61	-107
Earth	15	165	-67	61	-128
Sun	10	170	-126	61	-187

353 GHz					
	Aspect angle (°)	Theta value (°)	EOC directivity (dBi)	On axis max gain (dBi)	Rejection (dB)
Moon	32	148	-70	69	-139
Earth	15	165	-83	69	-152
Sun	10	170	-147	69	-216

857 GHz					
	Aspect angle (°)	Theta value (°)	EOC directivity (dBi)	On axis max gain (dBi)	Rejection (dB)
Moon	32	148	TBD	TBD	TBD
Earth	15	165	TBD	TBD	TBD
Sun	10	170	TBD	TBD	TBD

Tableau 6.6-1 : performance synthesis.

7. FAR OUT SIDE LOBE PERFORMANCE SYNTHESIS.

7.1 Performance toward Earth Sun and Moon of the Planck Spacecraft with perfect reflector surfaces

The following table shows that a nice margin is obtained for the rejection toward the Earth Sun and Moon for the Planck spacecraft equipped with ideal ellipsoidal reflector with no dust and no moon illumination of the primary.

30 GHz	Rejection (dB)	Rejection (dB)	Rejection (dB)
	wo baffle extension	with baffle extension & gaussian feed	with baffle extension & instrument feed models
Moon	-93	-83	TBC
Earth	-123	-100	TBC
Sun	-147	-136	TBC

100 GHz	Rejection (dB)	Rejection (dB)	Rejection (dB)	Rejection (dB)
	wo baffle extension	with baffle extension & gaussian feed	with baffle extension & instrument feed models polarization 1	with baffle extension & instrument feed models polarization 2
Moon	-118	-107	-116	-107
Earth	-158	-125	-141	-128
Sun	-186	-183	-198	-187

353 GHz	Rejection (dB)	Rejection (dB)	Rejection (dB)
	wo baffle extension	with baffle extension & gaussian feed	with baffle extension & instrument feed models
Moon	-159	-150	-139
Earth	-159	-170	-152
Sun	-159	-234	-216

857 GHz	Rejection (dB)	Rejection (dB)	Rejection (dB)
	wo baffle extension	with baffle extension & gaussian feed	with baffle extension & instrument feed models
Moon	-169	-170	TBD
Earth	-215	-187	TBD
Sun	-278	-259	TBD

Table 7.1-1 : rejection performance synthesis.

7.2 Quilting or Grating lobe impact on the far out side lobe level.

The Annex 1 contains the analysis of the reflector quilting. This analysis has already been broadcasted as answer to a PDR rid in 2002. The quilting is a regular distortion of the reflectors surfaces. This is in fact a regular array of spacing higher than the wavelength hence the grating lobe are recombined in the real angular domain of the pattern. The quilting on the secondary reflector is equivalent to an array as well as the quilting of the primary. Hence it can be found two arrays of grating lobe around each main lobe. The objective of this section is then to assess the impact of the grating lobes on the rejection level toward Earth sun and Moon area.

The following table (7.2-1) displays the levels of the first grating lobe. The results is extracted from the referenced figure provided in the last column. "Not visible" has to be understood as "grating lobe not higher than the nominal side lobe levels".

Firstly it is interesting to observe that the highest the frequency is the highest the grating lobe relative level is.

Then, it has to be noticed the relative level of the grating lobe wrt to the usual side lobe level. Hence at 100 GHz the first grating lobe is hardly visible among the side lobes. This allows to conclude that the second 100 GHz grating lobe will not be visible wrt to the side lobe (same conclusion for the 3rd, the 4th side lobe etc…).

Secondly it is interesting to observe the relative level of the first and second grating lobe level wrt to the main beam maximum. For instance at 353 GHz, the first grating lobe is 45 dB below the maximum gain, the second grating lobe is 100 dB below. This observation allows to deduce that the next grating lobe cannot be visible among the side lobe. The same conclusion can be obtained at 545 GHz where a rule of the thumb for the grating lobe level variation can be established : -45/-50 dB between two grating lobesx of different order. Hence the first one is @-40 dB the second one @-40-50 = @-90 the third one @-90dB - 45 dB = @-135 dB etc etc… The grating lobes relative levels are provided in table 7.2-1.
From this observation the 4th grating lobe at the worst case frequency is expected to be at the same level as the usual side lobe.

The table 7.2-2 and 7.2-3 displays the angular position of the grating lobes. It is interesting to observe as expected by theory that the highest the frequency is, the closest are the grating lobe wrt to the main beam. Hence as a conclusion all the visible grating lobe are located around the main beam (especially at 857 GHz where the 4th grating lobe is located at 3.08 ° away from the main beam). This angular direction is far away the direction of the Earth Sun and Moon.

Hence as a conlusion the grating lobes induced by the reflector quilting have no impact on the rejection performance.

Fequency (GHZ)	1st grating lobe level (dB/max)	2nd grating lobe level (dB/max)	3rd grating lobe level (dB/max)	4th grating lobe level (dB/max)	ref figure
100	not visible	Not visible	not visible	not visible	A9
143	-60	Not visible	not visible	not visible	A10
217	-55	Not visible	not visible	not visible	A13 / A14
353	-45	-100	not visible	not visible	A16 / A17
545	-40	-90	estimated to -135	probably not visible	A19 / A20
857	-35	-75	estimated to -115	probably not visible	A22 /A23

Table 7.2-1 : grating lobes level

Secondary

fequency (GHZ)	1st grating lobe location (°)	2nd grating lobe location (°)	3rd grating lobe location (°)	4th grating lobe location (°)
100	3.68	7.36	11.04	14.72
143	2.55	5.1	7.65	10.2
217	1.67	3.34	5.01	6.68
353	1.034	2.068	3.102	4.136
545	0.67	1.34	2.01	2.68
857	0.434	0.868	1.302	1.736

Table 7.2-2 : angular position of the grating lobe induced by the secondary reflector quilting

Primary

fequency (GHZ)	1st grating lobe location (°)	2nd grating lobe location (°)	3rd grating lobe location (°)	4th grating lobe location (°)
100	6.6	13.2	19.8	26.4
143	4.62	9.24	13.86	18.48
217	3.03	6.06	9.09	12.12
353	1.87	3.74	5.61	7.48
545	1.21	2.42	3.63	4.84
857	0.77	1.54	2.31	3.08

Table 7.2-3 : angular position of the grating lobe induced by the primary reflector quilting

7.3 Impact of dust contamination on the far out side lobe level.

All the details of the dust contamination analysis is provided in [RD 15].

This section presents only the performance budget and details the margins.

The numerical model in [RD 15] is based upon the computation of the BRDF and the BRDF variation with the incident angle. The BRDF values have been computed using a given contamination level as well as a given dust composition (see [RD 15]).

No computation have been performed at 30 GHz as far as the effect is negligible. In addition RF test on the RFDM have shown no impact on the measurement.

857 GHz	directivity		
	Go (dBi)	**BRDFmax**	**Rejection (dB)**
5000 ppm	76.7	3.90E-03	-92.8
7000 ppm	76.7	5.50E-03	-91.3
		BRDF/angle	
MOON (148-85=63°)	76.7	1.00E-04	-108.7
EARTH (165-85=80°)	76.7	6.00E-05	-110.9
SUN (170-85=85°)	76.7	2.00E-05	-115.7

Table 7.3-1 :Rejection level @857 GHz induced by reflector contamination.

Spec (dB)	Margin /spec (dB)	Goal (dB)	Margin / Goal (dB)
-78	30.7	-95	13.7
-85	25.9	-109	1.9
-98	17.7	-122	-6.3

Table 7.3-2 : margin @857 GHz wrt the requirements and the goals.

353 GHz	directivity		
	Go (dBi)	BRDF/max	Rejection (dB)
5000 ppm	69.7	1.48E-03	-90.0
7000 ppm	69.7	1.48E-03	-90.0
		BRDF/angle	
MOON (148-85=63°)	69.7	7.40E-05	-103.0
EARTH (165-85=80°)	69.7	1.78E-04	-99.2
SUN (170-85=85°)	69.7	2.66E-04	-97.5

Table 7.3-3 : Rejection level @353 GHz induced by reflector contamination.

Spec (dB)	Margin /spec (dB)	Goal (dB)	Margin / Goal (dB)
-72	31.0	-81	22.0
-79	20.2	-95	4.2
-92	5.5	-108	-10.5

Table 7.3-4 : margin @353 GHz wrt the requirements and the goals.

100 GHz	directivity		
	G0	BRDF/max	Rejection (dB)
5000 ppm	61.7	2.30E-04	-90.1
7000 ppm	61.7	2.30E-04	-90.1
		BRDF/angle	
MOON (148-85=63°)	61.7	1.15E-05	-103.1
EARTH (165-85=80°)	61.7	2.76E-05	-99.3
SUN (170-85=85°)	61.7	4.14E-05	-97.5

Table 7.3-5 Rejection level @100 GHz induced by reflector contamination.

Spec (dB)	Margin /spec (dB)	Goal (dB)	Margin / Goal (dB)
-72	31.1	-81	22.1
-79	20.3	-95	4.3
-92	5.5	-108	-10.5

Table 7.3-6 : margin @100 GHz wrt the requirements and the goals.

Hence the rejection performance toward the Earth, Sun and Moon direction remains below the requirement at all frequencies but not below the goals. Anyhow the dust model is conservative.

7.4 Impact of diffusion by primary reflector on the far out side lobe levels.

This section summarizes the computation of the effective antenna temperature by using the same method as the one used by the Wilkinson MAP engineering team.The effective antenna temperature is dependant of the particles composition as well as the particles shape and size. In this section the particle composition is the same as the one used for the dust contamination analysis. The end of life contamination level is taken as 7000 ppm as a worst case.

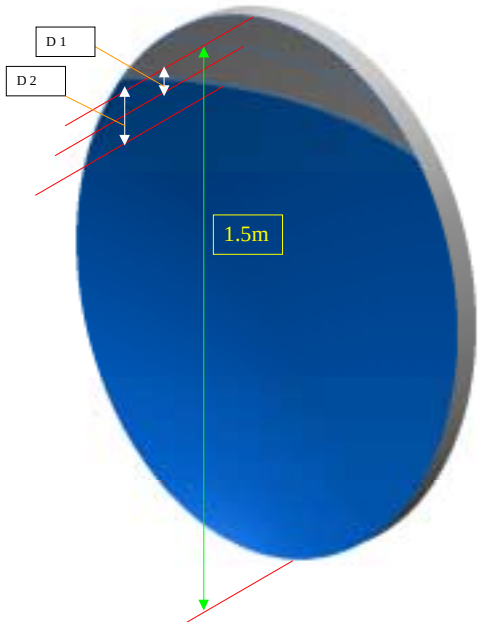

Figure 7.4-1 :Planck reflector illuminated area

The analysis summary displayed in this section shows that the noise induced by the diffusion of the particles on the primary reflector surface is negligible using the proposed method of MAP. This is due to the relative small illuminated surface as well as to the low coupling factor with the detector. Anyhow the main contribution is strongly dependant on the nature of the particles. But even in the extreme case where the particle composition would be made of 100% of graphite, the effective antenna temperature would remain below 1 µK.

The following table summarizes all the computed effective antenna temperature for a classical particle composition.

Spheres of 10.5 micro meter diameter				
f(GHz)	30	100	353	857
T(Micro_K)	6.94E-18	6.99E-16	8.20E-14	2.61E-12

Needles of 20 * 100 micro meter diameter				
f(GHz)	30	100	353	857
T(Micro_K)	9.32E-15	5.89E-13	4.42E-11	9.24E-10

Table 7.4-1 : summary of effective antenna temperature.

The particle nature impact is significant but the final results remain well below 1 µK even if the primary reflector is contaminated by 7000 ppm end of life (graphite particle only).

All technical detail of the analysis summarized in this section can be found in RD 14.

As a conclusion the primary reflector diffusion when illuminated by the Moon has a neglectable impact on the required rejection.

7.5 Final performance rejection toward Earth Sun and Moon.

The following table synthesizes all contributors to the rejection modification. The nominal performance is the one of the Planck spacecraft with ideal reflector, the baffle extension and the gaussian feed model. This nominal performance is degraded by different contributor. In fact the only contributor of importance is the dust contamination at the highest frequency. The far out side lobe are then dominated by the dust effect. In the following table the total rejection is obtained as the maximum of the different rejection computd alone (ie total rejection = max (rejection with no dust , rejection from dust model). As a conclusion, positive margin are obtained at all frequencies wrt the requirement whereas small negative margin is observed for the Sun for the comparison with the goals.

30 GHz

	Rejection with no dust (dB)	Rejection from dust model	Rejection from grating lobes	Rejection from primary diffusion	Total rejection (dB)	Rejection requirement (dB)	Rejection goal (dB)	Margin / requirement (dB)	Margin / goal (dB)
Moon	-83	NA	NA	NA	-83	-71	NA	12	NA
Earth	-100	NA	NA	NA	-100	-78	NA	22	NA
Sun	-136	NA	NA	NA	-136	-91	NA	45	NA

100 GHz

	Rejection with no dust (dB)	Rejection from dust model	Rejection from grating lobes	Rejection from primary diffusion	Total rejection (dB)	Rejection requirement (dB)	Rejection goal (dB)	Margin / requirement (dB)	Margin / goal (dB)
Moon	-107	-103	NA	NA	-103	-71.5	-73	32	30
Earth	-125	-99	NA	NA	-99	-78.5	-86	21	13
Sun	-183	-98	NA	NA	-98	-91.5	-99	6	-1

353 GHz

	Rejection with no dust (dB)	Rejection from dust model	Rejection from grating lobes	Rejection from primary diffusion	Total rejection (dB)	Rejection requirement (dB)	Rejection goal (dB)	Margin / requirement (dB)	Margin / goal (dB)
Moon	-150	-103	NA	NA	-103	-72	-81	31	22
Earth	-170	-99	NA	NA	-99	-79	-95	20	4
Sun	-234	-97	NA	NA	-97	-92	-108	5	-11

857 GHz

	Rejection with no dust (dB)	Rejection from dust model	Rejection from grating lobes	Rejection from primary diffusion	Total rejection (dB)	Rejection requirement (dB)	Rejection goal (dB)	Margin / requirement (dB)	Margin / goal (dB)
Moon	-170	-109	NA	NA	-109	-78	-95	31	14
Earth	-187	-111	NA	NA	-111	-85	-109	26	2
Sun	-259	-116	NA	NA	-116	-98	-122	18	-6

Table 7.5-1 : Final performance rejection comparison wrt to the requirements and the goals.

8. MAIN LOBE PERFORMANCE ANALYSIS

8.1 Introduction

The purpose of this chapter is to establish the Planck Telescope RF Performance analysis for the main lobe.

-In the first part the hypotheses and the input data used to perform the analysis are reviewed : telescope geometry, feed definitions, orientation and positions.

-In the second part, the hypotheses, the method of analysis applied for main lobes simulation is presented as well as discussions on convergency and on the performance estimation.

-The third part concerns the description of the RF budget which is based on 2 types of data : deterministic and random. The origin of the data corresponding to these two types is given.

-The fourth part gives the final bugdet of the telescope.

8.2 Hypotheses and data used for RF Budget

8.2.1 Planck telescope geometry

The geometry of the telescope is shown in Figure 8.2-1 and is the one referenced in [AD 2]. The telescope is composed of two reflectors in a gregorian off-axis configuration. The OM1 (M1), OM2 (M2) and ORDP (RDP) coordinates systems are defined in [AD 2]. M1 and M2 are located in the vertex of the ellipsoids and the RDP is the coordinate system of the FPU (Focal Plane Unit). Two additionnal coordinate systems OM1C and OM2C are introduced and are the coordinates systems associated with the mechanical interface of the reflectors and are defined in [RD 12].

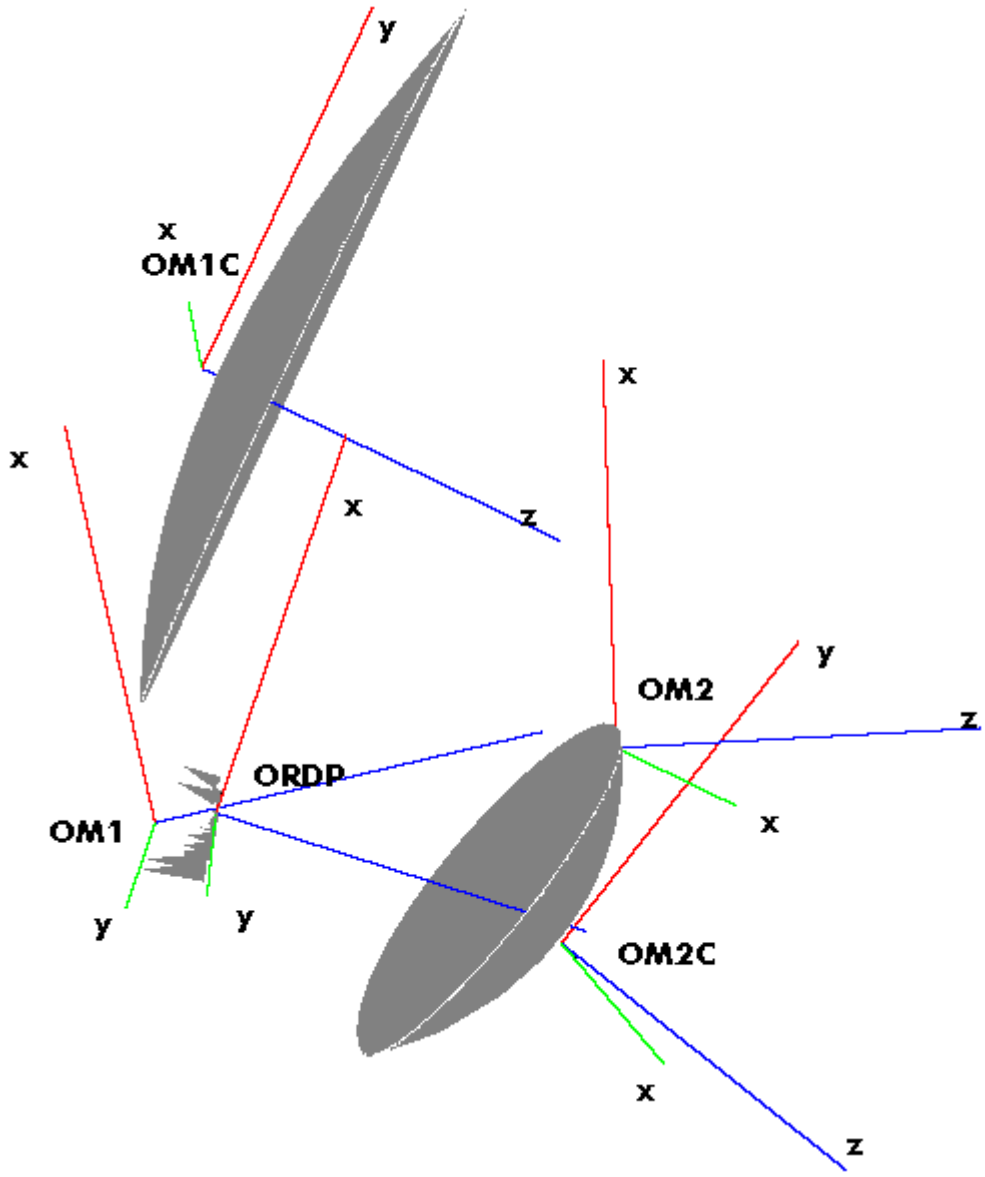

Figure 8.2-8.2-1: Planck Telescope coordinate systems

8.2.2 Horns definition

The FPU (focal plane unit) is composed of two type of horns : LFI (low frequency instruments) and HFI (High frequency instruments). The HFI horns are placed at the center of the FPU and are surrounded by the LFI horns.
The operating frequency of the horns is defined by their center frequency. LFI includes third types of horns defined by their central frequencies : 30, 44 and 70 and HFI includes six types defined by their center frequencies : 100, 143, 217, 353, 545 and 857 GHz.

For the analysis of the Planck performance, the feed model used is a gaussian beam defined by a far-field taper (apodisation) as given in Table 2-1 (extracted from [AD 2]).

Frequency	Angle 30 dB from Peak (°)
30 GHz (LFI-30-27 to LFI-30-28)	23.6
44 GHz (LFI-44-23 to LFI-44-26)	23.6
70 GHz (LFI-70-18 to LFI-70-22)	21.9
100 GHz (HFI-100-1 to HFI_100_4)	26.8
143 GHz (HFI-143-1 to HFI_100_8)	23.7
217 GHz (HFI-217-1 to HFI_100_8)	21.8
353 GHz (HFI-353-1 to HFI_353_8)	19.4
545 GHz (HFI-545-1 to HFI_545_4)	19.4
857 GHz (HFI-857-1 to HFI_857_4)	19.4

Table 8.2-1 Taper of Horns

These feeds are then directly defined in the Grasp8 model.

8.2.3 Horns position in the ORDP plane

The horns defined in the former section are accommodated in the FPU in a given way. The data concerning the location and orientation of the horns is provided by the instrument teams.

8.2.3.1 LFI Horns

The horns positions used for the analysis are the ones given in [AD 2] (see Table 8.2-2). 11 detectors defined by their center working frequency between 30 GHz to 70 GHz. The phase center at the location given by (X_{rdp}, Y_{rdp}, Z_{rdp}) . The local X_axis, Y_axis, Z_axis vector are expresse with the cosine directors.

				X_axis			Y_axis			Z_axis			
Detectors	**Xrdp**	**Yrdp**	**Zrdp**	**Ux**	**Uy**	**Uz**	**Ux**	**Uy**	**Uz**	**Ux**	**Uy**	**Uz**	**frequency**
N#	**mm**	**mm**	**mm**										**GHz**
LFI_70_18	-76.38	-69.37	14.54	0.936379	0.299574	-0.182891	-0.320318	0.942398	-0.096346	0.143494	0.1488	0.978401	70
LFI_70_19	-92.41	-43.29	18.66	0.922853	0.32965	-0.19918	-0.342171	0.939123	-0.031084	0.176808	0.096839	0.97947	70
LFI_70_20	-101.86	-17.69	20.86	0.912768	0.359322	-0.194275	-0.359717	0.932423	0.034501	0.193544	0.038393	0.98034	70
LFI_70_21	-101.86	17.69	20.86	0.912768	-0.359322	-0.194275	0.359717	0.932423	-0.034501	0.193544	-0.038393	0.98034	70
LFI_70_22	-92.41	43.29	18.66	0.922853	-0.32965	-0.19918	0.342171	0.939123	0.031084	0.176808	-0.096839	0.97947	70
LFI_70_23	-76.38	69.37	14.54	0.936379	-0.299574	-0.182891	0.320318	0.942398	0.096346	0.143494	-0.1488	0.978401	70
LFI_44_24	-138.41	0.	21.29	0.9666	0.0	-0.256289	0.	1.	0.	0.256289	0.	0.9666	44
LFI_44_25	55.32	133.27	-17.90	-0.262536	-0.923175	-0.280755	0.958343	-0.283384	0.035667	-0.112488	-0.259696	0.959117	44
LFI_44_26	55.32	-133.27	-17.90	-0.262536	0.923175	-0.280755	-0.958343	-0.283384	-0.035667	-0.112488	0.259696	0.959117	44
LFI_30_27	-136.95	54.94	18.60	0.910601	-0.314901	-0.267661	0.331426	0.943315	0.017731	0.246905	-0.104856	0.96335	30
LFI_30_28	-136.95	-54.94	18.60	0.910601	0.314901	-0.267661	-0.331426	0.943315	-0.017731	0.246905	0.104856	0.96335	30

Table 8.2-2 : LFI Horns positions and orientations

The overview of the LFI horns is shown in the Figure 8.2-2.

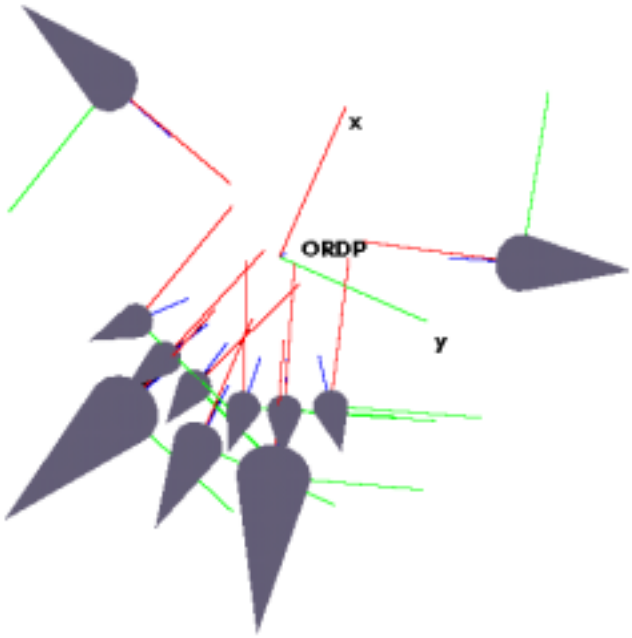

Figure 8.2-2 : LFI horns in the ORDP plane

8.2.3.2 HFI Horns

The position of the horns is provided by HFI team. The HFI instrument is composed of 36 detectors working in the center frequency range of 100 GHz to 847 GHz. The positions of the horns are given in the RDP coordinate system (X_{rdp}, Y_{rdpf}, Z_{rdp}) (see Table 8.2-3) the orientation of the horns at the date of the simulation is not fixed (ψ angle) , and for the need of the simulation is set arbitrarily at zero.

				X_axis			Y_axis			Z_axis			
Detectors	Xrdp	Yrdp	Zrdp	Ux	Uy	Uz	Ux	Uy	Uz	Ux	Uy	Uz	frequency
N#	mm	mm	mm										GHz
HFI_100_1	-47.57	-32.966	14.847	0.995407	-0.003320	-0.095675	-0.003320	0.997600	-0.069161	0.095675	0.069161	0.993007	100
HFI_100_2	-55.114	-10.622	16.831	0.993785	-0.001245	-0.111314	-0.001245	0.999750	-0.022304	0.111314	0.022304	0.993535	100
HFI_100_3	-55.114	10.622	16.831	0.993785	0.001245	-0.111314	0.001245	0.999750	0.022304	0.111314	-0.022304	0.993535	100
HFI_100_4	-47.57	32.966	14.847	0.995407	0.003320	-0.095675	0.003320	0.997600	0.069161	0.095675	-0.069161	0.993007	100
HFI_143_1	33.184	-39.106	-1.28	0.997576	0.002875	0.069528	0.002875	0.996591	-0.082449	-0.069528	0.082449	0.994167	143
HFI_143_2	35.142	-16.019	-0.572	0.997306	0.001247	0.073346	0.001247	0.999423	-0.033937	-0.073346	0.033937	0.996729	143
HFI_143_3	34.424	16.013	-0.39	0.997415	-0.001221	0.071848	-0.001221	0.999423	0.033940	-0.071848	-0.033940	0.996838	143
HFI_143_4	33.912	41.141	-1.613	0.997466	-0.003090	0.071078	-0.003090	0.996232	0.086673	-0.071078	-0.086673	0.993698	143
HFI_143_5	48.96	-32.843	-4.919	0.994759	0.003545	0.102182	0.003545	0.997603	-0.069112	-0.102182	0.069112	0.992362	143
HFI_143_6	50.593	-8.581	-4.455	0.994421	0.000958	0.105483	0.000958	0.999835	-0.018119	-0.105483	0.018119	0.994256	143
HFI_143_7	49.882	8.578	-4.263	0.994576	-0.000945	0.104011	-0.000945	0.999835	0.018122	-0.104011	-0.018122	0.994411	143
HFI_143_8	49.672	32.856	-5.108	0.994608	-0.003596	0.103642	-0.003596	0.997602	0.069120	-0.103642	-0.069120	0.992210	143
HFI_217_1	-31.18	-27.749	12.776	0.997992	-0.001858	-0.063313	-0.001858	0.998281	-0.058579	0.063313	0.058579	0.996273	217
HFI_217_2	-29.527	-8.754	13.236	0.998168	-0.000561	-0.060502	-0.000561	0.999828	-0.018533	0.060502	0.018533	0.997996	217
HFI_217_3	-30.307	8.752	13.362	0.998071	0.000576	-0.062081	0.000576	0.999828	0.018535	0.062081	-0.018535	0.997899	217
HFI_217_4	-30.399	27.756	12.651	0.998090	0.001813	-0.061746	0.001813	0.998280	0.058603	0.061746	-0.058603	0.996370	217
HFI_217_5	-16.174	-34.288	9.791	0.999467	-0.001184	-0.032614	-0.001184	0.997369	-0.072487	0.032614	0.072487	0.996836	217
HFI_217_6	-14.291	-15.164	10.422	0.999569	-0.000473	-0.029368	-0.000473	0.999481	-0.032197	0.029368	0.032197	0.999050	217
HFI_217_7	-15.051	15.16	10.563	0.999522	0.000498	-0.030916	0.000498	0.999482	0.032174	0.030916	-0.032174	0.999004	217
HFI_217_8	-15.412	34.298	9.651	0.999517	0.001128	-0.031062	0.001128	0.997367	0.072508	0.031062	-0.072508	0.996884	217
HFI_353_1	-3.268	-58.369	5.117	0.999987	-0.000308	-0.005009	-0.000308	0.992474	-0.122458	0.005009	0.122458	0.992461	353
HFI_353_2	-0.512	-39.964	6.325	1.000000	-0.000011	-0.000262	-0.000011	0.996427	-0.084458	0.000262	0.084458	0.996427	353
HFI_353_3	-0.073	-23.141	7.308	1.000000	0.000003	0.000122	0.000003	0.998792	-0.049138	-0.000122	0.049138	0.998792	353
HFI_353_4	1.231	-5.905	7.552	0.999997	0.000016	0.002562	0.000016	0.999921	-0.012547	-0.002562	0.012547	0.999918	353
HFI_353_5	0.409	10.332	7.649	1.000000	-0.000010	0.000908	-0.000010	0.999758	0.021980	-0.000908	-0.021980	0.999758	353
HFI_353_6	0.451	27.097	6.996	0.999999	-0.000038	0.001309	-0.000038	0.998347	0.057477	-0.001309	-0.057477	0.998346	353
HFI_353_7	-1.536	42.928	6.29	0.999997	0.000101	-0.002234	0.000101	0.995885	0.090631	0.002234	-0.090631	0.995882	353
HFI_353_8	-2.513	58.387	4.964	0.999994	0.000212	-0.003456	0.000212	0.992469	0.122496	0.003456	-0.122496	0.992463	353
HFI_545_1	12.049	-58.768	1.867	0.999650	0.001635	0.026421	0.001635	0.992370	-0.123281	-0.026421	0.123281	0.992020	545
HFI_545_2	14.698	-40.242	3.022	0.999512	0.001329	0.031201	0.001329	0.996378	-0.085027	-0.031201	0.085027	0.995890	545
HFI_545_3	13.702	43.225	3.004	0.999572	-0.001337	0.029230	-0.001337	0.995828	0.091238	-0.029230	-0.091238	0.995400	545
HFI_545_4	12.784	58.788	1.703	0.999609	-0.001729	0.027922	-0.001729	0.992366	0.123312	-0.027922	-0.123312	0.991975	545
HFI_857_1	15.072	-23.799	3.974	0.999501	0.000798	0.031581	0.000798	0.998724	-0.050492	-0.031581	0.050492	0.998225	857
HFI_857_2	16.357	-6.442	4.207	0.999420	0.000233	0.034060	0.000233	0.999906	-0.013691	-0.034060	0.013691	0.999326	857
HFI_857_3	15.568	9.909	4.332	0.999474	-0.000342	0.032430	-0.000342	0.999778	0.021065	-0.032430	-0.021065	0.999252	857
HFI_857_4	15.617	27.287	3.672	0.999462	-0.000950	0.032788	-0.000950	0.998324	0.057862	-0.032788	-0.057862	0.997786	857

Table 8.2-3 Positions of HFI horns

In Figure 8.2-3 and 8.2-4, the overview the the HFI horns in the focal plane is shown.

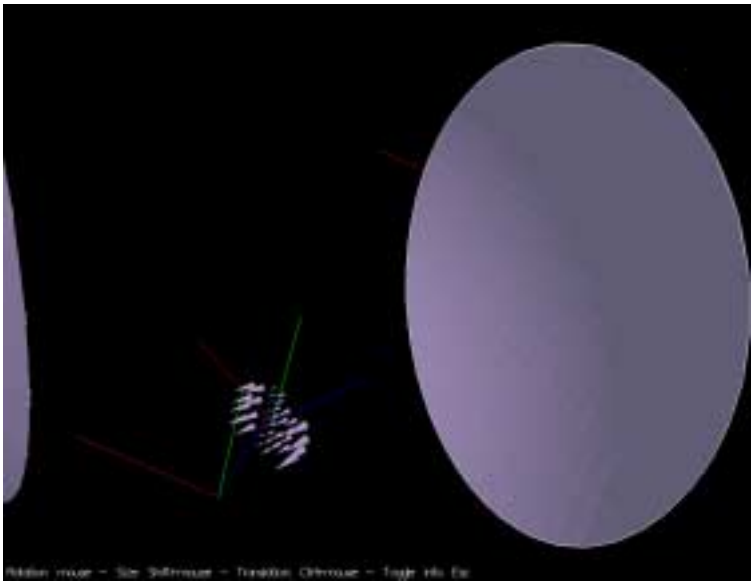

Figure 8.2-3: HFI horns in the ORDP plane

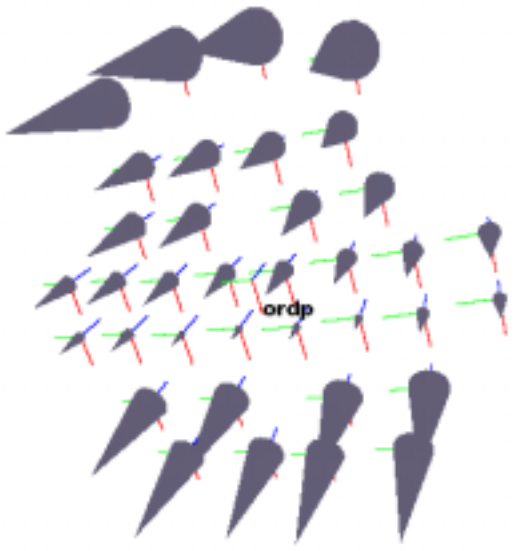

Figure 8.2-4 Detectors view in the focal Plane

8.3 Main lobes computation

8.3.1 introduction

The telescope performance evaluation is defined in term of main lobe gain degradation. In order to reach the requirements verification, the computation of the gain must be achieved with a sufficient accuracy. The gain degradation evaluation is based on different type of inputs (displacement of the reflector and feeds, distorsion of the surface ….). In order to achieve the computation with a given accuracy and with a reasonnable computation time, the convergency parameters and the method of analysis must be optimized. These last points are detailed in the following sections.

8.3.2 Requirements

The requirements for the Planck telescope performance is given in [AD 2].

Frequency	Max reduction in gain
GHz	dB
30	0,5
44	0,5
70	0,5
100	0,5
143	0,5
217	1
353	1
545	1,4
857	2,5

Figure 8.3-1 Telescope specifications: Gain degradation

PTPE-035 The telescope shall achieve a Gain at the defined position of the detectors and operational conditions that does not reduce the theoretical value by more than see table Figure 2-5)

8.3.3 Assessment in terms of directivity degradation

Directivity degradation :

The horns are placed in the focal plane but not at the focus point. As a consequence, according to the usual definition of the crosspol, the copol direction is given by the feed horn polarisation. Hence in order to obtain the diagram in copol and crosspol, the coordinate system of the uv pattern of the telescope main lobe grid must be calculated for each horn and each displacement. So as to avoid this additionnal computation which could become heavy with regards to the number of detectors and displacements to analyse, the directivity degradation is computed through the power diagram.

The term E_x given by Grasp8 is normalized to a square root of power ($P = |E|^2$).

Component 1:

$$|E_1| = \sqrt{{E_{1r}}^2 + {E_{1i}}^2}$$

Component 2 :

$$|E_2| = \sqrt{{E_{2r}}^2 + {E_{2i}}^2}$$

directivity in term of principal component

$$D_{dB} = 20\log_{10}(\sqrt{|E_1|^2 + |E_2|^2})$$

8.3.4 Simulation Tool

For the computation of the RF performance, a method of simulation with a good accuracy must be choosen because the model must be sensitive enough to asses impact of small disturbances. In fact, the contributors to the performance degradation have a small magnitude. More precisely, the computation will have to take into account small displacements (translations and rotations) and surface deformations of small amplitude (of order of a few microns).

As long as small disturbances could have a great impact on directivity, it is necessary to be sure of the numerical convergence of the results. For instance, according to the Ruze formula at 857 GHz few microns of surface error could have a large impact in directivity degradation :

delta rms	delta directivity (dB)
1	0,005
2	0,02
3	0,05
4	0,09
5	0,14
6	0,20
7	0,27

Table 8.3-1 : Surface error (µm rms) and gain degradation by Ruze

Thus, in order to have enough sensitivity in directivity, one must be able to quantify gain variation less than 0.01 dB.

Two type of data have to be considered : Impact of BFE displacement (rotation, translation conicity and radius variations) and surface errors on the reflectors:

8.3.4.1 Main lobe and displacement computation

There are two ways to simulate the telescope performance : MGTD (multi-geometrical-theory of diffraction) and PO (physical optics) or an hybird combination of the two methods. In the case of main lobe computation the use of PO is more accurate but time consuming even if a the pattern grid is reduced and centered just around on the main beam maximum. In the frame of determining the reflector surface discretization parameters for physical optics, a convergence study on the directivity computation have been performed with an accuracy better than 0.01 dB.
Generally used for fast computation away from the main lobes, full MGTD method is not correct for main lobe computation because of caustic problem. Anyway, it is possible to use MGTD on the subreflector and PO on the main reflector.
The advantage ofthe hybrid method is to be faster than the full PO and this approach will gain in accuracy as long as the theory of geometrical diffraction is based on higher frequency approximation.

A preliminary comparison study is summarised in the Table 8.3-2 below for LFI and HFI horns. The comparison between the two computations mgtd - PO (Reflection on the sub and PO on the main) and PO-PO is shown in Table 8.3-2.. The last column provides the difference in directivity in dB.

One can notice that at higher frequencies there is no difference in directivity (less than 0.006 dB up to 100 GHz). At lower frequencies the difference remains small , around 0.024 dB at 30 GHz, 0.022 dB at 44 GHz and 0.012 dB at 70 GHz). These results are in line with the fact that GTD method is accurate at high

frequences. Thus, the case of perfect reflectors, MGTD with PO could be used for the computation of the impact of displacement at higher frequencies.

8.3.4.2 Impact of deformation on surface

When the surface distortions have to be taken into account, full PO computation must be chosen as it is the only way to take into account the deformation and the distorsion on the surface. This means that the surface must initially be represented in term of surface distorsion.
The different method are :

- -to create a surface of points representative of the surface
- -to expand the deformation in term of Zernike polynomials for small spatial frequency
- -to generate a distorsion file which will be added to the perfect surface

The choice of the method is driven by the knowledge of deformations. If a cloud of points is used to represent the surface, the discretisation must be dense enough to avoid additionnal grating lobes. These latter could occur if the deformation magnitude is significant. Obviously, a compromise must be found with regards to the accuracy and computation time.

The other manner to represent the deformations on the reflectors is to use a basis functions expansion in Zernike polynomials. In that case one must assumes a sufficient number of functions to represent accurately the surface deformation. This method could not be applied for deformations which have a high spatial periodicity as quilting and random surface errors.

detector	GTD-PO	PO-PO	delta G
LFI_70_18	57,2117	57,2209	-0,0092
LFI_70_19	57,3694	57,3820	-0,0126
LFI_70_20	57,4513	57,4629	-0,0117
LFI_70_21	57,4513	57,4629	-0,0117
LFI_70_22	57,3694	57,3820	-0,0126
LFI_70_23	57,2117	57,2205	-0,0088
LFI_44_24	54,2521	54,2739	-0,0217
LFI_44_25	52,4603	52,4583	0,0020
LFI_44_26	52,4603	52,4583	0,0020
LFI_30_27	50,9666	50,9898	-0,0232
LFI_30_28	50,9666	50,9898	-0,0232
HFI_100_1	61,5997	61,6052	-0,0056
HFI_100_2	61,6568	61,6627	-0,0059
HFI_100_3	61,6568	61,6627	-0,0059
HFI_100_4	61,5997	61,6052	-0,0056
HFI_143_1	63,3077	63,3124	-0,0046
HFI_143_2	63,3577	63,3624	-0,0047
HFI_143_3	63,3654	63,3695	-0,0041
HFI_143_4	63,2852	63,2876	-0,0024
HFI_143_5	63,1215	63,1234	-0,0019
HFI_143_6	63,1942	63,1973	-0,0031
HFI_143_7	63,2046	63,2087	-0,0040
HFI_143_8	63,1083	63,1104	-0,0021
HFI_217_1	66,7002	66,7007	-0,0005
HFI_217_2	66,7143	66,7157	-0,0014
HFI_217_3	66,7186	66,7210	-0,0024
HFI_217_4	66,6984	66,6997	-0,0013
HFI_217_5	66,6210	66,6231	-0,0020
HFI_217_6	66,6246	66,6260	-0,0014
HFI_217_7	66,6289	66,6295	-0,0006
HFI_217_8	66,6173	66,6190	-0,0018
HFI_353_1	69,2531	69,2474	0,0057
HFI_353_2	69,6751	69,6708	0,0043
HFI_353_3	69,7500	69,7470	0,0031
HFI_353_4	69,7265	69,7246	0,0019
HFI_353_5	69,7339	69,7341	-0,0002
HFI_353_6	69,7432	69,7409	0,0023
HFI_353_7	69,6462	69,6429	0,0034
HFI_353_8	69,2464	69,2408	0,0055
HFI_545_1	71,8578	71,8516	0,0062
HFI_545_2	72,9061	72,9011	0,0050
HFI_545_3	72,8181	72,8126	0,0055
HFI_545_4	71,8342	71,8288	0,0053
HFI_857_1	76,6257	76,6232	0,0025
HFI_857_2	76,6672	76,6642	0,0031
HFI_857_3	76,6807	76,6769	0,0038
HFI_857_4	76,5524	76,5492	0,0032

Table 8.3-2 Convergence between PO-PO and MGTD (reflection)-PO

8.3.5 LFI radiation pattern

The radiation patterns for LFI horns are shown in Figure 8.3-2. The contour levels correspond to -3 dB below the maximum.

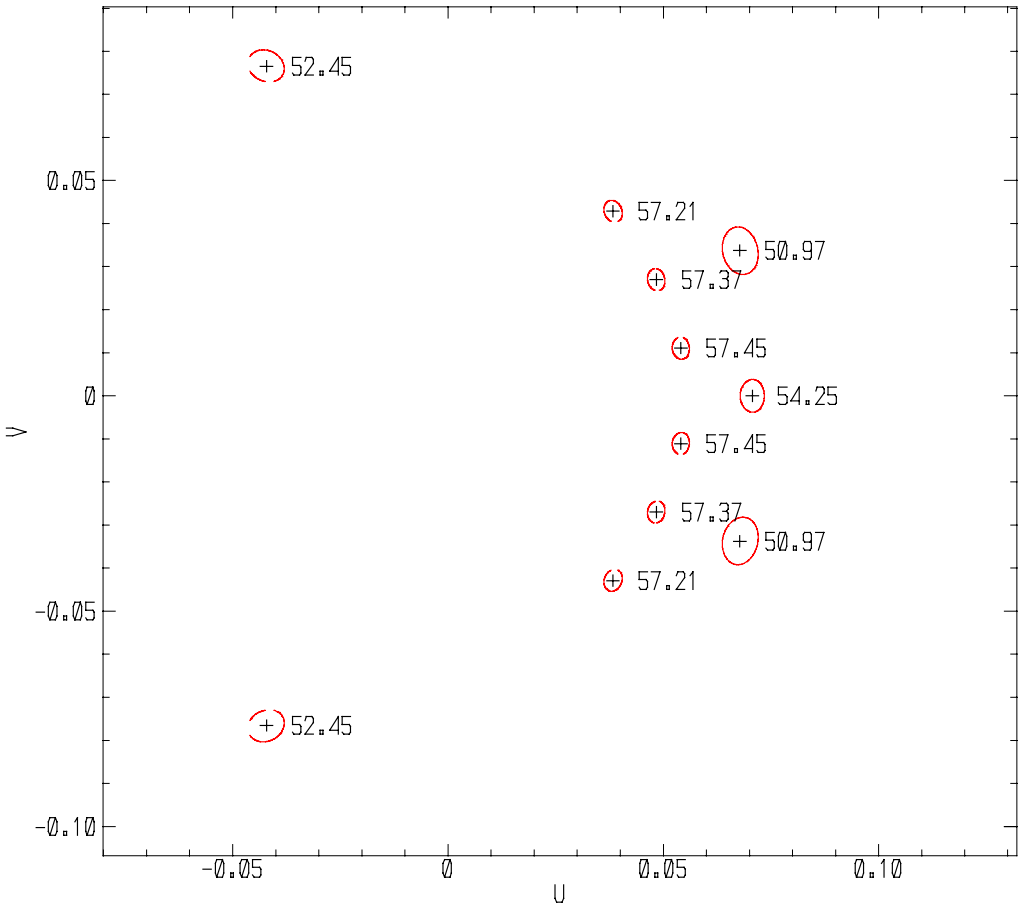

Figure 8.3-2: Radiation pattern of the telescope for LFI horns

8.3.6 HFI radiation pattern

In the same way the radiation patterns for HFI horns are plotted in Figure 8.3-3. The contour levels correspond to –3 dB and –6 dB.

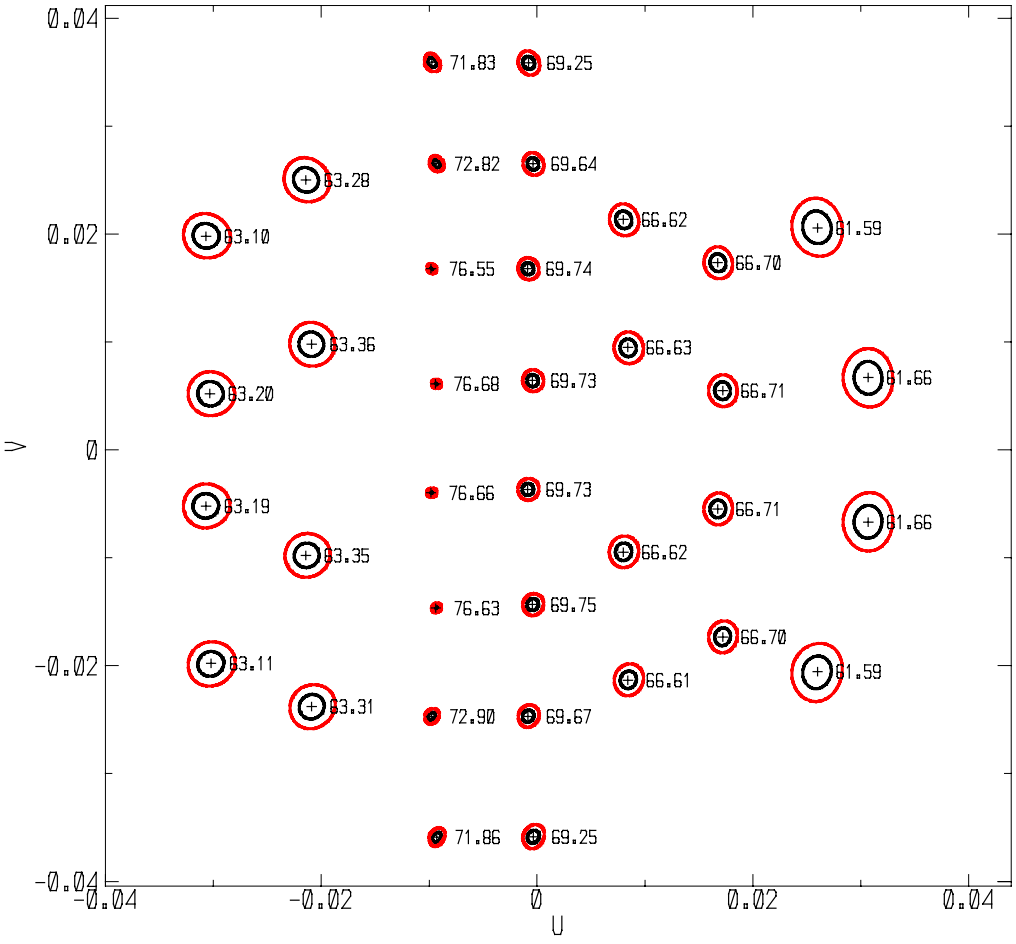

Figure 8.3-3. Radiation pattern of the telescope for HFI horns

8.4 CONTRIBUTORS ANALYSIS

This section deals with the identification of the contributors and their translation in terms of degradation of the RF performance. For this purpose, it is necessary to decompose each contributors and to define the best way to insert them in terms of RF modelling.

The major part of the inputs for the budget comes from [RD 12] where the impact of the contributors have been quantified by simulation (under several load cases) and the other part comes from analysis and allocation.

8.4.1 Contributors identification

Two types of contributors could be identified : deterministic (signed) and statistic (not signed) contributors (see Figure 8.4-1).

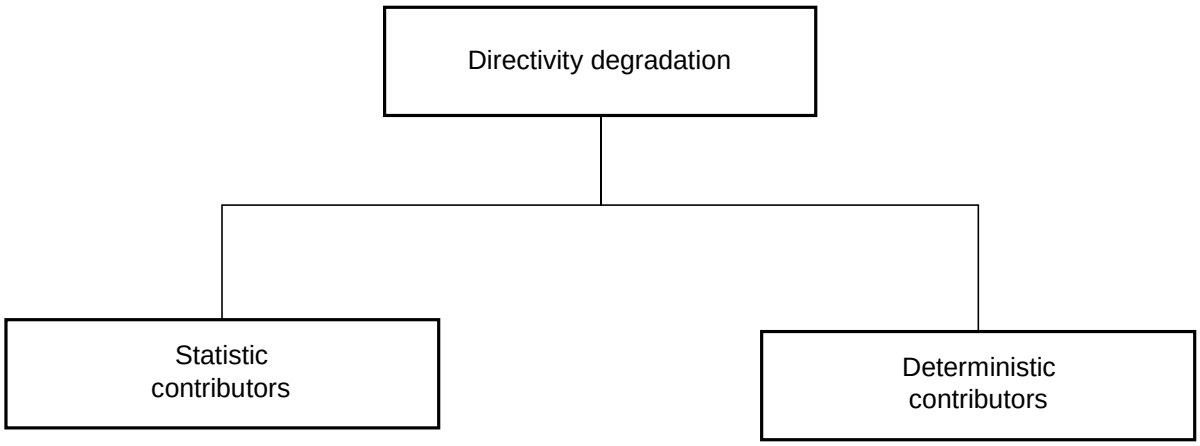

Figure 8.4-1 Contributors identification

For statistic contributors the degradation of the performance will be obtained by a quadratic summation and for the deterministic one by a linear summation.

Each contributor is divided into several sub-contributors in order to precisely identify the origin (see [RD 12]).

8.4.2 Deterministic contributor

The deterministic case at operational is composed of a deterministic load case defined in [RD 12] and other contributors (see Figure 8.4-2).

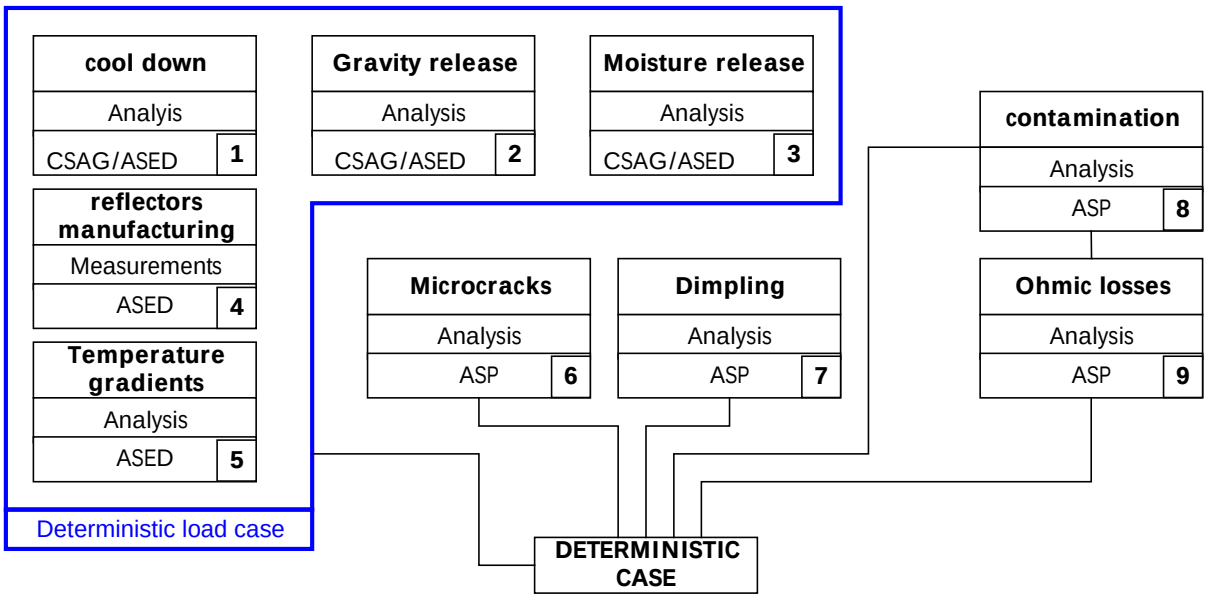

Figure 8.4-2 deterministic case

8.4.2.1 Input for deterministic load case

The deterministic load case is obtained by a summation of numerous sub level contributors and is defined by one set of parameters (BFE+distorsion) issued from [RD 12].

The deterministic load case is defined in the data format :

1) BFE defined by ΔR and ΔK from the initial conics defining the main and the sub reflectors.
2) Position of the BFE vertex in OM1 and OM2 (T_x, T_y, T_z, R_x, R_y)
3) Defocus of the ORDP plane (T_z)
4) Residual distorsion (also mentionned HF (high frequency distorsion)) in the coordinate system centered on the BFE vertex postion in the format of a cloud of points.

These values are defined in the following table :

BFE	Tx	Ty	Tz	Rx	Ry	ΔR	ΔK
unit	µm	µm	µm	µrad	µrad	µm	
PR	-0,9	-7,8	302,3	-2,1	-206,9	-18,5	0,0000401
SR	116,8	-11,8	28,3	-1,3	243,9	14,7	0,0000053

defocus					
unit	µm	µm	µm	µrad	µrad
RDP	0	0	-100	0	0

Table 8.4-1 deterministic load case : BFE and defocus

The residual surface error are given as cloud of point x, y, Δz. These surface distorsions are plotted in Figure 8.4-3 and 8.4-4.

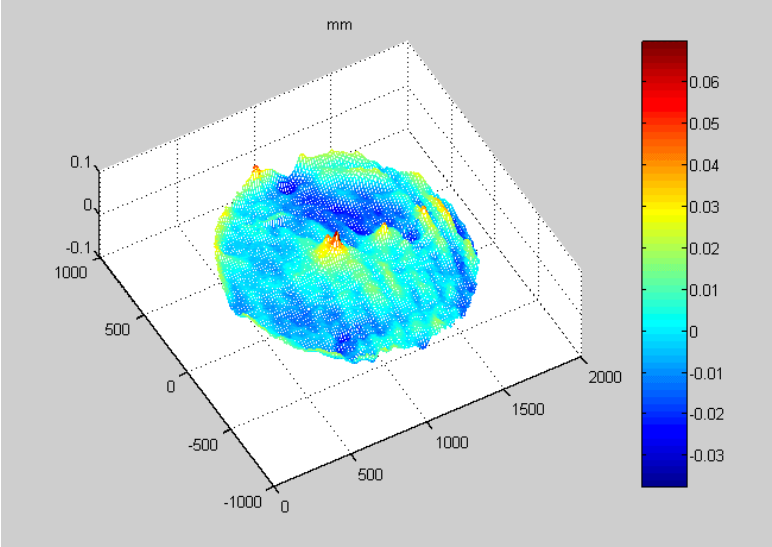

Figure 8.4-3 Residual deformations on the main reflector (unity in figure :mm) (rms≈ 10 µm)

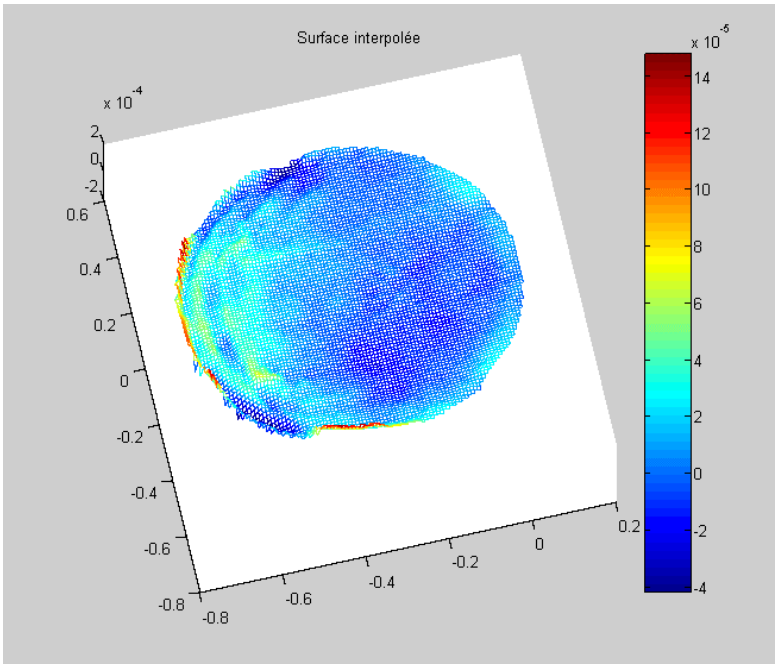

Figure 8.4-4 Residual deformations on the sub reflector (unity in figure :m) (rms ≈ 20 µm)

8.4.2.2 Results of computation of the deterministic load case

The input data defined in the previous section (§ 8.4.2.1) have been used to simulate the gain degradation.

- The BF (BFE + defocus) could be computed with GTD-PO or PO-PO method.
- The HF(residual surface distorsion) must be computed by PO-PO method

The results are plotted in Figure 2-12 and the details given in Table 2-7.

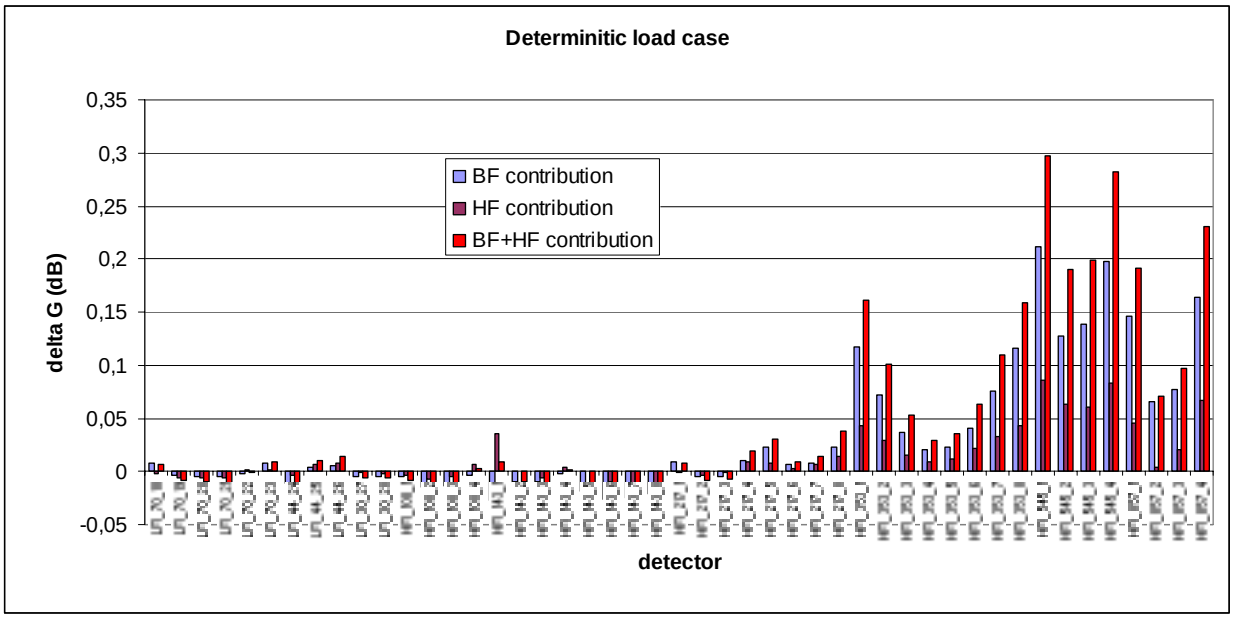

Figure 8.4-5 Gain degradation due to deterministic load case

The table 8.4-2 contains the numerical results of the analysis
The legend of each column is detailled hereafter :

ref_GTD : Reference gain computed by GTD method
ref_PO : Reference gain computed by physical optics method
BF_GTD : Gain of the best fit computed by GTD method
BF_PO : Gain of the best fit computed by physical optics method
BF_HF_PO : Gain of the best fit + residuals by physical optics method

								BF	HF	HF BF
	ref_GTD	ref_PO	BF_GTD	BF_PO	BF_HF_PO	ref_GTD-ref_PO	BF_GTD-BF_PO	BF_PO-ref_PO	BF_HF_PO-BF_PO	BF_HF_PO-ref_PO
detector	dBi	dBi	dBi	dBi	dBi	dB	dB	dB	dB	dB
LFI_70_18	57,2117	57,2209	57,2166	57,2292	57,2271	-0,0092	-0,0126	0,0084	-0,0021	0,0063
LFI_70_19	57,3695	57,3820	57,3646	57,3789	57,3735	-0,0126	-0,0143	-0,0032	-0,0054	-0,0086
LFI_70_20	57,4513	57,4629	57,4398	57,4587	57,4532	-0,0116	-0,0189	-0,0042	-0,0056	-0,0098
LFI_70_21	57,4513	57,4629	57,4402	57,4583	57,4521	-0,0116	-0,0180	-0,0046	-0,0062	-0,0108
LFI_70_22	57,3695	57,3820	57,3653	57,3799	57,3810	-0,0126	-0,0146	-0,0022	0,0012	-0,0010
LFI_70_23	57,2117	57,2205	57,2163	57,2282	57,2295	-0,0088	-0,0119	0,0077	0,0013	0,0091
LFI_44_24	54,2521	54,2739	54,2404	54,2627	54,2588	-0,0217	-0,0223	-0,0112	-0,0039	-0,0150
LFI_44_25	52,4603	52,4583	52,4604	52,4627	52,4689	0,0021	-0,0023	0,0044	0,0062	0,0106
LFI_44_26	52,4603	52,4583	52,4615	52,4640	52,4719	0,0021	-0,0025	0,0057	0,0079	0,0136
LFI_30_27	50,9666	50,9898	50,9646	50,9847	50,9839	-0,0232	-0,0201	-0,0051	-0,0008	-0,0059
LFI_30_28	50,9666	50,9898	50,9643	50,9849	50,9832	-0,0232	-0,0206	-0,0049	-0,0016	-0,0065
HFI_100_1	61,5996	61,6052	61,5922	61,5999	61,5965	-0,0056	-0,0077	-0,0053	-0,0034	-0,0087
HFI_100_2	61,6569	61,6627	61,6399	61,6478	61,6404	-0,0058	-0,0079	-0,0148	-0,0074	-0,0222
HFI_100_3	61,6569	61,6627	61,6418	61,6497	61,6453	-0,0058	-0,0079	-0,0130	-0,0044	-0,0174
HFI_100_4	61,5996	61,6052	61,5942	61,6019	61,6086	-0,0056	-0,0077	-0,0033	0,0067	0,0034
HFI_143_1	63,3077	63,3124	63,2802	63,2851	63,3209	-0,0047	-0,0049	-0,0273	0,0358	0,0085
HFI_143_2	63,3578	63,3624	63,3456	63,3526	63,3530	-0,0046	-0,0070	-0,0098	0,0003	-0,0095
HFI_143_3	63,3654	63,3695	63,3529	63,3600	63,3541	-0,0041	-0,0071	-0,0095	-0,0060	-0,0155
HFI_143_4	63,2852	63,2876	63,2802	63,2851	63,2890	-0,0024	-0,0049	-0,0025	0,0039	0,0014
HFI_143_5	63,1215	63,1234	63,1012	63,1053	63,1055	-0,0019	-0,0040	-0,0181	0,0003	-0,0179
HFI_143_6	63,1942	63,1973	63,1660	63,1718	63,1616	-0,0031	-0,0058	-0,0255	-0,0102	-0,0357
HFI_143_7	63,2047	63,2087	63,1777	63,1836	63,1673	-0,0040	-0,0059	-0,0251	-0,0163	-0,0414
HFI_143_8	63,1084	63,1104	63,0863	63,0897	63,0781	-0,0020	-0,0034	-0,0207	-0,0116	-0,0323
HFI_217_1	66,7002	66,7007	66,7048	66,7099	66,7084	-0,0005	-0,0051	0,0092	-0,0015	0,0077
HFI_217_2	66,7143	66,7157	66,7063	66,7110	66,7076	-0,0014	-0,0047	-0,0047	-0,0035	-0,0081
HFI_217_3	66,7186	66,7210	66,7112	66,7159	66,7144	-0,0024	-0,0047	-0,0051	-0,0016	-0,0067
HFI_217_4	66,6984	66,6997	66,7053	66,7099	66,7194	-0,0012	-0,0046	0,0103	0,0095	0,0197
HFI_217_5	66,6211	66,6231	66,6413	66,6461	66,6541	-0,0020	-0,0048	0,0231	0,0079	0,0310
HFI_217_6	66,6246	66,6260	66,6278	66,6324	66,6352	-0,0014	-0,0046	0,0064	0,0029	0,0093
HFI_217_7	66,6288	66,6295	66,6317	66,6367	66,6438	-0,0006	-0,0050	0,0072	0,0071	0,0144
HFI_217_8	66,6172	66,6190	66,6388	66,6423	66,6566	-0,0018	-0,0035	0,0233	0,0144	0,0376
HFI_353_1	69,2529	69,2474	69,3688	69,3648	69,4084	0,0055	0,0040	0,1174	0,0435	0,1610
HFI_353_2	69,6751	69,6708	69,7434	69,7429	69,7716	0,0043	0,0005	0,0721	0,0288	0,1008
HFI_353_3	69,7500	69,7470	69,7827	69,7844	69,8002	0,0031	-0,0017	0,0374	0,0158	0,0532
HFI_353_4	69,7265	69,7246	69,7429	69,7448	69,7542	0,0019	-0,0020	0,0202	0,0093	0,0296
HFI_353_5	69,7338	69,7341	69,7561	69,7568	69,7690	-0,0003	-0,0007	0,0228	0,0122	0,0349
HFI_353_6	69,7431	69,7409	69,7813	69,7820	69,8037	0,0022	-0,0007	0,0411	0,0217	0,0628
HFI_353_7	69,6460	69,6429	69,7196	69,7186	69,7521	0,0032	0,0009	0,0758	0,0335	0,1093
HFI_353_8	69,2463	69,2408	69,3604	69,3565	69,3997	0,0054	0,0040	0,1156	0,0433	0,1589
HFI_545_1	71,8576	71,8516	72,0681	72,0628	72,1488	0,0059	0,0053	0,2112	0,0860	0,2972
HFI_545_2	72,9059	72,9011	73,0289	73,0279	73,0907	0,0048	0,0010	0,1268	0,0628	0,1897
HFI_545_3	72,8179	72,8126	72,9547	72,9516	73,0122	0,0053	0,0031	0,1391	0,0605	0,1996
HFI_545_4	71,8339	71,8288	72,0681	72,0272	72,1106	0,0051	0,0408	0,1984	0,0833	0,2818
HFI_857_1	76,6255	76,6232	76,7728	76,7697	76,8150	0,0023	0,0031	0,1465	0,0453	0,1918
HFI_857_2	76,6671	76,6642	76,7317	76,7304	76,7350	0,0029	0,0014	0,0662	0,0046	0,0708
HFI_857_3	76,6804	76,6769	76,7544	76,7542	76,7741	0,0035	0,0003	0,0772	0,0200	0,0972
HFI_857_4	76,5519	76,5492	76,7124	76,7125	76,7798	0,0027	-0,0001	0,1633	0,0674	0,2306

Table 8.4-2 : Gain degradation due to the deterministic load case

8.4.2.2.1 Quilting effect

The quilting effect results from the telescope manufacturing. The telescope is supported by a honeycomb structure. The machining of the surface induces a bump at the center of each cell consequence of the rigidity at the edge of cell. The depth of the bump has been identified to be 4 µm. The honeycomb cells have a diameter of 60 mm. The two reflectors are based on the same type of honeycomb structure.

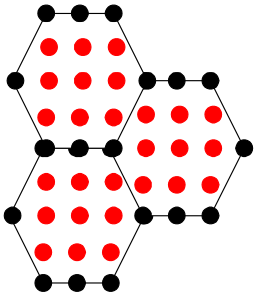

Figure 8.4-6 Cell decomposition

In order to handle the actual surface of the reflector in the simulation, the surfaces of the reflectors are meshed into 11000 points for the main reflector and 4000 points for the subreflector. Each hexagonal cell is described by 17 points (see Figure 8.4-6) where the depths of the central points of hexagons (in red in the figure) are adjusted to simulate the quilting effect. The discretisation is defined on the reflector surface in two directions : 15 mm in one direction and 12.99038 mm in the other direction to obtain the equivalent cell on the surface.

Figure 8.4-7 shows the unit cell decomposition and the decomposition of the main reflector in cells in the coordinate system used to define the reflector. Only the point at the edge is represented and the dimension of the cell is shown magnified for illustration of the method.

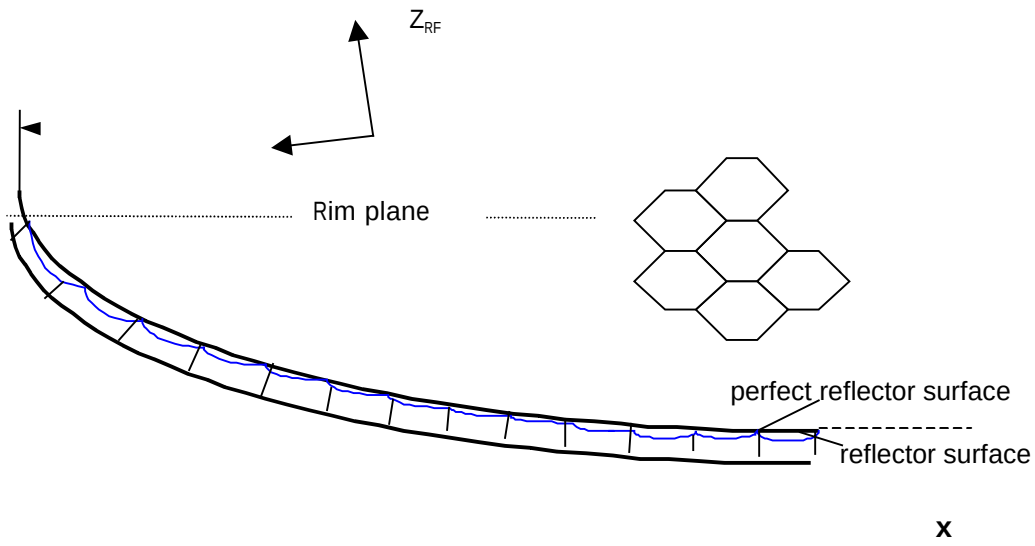

Figure 8.4-7 Quilting impact on reflector

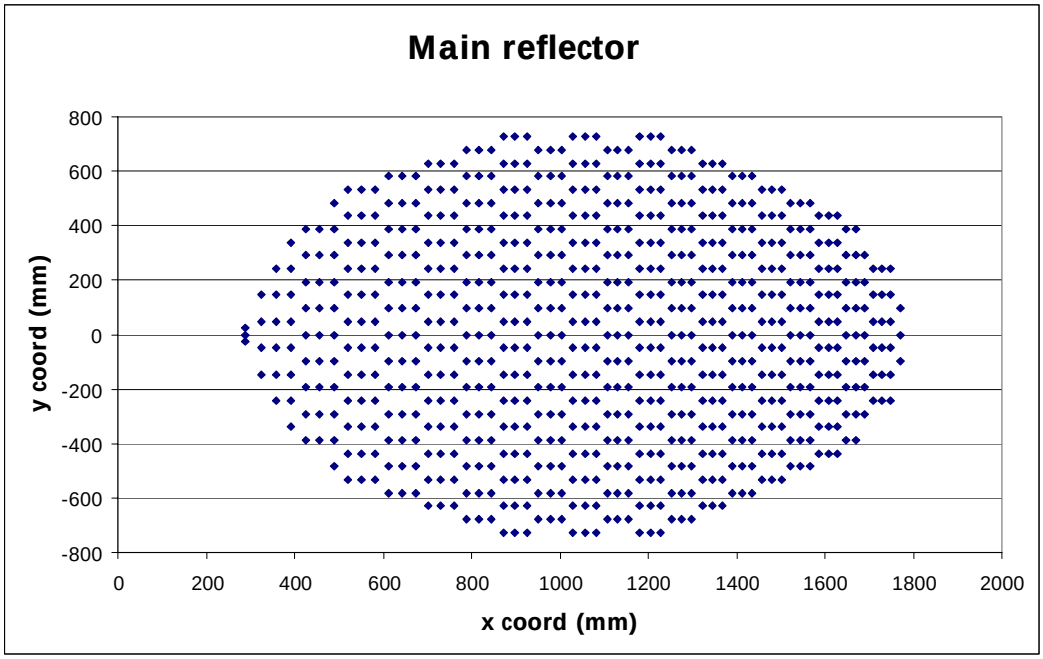

Figure 8.4-8 Cell decomposition of the reflector (magnified)

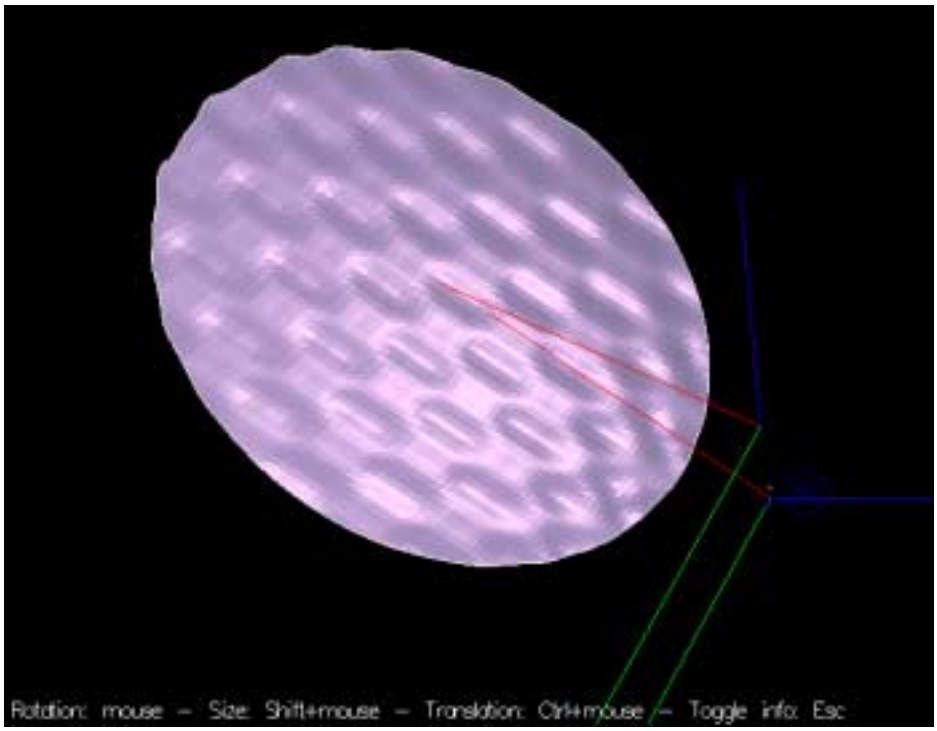

Figure 8.4-9 Quilting impact on the reflector (cell magnified)

The modified grid of points is then used in a Grasp8 simulation to analyse the performance degradation. The Figure 8.4-9 shows the 3D representation of the surface (the cells are drawn larger than reality and the depth is magnified for illustration). All the central points are set at the same depth from the perfect reflector surface.

The gain degradation of the telescope have been computed and is shown in Figure 8.4-10. The gain degradation remains small, less than 0.025 dB at higher frequency. As presented in telescope working group meeting the impact of quilting is more significant in the side lobes than in the main lobes.

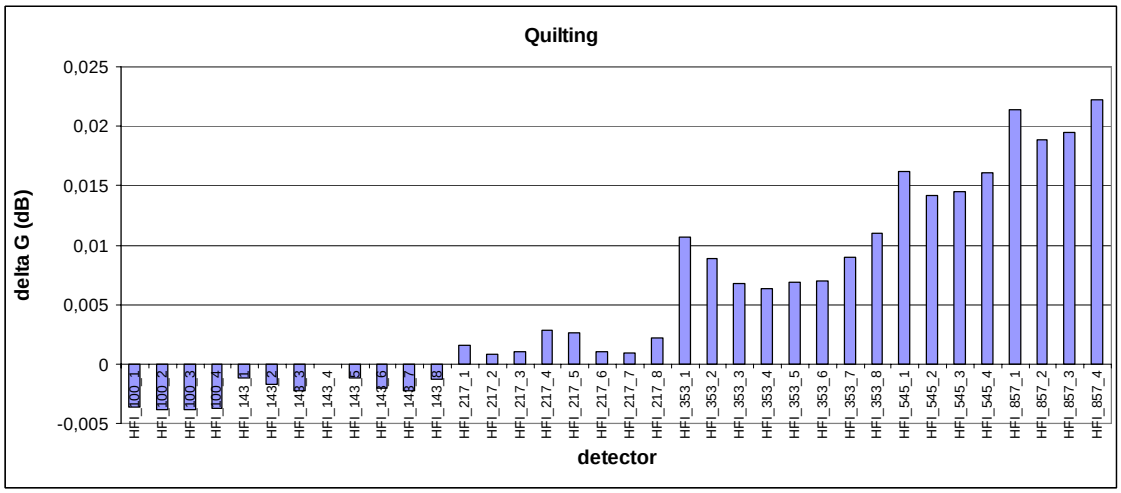

Figure 8.4-10 : Gain degradation due to quilting effects

8.4.2.2.2 Ohmic losses

The ohmic losses depend on the surface materials used for the reflectors manufacturing and more precisely on the conductivity of the metal which itself depends on surface finishing and on the nature of the metal. The exact knowledge of the conductivity is difficult to obtain. Some measurement results could be found [1] and [2] up to 377 GHz.
In the scope of the assesment of the ohmic losses, a realistic values for the conductivity has been taken based on the remark in [1] : " the resistivity is twice as high as calculated from nominal DC conductivity" and on the actual quality of the reflector surface : the reflectors are made on pure aluminium.

Based on measurements and empirical assumptions [2] [1], the reflection losses at a frequency F (in GHz) in submillimeter frequencies range, for bulk aluminium materials is found to be equal to :

$$L = 0.21\ \% \sqrt{\frac{F}{100}} \qquad (1)$$

which correspond to a conductivity of $\sigma = 2\ 10^{+7}$ S m^{-1} at submillimeter frequencies range ($\sigma = 4\ 10^{+7}$ S m^{-1} at DC)
For other conductivities the formula found in [1] could be used (with F expressed in GHz).:

$$L = \frac{10.88.10^{-3}}{30\pi} \sqrt{\frac{10^{10}}{3\sigma}} \sqrt{\frac{F}{100}} \qquad (2)$$

Differents value of conductivity for Aluminum could be found in [1][2] measured at ambiant temperature and at frequencies up to 377 GHz. Ohmic losses decrease with temperature and the reflectors are assumed to be at 50 K.

[1] [1] J. W. Zwart, V. O. Heinen, K. Long and N. Stankiewicz :"Surface resistance measurements at 377 GHz", *Int. J. IR and Millimeter Waves*, Vol. 17, no. 2, pp. 349-357, Dec. 1996.
[2] [2] J. W. Lamb, "Miscellaneous data on materials for millimetre and submillimetere optics", *Int. J. IR and Millimeter Waves*, Vol. 17, no. 12, pp. 1997-2034, Dec. 1996.

The Table 8-4.3 summarizes the value taken for the budget.

frequency (GHz)	delta directivity (dB)
30	0,0071
44	0,0086
70	0,0109
100	0,0130
143	0,0156
217	0,0192
353	0,0245
545	0,0305
857	0,0382

Table 8.4-3 Gain degradation due to ohmic losses

8.4.2.2.3 Roughness

The roughness also intervenes implicitly in the ohmic losses by increasing the resistivity of the surface, thus reducing the efficiency of the reflector surface.

The roughness could be characterised by a peak-to-peak value and a correlation lenght. As long as this type of contribution is by nature random with small spatial frequency, the directivity degradation could be calculated by using Ruze formulaμ. According to the reflector specification, the surface is assumed to have a roughness of order of 0.2 μm rms.
For a roughness of 0.2 μm rms, the table 8.4-4 shows that the roughness have neglectable impact on the gain degadation.

Frequency GHz	WFE inputs (μm)	delta G (dB) (Ruze)
30	0,2	NS
44	0,2	NS
70	0,2	NS
100	0,2	NS
143	0,2	NS
217	0,2	NS
353	0,2	NS
545	0,2	NS
857	0,2	0,0001

Table 8.4-4 Gain degradation due to roughness

8.4.2.2.4 Micro-cracks effect

For the CDR budget , it has been agreed that there is no microcraks on the reflectors. Hence no RF impact.

8.4.2.2.5 Contamination

An allocation is provided on the basis of a 2 μm rms surface error which is representative of particular contamination :

Frequency GHz	WFE inputs (μm)	delta G (dB) (Ruze)
30	2	NS
44	2	NS
70	2	NS
100	2	0,0001
143	2	0,0002
217	2	0,0004
353	2	0,0009
545	2	0,0023
857	2	0,0056

Table 8.4-5 Gain degradation due to contamination (NS :not significant)

8.4.2.3 Deterministic contributor budget

In Table 8.4-6 and Figure 8.4-11, the total budget for the deterministic contributors is presented.

detector n°	deterministic load case	quilting	ohmic losses	contamination	Total determinist
	dB	dB	dB	dB	dB
LFI_70_18	0,0063	ns	0,0109	ns	0,0172
LFI_70_19	-0,0086	ns	0,0109	ns	0,0195
LFI_70_20	-0,0098	ns	0,0109	ns	0,0207
LFI_70_21	-0,0108	ns	0,0109	ns	0,0217
LFI_70_22	-0,0010	ns	0,0109	ns	0,0119
LFI_70_23	0,0091	ns	0,0109	ns	0,0200
LFI_44_24	-0,0150	ns	0,0086	ns	0,0236
LFI_44_25	0,0106	ns	0,0086	ns	0,0192
LFI_44_26	0,0136	ns	0,0086	ns	0,0222
LFI_30_27	-0,0059	ns	0,0071	ns	0,0130
LFI_30_28	-0,0065	ns	0,0071	ns	0,0136
HFI_100_1	-0,0087	-0,0037	0,013	0,0001	0,0255
HFI_100_2	-0,0222	-0,0039	0,013	0,0001	0,0392
HFI_100_3	-0,0174	-0,0039	0,013	0,0001	0,0344
HFI_100_4	0,0034	-0,0037	0,013	0,0001	0,0202
HFI_143_1	0,0085	-0,0012	0,0156	0,0002	0,0256
HFI_143_2	-0,0095	-0,0017	0,0156	0,0002	0,0269
HFI_143_3	-0,0155	-0,0022	0,0156	0,0002	0,0335
HFI_143_4	0,0014	-0,0001	0,0156	0,0002	0,0173
HFI_143_5	-0,0179	-0,0012	0,0156	0,0002	0,0349
HFI_143_6	-0,0357	-0,0021	0,0156	0,0002	0,0536
HFI_143_7	-0,0414	-0,0022	0,0156	0,0002	0,0595
HFI_143_8	-0,0323	-0,0013	0,0156	0,0002	0,0494
HFI_217_1	0,0077	0,0016	0,0192	0,0004	0,0289
HFI_217_2	-0,0081	0,0008	0,0192	0,0004	0,0285
HFI_217_3	-0,0067	0,0011	0,0192	0,0004	0,0274
HFI_217_4	0,0197	0,0029	0,0192	0,0004	0,0422
HFI_217_5	0,0310	0,0026	0,0192	0,0004	0,0532
HFI_217_6	0,0093	0,0010	0,0192	0,0004	0,0299
HFI_217_7	0,0144	0,0009	0,0192	0,0004	0,0349
HFI_217_8	0,0376	0,0022	0,0192	0,0004	0,0594
HFI_353_1	0,1610	0,0107	0,0245	0,0009	0,1971
HFI_353_2	0,1008	0,0089	0,0245	0,0009	0,1352
HFI_353_3	0,0532	0,0067	0,0245	0,0009	0,0853
HFI_353_4	0,0296	0,0063	0,0245	0,0009	0,0613
HFI_353_5	0,0349	0,0068	0,0245	0,0009	0,0672
HFI_353_6	0,0628	0,0070	0,0245	0,0009	0,0952
HFI_353_7	0,1093	0,0090	0,0245	0,0009	0,1437
HFI_353_8	0,1589	0,0110	0,0245	0,0009	0,1953
HFI_545_1	0,2972	0,0162	0,0305	0,0023	0,3462
HFI_545_2	0,1897	0,0141	0,0305	0,0023	0,2366
HFI_545_3	0,1996	0,0145	0,0305	0,0023	0,2468
HFI_545_4	0,2818	0,0161	0,0305	0,0023	0,3307
HFI_857_1	0,1918	0,0214	0,0382	0,0056	0,2570
HFI_857_2	0,0708	0,0189	0,0382	0,0056	0,1335
HFI_857_3	0,0972	0,0194	0,0382	0,0056	0,1605
HFI_857_4	0,2306	0,0223	0,0382	0,0056	0,2967

Table 8.4-6 Determinist : Budget (ns : not significant)

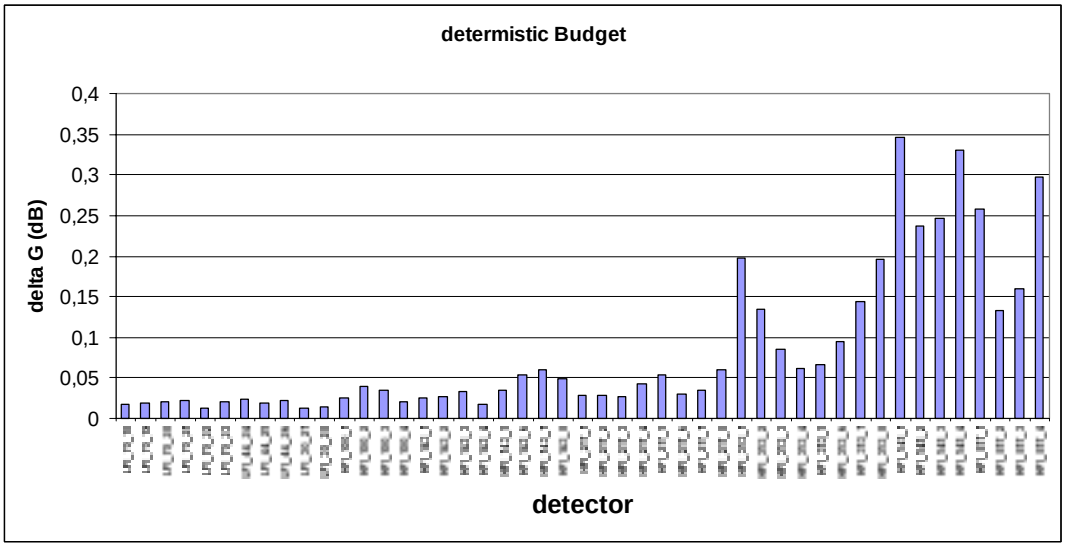

Figure 8.4-11 Determinist: Budget

8.4.3 Statistic contributors

8.4.3.1 Origin of inputs

These contributors could be divided into different levels :

Telescope level

Focal Plane Unit

Telescope-FPU integration

Contingency

The random case at operational is composed of numerous contributors. The data are of two main types : inputs provided in WFE rms per horn, and inputs described in term of BFE random displacements and distorsions (translation, rotation , conicity, radius variations, surface errors). The details of these data are presented in [RD 12]. In this section, only a recall of the inputs is presented followed by the corresponding gain dagradation.

8.4.3.2 WFE per horn

Frequency GHz	WFE inputs (µm)	delta G (dB) (Ruze)
30	14,5	0,0004
44	13,4	0,0007
70	12,3	0,0014
100	11,4	0,0025
143	9,7	0,0037
217	9,6	0,0083
353	7,3	0,0126
545	7,2	0,0293
857	7,2	0,0725

Table 8.4-7 WFE per Horn

The Table 8.4-7 provides the WFE per horns. The quantification in term of gain degradation is obtained through Ruze formula :

$$\Delta G_{dB} = \frac{10}{\ln(10)}\left(\frac{2\pi\, WFE}{\lambda}\right)^2$$

8.4.3.3 BFE random displacements and distortions

From [RD 12] each contributor is expanded in the variations of seven parameters Rx, Ry, Tx, Ty, Tz, ΔK, ΔR in each coordinate system (OM1 , OM1C, OM2, OM2C and ORDP).

The contributors are listed in Table 8.4-8 and Table 8.4-9 with the details on data organisation. The table 8.4-10 presents the description of each columns of former tables. Each contributor impact is computed,the numerical results are presented in Table 8.4-11 to table 8.4-17.

Then the graphical results are displayed in figure 8.4-12.

			case	Tx	Ty	Tz	Rx	Ry	dR	dK	Correlated?	Nature	coord Sys
			n°	µm	µm	µm	µrad	µrad	µm				
PR	QM Videogram,		C1	48,0	0,0	168,0	0,0	69,1	0,0	0	No	2sig	OM1C
PR	QM T scaling		C2	-4,8	0,0	-2,7	0,0	0,1	0,0	0	Yes(*)	2sig	OM1C
PR	QM T know		C3	-1,0	0,0	-0,6	0,0	0,0	0,0	0	Yes(*)	2sig	OM1C
PR	CTE non-unif	Frame	C4	1,8	0,1	-2,1	0,0	-0,7	0,0	0	Yes(*)	2sig	OM1C
PR	CTE non-unif	Pr pan	C5	-7,0	0,0	-3,4	0,0	-9,4	0,0	0	Yes(*)	2sig	OM1C
PR	CTE non-unif	SR pan	C6	-0,1	0,0	-0,2	0,0	-0,1	0,0	0	Yes(*)	2sig	OM1C
PR	CTE non-unif	Fr st1	C7	-0,2	0,8	-7,0	-6,9	0,3	0,0	0	Yes(*)	2sig	OM1C
PR	CTE non-unif	Fr st2	C8	-0,2	-0,8	-6,9	9,0	0,3	0,0	0	Yes(*)	2sig	OM1C
PR	CTE non-unif	BBS	C9	-0,2	0,0	7,7	0,0	-8,2	0,0	0	Yes(*)	2sig	OM1C
PR	CTE non-unif	BTS	C10	-0,2	0,0	6,9	0,0	-7,4	0,0	0	Yes(*)	2sig	OM1C
PR	CTE non-unif	Sr st1	C11	0,0	0,1	0,0	-0,1	0,0	0,0	0	Yes(*)	2sig	OM1C
PR	CTE non-unif	SR st2	C12	0,0	-0,1	0,0	0,1	0,0	0,0	0	Yes(*)	2sig	OM1C
PR	CTE non-unif	Low st	C13	-0,2	0,0	0,0	0,0	-0,4	0,0	0	Yes(*)	2sig	OM1C
PR	CS IF load		C14	3,3	-0,5	-1,1	0,2	8,6	0,0	0	No	2sig	OM1C
PR	Baffle IF load		C15	1,8	0,0	9,6	-0,1	-0,7	0,0	0	No	2sig	OM1C
PR	FPU IF load		C16	3,9	0,0	-0,9	0,0	11,5	0,0	0	No	2sig	OM1C
PR	PR, SR, JFET		C17	-0,7	0,0	0,0	0,0	-1,0	0,0	0	No	2sig	OM1C
PR	Gravity release		C18	5,7	0,0	-11,5	0,0	20,0	0,0	0	No	2sig	OM1C
PR	Moist release	Struc	C19	-4,6	0,0	2,1	0,0	-9,3	0,0	0	No	2sig	OM1C
PR	Moist release	refl	C20	-12,0	0,0	1,4	0,0	12,3	-13,2	0	Yes	2sig	OM1
PR	Alignment		C21	60,8	152,0	121,6	22,4	7,2	0,0	0	No	2sig	OM1C
PR	CS planarity	E	C22	-0,6	0,0	-37,2	0,0	92,6	0,0	0	Yes(*)	2sig	OM1C
PR	CS planarity	N-E	C23	-31,7	53,6	1,6	-21,7	-48,2	0,0	0	Yes(*)	2sig	OM1C
PR	CS planarity	N-W	C24	4,2	-8,5	47,4	50,3	-4,1	0,0	0	Yes(*)	2sig	OM1C
PR	CS planarity	W	C25	0,4	0,0	-0,8	0,0	1,4	0,0	0	Yes(*)	2sig	OM1C
PR	CS planarity	S-W	C26	4,2	8,5	47,4	-50,3	-4,1	0,0	0	Yes(*)	2sig	OM1C
PR	CS planarity	S-E	C27	-31,7	-53,6	1,6	21,7	-48,2	0,0	0	Yes(*)	2sig	OM1C
PR	TTA	E	C28	-1,1	0,0	-8,1	0,0	18,7	0,0	0	Yes(*)	2sig	OM1C
PR	TTA	N-E	C29	-6,3	10,8	-0,2	-4,0	-7,8	0,0	0	Yes(*)	2sig	OM1C
PR	TTA	N-W	C30	0,3	-0,4	7,8	7,5	-1,7	0,0	0	Yes(*)	2sig	OM1C
PR	TTA	W	C31	0,1	0,0	0,2	0,0	0,2	0,0	0	Yes(*)	2sig	OM1C
PR	TTA	S-W	C32	0,3	0,4	7,8	-7,5	-1,7	0,0	0	Yes(*)	2sig	OM1C
PR	TTA	S-E	C33	-6,3	-10,8	-0,2	4,0	-7,8	0,0	0	Yes(*)	2sig	OM1C
PR	Structure launch		C34	20,0	20,0	20,0	20,0	20,0	0,0	0	No	2sig	OM1C
PR	Structure creeping		C35	20,0	20,0	20,0	20,0	20,0	0,0	0	No	2sig	OM1C
PR	Structure lifetime		C36	20,0	20,0	20,0	20,0	20,0	0,0	0	No	2sig	OM1C
PR	dT in-orbit	Struc	C37	-6,3	0,8	-1,8	0,8	0,1	0,0	0	Yes(*)	2sig	OM1C
PR	dT in-orbit	refl	C38	7,0	0,0	1,6	0,0	-0,2	-9,0	-0	Yes(*)	2sig	OM1
PR	ISMA	Rad	C39	11,1	0,0	-0,6	0,0	-8,5	6,6	-0	Yes	2sig	OM1
PR	ISMA	Tang	C40	0,0	-1,4	0,0	0,0	0,0	0,0	0	Yes	2sig	OM1
PR	ISMA	Out-of-pl	C41	25,4	0,0	-73,0	0,0	0,0	0,8	-0	Yes	2sig	OM1
PR	ISMA	Rotation	C42	0,0	1,7	0,0	0,0	0,0	0,0	0	Yes	2sig	OM1
PR	ISM-B	Rad	C43	-11,1	0,0	-0,6	0,0	8,5	6,6	-0	Yes	2sig	OM1
PR	ISM-B	Tang	C44	0,0	-1,4	0,0	0,0	0,0	0,0	0	Yes	2sig	OM1
PR	ISM-B	Out-of-pl	C45	25,4	0,0	-73,0	0,0	0,0	0,8	-0	Yes	2sig	OM1
PR	ISM-B	Rotation	C46	0,0	0,9	0,0	0,0	0,0	0,0	0	Yes	2sig	OM1
PR	FEM acc		C47	1,0	1,0	1,0	1,0	1,0	1,0	0	No	2sig	OM1

Table 8.4-8 Input parameters for the sensitivity analysis. Random case

SR	QM Videogram,		C48	52,0	0,0	55,2	0,0	175,7	0,0	0	No	2sig	OM2C
SR	QM T scaling		C2	6,9	0,0	4,7	0,0	31,6	0,0	0	Yes(*)	2sig	OM2C
SR	QM T know		C3	1,5	0,0	1,0	0,0	6,7	0,0	0	Yes(*)	2sig	OM2C
SR	CTE non-unif	Frame	C4	-5,1	0,0	3,4	0,0	23,6	0,0	0	Yes(*)	2sig	OM2C
SR	CTE non-unif	Pr pan	C5	-0,5	0,0	-0,8	0,0	-0,7	0,0	0	Yes(*)	2sig	OM2C
SR	CTE non-unif	SR pan	C6	1,4	0,0	-1,4	0,0	-5,2	0,0	0	Yes(*)	2sig	OM2C
SR	CTE non-unif	Fr st1	C7	0,0	0,0	0,0	0,0	0,0	0,0	0	Yes(*)	2sig	OM2C
SR	CTE non-unif	Fr st2	C8	0,0	0,0	0,0	0,0	0,0	0,0	0	Yes(*)	2sig	OM2C
SR	CTE non-unif	BBS	C9	0,0	0,0	-0,1	0,0	-0,1	0,0	0	Yes(*)	2sig	OM2C
SR	CTE non-unif	BTS	C10	1,0	0,9	-2,4	-9,9	-8,2	0,0	0	Yes(*)	2sig	OM2C
SR	CTE non-unif	Sr st1	C11	1,0	0,9	-2,4	-9,9	-8,2	0,0	0	Yes(*)	2sig	OM2C
SR	CTE non-unif	SR st2	C12	1,0	-0,9	-2,4	10,0	-8,2	0,0	0	Yes(*)	2sig	OM2C
SR	CTE non-unif	Low st	C13	0,0	0,0	0,1	0,0	0,1	0,0	0	Yes(*)	2sig	OM2C
SR	CS IF load		C49	12,1	0,1	4,0	0,3	-25,0	0,0	0	No	2sig	OM2C
SR	Baffle IF load		C50	-10,5	0,0	-18,6	0,1	7,9	0,0	0	No	2sig	OM2C
SR	FPU IF load		C51	0,5	0,0	1,4	0,0	0,6	0,0	0	No	2sig	OM2C
SR	PR, SR, JFET		C52	-0,5	0,0	-0,5	0,0	-0,4	0,0	0	No	2sig	OM2C
SR	Gravity release		C53	4,0	0,0	0,6	0,0	-8,5	0,0	0	No	2sig	OM2C
SR	Moist release	Struc	C54	1,5	0,0	0,5	0,0	-2,7	0,0	0	No	2sig	OM2C
SR	Moist release	ref	C55	6,5	0,0	-0,2	0,0	-11,0	1,4	0	Yes		OM2
SR	alignment		C56	65,9	152,0	70,0	22,4	10,0	0,0	0	No	2sig	OM2C
SR	CS planarity	E	C22	1,4	0,0	3,4	0,0	4,3	0,0	0	Yes(*)	2sig	OM2C
SR	CS planarity	N-E	C23	-2,0	-0,6	-2,0	-0,4	0,5	0,0	0	Yes(*)	2sig	OM2C
SR	CS planarity	N-W	C24	-10,7	-0,8	14,9	29,6	61,0	0,0	0	Yes(*)	2sig	OM2C
SR	CS planarity	W	C25	-46,9	0,0	36,1	0,0	-150,0	0,0	0	Yes(*)	2sig	OM2C
SR	CS planarity	S-W	C26	-10,7	0,8	14,9	-29,6	61,0	0,0	0	Yes(*)	2sig	OM2C
SR	CS planarity	S-E	C27	-2,0	0,6	-2,0	0,4	0,5	0,0	0	Yes(*)	2sig	OM2C
SR	TTA	E	C28	0,2	0,0	0,5	0,0	-0,4	0,0	0	Yes(*)	2sig	OM2C
SR	TTA	N-E	C29	0,0	0,1	0,6	0,8	1,2	0,0	0	Yes(*)	2sig	OM2C
SR	TTA	N-W	C30	-1,9	-0,6	2,5	4,1	9,4	0,0	0	Yes(*)	2sig	OM2C
SR	TTA	W	C31	-7,1	0,0	4,6	0,0	-21,0	0,0	0	Yes(*)	2sig	OM2C
SR	TTA	S-W	C32	-1,9	0,6	2,5	-4,1	9,4	0,0	0	Yes(*)	2sig	OM2C
SR	TTA	S-E	C33	0,0	-0,1	0,6	-0,8	1,2	0,0	0	Yes(*)	2sig	OM2C
SR	Structure launch		C57	20,0	20,0	20,0	20,0	20,0	0,0	0	No	2sig	OM2C
SR	Structure creeping		C58	20,0	20,0	20,0	20,0	20,0	0,0	0	No	2sig	OM2C
SR	Structure lifetime		C59	20,0	20,0	20,0	20,0	20,0	0,0	0	No	2sig	OM2C
SR	dT in-orbit	Struc	C37	8,5	-0,3	5,5	0,6	37,3	0,0	0	Yes(*)	2sig	OM2C
SR	dT in-orbit	refl	C38	-3,3	-0,1	-0,7	-0,2	-0,6	4,0	0	Yes(*)	2sig	OM2
SR	ISM-A	Rad	C60	-11,5	0,0	-1,5	0,0	-15,5	-2,0	0	Yes	2sig	OM2
SR	ISM-A	Tang	C61	0,0	-46,0	0,0	0,0	0,0	0,0	0	Yes	2sig	OM2
SR	ISM-A	Out-of-pl	C62	-34,0	0,0	60,0	0,0	0,0	0,3	-0	Yes	2sig	OM2
SR	ISM-A	Rotation	C63	0,0	6,0	0,0	0,0	0,0	0,0	0	Yes	2sig	OM2
SR	ISM-B	Rad	C64	11,5	0,0	-1,5	0,0	15,5	-2,0	0	Yes	2sig	OM2
SR	ISM-B	Tang	C65	0,0	-46,0	-0,1	0,0	0,0	0,0	0	Yes	2sig	OM2
SR	ISM-B	Out-of-pl	C66	-34,0	0,0	60,0	0,0	0,0	0,3	-0	Yes	2sig	OM2
SR	ISM-B	Rotation	C67	0,0	6,0	0,0	0,0	0,0	0,0	0	Yes	2sig	OM2
SR	FEM acc		C68	1,0	1,0	1,0	1,0	1,0	1,0	0	No	2sig	OM2
FPU	Shimming accuracy		C69	592	412	414	-	-	-	-	No	2sig	RDP
	Stability		C70	400	400	100	-	-	-	-	No	2sig	RDP

Table 8.4-9 Input parameters for sensitivity analysis : Random case

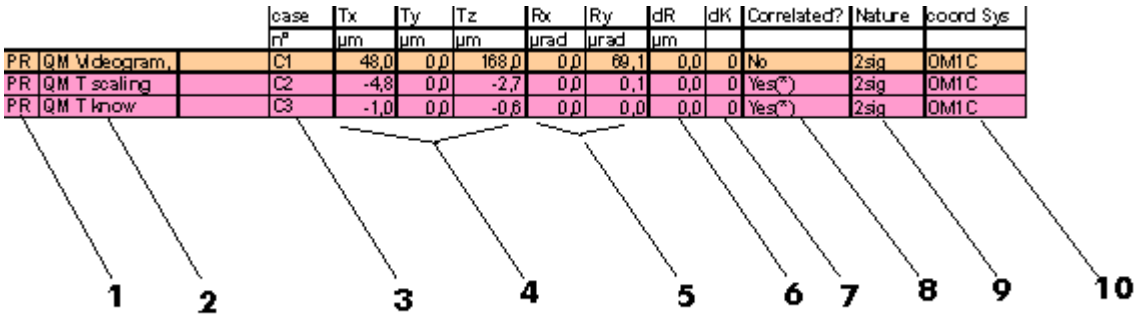

		case	Tx	Ty	Tz	Rx	Ry	dR	dK	Correlated?	Nature	coord Sys
		n°	µm	µm	µm	µrad	µrad	µm				
PR	QM Videogram,	C1	48,0	0,0	168,0	0,0	69,1	0,0	0	No	2sig	OM1C
PR	QM T scaling	C2	-4,8	0,0	-2,7	0,0	0,1	0,0	0	Yes(*)	2sig	OM1C
PR	QM T know	C3	-1,0	0,0	-0,6	0,0	0,0	0,0	0	Yes(*)	2sig	OM1C

1 2 3 4 5 6 7 8 9 10

Table 8.4-10 Descriptions of the columns

1 : **SR** (secondary reflector), **PR**(primary reflector) or **FPU** (focal plane unit)
2 : sub load case **name**
3 : case identification **CX**
4 : translation variation : **Tx, Ty,Tz**
5 : rotation variation : **Rx , Ry**
6 : radius variation **dR**
7 : conicity variation **dK**
8 : correlation type : **No, Yes, Yes (*) :**

No : means that the gain degradation of all individual variation and his opposite variation (translation, rotation, radius or conicity) have been computed. The total gain degradation is obtained by a RSS summation of induvidual degradation due to each variation (or his opposite variation if it constitute the worst case).

Yes : means that the gain degradation of the set of variations (translations, rotation, radius and conicity) and his opposite set) for the PR or the SR have been computed. The worst case between the set of variation and the opposite have been taken as gain degradation for this case.

Yes(*) : means that the gain degradation of the set of variations (translations, rotations, radius and conicity) and his opposite set) the SR and PR have been computed. The worst case between the set of variation and the opposite have been taken as gain degradation for this case.

9 : Error type
10 : Coordinate system (**OM1, OM2, OM1C, OM2C, ORDP**)

The geometry of the telescope is modified for each variation and the simulation of the telescope gives the far field radiation pattern which is then compared to the computed reference pattern.
The total (RSS summation) of these contributors is given in Table 8.4-18.

detector n°	case1	case2	case3	case4	case5	case6	case7	case8	case9	case10
	dB	dB	dB	dB	dB	dB	dB	dB	dB	dB
lfi_70_18	0.0036	0.0006	0.0002	0.0004	0.0006	0.0003	0.0003	0.0003	0.0001	0.0003
lfi_70_19	0.0036	0.0008	0.0002	0.0014	0.0010	0.0003	0.0007	0.0006	0.0004	0.0014
lfi_70_20	0.0071	0.0013	0.0002	0.0025	0.0021	0.0006	0.0007	0.0003	0.0008	0.0016
lfi_70_21	0.0071	0.0013	0.0002	0.0025	0.0021	0.0006	0.0002	0.0008	0.0008	0.0012
lfi_70_22	0.0036	0.0008	0.0002	0.0014	0.0010	0.0003	0.0004	0.0009	0.0004	0.0005
lfi_70_23	0.0036	0.0006	0.0002	0.0004	0.0006	0.0003	0.0002	0.0004	0.0001	0.0005
lfi_44_24	0.0052	0.0005	0.0001	0.0013	0.0010	0.0003	0.0003	0.0004	0.0002	0.0004
lfi_44_25	0.0039	0.0004	0.0001	0.0002	0.0006	0.0000	0.0007	0.0006	0.0004	0.0005
lfi_44_26	0.0039	0.0004	0.0001	0.0003	0.0006	0.0000	0.0004	0.0009	0.0004	0.0012
lfi_30_27	0.0030	0.0006	0.0001	0.0009	0.0006	0.0002	0.0001	0.0002	0.0003	0.0004
lfi_30_28	0.0030	0.0006	0.0001	0.0009	0.0006	0.0002	0.0002	0.0001	0.0003	0.0006
hfi_100_1	0.0030	0.0022	0.0004	0.0011	0.0015	0.0008	0.0012	0.0020	0.0017	0.0007
hfi_100_2	0.0083	0.0031	0.0005	0.0032	0.0035	0.0012	0.0017	0.0012	0.0019	0.0050
hfi_100_3	0.0083	0.0031	0.0005	0.0032	0.0035	0.0012	0.0007	0.0021	0.0019	0.0027
hfi_100_4	0.0030	0.0022	0.0004	0.0011	0.0015	0.0008	0.0015	0.0017	0.0017	0.0038
hfi_143_1	0.0035	0.0015	0.0005	0.0009	0.0006	0.0010	0.0021	0.0025	0.0015	0.0033
hfi_143_2	0.0066	0.0028	0.0008	0.0038	0.0032	0.0014	0.0009	0.0009	0.0018	0.0026
hfi_143_3	0.0056	0.0003	0.0003	0.0020	0.0007	0.0006	0.0004	0.0006	0.0013	0.0003
hfi_143_4	0.0035	0.0015	0.0005	0.0009	0.0006	0.0010	0.0021	0.0025	0.0015	0.0033
hfi_143_5	0.0090	0.0009	0.0001	0.0025	0.0014	0.0002	0.0004	0.0004	0.0006	0.0013
hfi_143_6	0.0153	0.0010	0.0002	0.0037	0.0025	0.0002	0.0009	0.0008	0.0007	0.0016
hfi_143_7	0.0146	0.0005	0.0001	0.0032	0.0018	0.0002	0.0005	0.0012	0.0006	0.0006
hfi_143_8	0.0092	0.0025	0.0005	0.0025	0.0028	0.0012	0.0005	0.0003	0.0018	0.0027
hfi_217_1	0.0114	0.0027	0.0009	0.0023	0.0026	0.0016	0.0020	0.0021	0.0024	0.0048
hfi_217_2	0.0099	0.0012	0.0006	0.0030	0.0021	0.0012	0.0007	0.0024	0.0006	0.0021
hfi_217_3	0.0102	0.0008	0.0005	0.0028	0.0019	0.0011	0.0018	0.0015	0.0004	0.0003
hfi_217_4	0.0120	0.0023	0.0009	0.0016	0.0022	0.0014	0.0015	0.0020	0.0020	0.0031
hfi_217_5	0.0200	0.0008	0.0006	0.0018	0.0024	0.0012	0.0007	0.0004	0.0007	0.0015
hfi_217_6	0.0120	0.0018	0.0005	0.0014	0.0012	0.0012	0.0008	0.0008	0.0023	0.0006
hfi_217_7	0.0102	0.0006	0.0006	0.0018	0.0008	0.0013	0.0005	0.0015	0.0007	0.0017
hfi_217_8	0.0197	0.0006	0.0006	0.0007	0.0014	0.0015	0.0016	0.0017	0.0020	0.0009
hfi_353_1	0.0838	0.0022	0.0014	0.0090	0.0083	0.0027	0.0036	0.0027	0.0021	0.0040
hfi_353_2	0.0559	0.0023	0.0008	0.0034	0.0045	0.0019	0.0036	0.0029	0.0017	0.0032
hfi_353_3	0.0415	0.0014	0.0008	0.0010	0.0013	0.0015	0.0022	0.0014	0.0012	0.0012
hfi_353_4	0.0357	0.0009	0.0007	0.0023	0.0005	0.0019	0.0020	0.0013	0.0023	0.0018
hfi_353_5	0.0328	0.0018	0.0008	0.0015	0.0010	0.0013	0.0028	0.0027	0.0028	0.0037
hfi_353_6	0.0430	0.0011	0.0008	0.0014	0.0012	0.0013	0.0034	0.0029	0.0006	0.0025
hfi_353_7	0.0612	0.0010	0.0012	0.0050	0.0043	0.0019	0.0032	0.0032	0.0011	0.0007
hfi_353_8	0.0842	0.0033	0.0004	0.0074	0.0090	0.0017	0.0021	0.0032	0.0020	0.0040
hfi_545_1	0.1421	0.0046	0.0014	0.0144	0.0152	0.0044	0.0091	0.0019	0.0030	0.0107
hfi_545_2	0.1164	0.0021	0.0007	0.0055	0.0073	0.0024	0.0078	0.0006	0.0015	0.0041
hfi_545_3	0.1234	0.0020	0.0008	0.0072	0.0076	0.0015	0.0013	0.0073	0.0007	0.0026
hfi_545_4	0.1405	0.0050	0.0019	0.0139	0.0154	0.0046	0.0015	0.0098	0.0032	0.0021
hfi_857_1	0.1937	0.0014	0.0007	0.0011	0.0004	0.0005	0.0100	0.0031	0.0068	0.0032
hfi_857_2	0.1643	0.0023	0.0017	0.0088	0.0064	0.0033	0.0067	0.0039	0.0086	0.0097
hfi_857_3	0.1706	0.0020	0.0006	0.0083	0.0048	0.0031	0.0058	0.0095	0.0079	0.0120
hfi_857_4	0.2025	0.0013	0.0010	0.0005	0.0035	0.0006	0.0042	0.0135	0.0058	0.0098

Table 8.4-11 random case (1 to 10) (2σ)

detector n°	case11	case12	case13	case14	case15	case16	case17	case18	case19	case20
	dB	dB	dB	dB	dB	dB	dB	dB	dB	dB
lfi_70_18	0.0006	0.0001	0.0000	0.0001	0.0001	0.0003	0.0000	0.0009	0.0001	0.0004
lfi_70_19	0.0010	0.0004	0.0000	0.0006	0.0002	0.0008	0.0001	0.0013	0.0006	0.0004
lfi_70_20	0.0011	0.0004	0.0001	0.0013	0.0005	0.0017	0.0001	0.0021	0.0014	0.0000
lfi_70_21	0.0006	0.0009	0.0001	0.0013	0.0005	0.0017	0.0001	0.0021	0.0014	0.0000
lfi_70_22	0.0002	0.0009	0.0000	0.0006	0.0002	0.0008	0.0001	0.0013	0.0006	0.0004
lfi_70_23	0.0000	0.0005	0.0000	0.0001	0.0001	0.0003	0.0000	0.0009	0.0001	0.0004
lfi_44_24	0.0004	0.0003	0.0000	0.0005	0.0003	0.0007	0.0001	0.0014	0.0005	0.0005
lfi_44_25	0.0007	0.0008	0.0000	0.0003	0.0002	0.0004	0.0000	0.0008	0.0003	0.0005
lfi_44_26	0.0008	0.0007	0.0000	0.0003	0.0002	0.0004	0.0000	0.0008	0.0003	0.0005
lfi_30_27	0.0002	0.0003	0.0000	0.0004	0.0002	0.0005	0.0001	0.0008	0.0004	0.0003
lfi_30_28	0.0004	0.0001	0.0000	0.0004	0.0002	0.0005	0.0001	0.0008	0.0004	0.0003
hfi_100_1	0.0009	0.0024	0.0001	0.0022	0.0004	0.0020	0.0002	0.0015	0.0024	0.0018
hfi_100_2	0.0030	0.0005	0.0001	0.0028	0.0008	0.0036	0.0003	0.0029	0.0031	0.0013
hfi_100_3	0.0006	0.0025	0.0001	0.0028	0.0008	0.0036	0.0003	0.0029	0.0031	0.0013
hfi_100_4	0.0027	0.0011	0.0001	0.0022	0.0004	0.0020	0.0002	0.0015	0.0024	0.0018
hfi_143_1	0.0036	0.0016	0.0001	0.0016	0.0004	0.0008	0.0002	0.0009	0.0014	0.0006
hfi_143_2	0.0015	0.0008	0.0002	0.0024	0.0009	0.0029	0.0004	0.0036	0.0026	0.0020
hfi_143_3	0.0012	0.0009	0.0001	0.0009	0.0003	0.0003	0.0001	0.0019	0.0007	0.0007
hfi_143_4	0.0036	0.0016	0.0001	0.0016	0.0004	0.0008	0.0002	0.0009	0.0014	0.0006
hfi_143_5	0.0007	0.0008	0.0000	0.0009	0.0001	0.0008	0.0000	0.0028	0.0010	0.0015
hfi_143_6	0.0010	0.0012	0.0000	0.0005	0.0003	0.0015	0.0001	0.0039	0.0008	0.0003
hfi_143_7	0.0011	0.0010	0.0000	0.0006	0.0004	0.0010	0.0000	0.0034	0.0007	0.0006
hfi_143_8	0.0017	0.0011	0.0001	0.0026	0.0008	0.0027	0.0003	0.0023	0.0029	0.0005
hfi_217_1	0.0039	0.0026	0.0002	0.0024	0.0008	0.0027	0.0004	0.0021	0.0026	0.0015
hfi_217_2	0.0010	0.0027	0.0001	0.0007	0.0010	0.0015	0.0003	0.0028	0.0010	0.0003
hfi_217_3	0.0029	0.0012	0.0001	0.0004	0.0009	0.0012	0.0003	0.0027	0.0006	0.0003
hfi_217_4	0.0020	0.0031	0.0002	0.0019	0.0005	0.0023	0.0004	0.0018	0.0020	0.0010
hfi_217_5	0.0008	0.0012	0.0001	0.0008	0.0003	0.0018	0.0002	0.0032	0.0011	0.0004
hfi_217_6	0.0009	0.0014	0.0001	0.0019	0.0002	0.0009	0.0002	0.0010	0.0017	0.0017
hfi_217_7	0.0008	0.0014	0.0001	0.0009	0.0011	0.0006	0.0003	0.0018	0.0009	0.0002
hfi_217_8	0.0018	0.0015	0.0002	0.0020	0.0014	0.0015	0.0004	0.0025	0.0019	0.0008
hfi_353_1	0.0035	0.0016	0.0005	0.0052	0.0049	0.0061	0.0010	0.0133	0.0057	0.0021
hfi_353_2	0.0037	0.0025	0.0001	0.0039	0.0030	0.0042	0.0002	0.0079	0.0041	0.0023
hfi_353_3	0.0010	0.0020	0.0001	0.0014	0.0015	0.0020	0.0003	0.0024	0.0019	0.0034
hfi_353_4	0.0023	0.0027	0.0001	0.0014	0.0013	0.0011	0.0003	0.0027	0.0019	0.0032
hfi_353_5	0.0028	0.0025	0.0002	0.0017	0.0024	0.0012	0.0005	0.0033	0.0018	0.0015
hfi_353_6	0.0013	0.0016	0.0002	0.0008	0.0029	0.0010	0.0005	0.0044	0.0010	0.0021
hfi_353_7	0.0019	0.0013	0.0004	0.0033	0.0040	0.0031	0.0008	0.0084	0.0035	0.0020
hfi_353_8	0.0014	0.0013	0.0002	0.0055	0.0033	0.0073	0.0003	0.0120	0.0060	0.0037
hfi_545_1	0.0099	0.0042	0.0003	0.0084	0.0074	0.0113	0.0009	0.0209	0.0089	0.0038
hfi_545_2	0.0044	0.0030	0.0003	0.0038	0.0060	0.0053	0.0005	0.0114	0.0042	0.0064
hfi_545_3	0.0009	0.0032	0.0002	0.0047	0.0055	0.0056	0.0002	0.0121	0.0049	0.0058
hfi_545_4	0.0012	0.0069	0.0007	0.0084	0.0079	0.0118	0.0014	0.0213	0.0091	0.0036
hfi_857_1	0.0028	0.0043	0.0003	0.0029	0.0097	0.0031	0.0006	0.0125	0.0038	0.0131
hfi_857_2	0.0024	0.0048	0.0005	0.0051	0.0088	0.0051	0.0012	0.0131	0.0063	0.0126
hfi_857_3	0.0048	0.0018	0.0003	0.0030	0.0084	0.0037	0.0006	0.0112	0.0044	0.0134
hfi_857_4	0.0045	0.0040	0.0006	0.0035	0.0109	0.0037	0.0009	0.0143	0.0045	0.0142

Table 8.4-12 random case (11 to 20) (2σ)

detector n°	case21	case22	case23	case24	case25	case26	case27	case28	case29	case30
	dB	dB	dB	dB	dB	dB	dB	dB	dB	dB
lfi_70_18	0.0120	0.0041	0.0051	0.0029	0.0008	0.0054	0.0003	0.0007	0.0007	0.0007
lfi_70_19	0.0118	0.0015	0.0006	0.0062	0.0031	0.0019	0.0042	0.0010	0.0001	0.0015
lfi_70_20	0.0081	0.0041	0.0035	0.0057	0.0049	0.0022	0.0058	0.0020	0.0013	0.0015
lfi_70_21	0.0081	0.0041	0.0058	0.0016	0.0049	0.0062	0.0035	0.0020	0.0019	0.0009
lfi_70_22	0.0118	0.0015	0.0042	0.0023	0.0031	0.0060	0.0006	0.0010	0.0013	0.0003
lfi_70_23	0.0120	0.0041	0.0003	0.0052	0.0008	0.0025	0.0051	0.0007	0.0005	0.0004
lfi_44_24	0.0057	0.0035	0.0043	0.0040	0.0063	0.0047	0.0043	0.0008	0.0006	0.0007
lfi_44_25	0.0166	0.0037	0.0067	0.0081	0.0034	0.0064	0.0004	0.0008	0.0012	0.0012
lfi_44_26	0.0166	0.0037	0.0004	0.0061	0.0034	0.0076	0.0067	0.0008	0.0003	0.0009
lfi_30_27	0.0057	0.0007	0.0021	0.0019	0.0033	0.0048	0.0011	0.0005	0.0007	0.0003
lfi_30_28	0.0057	0.0007	0.0011	0.0048	0.0033	0.0018	0.0021	0.0005	0.0003	0.0005
hfi_100_1	0.0160	0.0012	0.0060	0.0104	0.0052	0.0043	0.0034	0.0017	0.0034	0.0017
hfi_100_2	0.0092	0.0041	0.0052	0.0073	0.0053	0.0020	0.0096	0.0023	0.0029	0.0044
hfi_100_3	0.0092	0.0041	0.0096	0.0011	0.0053	0.0081	0.0052	0.0023	0.0040	0.0009
hfi_100_4	0.0160	0.0012	0.0034	0.0039	0.0052	0.0095	0.0060	0.0017	0.0016	0.0037
hfi_143_1	0.0225	0.0001	0.0076	0.0085	0.0023	0.0069	0.0053	0.0004	0.0006	0.0043
hfi_143_2	0.0107	0.0068	0.0068	0.0016	0.0064	0.0083	0.0042	0.0031	0.0029	0.0016
hfi_143_3	0.0112	0.0043	0.0044	0.0090	0.0054	0.0031	0.0068	0.0011	0.0006	0.0018
hfi_143_4	0.0225	0.0001	0.0076	0.0085	0.0023	0.0069	0.0053	0.0004	0.0006	0.0043
hfi_143_5	0.0258	0.0079	0.0126	0.0031	0.0077	0.0159	0.0045	0.0015	0.0015	0.0008
hfi_143_6	0.0152	0.0114	0.0116	0.0069	0.0105	0.0130	0.0109	0.0025	0.0012	0.0020
hfi_143_7	0.0150	0.0109	0.0113	0.0120	0.0108	0.0085	0.0120	0.0019	0.0011	0.0015
hfi_143_8	0.0256	0.0090	0.0029	0.0157	0.0068	0.0016	0.0110	0.0020	0.0025	0.0027
hfi_217_1	0.0232	0.0014	0.0074	0.0072	0.0038	0.0092	0.0071	0.0020	0.0038	0.0043
hfi_217_2	0.0116	0.0075	0.0041	0.0094	0.0033	0.0028	0.0081	0.0024	0.0008	0.0019
hfi_217_3	0.0118	0.0082	0.0088	0.0022	0.0034	0.0091	0.0046	0.0022	0.0014	0.0033
hfi_217_4	0.0227	0.0009	0.0059	0.0095	0.0038	0.0066	0.0068	0.0018	0.0032	0.0030
hfi_217_5	0.0167	0.0081	0.0090	0.0026	0.0058	0.0091	0.0054	0.0022	0.0011	0.0013
hfi_217_6	0.0094	0.0019	0.0007	0.0020	0.0018	0.0014	0.0018	0.0020	0.0021	0.0013
hfi_217_7	0.0105	0.0030	0.0021	0.0025	0.0017	0.0023	0.0012	0.0012	0.0009	0.0018
hfi_217_8	0.0182	0.0069	0.0047	0.0103	0.0065	0.0031	0.0078	0.0007	0.0020	0.0030
hfi_353_1	0.0577	0.0370	0.0332	0.0418	0.0405	0.0313	0.0390	0.0072	0.0060	0.0073
hfi_353_2	0.0396	0.0146	0.0140	0.0207	0.0241	0.0172	0.0172	0.0027	0.0032	0.0057
hfi_353_3	0.0281	0.0021	0.0016	0.0093	0.0169	0.0097	0.0028	0.0010	0.0012	0.0012
hfi_353_4	0.0243	0.0094	0.0076	0.0047	0.0134	0.0050	0.0071	0.0022	0.0014	0.0014
hfi_353_5	0.0239	0.0083	0.0044	0.0039	0.0115	0.0042	0.0052	0.0014	0.0027	0.0028
hfi_353_6	0.0300	0.0031	0.0074	0.0113	0.0191	0.0130	0.0057	0.0010	0.0005	0.0014
hfi_353_7	0.0419	0.0183	0.0209	0.0193	0.0291	0.0262	0.0176	0.0039	0.0029	0.0030
hfi_353_8	0.0597	0.0360	0.0382	0.0277	0.0405	0.0438	0.0319	0.0058	0.0072	0.0035
hfi_545_1	0.1396	0.0565	0.0356	0.0976	0.0727	0.0277	0.0781	0.0107	0.0062	0.0168
hfi_545_2	0.1102	0.0185	0.0069	0.0660	0.0582	0.0131	0.0395	0.0031	0.0015	0.0110
hfi_545_3	0.1165	0.0253	0.0446	0.0146	0.0632	0.0730	0.0130	0.0053	0.0098	0.0026
hfi_545_4	0.1407	0.0559	0.0771	0.0196	0.0718	0.1024	0.0350	0.0108	0.0155	0.0032
hfi_857_1	0.1624	0.0288	0.0309	0.0749	0.0946	0.0140	0.0101	0.0054	0.0060	0.0118
hfi_857_2	0.1222	0.0575	0.0464	0.0374	0.0743	0.0115	0.0360	0.0119	0.0085	0.0049
hfi_857_3	0.1302	0.0554	0.0313	0.0189	0.0780	0.0396	0.0466	0.0115	0.0044	0.0022
hfi_857_4	0.1763	0.0187	0.0226	0.0174	0.1019	0.0854	0.0250	0.0045	0.0073	0.0035

Table 8.4-13 random case (21 to 30) (2σ)

detector n°	case31	case32	case33	case34	case35	case36	case37	case38	case39	case40
	dB	dB	dB	dB	dB	dB	dB	dB	dB	dB
lfi_70_18	0.0007	0.0004	0.0005	0.0020	0.0020	0.0020	0.0007	0.0004	0.0004	0.0001
lfi_70_19	0.0007	0.0003	0.0013	0.0031	0.0031	0.0031	0.0011	0.0001	0.0001	0.0001
lfi_70_20	0.0011	0.0009	0.0019	0.0032	0.0032	0.0032	0.0017	0.0003	0.0003	0.0001
lfi_70_21	0.0011	0.0015	0.0013	0.0032	0.0032	0.0032	0.0014	0.0003	0.0003	0.0001
lfi_70_22	0.0007	0.0015	0.0001	0.0031	0.0031	0.0031	0.0007	0.0001	0.0001	0.0001
lfi_70_23	0.0007	0.0007	0.0007	0.0020	0.0020	0.0020	0.0006	0.0004	0.0004	0.0001
lfi_44_24	0.0006	0.0007	0.0006	0.0018	0.0018	0.0018	0.0006	0.0001	0.0001	0.0000
lfi_44_25	0.0005	0.0009	0.0003	0.0031	0.0031	0.0031	0.0008	0.0004	0.0004	0.0001
lfi_44_26	0.0005	0.0012	0.0012	0.0031	0.0031	0.0031	0.0003	0.0004	0.0004	0.0001
lfi_30_27	0.0006	0.0005	0.0003	0.0012	0.0012	0.0012	0.0006	0.0002	0.0002	0.0000
lfi_30_28	0.0006	0.0003	0.0007	0.0012	0.0012	0.0012	0.0007	0.0002	0.0002	0.0000
hfi_100_1	0.0010	0.0037	0.0016	0.0053	0.0053	0.0053	0.0013	0.0010	0.0010	0.0002
hfi_100_2	0.0021	0.0009	0.0040	0.0054	0.0054	0.0054	0.0040	0.0014	0.0014	0.0002
hfi_100_3	0.0021	0.0044	0.0029	0.0054	0.0054	0.0054	0.0034	0.0014	0.0014	0.0002
hfi_100_4	0.0010	0.0017	0.0034	0.0053	0.0053	0.0053	0.0022	0.0010	0.0010	0.0002
hfi_143_1	0.0019	0.0021	0.0027	0.0058	0.0058	0.0058	0.0018	0.0013	0.0013	0.0003
hfi_143_2	0.0022	0.0014	0.0024	0.0053	0.0053	0.0053	0.0030	0.0009	0.0009	0.0000
hfi_143_3	0.0011	0.0018	0.0002	0.0036	0.0036	0.0036	0.0004	0.0009	0.0009	0.0000
hfi_143_4	0.0019	0.0021	0.0027	0.0058	0.0058	0.0058	0.0018	0.0013	0.0013	0.0003
hfi_143_5	0.0006	0.0008	0.0016	0.0050	0.0050	0.0050	0.0008	0.0005	0.0005	0.0001
hfi_143_6	0.0004	0.0012	0.0012	0.0045	0.0045	0.0045	0.0016	0.0008	0.0008	0.0000
hfi_143_7	0.0006	0.0021	0.0011	0.0041	0.0041	0.0041	0.0007	0.0006	0.0006	0.0000
hfi_143_8	0.0022	0.0012	0.0040	0.0062	0.0062	0.0062	0.0023	0.0011	0.0011	0.0001
hfi_217_1	0.0018	0.0041	0.0038	0.0059	0.0059	0.0059	0.0034	0.0022	0.0022	0.0004
hfi_217_2	0.0009	0.0029	0.0017	0.0049	0.0049	0.0049	0.0018	0.0018	0.0018	0.0001
hfi_217_3	0.0011	0.0022	0.0004	0.0048	0.0048	0.0048	0.0009	0.0016	0.0016	0.0001
hfi_217_4	0.0014	0.0036	0.0031	0.0048	0.0048	0.0048	0.0022	0.0014	0.0014	0.0004
hfi_217_5	0.0005	0.0016	0.0013	0.0043	0.0043	0.0043	0.0010	0.0006	0.0006	0.0001
hfi_217_6	0.0019	0.0013	0.0013	0.0037	0.0037	0.0037	0.0009	0.0014	0.0014	0.0002
hfi_217_7	0.0012	0.0017	0.0004	0.0035	0.0035	0.0035	0.0013	0.0014	0.0014	0.0001
hfi_217_8	0.0025	0.0022	0.0017	0.0056	0.0056	0.0056	0.0004	0.0011	0.0011	0.0001
hfi_353_1	0.0055	0.0045	0.0059	0.0164	0.0164	0.0164	0.0025	0.0019	0.0019	0.0001
hfi_353_2	0.0045	0.0052	0.0053	0.0104	0.0104	0.0104	0.0029	0.0031	0.0031	0.0003
hfi_353_3	0.0018	0.0022	0.0024	0.0041	0.0041	0.0041	0.0014	0.0012	0.0012	0.0002
hfi_353_4	0.0018	0.0022	0.0016	0.0048	0.0048	0.0048	0.0008	0.0006	0.0006	0.0002
hfi_353_5	0.0029	0.0033	0.0016	0.0061	0.0061	0.0061	0.0005	0.0032	0.0032	0.0003
hfi_353_6	0.0023	0.0031	0.0007	0.0062	0.0062	0.0062	0.0004	0.0019	0.0019	0.0001
hfi_353_7	0.0042	0.0049	0.0035	0.0106	0.0106	0.0106	0.0014	0.0024	0.0024	0.0001
hfi_353_8	0.0052	0.0066	0.0066	0.0159	0.0159	0.0159	0.0044	0.0016	0.0016	0.0000
hfi_545_1	0.0103	0.0033	0.0155	0.0325	0.0325	0.0325	0.0073	0.0035	0.0035	0.0011
hfi_545_2	0.0079	0.0013	0.0079	0.0213	0.0213	0.0213	0.0039	0.0029	0.0029	0.0003
hfi_545_3	0.0086	0.0122	0.0011	0.0216	0.0216	0.0216	0.0015	0.0038	0.0038	0.0010
hfi_545_4	0.0100	0.0167	0.0053	0.0326	0.0326	0.0326	0.0047	0.0037	0.0037	0.0010
hfi_857_1	0.0105	0.0015	0.0053	0.0275	0.0275	0.0275	0.0045	0.0082	0.0082	0.0014
hfi_857_2	0.0089	0.0025	0.0055	0.0229	0.0229	0.0229	0.0015	0.0092	0.0092	0.0008
hfi_857_3	0.0095	0.0059	0.0087	0.0221	0.0221	0.0221	0.0011	0.0089	0.0089	0.0009
hfi_857_4	0.0131	0.0154	0.0059	0.0293	0.0293	0.0293	0.0037	0.0092	0.0092	0.0008

Table 8.4-14 random case (31 to 40) (2σ)

detector n°	case41	case42	case43	case44	case45	case46	case47	case48	case49	case50
	dB	dB	dB	dB	dB	dB	dB	dB	dB	dB
lfi_70_18	0.0015	0.0001	0.0005	0.0001	0.0015	0.0001	0.0001	0.0022	0.0005	0.0005
lfi_70_19	0.0023	0.0002	0.0001	0.0001	0.0023	0.0001	0.0001	0.0057	0.0015	0.0009
lfi_70_20	0.0039	0.0001	0.0002	0.0001	0.0039	0.0001	0.0001	0.0091	0.0027	0.0015
lfi_70_21	0.0039	0.0001	0.0002	0.0001	0.0039	0.0001	0.0001	0.0091	0.0027	0.0015
lfi_70_22	0.0023	0.0002	0.0001	0.0001	0.0023	0.0001	0.0001	0.0057	0.0015	0.0009
lfi_70_23	0.0015	0.0001	0.0005	0.0001	0.0015	0.0001	0.0001	0.0022	0.0005	0.0005
lfi_44_24	0.0037	0.0000	0.0002	0.0000	0.0037	0.0000	0.0001	0.0088	0.0014	0.0009
lfi_44_25	0.0008	0.0002	0.0004	0.0001	0.0008	0.0001	0.0001	0.0032	0.0005	0.0008
lfi_44_26	0.0008	0.0002	0.0004	0.0001	0.0008	0.0001	0.0001	0.0032	0.0005	0.0008
lfi_30_27	0.0017	0.0000	0.0002	0.0000	0.0017	0.0000	0.0000	0.0041	0.0010	0.0007
lfi_30_28	0.0017	0.0000	0.0002	0.0000	0.0017	0.0000	0.0000	0.0041	0.0010	0.0007
hfi_100_1	0.0018	0.0003	0.0010	0.0002	0.0018	0.0002	0.0003	0.0073	0.0022	0.0019
hfi_100_2	0.0047	0.0002	0.0012	0.0002	0.0047	0.0001	0.0003	0.0096	0.0048	0.0030
hfi_100_3	0.0047	0.0002	0.0012	0.0002	0.0047	0.0001	0.0003	0.0096	0.0048	0.0030
hfi_100_4	0.0018	0.0003	0.0010	0.0002	0.0018	0.0002	0.0003	0.0073	0.0022	0.0019
hfi_143_1	0.0025	0.0004	0.0011	0.0003	0.0025	0.0002	0.0003	0.0042	0.0021	0.0024
hfi_143_2	0.0039	0.0000	0.0008	0.0000	0.0039	0.0000	0.0003	0.0110	0.0045	0.0030
hfi_143_3	0.0047	0.0001	0.0010	0.0000	0.0047	0.0000	0.0001	0.0107	0.0014	0.0011
hfi_143_4	0.0025	0.0004	0.0011	0.0003	0.0025	0.0002	0.0003	0.0042	0.0021	0.0024
hfi_143_5	0.0064	0.0001	0.0006	0.0001	0.0064	0.0001	0.0001	0.0138	0.0020	0.0008
hfi_143_6	0.0094	0.0001	0.0009	0.0000	0.0094	0.0000	0.0001	0.0204	0.0032	0.0012
hfi_143_7	0.0098	0.0001	0.0008	0.0000	0.0098	0.0000	0.0001	0.0201	0.0026	0.0013
hfi_143_8	0.0046	0.0001	0.0008	0.0001	0.0046	0.0001	0.0002	0.0149	0.0041	0.0031
hfi_217_1	0.0035	0.0005	0.0020	0.0004	0.0035	0.0003	0.0006	0.0053	0.0034	0.0030
hfi_217_2	0.0007	0.0001	0.0018	0.0001	0.0007	0.0001	0.0003	0.0106	0.0025	0.0016
hfi_217_3	0.0009	0.0002	0.0017	0.0001	0.0009	0.0001	0.0002	0.0108	0.0021	0.0015
hfi_217_4	0.0036	0.0004	0.0012	0.0004	0.0036	0.0003	0.0006	0.0049	0.0028	0.0027
hfi_217_5	0.0074	0.0001	0.0009	0.0001	0.0074	0.0001	0.0003	0.0089	0.0019	0.0017
hfi_217_6	0.0024	0.0002	0.0012	0.0002	0.0024	0.0001	0.0003	0.0062	0.0026	0.0031
hfi_217_7	0.0032	0.0002	0.0014	0.0001	0.0032	0.0001	0.0003	0.0051	0.0013	0.0017
hfi_217_8	0.0085	0.0002	0.0010	0.0001	0.0085	0.0001	0.0004	0.0101	0.0019	0.0029
hfi_353_1	0.0377	0.0001	0.0018	0.0001	0.0377	0.0000	0.0008	0.0661	0.0099	0.0094
hfi_353_2	0.0231	0.0004	0.0027	0.0003	0.0231	0.0002	0.0006	0.0344	0.0055	0.0068
hfi_353_3	0.0150	0.0002	0.0008	0.0002	0.0150	0.0001	0.0004	0.0174	0.0018	0.0045
hfi_353_4	0.0101	0.0002	0.0003	0.0002	0.0101	0.0001	0.0004	0.0138	0.0012	0.0045
hfi_353_5	0.0088	0.0003	0.0032	0.0003	0.0088	0.0002	0.0006	0.0144	0.0023	0.0050
hfi_353_6	0.0156	0.0001	0.0018	0.0001	0.0156	0.0001	0.0004	0.0210	0.0020	0.0052
hfi_353_7	0.0257	0.0001	0.0020	0.0001	0.0257	0.0001	0.0006	0.0405	0.0057	0.0072
hfi_353_8	0.0391	0.0001	0.0019	0.0000	0.0391	0.0000	0.0005	0.0665	0.0103	0.0091
hfi_545_1	0.0657	0.0013	0.0034	0.0011	0.0657	0.0007	0.0014	0.1127	0.0182	0.0167
hfi_545_2	0.0472	0.0004	0.0020	0.0003	0.0472	0.0002	0.0008	0.0703	0.0102	0.0145
hfi_545_3	0.0520	0.0012	0.0031	0.0010	0.0520	0.0007	0.0013	0.0790	0.0105	0.0142
hfi_545_4	0.0648	0.0012	0.0033	0.0010	0.0648	0.0007	0.0015	0.1127	0.0178	0.0164
hfi_857_1	0.0650	0.0017	0.0080	0.0014	0.0650	0.0010	0.0023	0.0931	0.0086	0.0246
hfi_857_2	0.0424	0.0010	0.0085	0.0008	0.0424	0.0006	0.0020	0.0737	0.0077	0.0227
hfi_857_3	0.0469	0.0011	0.0085	0.0009	0.0469	0.0006	0.0017	0.0780	0.0066	0.0241
hfi_857_4	0.0707	0.0012	0.0080	0.0008	0.0707	0.0004	0.0016	0.1024	0.0111	0.0273

Table 8.4-15 random case (41 to 50) (2σ)

detector n°	case51	case52	case53	case54	case55	case56	case57	case58	case59	case60
	dB	dB	dB	dB	dB	dB	dB	dB	dB	dB
lfi_70_18	0.0000	0.0000	0.0004	0.0001	0.0002	0.0113	0.0014	0.0014	0.0014	0.0002
lfi_70_19	0.0001	0.0000	0.0005	0.0002	0.0005	0.0113	0.0030	0.0030	0.0030	0.0002
lfi_70_20	0.0001	0.0001	0.0008	0.0003	0.0011	0.0076	0.0034	0.0034	0.0034	0.0004
lfi_70_21	0.0001	0.0001	0.0008	0.0003	0.0011	0.0076	0.0034	0.0034	0.0034	0.0004
lfi_70_22	0.0001	0.0000	0.0005	0.0002	0.0005	0.0113	0.0030	0.0030	0.0030	0.0002
lfi_70_23	0.0000	0.0000	0.0004	0.0001	0.0002	0.0113	0.0014	0.0014	0.0014	0.0002
lfi_44_24	0.0001	0.0000	0.0004	0.0001	0.0004	0.0066	0.0017	0.0017	0.0017	0.0002
lfi_44_25	0.0001	0.0000	0.0001	0.0000	0.0003	0.0187	0.0029	0.0029	0.0029	0.0003
lfi_44_26	0.0001	0.0000	0.0001	0.0000	0.0003	0.0187	0.0029	0.0029	0.0029	0.0003
lfi_30_27	0.0000	0.0000	0.0004	0.0001	0.0004	0.0048	0.0013	0.0013	0.0013	0.0001
lfi_30_28	0.0000	0.0000	0.0004	0.0001	0.0004	0.0048	0.0013	0.0013	0.0013	0.0001
hfi_100_1	0.0001	0.0001	0.0010	0.0003	0.0018	0.0183	0.0054	0.0054	0.0054	0.0002
hfi_100_2	0.0002	0.0001	0.0017	0.0005	0.0025	0.0090	0.0061	0.0061	0.0061	0.0006
hfi_100_3	0.0002	0.0001	0.0017	0.0005	0.0025	0.0090	0.0061	0.0061	0.0061	0.0006
hfi_100_4	0.0001	0.0001	0.0010	0.0003	0.0018	0.0183	0.0054	0.0054	0.0054	0.0002
hfi_143_1	0.0001	0.0001	0.0014	0.0004	0.0020	0.0246	0.0046	0.0046	0.0046	0.0003
hfi_143_2	0.0002	0.0002	0.0020	0.0008	0.0022	0.0120	0.0056	0.0056	0.0056	0.0007
hfi_143_3	0.0000	0.0000	0.0008	0.0002	0.0012	0.0097	0.0031	0.0031	0.0031	0.0002
hfi_143_4	0.0001	0.0001	0.0014	0.0004	0.0020	0.0246	0.0046	0.0046	0.0046	0.0003
hfi_143_5	0.0000	0.0000	0.0003	0.0001	0.0007	0.0237	0.0043	0.0043	0.0043	0.0003
hfi_143_6	0.0001	0.0000	0.0003	0.0001	0.0003	0.0127	0.0045	0.0045	0.0045	0.0004
hfi_143_7	0.0001	0.0000	0.0004	0.0001	0.0009	0.0121	0.0039	0.0039	0.0039	0.0004
hfi_143_8	0.0002	0.0001	0.0018	0.0005	0.0027	0.0254	0.0059	0.0059	0.0059	0.0006
hfi_217_1	0.0002	0.0002	0.0020	0.0008	0.0028	0.0229	0.0054	0.0054	0.0054	0.0006
hfi_217_2	0.0001	0.0001	0.0013	0.0005	0.0006	0.0130	0.0043	0.0043	0.0043	0.0003
hfi_217_3	0.0001	0.0001	0.0015	0.0004	0.0002	0.0132	0.0040	0.0040	0.0040	0.0003
hfi_217_4	0.0002	0.0002	0.0017	0.0008	0.0025	0.0226	0.0043	0.0043	0.0043	0.0005
hfi_217_5	0.0001	0.0001	0.0015	0.0004	0.0011	0.0136	0.0038	0.0038	0.0038	0.0003
hfi_217_6	0.0001	0.0001	0.0016	0.0004	0.0027	0.0086	0.0031	0.0031	0.0031	0.0003
hfi_217_7	0.0001	0.0001	0.0018	0.0005	0.0003	0.0097	0.0033	0.0033	0.0033	0.0003
hfi_217_8	0.0002	0.0001	0.0021	0.0006	0.0013	0.0154	0.0043	0.0043	0.0043	0.0007
hfi_353_1	0.0007	0.0005	0.0044	0.0018	0.0022	0.0462	0.0136	0.0136	0.0136	0.0028
hfi_353_2	0.0004	0.0002	0.0030	0.0006	0.0026	0.0266	0.0080	0.0080	0.0080	0.0002
hfi_353_3	0.0003	0.0001	0.0012	0.0005	0.0016	0.0195	0.0053	0.0053	0.0053	0.0005
hfi_353_4	0.0003	0.0002	0.0022	0.0006	0.0025	0.0198	0.0047	0.0047	0.0047	0.0007
hfi_353_5	0.0004	0.0002	0.0018	0.0008	0.0038	0.0184	0.0050	0.0050	0.0050	0.0010
hfi_353_6	0.0004	0.0002	0.0020	0.0009	0.0019	0.0217	0.0055	0.0055	0.0055	0.0008
hfi_353_7	0.0006	0.0003	0.0030	0.0014	0.0017	0.0309	0.0087	0.0087	0.0087	0.0018
hfi_353_8	0.0005	0.0002	0.0029	0.0006	0.0025	0.0459	0.0142	0.0142	0.0142	0.0018
hfi_545_1	0.0010	0.0004	0.0071	0.0021	0.0028	0.1314	0.0303	0.0303	0.0303	0.0029
hfi_545_2	0.0010	0.0004	0.0047	0.0011	0.0030	0.0992	0.0215	0.0215	0.0215	0.0016
hfi_545_3	0.0010	0.0004	0.0033	0.0007	0.0019	0.1030	0.0215	0.0215	0.0215	0.0015
hfi_545_4	0.0011	0.0006	0.0074	0.0028	0.0029	0.1335	0.0294	0.0294	0.0294	0.0027
hfi_857_1	0.0018	0.0007	0.0029	0.0011	0.0116	0.1367	0.0302	0.0302	0.0302	0.0042
hfi_857_2	0.0018	0.0008	0.0031	0.0019	0.0131	0.1012	0.0253	0.0253	0.0253	0.0049
hfi_857_3	0.0017	0.0006	0.0016	0.0015	0.0120	0.1080	0.0269	0.0269	0.0269	0.0057
hfi_857_4	0.0022	0.0009	0.0029	0.0020	0.0104	0.1485	0.0337	0.0337	0.0337	0.0048

Table 8.4-16 random case (51 to 60) (2σ)

detector n°	case61	case62	case63	case64	case65	case66	case67	case68	case69	case70
	dB	dB	dB	dB	dB	dB	dB	dB	dB	dB
lfi_70_18	0.0039	0.0015	0.0003	0.0003	0.0039	0.0015	0.0003	0.0001	0.0084	0.0033
lfi_70_19	0.0039	0.0027	0.0006	0.0002	0.0039	0.0027	0.0006	0.0001	0.0084	0.0027
lfi_70_20	0.0022	0.0040	0.0004	0.0003	0.0022	0.0040	0.0004	0.0002	0.0087	0.0023
lfi_70_21	0.0022	0.0040	0.0004	0.0003	0.0022	0.0040	0.0004	0.0002	0.0087	0.0023
lfi_70_22	0.0039	0.0027	0.0006	0.0002	0.0039	0.0027	0.0006	0.0001	0.0084	0.0027
lfi_70_23	0.0039	0.0015	0.0003	0.0003	0.0039	0.0015	0.0003	0.0001	0.0084	0.0033
lfi_44_24	0.0001	0.0031	0.0001	0.0002	0.0001	0.0031	0.0001	0.0001	0.0157	0.0122
lfi_44_25	0.0055	0.0029	0.0007	0.0004	0.0055	0.0029	0.0007	0.0001	0.0165	0.0112
lfi_44_26	0.0055	0.0029	0.0007	0.0004	0.0055	0.0029	0.0007	0.0001	0.0165	0.0112
lfi_30_27	0.0018	0.0023	0.0001	0.0002	0.0018	0.0023	0.0001	0.0001	0.0072	0.0024
lfi_30_28	0.0018	0.0023	0.0001	0.0002	0.0018	0.0023	0.0001	0.0001	0.0072	0.0024
hfi_100_1	0.0039	0.0016	0.0013	0.0001	0.0039	0.0016	0.0013	0.0003	0.0131	0.0048
hfi_100_2	0.0007	0.0064	0.0010	0.0005	0.0008	0.0064	0.0010	0.0003	0.0102	0.0044
hfi_100_3	0.0007	0.0064	0.0010	0.0005	0.0007	0.0064	0.0010	0.0003	0.0102	0.0044
hfi_100_4	0.0039	0.0016	0.0013	0.0001	0.0040	0.0016	0.0013	0.0003	0.0131	0.0048
hfi_143_1	0.0067	0.0018	0.0018	0.0005	0.0067	0.0018	0.0018	0.0004	0.0151	0.0066
hfi_143_2	0.0024	0.0039	0.0002	0.0007	0.0024	0.0039	0.0002	0.0004	0.0130	0.0072
hfi_143_3	0.0020	0.0025	0.0002	0.0003	0.0020	0.0025	0.0002	0.0001	0.0125	0.0067
hfi_143_4	0.0067	0.0018	0.0018	0.0005	0.0067	0.0018	0.0018	0.0004	0.0151	0.0066
hfi_143_5	0.0069	0.0035	0.0002	0.0003	0.0069	0.0035	0.0002	0.0001	0.0138	0.0092
hfi_143_6	0.0017	0.0056	0.0005	0.0003	0.0017	0.0056	0.0005	0.0001	0.0153	0.0085
hfi_143_7	0.0017	0.0059	0.0005	0.0003	0.0017	0.0059	0.0005	0.0001	0.0155	0.0083
hfi_143_8	0.0074	0.0045	0.0002	0.0004	0.0074	0.0045	0.0002	0.0003	0.0162	0.0083
hfi_217_1	0.0067	0.0045	0.0018	0.0005	0.0067	0.0045	0.0018	0.0006	0.0067	0.0058
hfi_217_2	0.0038	0.0021	0.0011	0.0008	0.0038	0.0021	0.0011	0.0003	0.0105	0.0080
hfi_217_3	0.0038	0.0025	0.0011	0.0007	0.0038	0.0025	0.0011	0.0002	0.0107	0.0079
hfi_217_4	0.0061	0.0038	0.0019	0.0004	0.0060	0.0038	0.0019	0.0006	0.0065	0.0047
hfi_217_5	0.0037	0.0054	0.0007	0.0004	0.0037	0.0054	0.0007	0.0003	0.0086	0.0038
hfi_217_6	0.0028	0.0036	0.0007	0.0001	0.0028	0.0036	0.0007	0.0003	0.0128	0.0050
hfi_217_7	0.0033	0.0031	0.0007	0.0006	0.0033	0.0031	0.0007	0.0003	0.0137	0.0068
hfi_217_8	0.0050	0.0067	0.0007	0.0006	0.0050	0.0067	0.0007	0.0004	0.0093	0.0051
hfi_353_1	0.0049	0.0329	0.0005	0.0022	0.0050	0.0329	0.0005	0.0011	0.0348	0.0134
hfi_353_2	0.0033	0.0230	0.0013	0.0003	0.0033	0.0230	0.0013	0.0006	0.0292	0.0065
hfi_353_3	0.0011	0.0195	0.0016	0.0007	0.0011	0.0195	0.0016	0.0004	0.0267	0.0075
hfi_353_4	0.0008	0.0167	0.0015	0.0009	0.0008	0.0167	0.0015	0.0004	0.0247	0.0054
hfi_353_5	0.0009	0.0150	0.0011	0.0011	0.0009	0.0150	0.0011	0.0007	0.0248	0.0067
hfi_353_6	0.0016	0.0196	0.0015	0.0019	0.0015	0.0196	0.0015	0.0005	0.0279	0.0074
hfi_353_7	0.0021	0.0259	0.0011	0.0022	0.0021	0.0259	0.0011	0.0008	0.0300	0.0076
hfi_353_8	0.0068	0.0339	0.0004	0.0009	0.0068	0.0339	0.0004	0.0005	0.0354	0.0129
hfi_545_1	0.0332	0.0587	0.0055	0.0022	0.0333	0.0587	0.0055	0.0015	0.0767	0.0297
hfi_545_2	0.0232	0.0553	0.0041	0.0038	0.0232	0.0553	0.0041	0.0010	0.0848	0.0191
hfi_545_3	0.0247	0.0570	0.0033	0.0030	0.0247	0.0570	0.0033	0.0013	0.0850	0.0209
hfi_545_4	0.0337	0.0585	0.0044	0.0018	0.0336	0.0585	0.0044	0.0018	0.0765	0.0304
hfi_857_1	0.0259	0.0983	0.0043	0.0071	0.0259	0.0983	0.0043	0.0023	0.1816	0.0425
hfi_857_2	0.0101	0.0843	0.0005	0.0060	0.0102	0.0843	0.0005	0.0025	0.1707	0.0407
hfi_857_3	0.0117	0.0891	0.0008	0.0083	0.0116	0.0891	0.0008	0.0020	0.1750	0.0435
hfi_857_4	0.0290	0.1029	0.0047	0.0072	0.0288	0.1029	0.0047	0.0024	0.1845	0.0439

Table 8.4-17 random case (61 to 70) (2σ)

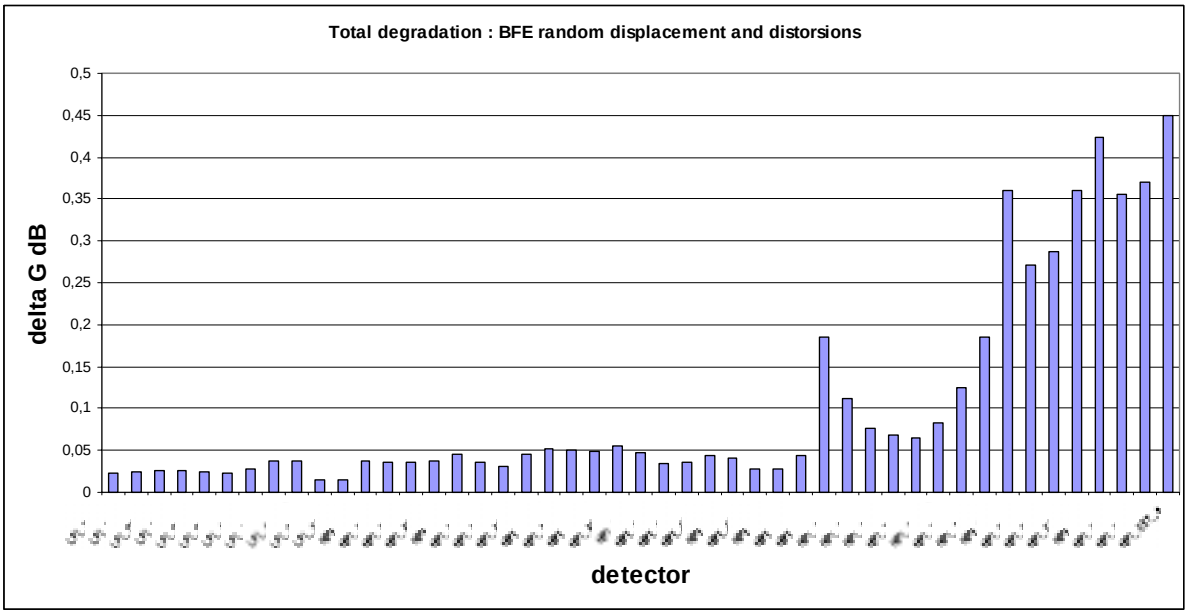

Figure 8.4-12 : Random cases 1 to 70 (2σ)

8.4.3.4 Total random case

The complete budget for the random contributors is presented in the Table 8.4-19.

detector n°	WFE per Horn contribution	Random BFE distorsion and displacements contribution	Total Random
	dB	dB	dB
LFI_70_18	0,0014	0,0227	**0,0228**
LFI_70_19	0,0014	0,0244	**0,0245**
LFI_70_20	0,0014	0,0256	**0,0257**
LFI_70_21	0,0014	0,0257	**0,0257**
LFI_70_22	0,0014	0,0243	**0,0244**
LFI_70_23	0,0014	0,0226	**0,0227**
LFI_44_24	0,0007	0,0280	**0,0280**
LFI_44_25	0,0007	0,0370	**0,0370**
LFI_44_26	0,0007	0,0369	**0,0369**
LFI_30_27	0,0004	0,0149	**0,0149**
LFI_30_28	0,0004	0,0149	**0,0149**
HFI_100_1	0,0025	0,0370	**0,0370**
HFI_100_2	0,0025	0,0351	**0,0352**
HFI_100_3	0,0025	0,0349	**0,0350**
HFI_100_4	0,0025	0,0369	**0,0370**
HFI_143_1	0,0037	0,0449	**0,0450**
HFI_143_2	0,0037	0,0359	**0,0361**
HFI_143_3	0,0037	0,0306	**0,0308**
HFI_143_4	0,0037	0,0449	**0,0450**
HFI_143_5	0,0037	0,0521	**0,0522**
HFI_143_6	0,0037	0,0500	**0,0502**
HFI_143_7	0,0037	0,0494	**0,0496**
HFI_143_8	0,0037	0,0549	**0,0550**
HFI_217_1	0,0083	0,0464	**0,0471**
HFI_217_2	0,0083	0,0346	**0,0356**
HFI_217_3	0,0083	0,0349	**0,0359**
HFI_217_4	0,0083	0,0436	**0,0444**
HFI_217_5	0,0083	0,0410	**0,0419**
HFI_217_6	0,0083	0,0275	**0,0287**
HFI_217_7	0,0083	0,0279	**0,0291**
HFI_217_8	0,0083	0,0446	**0,0453**
HFI_353_1	0,0126	0,1845	**0,1849**
HFI_353_2	0,0126	0,1124	**0,1131**
HFI_353_3	0,0126	0,0769	**0,0779**
HFI_353_4	0,0126	0,0674	**0,0685**
HFI_353_5	0,0126	0,0643	**0,0655**
HFI_353_6	0,0126	0,0829	**0,0838**
HFI_353_7	0,0126	0,1252	**0,1259**
HFI_353_8	0,0126	0,1856	**0,1860**
HFI_545_1	0,0293	0,3598	**0,3610**
HFI_545_2	0,0293	0,2710	**0,2726**
HFI_545_3	0,0293	0,2877	**0,2892**
HFI_545_4	0,0293	0,3598	**0,3610**
HFI_857_1	0,0725	0,4231	**0,4292**
HFI_857_2	0,0725	0,3552	**0,3625**
HFI_857_3	0,0725	0,3704	**0,3774**
HFI_857_4	0,0725	0,4492	**0,4550**

Table 8.4-18 Total Random case (2σ)

8.4.4 Complete Budget

The RF main lobe performance budget of Planck Telescope is shown in Table 8.4-19 and graphically displayed in Figure 8.4-13. The column “Total Budget” is obtained by summing linearly the determinist and random contribution.

detector n°	Total Deterministe	Total Random	Total Budget	Specifications
	dB	dB	dB	dB
LFI_70_18	0,0172	0,0228	0,0399	0,5
LFI_70_19	0,0195	0,0245	0,0439	0,5
LFI_70_20	0,0207	0,0257	0,0463	0,5
LFI_70_21	0,0217	0,0257	0,0474	0,5
LFI_70_22	0,0119	0,0244	0,0363	0,5
LFI_70_23	0,0200	0,0227	0,0426	0,5
LFI_44_24	0,0236	0,0280	0,0516	0,5
LFI_44_25	0,0192	0,0370	0,0562	0,5
LFI_44_26	0,0222	0,0369	0,0591	0,5
LFI_30_27	0,0130	0,0149	0,0279	0,5
LFI_30_28	0,0136	0,0149	0,0285	0,5
HFI_100_1	0,0255	0,0370	0,0625	0,5
HFI_100_2	0,0392	0,0352	0,0744	0,5
HFI_100_3	0,0344	0,0350	0,0694	0,5
HFI_100_4	0,0202	0,0370	0,0572	0,5
HFI_143_1	0,0256	0,0450	0,0706	0,5
HFI_143_2	0,0269	0,0361	0,0631	0,5
HFI_143_3	0,0335	0,0308	0,0643	0,5
HFI_143_4	0,0173	0,0450	0,0623	0,5
HFI_143_5	0,0349	0,0522	0,0870	0,5
HFI_143_6	0,0536	0,0502	0,1038	0,5
HFI_143_7	0,0595	0,0496	0,1090	0,5
HFI_143_8	0,0494	0,0550	0,1043	0,5
HFI_217_1	0,0289	0,0471	0,0760	1
HFI_217_2	0,0285	0,0356	0,0641	1
HFI_217_3	0,0274	0,0359	0,0632	1
HFI_217_4	0,0422	0,0444	0,0866	1
HFI_217_5	0,0532	0,0419	0,0951	1
HFI_217_6	0,0299	0,0287	0,0586	1
HFI_217_7	0,0349	0,0291	0,0640	1
HFI_217_8	0,0594	0,0453	0,1048	1
HFI_353_1	0,1971	0,1849	0,3820	1
HFI_353_2	0,1352	0,1131	0,2482	1
HFI_353_3	0,0853	0,0779	0,1632	1
HFI_353_4	0,0613	0,0685	0,1299	1
HFI_353_5	0,0672	0,0655	0,1327	1
HFI_353_6	0,0952	0,0838	0,1790	1
HFI_353_7	0,1437	0,1259	0,2696	1
HFI_353_8	0,1953	0,1860	0,3813	1
HFI_545_1	0,3462	0,3610	0,7072	1,4
HFI_545_2	0,2366	0,2726	0,5092	1,4
HFI_545_3	0,2468	0,2892	0,5361	1,4
HFI_545_4	0,3307	0,3610	0,6917	1,4
HFI_857_1	0,2570	0,4292	0,6863	2,5
HFI_857_2	0,1335	0,3625	0,4959	2,5
HFI_857_3	0,1605	0,3774	0,5379	2,5
HFI_857_4	0,2967	0,4550	0,7517	2,5

Table 8.4-19 Complete Budget (2σ)

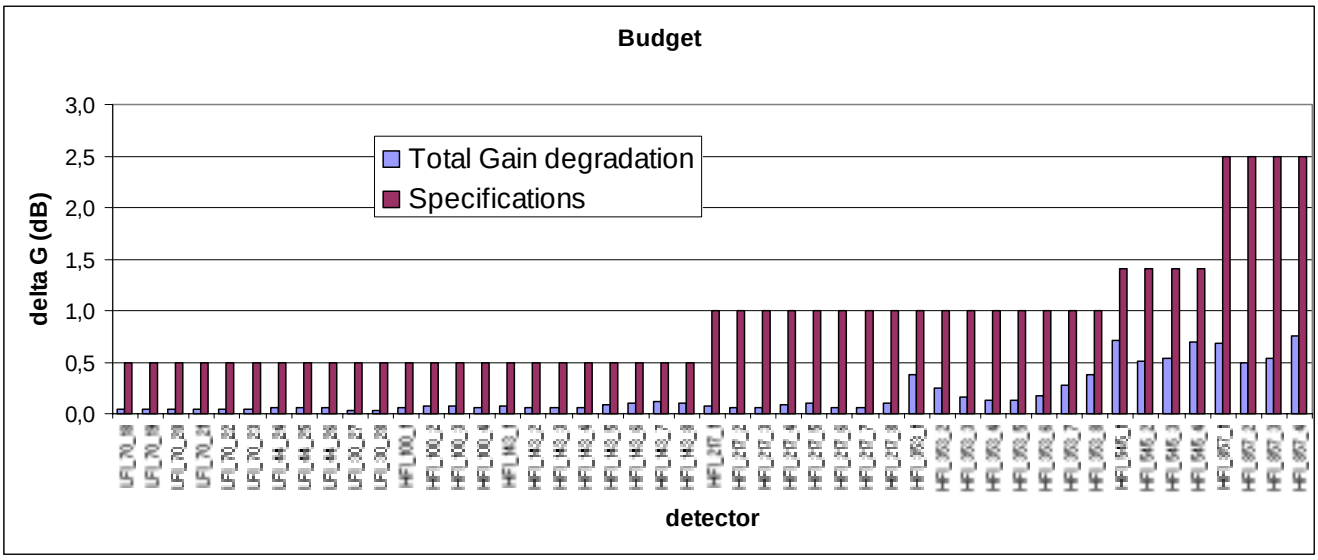

Figure 8.4-13 Total RF Budget of Planck Telescope (2σ)

8.4.5 Ellipticity deviation

For the ellipticity performance, no additionnal analysis have been performed since the PDR. Discussion on the method to be aplied to compute this performance is still open.

8.5 Conclusion

In this section, the RF main lobe performance of Planck Telescope budget is presented. Compared to the specifications, the results show a confortable margin.

9. CONCLUSION

For the requirement toward the Earth Sun and Moon, the results of the computation performed in the frame of the RF expertise (ideal reflector surfaces, no dust, sharp edges) show a significant margin. Anyhow this margin is dominated by the reflector dust contamination.

For the self spacecraft emission level the seleced appoach is consevative. In that case a significant margin of few order of magnitude is obtained. The most critical surface is the reflector then the other elements in the optical cavity.

On final the main lobe performance degradation is well below the allowed degradation.

Annex 1 : Quilting effect

Far-out sides lobes

The array configuration of the bumps on the reflectors generates grating lobes.
For detectors HFI_100_1, HFI_143_1, , HFI_217_1, HFI_353_1, HFI_545_1 and HFI_857_1, the radiation patterns have been computed in a large window (see Figure A1-A6 Annex A). The cuts in $\phi = 90$ plane (plane of symmetry of the telescope) are plotted in Figure B1 to B18 in Annex B. For the large patterns, the horns have been placed at the origin of the ORDP coordinate system, the initial orientation has been conserved for a first computation in order to have centered patterns and to avoid any research of the centers.

First, the angles θ for which the grating lobes have a maximum are determined and by using (1), the spacings have been computed. It appears that each of the reflector creates grating lobes. The grating lobes created by the secondary are re-concentrated by the main reflector. The distance d ≈ 52 mm corresponds to the geometrical spacing between cells on the main reflector. The second value d ≈ 94 mm correspond to the grating lobes equivalent spacing re-concentrated by the main reflector.

$$d = \frac{2\lambda}{\sin\theta} \qquad (1)$$

	Secondary	Primary		
Frequency	angle 1 (degres)	angle2 (degres)	spacing d	spacing d
100	3,68	6,6	93,4840441	52,2039754
143	2,55	4,623	94,3091537	52,0592693
217	1,67	3,027	94,8794103	52,3620417
353	1,034	1,87	94,1922172	52,0891752
545	0,67	1,208	94,1510751	52,2222319
857	0,434	0,768	92,4315621	52,2345255

Table : grating lobe angular spacing.

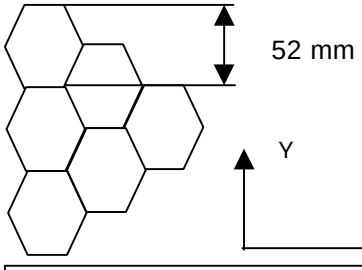

Figure : cell spacing

Due to the hexagonal shape of the cells the maximum of grating lobes occurs in the plane $\phi = 30$ and 60 degrees. (See patterns Figure A1 to Figure A6).

The level of rejection of the grating lobes is detailed and could reach 34.1 dB below the main beam peak at 857 GHz.

Frequency	rejection dB
100	56,9
143	52,75
217	48,1
353	42,8
545	38
857	34,1

RADIATION PATTERNS

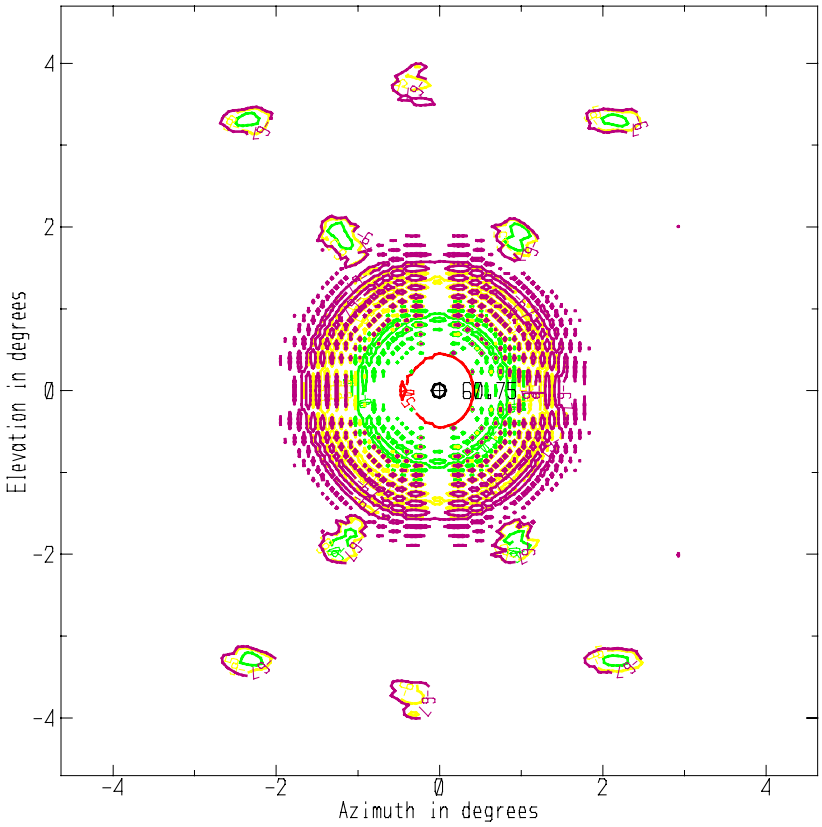

FIGURE A1 : Radiation pattern : HFI_100_1, iso contour : -3 –50 –60 –65 –67 dB)

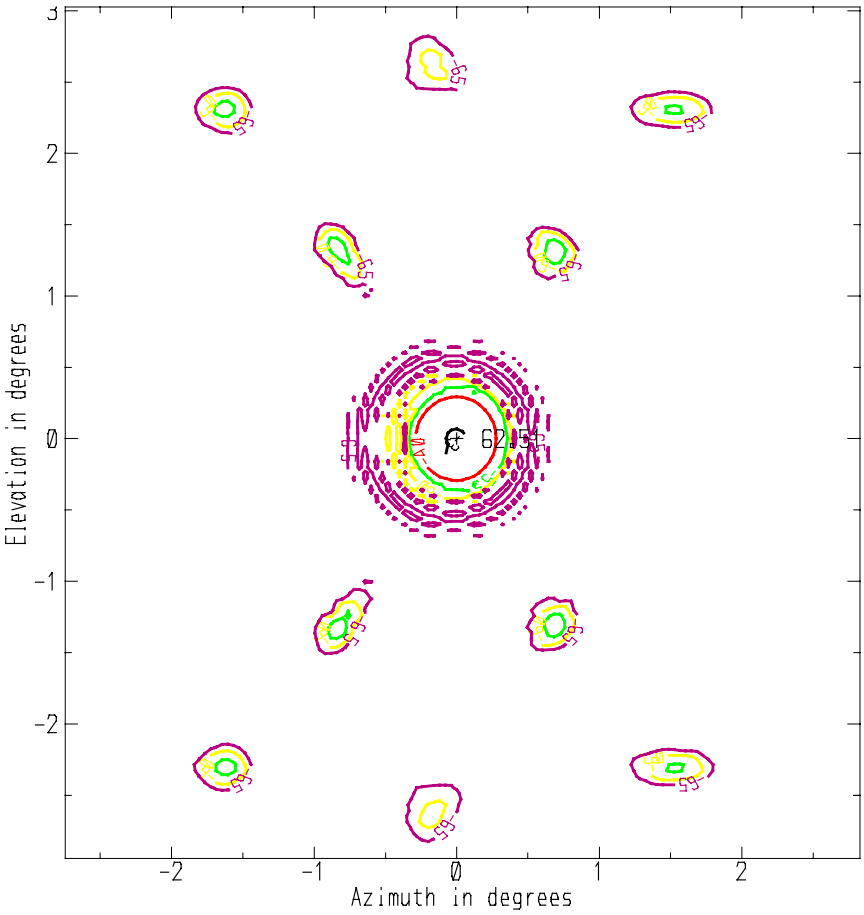

FIGURE A2 : Radiation pattern : HFI_143_1,iso contours (-3 –40 –55 –60 –65 dB)

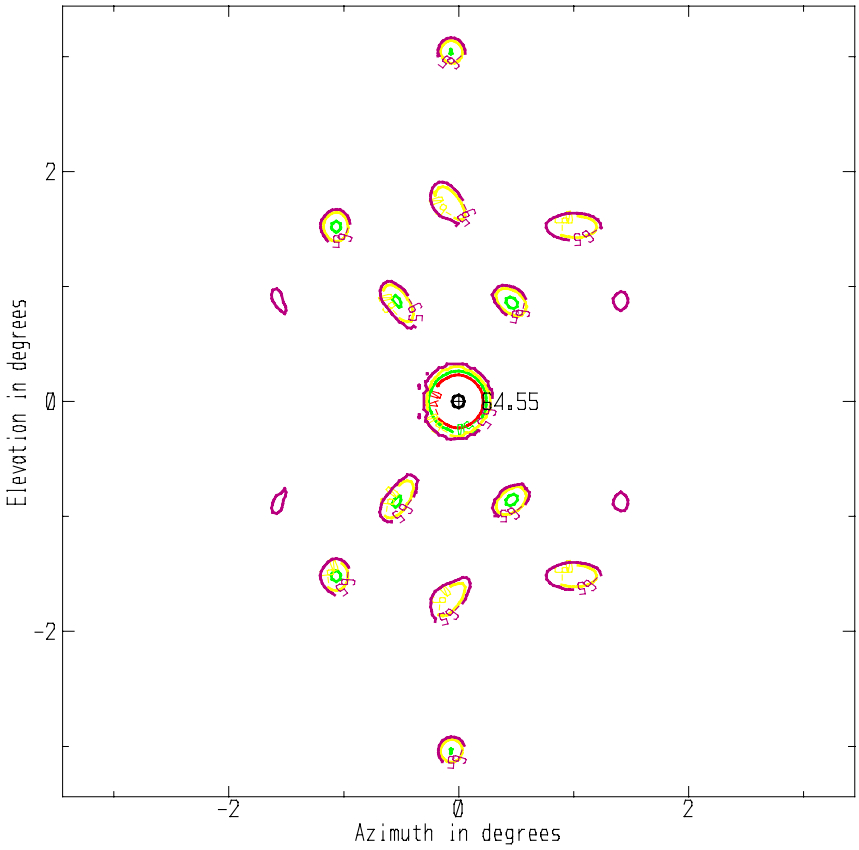

FIGURE A3 : HFI_217_1, iso-contour (-3 –40 –50 –60 –65 dB)

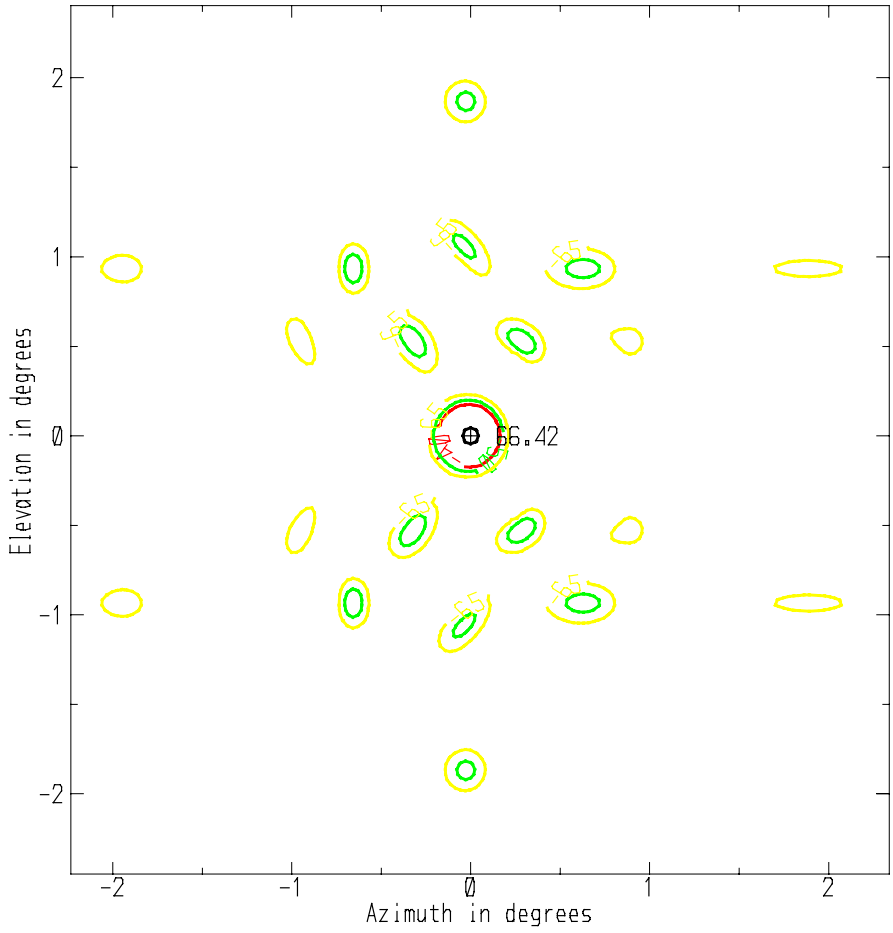

FIGURE A4 : HFI_353_1, iso contours (-3 –40 –50 –65 dB)

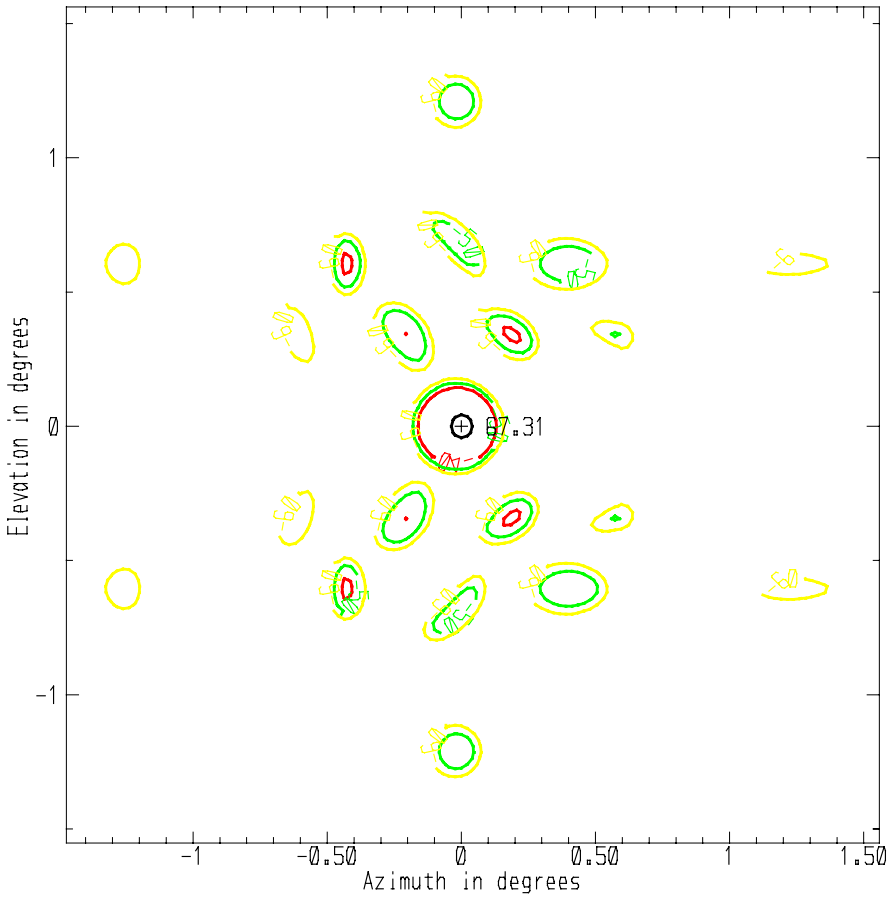

FIGURE A5 : HFI_ 545_1, iso contour (-3 –50 –60 dB)

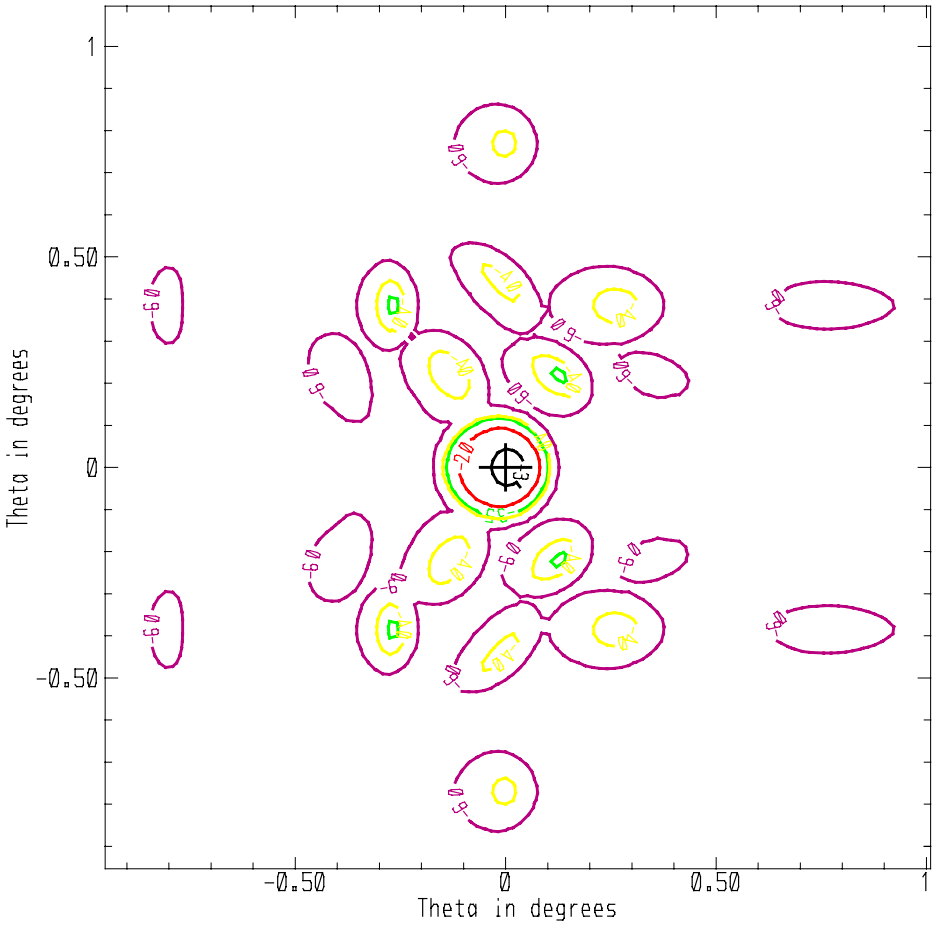

FIGURE A6 : HFI_857_1, iso contour (-3 –20 –35 –40 –60 dB)

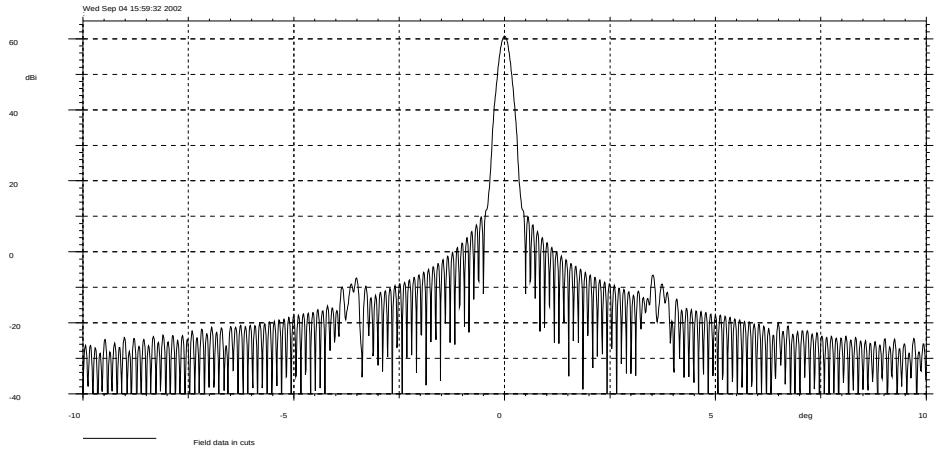

FIGURE A7 : HFI_100_1, quilting on main and sub reflectors

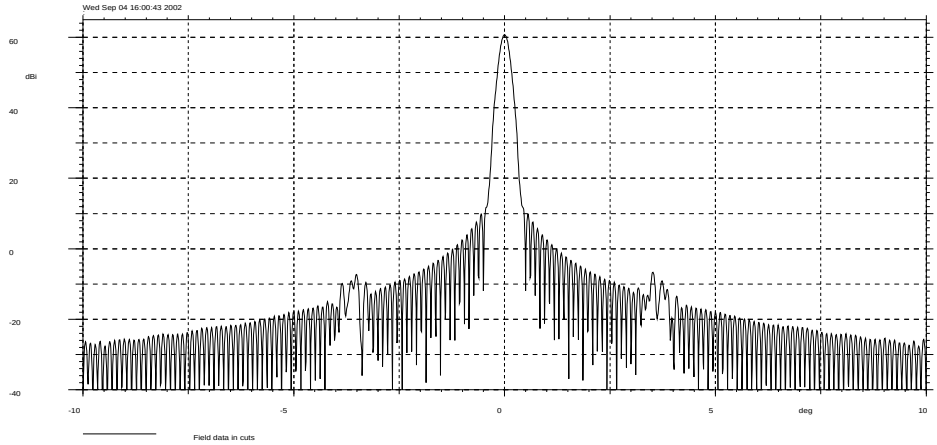

FIGURE A8 : HFI_100_1, quilting on sub reflector only

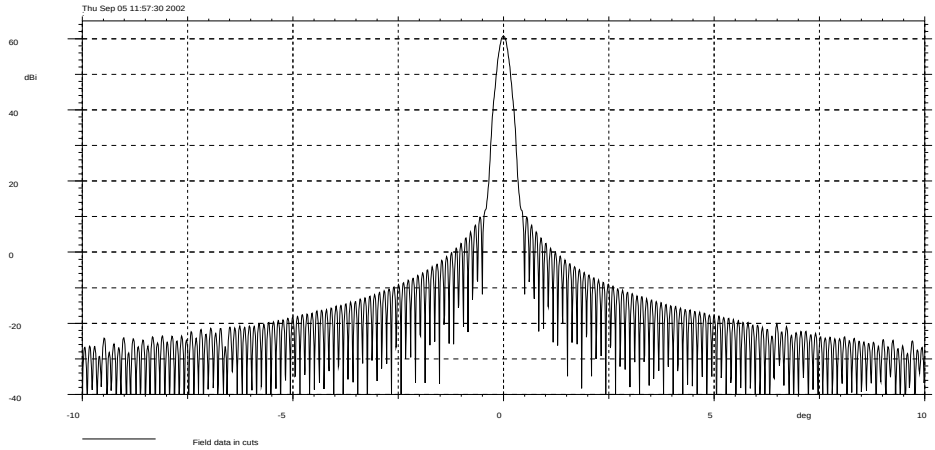

FIGURE A9 : HFI_100_1, quilting on main reflector only

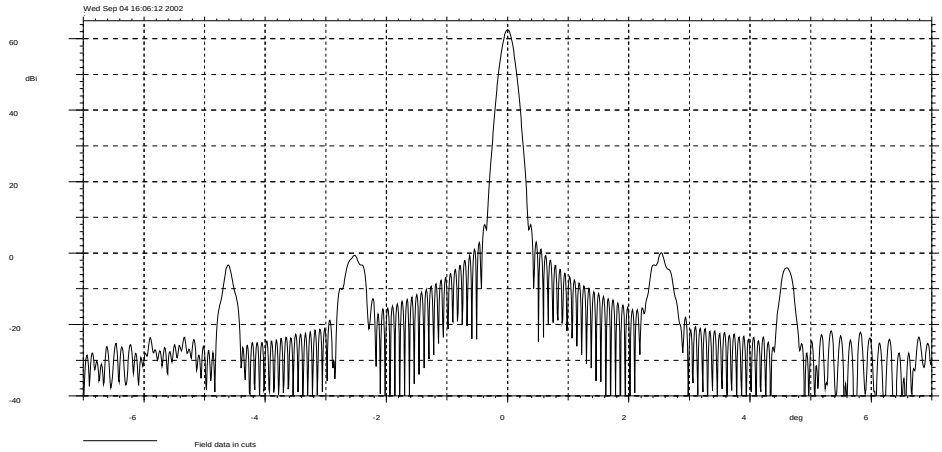

FIGURE A10 : HFI_143_1, quilting on main and sub reflectors

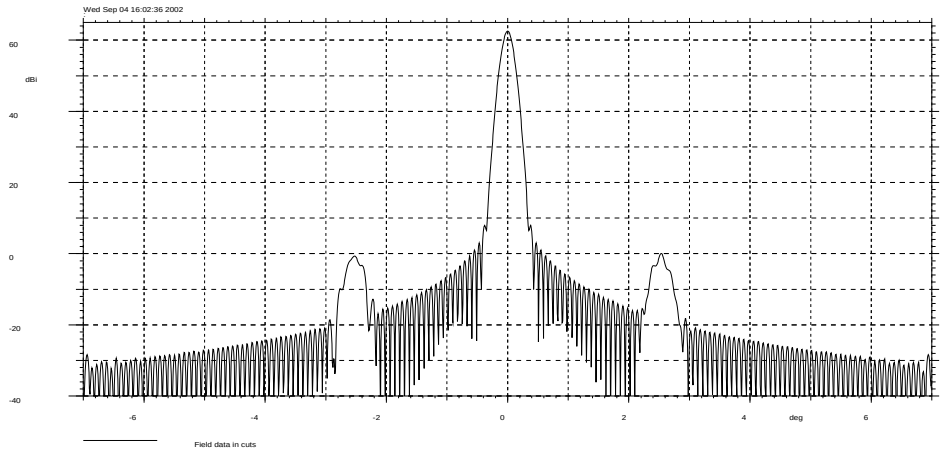

FIGURE A11 : HFI_143_1, quilting on sub reflector only

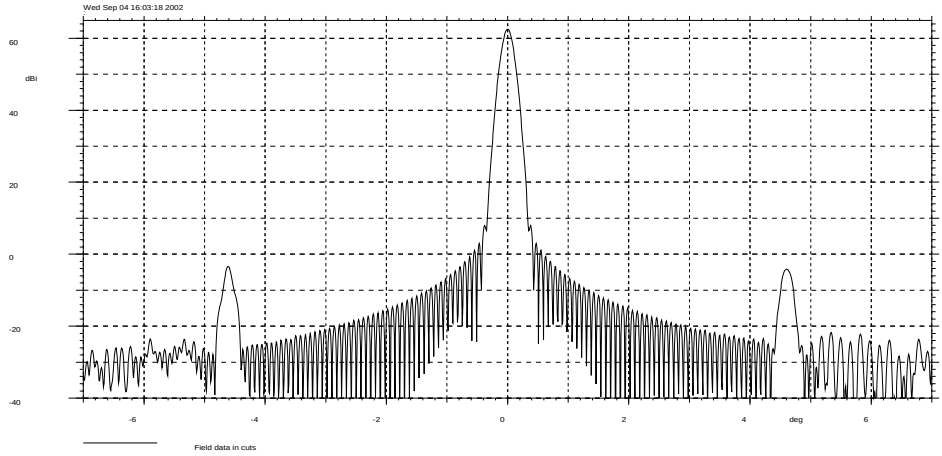

FIGURE A12 : HFI_143_1, quilting on main reflector only

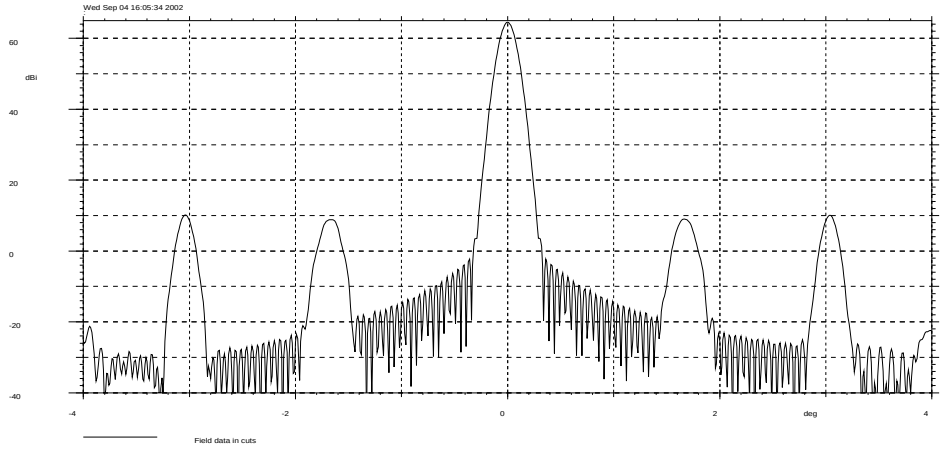

FIGURE A13 : HFI_217_1, quilting on main and sub reflectors

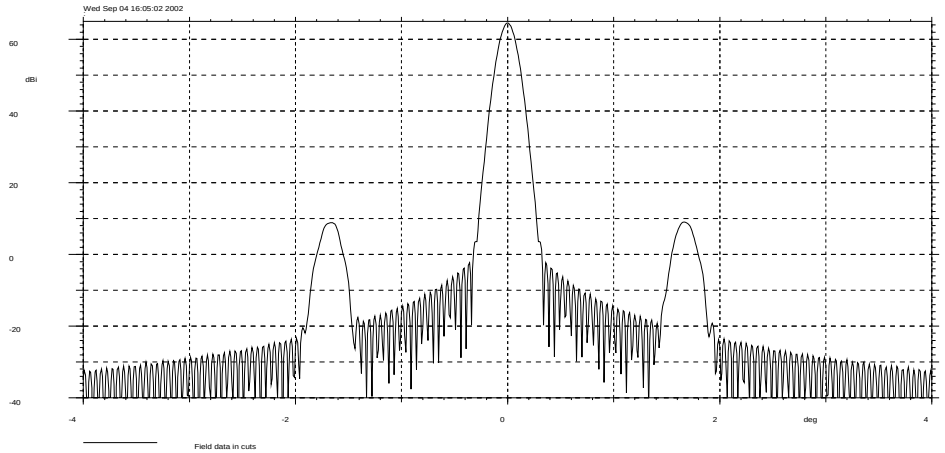

FIGURE A14 : HFI_ 217_1, quilting on sub reflector only

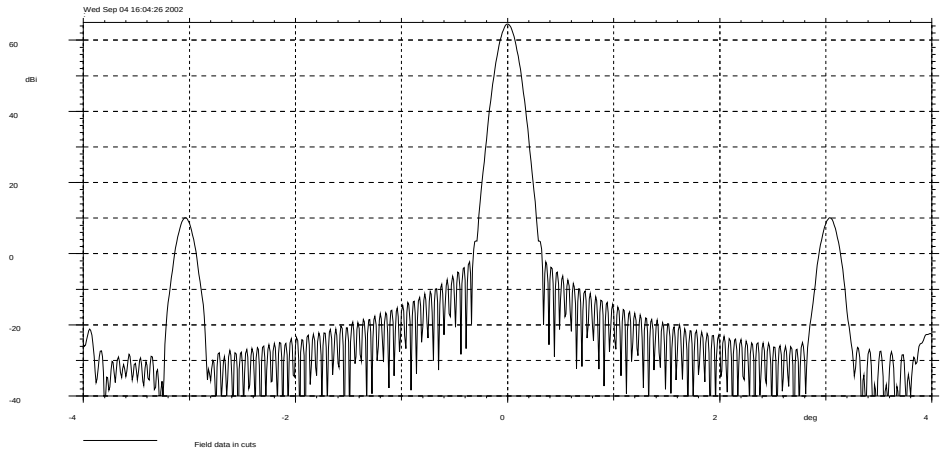

FIGURE A15 : HFI_ 217_1 : quilting on main reflector only

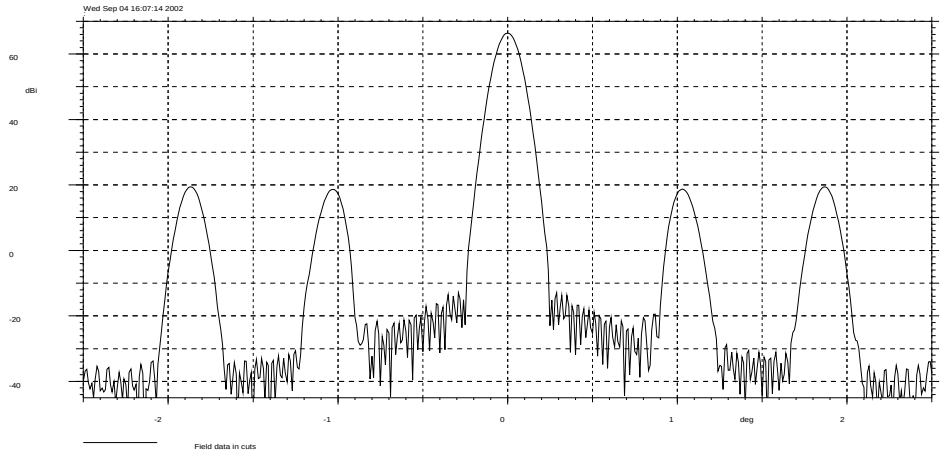

FIGURE A16 : HFI_353_1, quilting on main and sub reflectors

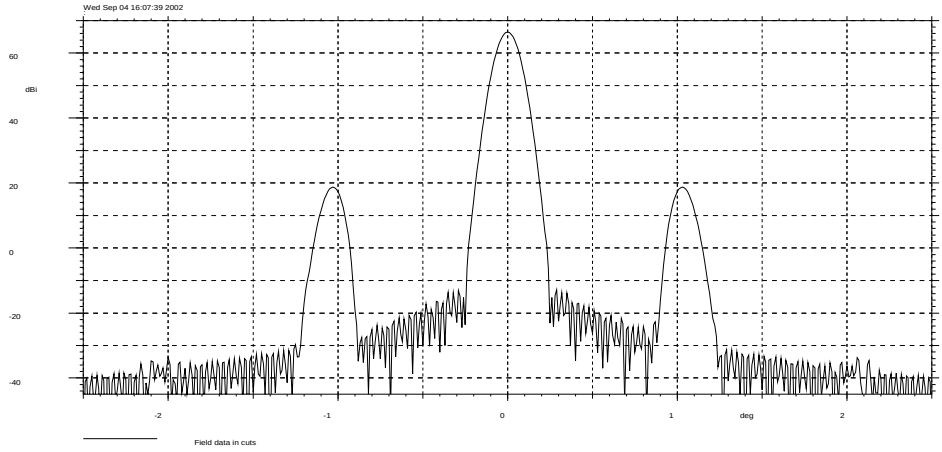

FIGURE A17 : HFI_353_1, quilting on sub reflector only

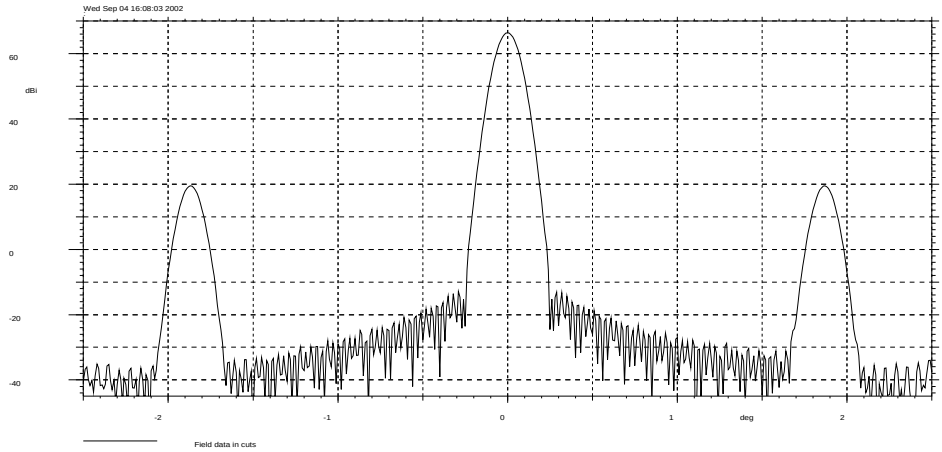

FIGURE A18 : HFI_353_1, quilting on main reflector only

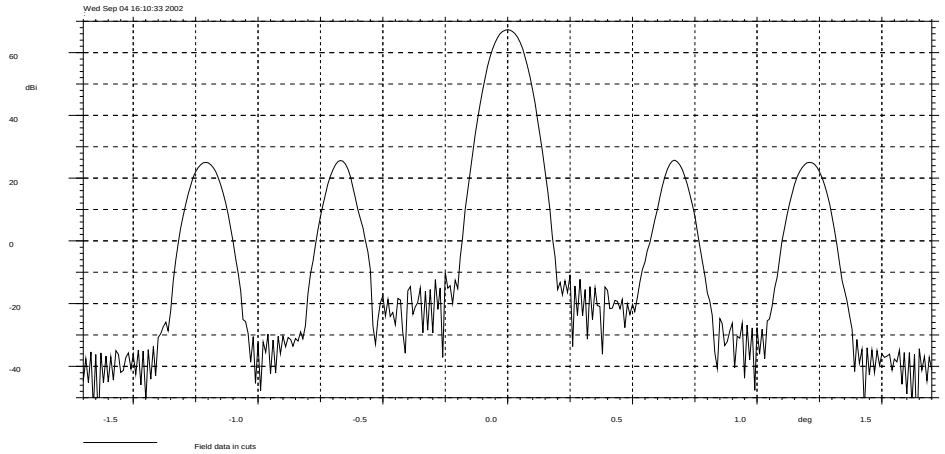

FIGURE A19 : HFI_545_1 quilting on main and sub reflectors.

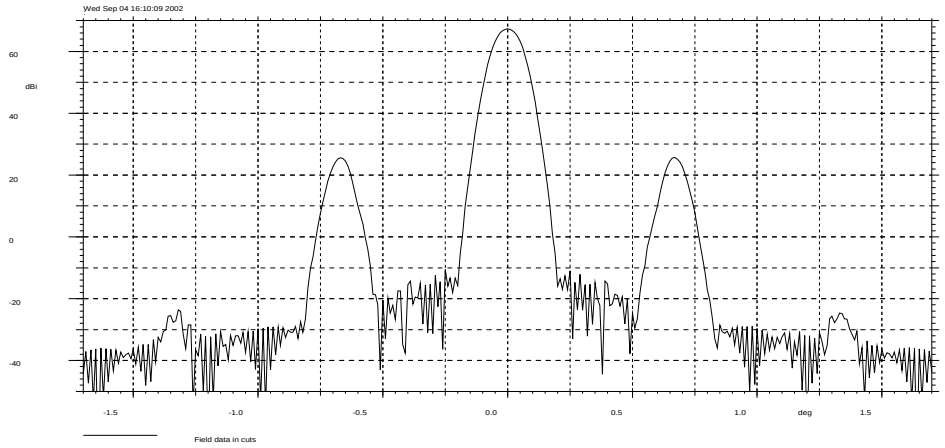

FIGURE A20 : HFI_545_1, quilting on sub reflector only

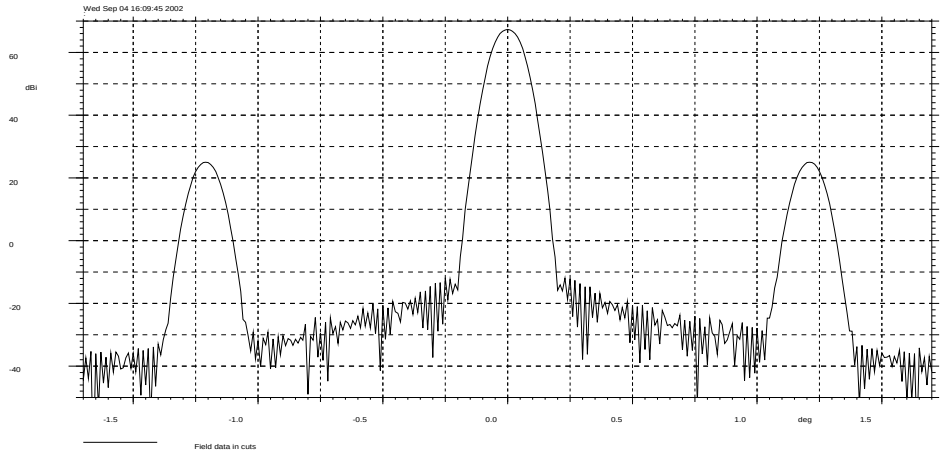

FIGURE A21 : HFI_545_1, quilting on main reflector only

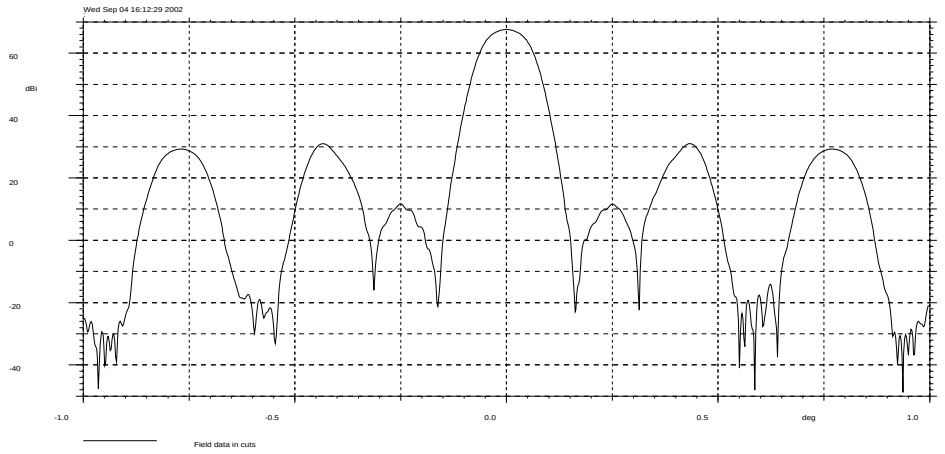

FIGURE A22 : HFI_857_1, quilting on main and sub reflector

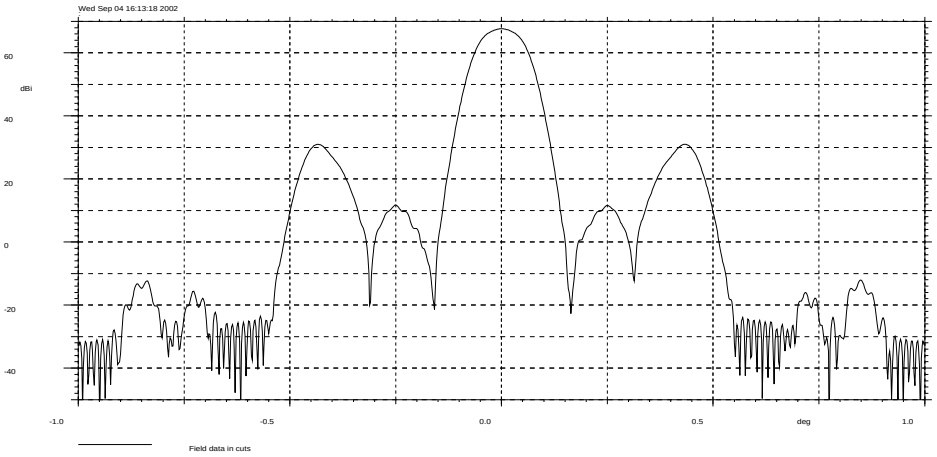

FIGURE A23 : HFI_857_1, quilting on sub reflector only

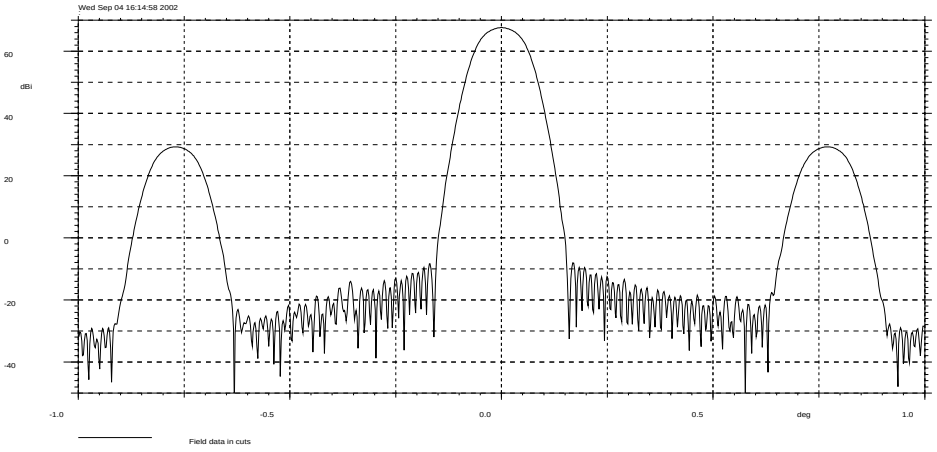

FIGURE A23 : HFI_857_1, quilting on main reflector only

END OF DOCUMENT